Modeling and Methodological Advances in Causal Inference

by

Shuxi Zeng

Department of Statistical Science
Duke University

Date: _____

Approved:

_____

Fan Li, Advisor

_____

Surya T. Tokdar

_____

Jason Xu

_____

Susan C. Alberts

Dissertation submitted in partial fulfillment of the requirements for the degree of
Doctor of Philosophy in the Department of Statistical Science
in the Graduate School of Duke University

2021

ABSTRACT

Modeling and Methodological Advances in Causal Inference

by

Shuxi Zeng

Department of Statistical Science
Duke University

Date: _____

Approved:

_____

Fan Li, Advisor

_____

Surya T. Tokdar

_____

Jason Xu

_____

Susan C. Alberts

An abstract of a dissertation submitted in partial fulfillment of the requirements for the degree of Doctor of Philosophy in the Department of Statistical Science in the Graduate School of Duke University

2021

Abstract

This thesis develops novel theory, methods, and models in three major areas in causal inference: (i) propensity score weighting methods for randomized experiments and observational studies; (ii) causal mediation analysis with sparse and irregular longitudinal data; and (iii) machine learning methods for causal inference. All theoretical and methodological developments are accompanied by extensive simulation studies and real world applications.

Our contribution to propensity score weighting method is presented in Chapter 2 and 3. In Chapter 2, we investigate the use of propensity score weighting in the randomized trials for covariate adjustment. We introduce the class of balancing weights and establish its theoretical properties. We demonstrate that it is asymptotically equivalent to the analysis of covariance (ANCOVA) and derive the closed-form variance estimator. We further recommend the overlap weighting estimator based on its semiparametric efficiency and good finite-sample performance. In Chapter 3, We proposed a class of propensity score weighting estimators causal inference for survival outcomes based on the pseudo-observations. This class of estimators are applicable to several different target populations, survival causal estimands, as well as binary and multiple treatments. We study the theoretical properties of the weighting estimator and derive a new closed-form variance estimator.

Our contribution to causal mediation analysis is presented in Chapter 4. Causal mediation analysis studies the causal relationships between treatment, outcome and an intermediate variable (i.e. mediator) that lies in between. We extend the existing causal mediation framework to the setting where both the mediator and outcome are measured repeatedly on sparse and irregular time grids. We view the observed mediator and outcome trajectories as realizations of underlying smooth stochastic processes and define causal estimands of direct and indirect effects accordingly. We provide assumptions to nonparametrically identify these estimands. We further de-

vise a functional principal component analysis (FPCA) approach to estimate the smooth processes and consequently causal effects. We adopt the Bayesian paradigm to properly quantify the uncertainties in estimation.

Our contribution to machine learning methods for causal inference is presented in Chapter 5 and 6. In Chapter 5, we develop a new algorithm that learns double-robust representations in observational studies, leading to consistent causal estimation if the model for either the propensity score or the outcome, but not necessarily both, is correctly specified. Specifically, we use the entropy balancing method to learn the weights that minimize the Jensen-Shannon divergence of the representation between the treated and control groups, based on which we make robust and efficient counterfactual predictions for both individual and average treatment effects. In Chapter 6, we study how to build a robust prediction model by exploiting the causal relationships among predictors. We propose a causal transfer random forest method learning the stable causal relationships efficiently from a large scale of observational data and a small amount of randomized data. We provide theoretical justifications and validate the algorithm empirically with synthetic experiments and real world prediction tasks.

Contents

List of Tables

List of Figures

Acknowledgements

I am very fortunate to spend the past four years in the Department of Statistical Science, Duke University. I would like to express my appreciation to the amazing people who make my life towards Ph.D. a valuable memory.

First, I want to thank my advisor, Dr. Fan Li, for being a great mentor in causal inference research. I benefit tremendously from her way of approaching research problems. During our first meeting, she proposed three pillars for being a "successful" Ph.D. in statistics, which include mathematics, programming and writing skills. Although I am far from being excel in all the three forementioned aspects, I have made great progress with her help during my Ph.D. study.

I also would like to thank Dr. Peng Ding at University of California, Berkeley, for his generous recommendation and guidance to the research of causal inference. I thank Dr. Bo Li at Tsinghua University for leading me into the statistics. which shapes the career path for an undergraduate with the Economics major.

I also want to thank my collaborators during my Ph.D. study. I particularly enjoy working with those researchers on the same project, including Dr. Fan (Frank) Li, Dr. Susan Alberts, Dr. Elizabeth Archie, Dr. Stacy Rosenbaum, Dr. Fernando Campos, Dr. Elizabeth Lange, Dr. Rui Wang, Dr. Liangyuan Hu, Dr. Lawrence Carin, Dr. Chenyang Tao, Dr. Shounak Datta, Serge Assaad, Paidamoyo Chapfuwa and Dr. Jason Poulos.

I would also like to thank my other thesis committee members, Dr. Surya Tokdar, Dr. Jason Xu and Dr. Susan Alberts for all the suggestions and discussions on my research. I also thank Dr. Emre Kiciman, Dr. Denis Charles and Dr. Murat Bayir for the collaboration on my summer project at Microsoft and Dr. Swati Rallapalli for hosting my internship at Facebook. I would also like to thank the staff in our department, Lori Rauch, Nicole Scott, Karen Whitesell, for being so supportive to the students.

I wish to thank Xu Chen, Bai Li, Jialiang Mao, Jiurui Tang and many others for being great friends. I also enjoy the time spending with my cohort, Fan Bu, Federico Ferrari, Yi Guo, Henry Kirveslahti, Heather Mathews, Hanyu Song. I appreciate the research discussions and game play with Sheng Jiang. I also owe a debt of gratitude to my rootmates, Kangnan Li and Keru Wu.

Finally, I want to thank my parents for all their constant support from the other side of the Earth, which is the strongest motivation along my endeavour.

1

Introduction

1.1 Motivation

Causal inference, or counterfactual prediction, is central to decision making in healthcare, policy and social sciences (Imbens and Rubin, 2015). The topic of causal inference concerns the causal effect of one specific treatment $T_i \in \mathcal{T}$, e.g. evaluating the treatment effect of a medicine, on certain outcomes Y_i of interests, based on the sample $i = 1, 2, \cdots, N$ drawn from a population. Rubin (1974) defines the causal effect in potential outcomes framework, which posits a set of potential outcomes $Y_i(t), t \in \mathcal{T}$ for each unit and only one of them is observed depending on the treatment assigned. Therefore, the fundamental problem in causal inference is to impute the missing potential outcomes (Holland, 1986). In observational study, the treatment assignment is usually depending on certain pretreatment covariates $\mathbf{X}_i$, which are also correlated with the potential outcomes. The direct comparison across different treatment groups can be biased as the distributions of some important covariates might imbalance across two groups, which is also known as the *confounding* problem (VanderWeele and Shpitser, 2013).

Several approaches like direct regression adjustment, matching (Abadie and Imbens, 2006) and weighting (Hirano et al., 2003) have been employed to address the confounding or adjust for the covariate imbalance. The use of propensity score weighting (Rosenbaum and Rubin, 1983), defined as the probability of being treated, $e(x) = \Pr(T_i = 1|\mathbf{X}_i = x)$, has been used to adjust for confounding bias in the observational study. However, the performance of weighting method deteriorates due to the extreme weights in severe imbalance scenario. This problem is pronounced

especially when the sample size is small, even in randomized controlled trials with imbalance only by chance (Senn, 1989; Ciolino et al., 2015; Thompson et al., 2015). Moreover, the propensity score weighting estimator is hard to adapt when the data is of a particular structure, such as the case dealing with survival outcomes with censoring (Austin, 2014; Mao et al., 2018). Commonly used propensity score weighting estimator is usually coupled with certain survival models and thus is vulnerable to model misspecifications (Austin, 2010a,b). Developing a propensity score weighting estimator without depending on the outcome modeling assumptions is of methodological interests.

Researchers might be not only interested in evaluating the effect of a certain treatment but also understanding the causal mechanism, especially how much of the effect can be attributed to a mediator M_i, which is also known as the mediation analysis (Baron and Kenny, 1986; Imai et al., 2010b). For example, in a motivating application, researchers study how much of the effect from early adversity on the health outcome can be explained by the social bonds among wild baboons (Rosenbaum et al., 2020). However, the mediators and outcomes might be measured on a sparse and irregular grid for each unit in practice. The sparse and irregularly-spaced longitudinal data are increasingly popular nowadays, such as in electronic health records (EHR), which brings challenges for modeling and inference on mediation analysis.

Recent advances in machine learning research has equipped causal inference with useful modeling or learning tools (Johansson et al., 2016; Shalit et al., 2017; Zhang et al., 2020). While the powerful techniques like neural networks have been added into the toolbox for outcome modeling, the importance of modeling the treatment assignment mechanism has not been fully recognized in machine learning community. Classic causal inference literature points out that combining both the propensity score and the outcome model can increase the efficiency of the estimator and bring the doubly robust property (Scharfstein et al., 1999; Lunceford and Davidian, 2004b; Kang et al., 2007; Chernozhukov et al., 2018). Namely, the estimator remains consistent if

either the outcome or the propensity score model is correctly specified. One natural question is how to attain the double robustness when we are faced with the high-dimensional dataset and employ the machine learning algorithms, like representation learning, for counterfactual predictions.

Causal inference also sheds light on other research areas such as the domain adaptation and transfer learning (Quionero-Candela et al., 2009; Bickel et al., 2009; Daume III and Marcu, 2006), even in the context without specific treatments. For instance, one obstacle for a model to transfer from training distribution to a target testing distribution is the spurious correlations. Namely, the algorithms exploiting the correlations might learn the non-robust relationships that do not hold on the testing data. One possible fix to use the direct causes of the labels, as the causal relationships are expected to be robust across different scenarios (Rojas-Carulla et al., 2018; Meinshausen, 2018; Kuang et al., 2018; Arjovsky et al., 2019). Some ads publisher (e.g. Bing ads) have run certain randomized experiments in the real traffic to build robust models for click predictions (Bayir et al., 2019). However. the randomized data are usually acquired at a larger cost and how to efficiently use it for building robust prediction model is of particular interests to many practitioners.

1.2 Research questions and main contributions

Motivated by the specific challenges in causal inference, this thesis proposes the several novel methods and modeling techniques. In this section, we briefly summarize the research questions and highlight the contributions of the thesis.

1.Propensity score weighting in randomized controlled trials

Chance imbalance in baseline characteristics is common in randomized controlled trials (RCT) (Senn, 1989; Ciolino et al., 2015). Regression adjustment such as the analysis of covariance (ANCOVA) is often used to account for imbalance and increase precision of the treatment effect estimate (Yang and Tsiatis, 2001; Kahan et al., 2016; Leon et al., 2003; Tsiatis et al., 2008; Lin, 2013). An objective alternative is

through inverse probability weighting (IPW) of the propensity scores (Tsiatis et al., 2008; Shen et al., 2014). Although IPW and ANCOVA are asymptotically equivalent (Williamson et al., 2014), the former may demonstrate inferior performance in finite samples. Whether we can retain the objectivity of weighting methods and meanwhile improve the finite sample performance is of particular interests to the practitioners analyzing the results for RCT.

In this thesis, we point out that IPW is a special case of the general class of balancing weights (Li et al., 2018a), and advocate to use overlap weighting (OW) for covariate adjustment. The OW method has a unique advantage of completely removing chance imbalance when the propensity score is estimated by logistic regression. We show that the OW estimator attains the same semiparametric variance lower bound as the most efficient ANCOVA estimator and the IPW estimator for a continuous outcome, and derive closed-form variance estimators for OW when estimating additive and ratio estimands. Through extensive simulations, we demonstrate OW consistently outperforms IPW in finite samples and improves the efficiency over ANCOVA and augmented IPW when the degree of treatment effect heterogeneity is moderate or when the outcome model is incorrectly specified.

2.Propensity score weighting with survival outcomes

Survival outcomes are common in comparative effectiveness studies. A standard approach for causal inference with survival outcomes is to fit a Cox proportional hazards model to an inversely probability weighted (IPW) sample (Austin, 2014; Austin and Stuart, 2017). However, this method is subject to model misspecification and the resulting hazard ratio estimate lacks causal interpretation (Hernán, 2010). Moreover, IPW often corresponds to an inappropriate target population when there is lack of covariate overlap between the treatment groups. A "once for all" approach constructs "pseudo" observations of the censored outcomes and allows less-model dependent methods such as propensity score weighting to proceed as if we have the completely observed outcomes (Andersen et al., 2017).

3. Causal mediation analysis with sparse and irregular data

Causal mediation analysis seeks to investigate how the treatment effect of an exposure on outcomes is mediated through intermediate variables (Robins and Greenland, 1992; Pearl, 2001; Sobel, 2008; Tchetgen Tchetgen and Shpitser, 2012; Daniels et al., 2012; VanderWeele, 2016). Although many applications involve longitudinal data (van der Laan and Petersen, 2008; Roth and MacKinnon, 2012), the existing methods are not directly applicable to settings where the mediator and outcome are measured on sparse and irregular time grids.

This thesis extends the existing causal mediation framework from a functional data analysis perspective, viewing the sparse and irregular longitudinal data as realizations of underlying smooth stochastic processes. We define causal estimands of direct and indirect effects accordingly and provide corresponding identification assumptions. For estimation and inference, we employ a functional principal component analysis approach for dimension reduction and use the first few functional principal components instead of the whole trajectories in the structural equation models (Yao et al., 2005; Jiang and Wang, 2010, 2011; Han et al., 2018). We adopt the Bayesian paradigm to accurately quantify the uncertainties (Kowal and Bourgeois, 2020). The operating characteristics of the proposed methods are examined via simulations. We apply the proposed methods to a longitudinal data set from a wild baboon population in Kenya to investigate the causal relationships between early adversity, strength of social bonds between animals, and adult glucocorticoid hormone concentrations (Rosenbaum et al., 2020).

4. Double robust representation learning

To de-bias causal estimators with high-dimensional data in observational studies, recent advances suggest the importance of combining machine learning models for both the propensity score and the outcome function (Belloni et al., 2014). Especially, (Chernozhukov et al., 2018) proposed to combine machine learning models for the propensity score and the outcome function to achieve $\sqrt{N}$ consistency in estimating

the average treatment effect (ATE). A closely related concept is double-robustness (Scharfstein et al., 1999; Lunceford and Davidian, 2004b; Kang et al., 2007), in which an estimator is consistent if either the propensity score model or the outcome model, but not necessarily both, is correctly specified.

This thesis proposes a novel scalable method to learn double-robust representations for counterfactual predictions, leading to consistent causal estimation if the model for either the propensity score or the outcome, but not necessarily both, is correctly specified. Specifically, we use the entropy balancing method (Hainmueller, 2012) to learn the weights that minimize the Jensen-Shannon divergence of the representation between the treated and control groups, based on which we make robust and efficient counterfactual predictions for both individual and average treatment effects. We provide theoretical justifications for the proposed method. The algorithm shows competitive performance with the state-of-the-art on real world and synthetic data.

5. Transfer learning based on causal relationships

It is often critical for prediction models to be robust to distributional shifts between training and testing data. From a causal perspective, the challenge is to distinguish the stable causal relationships from the unstable spurious correlations across shifts (Peters et al., 2016; Rojas-Carulla et al., 2018; Arjovsky et al., 2019). An efficient algorithm to disentangle the stable causal relationships from the a large amount of observational data and a small proportion of randomized data is of interests to many practitioners especially for the online advertisement industry (Cook et al., 2002; Kallus et al., 2018; Bayir et al., 2019).

We describe a *causal transfer random forest* (CTRF) that combines existing training data with a small amount of data from a randomized experiment to train a model which is robust to the feature shifts and therefore transfers to a new targeting distribution. Theoretically, we justify the robustness of the approach against feature shifts with the knowledge from causal learning. Empirically, we evaluate the CTRF

using both synthetic data experiments and real-world experiments in the Bing Ads platform, including a click prediction task and in the context of an end-to-end counterfactual optimization system. The proposed CTRF produces robust predictions and outperforms most baseline methods compared in the presence of feature shifts.

1.3 Outline

In Chapter 2, we study the use of a general class of propensity score weights, called the balancing weights in randomized trials for covariate adjustment. Within this class, we advocate to use the overlap weighting (OW). We provide theoretical guarantee and carry out extensive simulations studies on the proposed estimator. It turns out the propensity score weighting estimator based on OW achieves semiparametric efficiency under certain conditions as well as a good finite-sample performance.

In Chapter 3, we generalize the balancing weights in Li et al. (2018a) to time-to-event outcomes based on the pseudo-observation approach with multiple treatments. We study its theoretical property and derive closed-form variance estimators. The variance estimators account for the uncertainty from propensity score estimation as well as the pseudo observations. We examine both the point estimator and variance estimator through extensive simulations and compare it with a range of commonly used estimators.

In Chapter 4, we propose a causal mediation framework for sparse and irregular longitudinal data. We view the data from a functional data analysis perspective and define causal estimands of direct and indirect effects accordingly. We provide assumptions for nonparametric identification and modeling techniques based on functional principal component analysis (FPCA). We project the mediator and outcome trajectories to a low-dimensional representation and quantify the uncertainties accurately through a Bayesian paradigm.

In Chapter 5, we propose a novel algorithm to learn the double-robust representations for counterfactual predictions in observational studies, allowing for simultaneous

learning of the representations and balancing weights. We study its theoretical property and test its performance on several benchmark datasets. Though the proposed method is motivated by estimating the treatment on average, it also demonstrates comparable performance with state-of-the-art for individual treatment effects (ITE) estimation.

In Chapter 6, we introduce a novel and efficient method for building robust prediction models that combine large-scale observational data with a small amount of randomized data. We also offer a theoretical justification of the proposed method and its improved performance from the causal perspective. We evaluate the proposed method with synthetic experiments and multiple experiments in a real-world, large-scale online system at Bing Ads.

In Chapter 7, we conclude the thesis with highlights on the contributions and directions for future extensions.

2

Propensity score weighting in RCT

2.1 Introduction

Randomized controlled trials are the gold standard for evaluating the efficacy and safety of new treatments and interventions. Statistically, randomization ensures the optimal internal validity and balances both measured and unmeasured confounders in expectation. This makes the simple unadjusted difference-in-means estimator unbiased for the intervention effect (Rosenberger and Lachin, 2002). Frequently, important patient characteristics are collected at baseline; although over repeated experiments, they will be balanced between treatment arms, chance imbalance often arises in a single trial due to the random nature in allocating the treatment (Senn, 1989; Ciolino et al., 2015), especially when the sample size is limited (Thompson et al., 2015). If any of the baseline covariates are prognostic risk factors that are predictive of the outcome, adjusting for the imbalance of these factors in the analysis can improve the statistical power and provide a greater chance of identifying the treatment signals when they actually exist (Ciolino et al., 2015; Pocock et al., 2002; Hernández et al., 2004).

There are two general streams of methods for covariate adjustment in randomized trials: (outcome) regression adjustment (Yang and Tsiatis, 2001; Kahan et al., 2016; Leon et al., 2003; Tsiatis et al., 2008; Zhang et al., 2008) and the inverse probability of treatment weighting (IPW or IPTW) based on propensity scores (Williamson et al., 2014; Shen et al., 2014; Colantuoni and Rosenblum, 2015). For regression adjustment with continuous outcomes, the analysis of covariance (ANCOVA) model is often used, where the outcome is regressed on the treatment, covariates and possibly

their interactions (Tsiatis et al., 2008). The treatment effect is estimated by the coefficient of the treatment variable. With binary outcomes, a generalized linear model can be postulated to estimate the adjusted risk ratio or odds ratio, with the caveat that the regression coefficient of treatment may not represent the marginal effect due to non-collapsability (Williamson et al., 2014). Tsiatis and co-authors developed a suite of semiparametric ANCOVA estimators that improves efficiency over the unadjusted analysis in randomized trials (Yang and Tsiatis, 2001; Leon et al., 2003; Tsiatis et al., 2008). Lin (Lin, 2013) clarified that it is critical to incorporate covariate-by-treatment interaction terms in regression adjustment for efficiency gain. When the randomization probability is 1/2, ANCOVA returns consistent point and interval estimates even if the outcome model is misspecified (Yang and Tsiatis, 2001; Lin, 2013; Wang et al., 2019). However, misspecification of the outcome model can decrease precision in unbalanced experiments with treatment effect heterogeneity (Freedman, 2008). Another limitation of regression adjustment is the potential for inviting a 'fishing expedition': one may search for an outcome model that gives the most dramatic treatment effect estimate which jeopardizes the objectivity of causal inference with randomized trials (Tsiatis et al., 2008; Shen et al., 2014).

Originally developed in the context of survey sampling and observational studies (Lunceford and Davidian, 2004a), IPW has been advocated as an objective alternative to ANCOVA in randomized trials (Williamson et al., 2014). To implement IPW, one first fits a logistic *working* model to estimate the propensity scores – the conditional probability of receiving the treatment given the baseline covariates (Rosenbaum and Rubin, 1983), and then estimates the treatment effect by the difference of the weighted outcome – weighted by the inverse of the estimated propensity – between the treatment arms. In randomized trials, the treatment group is randomly assigned and the true propensity score is known. Therefore, the working propensity score model is always correctly specified, and the IPW estimator is consistent to the marginal treatment effect. For a continuous outcome, the IPW estimator with a logistic propensity

model has the same large-sample variance as the efficient ANCOVA estimator (Shen et al., 2014; Williamson et al., 2014), but it offers the following advantages.

First, IPW separates the design and analysis in the sense that the propensity score model only involves baseline covariates and the treatment indicator; it does not require the access to the outcome and hence avoids the 'fishing expedition.' As such, IPW offers better transparency and objectivity in pre-specifying the analytical adjustment before outcomes are observed. Second, IPW preserves the marginal treatment effect estimand with non-continuous outcomes, while the interpretation of the outcome regression coefficient may change according to different covariate specifications (Hauck et al., 1998; Robinson and Jewell, 1991). Third, IPW can easily obtain treatment effect estimates for rare binary or categorical outcomes whereas outcome models often fail to converge in such situations (Williamson et al., 2014). This is particularly the case when the target parameter is a risk ratio, where log-binomial models are known to have unsatisfying convergence properties (Zou, 2004). On the other hand, a major limitation of IPW is that it may be inefficient compared to ANCOVA with limited sample sizes and unbalanced treatment allocations (Raad et al., 2020) .

In this chapter, we point out that IPW is a special case of the general class of propensity score weights, called the balancing weights (Li et al., 2018a), many members of which could be used for covariate adjustment in randomized trials. Within this class, we advocate to use the overlap weighting (OW) (Li et al., 2018a, 2019; Schneider et al., 2001; Crump et al., 2006; Li and Li, 2019b). In the context of randomized trials, a particularly attractive feature of OW is that, if the propensity score is estimated from a logistic working model, then OW leads to *exact mean balance* of any baseline covariate in that model, and consequently remove the chance imbalance of that covariate. As a propensity score method, OW retains the aforementioned advantages of IPW while offers better finite-sample properties (Section 2.2). In Section 2.3, we demonstrate that the OW estimator, similar as IPW, achieves the

same semiparametric variance lower bound and hence is asymptotically equivalent to the efficient ANCOVA estimator for continuous outcomes. For binary outcomes, we further provide closed-form variance estimators of the OW estimator for estimating marginal risk difference, risk ratio and odds ratio, which incorporates the uncertainty in estimating the propensity scores and achieves close to nominal coverage in finite samples. Through extensive simulations in Section 2.4, we demonstrate the efficiency advantage of OW under small to moderate sample sizes, and also validate the proposed variance estimator for OW. Finally, in Section 2.5 we apply the proposed method to the Best Apnea Interventions for Research (BestAIR) randomized trial and evaluate the treatment effect of continuous positive airway pressure (CPAP) on several clinical outcomes.

2.2 Propensity score weighting for covariate adjustment

2.2.1 The balancing weights

We consider a randomized trial with two arms and N patients, where N_1 and N_0 patients are randomized into the treatment and control arm, respectively. Let $Z_i = z$ be the binary treatment indicator, with $z = 1$ indicates treatment and $z = 0$ control. Under the potential outcome framework (Neyman, 1990), each unit has a pair of potential outcomes $\{Y_i(1), Y_i(0)\}$, mapped to the treatment and control condition, respectively, of which only the one corresponding to the actual treatment assigned is observed. We denote the observed outcome as $Y_i = Z_i Y_i(1) + (1 - Z_i)Y_i(0)$. In randomized trials, a collection of p baseline variables could be recorded for each patient, denoted by $X_i = (X_{i1}, \ldots, X_{ip})^T$. Denote $\mu_z = E\{Y_i(z)\}$ and $\mu_z(x) = E\{Y_i(z)|X_i = x\}$ as the marginal and conditional expectation of the outcome in arm z ($z = 0, 1$), respectively. A common estimand on the additive scale is the average treatment effect (ATE):

$$\tau = E\{Y_i(1) - Y_i(0)\} = \mu_1 - \mu_0. \tag{2.1}$$

We assume that the treatment Z is randomly assigned to patients, where $\Pr(Z_i = 1|X_i, Y_i(1), Y_i(0)) = \Pr(Z_i = 1) = r$, and $0 < r < 1$ is the randomization probability (see Section 8.1.1 for additional discussions on randomization). The most typical study design uses balanced assignment with $r = 1/2$. Other values of r may be possible, for example, when there is a perceived benefit of the treatment, and a larger proportion of patients are randomized to the intervention. Under randomization of treatment and the consistency assumption, we have $\tau = E(Y_i|Z_i = 1) - E(Y_i|Z_i = 0)$, and thus the unadjusted difference-in-means estimator is:

$$\hat{\tau}^{\text{UNADJ}} = \frac{\sum_{i=1}^{N} Z_i Y_i}{\sum_{i=1}^{N} Z_i} - \frac{\sum_{i=1}^{N}(1 - Z_i)Y_i}{\sum_{i=1}^{N}(1 - Z_i)}. \tag{2.2}$$

Below we generalize the ATE to a class of weighted average treatment effect (WATE) estimands to construct alternative weighting methods. Assume the study sample is drawn from a probability density $f(x)$, and let $g(x)$ denote the covariate distribution density of a *target population*, possibly different from the one represented by the observed sample. The ratio $h(x) = g(x)/f(x)$ is called a *tilting function* (Li and Li, 2019b), which re-weights the distribution of the baseline characteristics of the study sample to represent the target population. We can represent the ATE on the target population g by a WATE estimand:

$$\tau^h = E_g[Y_i(1) - Y_i(0)] = \frac{E\{h(x)(\mu_1(x) - \mu_0(x))\}}{E\{h(x)\}}. \tag{2.3}$$

In practice, we usually pre-specify $h(x)$ instead of $g(x)$. Most commonly $h(x)$ is specified as a function of the propensity score or simply a constant. The propensity score (Rosenbaum and Rubin, 1983) is the conditional probability of treatment given the covariates, $e(x) = \Pr(Z_i = 1|X_i = x)$. Under the randomization assumption, $e(x) = \Pr(Z_i = 1) = r$ for any baseline covariate value x, and therefore as long as $h(x)$ is a function of the propensity score $e(x)$, different h corresponds to the same target population g, and the WATE reduces to ATE, i.e. $\tau^h = \tau$. This is *distinct from observational studies*, where the propensity scores are usually unknown and vary between units, and consequently different $h(x)$ corresponds to different

target populations and estimands (Thomas et al., 2020b). This special feature under randomized trials provides the basis for considering alternative weighting strategies to achieve better finite-sample performances.

In the context of confounding adjustment in observational studies, Li et al. proposed a class of propensity score weights, named the *balancing weights*, to estimate WATE(Li et al., 2018a). Specifically, given any $h(x)$, the balancing weights for patients in the treatment and control arm are defined as:

$$w_1(x) = h(x)/e(x), \quad w_0(x) = h(x)/\{1 - e(x)\}, \tag{2.4}$$

which balances the distributions of the covariates between treatment and control arms in the target population, so that $f_1(x)w_1(x) = f_0(x)w_0(x) = f(x)h(x)$, where $f_z(x)$ is the conditional distribution of covariates in treatment arm z (Wallace and Moodie, 2015; Li et al., 2018a). Then, one can use the following Hájek-type estimator to estimate τ^h:

$$\hat{\tau}^h = \hat{\mu}_1^h - \hat{\mu}_0^h = \frac{\sum_{i=1}^N w_1(x_i)Z_iY_i}{\sum_{i=1}^N w_1(x_i)Z_i} - \frac{\sum_{i=1}^N w_0(x_i)(1-Z_i)Y_i}{\sum_{i=1}^N w_0(x_i)(1-Z_i)}. \tag{2.5}$$

The function $h(x)$ can take any form, each corresponding to a specific weighting scheme. For example, when $h(x) = 1$, the balancing weights become the inverse probability weights, $(w_1, w_0) = (1/e(x), 1/\{1 - e(x)\})$; when $h(x) = e(x)(1 - e(x))$, we have the overlap weights (Li et al., 2018a), $(w_1, w_0) = (1 - e(x), e(x))$, which was also independently developed by Wallace and Moodie (Wallace and Moodie, 2015) in the context of dynamic treatment regimes. Other examples of the balancing weights include the average treatment effect among treated (ATT) weights (Hirano and Imbens, 2001) and the matching weights (Li and Greene, 2013).

IPW is the most well-known case of the balancing weights. Specific to covariate adjustment in randomized trials, Williamson et al. (Williamson et al., 2014) and Shen et al. (Shen et al., 2014) suggested the following IPW estimator of τ:

$$\hat{\tau}^{\text{IPW}} = \frac{\sum_{i=1}^N Z_iY_i/\hat{e}_i}{\sum_{i=1}^N Z_i/\hat{e}_i} - \frac{\sum_{i=1}^N (1-Z_i)Y_i/(1-\hat{e}_i)}{\sum_{i=1}^N (1-Z_i)/(1-\hat{e}_i)}. \tag{2.6}$$

We will point out in Section 2.3 that their findings on IPW are generally applicable to the balancing weights as long as $h(x)$ is a smooth function of the true propensity score. The choice of $h(x)$, however, will affect the finite-sample operating characteristics of the weighting estimator. In particular, below we will closely examine the overlap weights.

2.2.2 The overlap weights

In observational studies, the overlap weights correspond to a target population with the most overlap in the baseline characteristics, and have been shown theoretically to give the smallest asymptotic variance of $\hat{\tau}^h$ among all balancing weights (Li et al., 2018a) as well as empirically reduce the variance of τ^h in finite samples (Li et al., 2019). Illustrative examples of the overlap population distribution can be found in Figure 1 of Li et al. (Li et al., 2018a) with a single covariate as well as in the bubble plot of Thomas et al. (Thomas et al., 2020a) with two covariates. In randomized trials, as discussed before, because the true propensity score is constant, the overlap weights and IPW target the same population estimand τ, but their finite-sample operating characteristics can be markedly different, as elucidated below.

The OW estimator for the ATE in randomized trials is

$$\hat{\tau}^{\text{OW}} = \hat{\mu}_1 - \hat{\mu}_0 = \frac{\sum_{i=1}^{N}(1-\hat{e}_i)Z_iY_i}{\sum_{i=1}^{N}(1-\hat{e}_i)Z_i} - \frac{\sum_{i=1}^{N}\hat{e}_i(1-Z_i)Y_i}{\sum_{i=1}^{N}\hat{e}_i(1-Z_i)}, \tag{2.7}$$

where $\hat{e}_i = e(X_i;\hat{\theta})$ is the estimated propensity score from a working logistic regression model:

$$e_i = e(X_i;\theta) = \frac{\exp(\theta_0 + X_i^T\theta_1)}{1+\exp(\theta_0 + X_i^T\theta_1)}, \tag{2.8}$$

with parameters $\theta = (\theta_0, \theta_1^T)^T$ and $\hat{\theta}$ is the maximum likelihood estimate of θ. Regarding the selection of covariates in the propensity score model, the previous literature suggests to include stratification variables as well as a small number of key prognostic factors pre-specified in the design stage (Raab et al., 2000; Williamson et al., 2014). These guidelines are also applicable to the OW estimator.

The logistic propensity score model fit underpins a unique *exact balance* property of OW. Specifically, the overlap weights estimated from model (2.8) lead to exact mean balance of any predictor included in the model (Theorem 3 in Li et al. (Li et al., 2018a)):

$$\frac{\sum_{i=1}^{N}(1-\hat{e}_i)Z_iX_{ji}}{\sum_{i=1}^{N}(1-\hat{e}_i)Z_i} - \frac{\sum_{i=1}^{N}\hat{e}_i(1-Z_i)X_{ji}}{\sum_{i=1}^{N}\hat{e}_i(1-Z_i)} = 0, \quad \text{for } j = 1, ..., p. \tag{2.9}$$

This property has important practical implications in randomized trials, namely, for any baseline covariate included in the propensity score model, the associated chance imbalance in a single randomized trial vanishes once the overlap weights are applied. If one reports the weighted mean differences in baseline covariates between arms (frequently included in the standard "Table 1" in primary trial reports), those differences are identically zero. Thus the application of OW enhances the face validity of the randomized study.

More importantly, the exact mean balance property translates into better efficiency in estimating τ. To illustrate the intuition, consider the following simple example. Suppose the true outcome surface is $Y_i = \alpha + Z_i\tau + X_i^T\beta_0 + \varepsilon_i$ with $E(\varepsilon_i|Z_i, X_i) = 0$. Denote the weighted chance imbalance in the baseline covariates by

$$\Delta_X(w_0, w_1) = \frac{\sum_{i=1}^{N} w_1(X_i)Z_iX_i}{\sum_{i=1}^{N} w_1(X_i)Z_i} - \frac{\sum_{i=1}^{N} w_0(X_i)(1-Z_i)X_i}{\sum_{i=1}^{N} w_0(X_i)(1-Z_i)},$$

and the weighted difference in random noise by

$$\Delta_\varepsilon(w_0, w_1) = \frac{\sum_{i=1}^{N} w_1(X_i)Z_i\varepsilon_i}{\sum_{i=1}^{N} w_1(X_i)Z_i} - \frac{\sum_{i=1}^{N} w_0(X_i)(1-Z_i)\varepsilon_i}{\sum_{i=1}^{N} w_0(X_i)(1-Z_i)}.$$

For the unadjusted estimator, substituting the true outcome surface in equation (2.2) gives $\hat{\tau}^{\text{UNADJ}} - \tau = \Delta_X(1,1)^T\beta_0 + \Delta_\varepsilon(1,1)$.This expression implies that the estimation error of $\hat{\tau}^{\text{UNADJ}}$ is a sum of the chance imbalance and random noise, and becomes large when imbalanced covariates are highly prognostic (i.e. large magnitude of β_0). Similarly, if we substitute the true outcome surface in (2.6), we can show that the estimation error of IPW is $\hat{\tau}^{\text{IPW}} - \tau = \Delta_X(1/(1-\hat{e}), 1/\hat{e})^T\beta_0 + \Delta_\varepsilon(1/(1-$

$\hat{e}), 1/\hat{e})$. Intuitively, IPW controls for chance imbalance because we usually have $\|\Delta_X(1/(1-\hat{e}), 1/\hat{e})\| < \|\Delta_X(1,1)\|$, which reduces the variation of the estimation error over repeated experiments. However, because $\Delta_X(1/(1-\hat{e}), 1/\hat{e})$ is not zero, the estimation error remains sensitive to the magnitude of β_0. In contrast, because of the exact mean balance property of OW, we have $\Delta_X(\hat{e}, 1-\hat{e}) = 0$; consequently, substituting the true outcome surface in (2.7), we can see that the estimation error of OW equals $\hat{\tau}^{\text{OW}} - \tau = \Delta_\varepsilon(\hat{e}, 1-\hat{e})$, which is only noise and free of β_0. This simple example illustrates that, for each realized randomization, OW should have the smallest estimation error, which translates into larger efficiency in estimating τ over repeated experiments.

For non-continuous outcomes, we also consider ratio estimands. For example, while the ATE is also known as the causal risk difference with binary outcomes, $\tau = \tau_{\text{RD}}$. Two other standard estimands are the causal risk ratio (RR) and the causal odds ratio (OR) on the log scale, defined by

$$\tau_{\text{RR}} = \log\left(\frac{\mu_1}{\mu_0}\right), \qquad \tau_{\text{OR}} = \log\left\{\frac{\mu_1/(1-\mu_1)}{\mu_0/(1-\mu_0)}\right\}. \tag{2.10}$$

The OW estimator for risk ratio and odds ratio are $\hat{\tau}_{\text{RR}} = \log\{\hat{\mu}_1/\hat{\mu}_0\}$, and $\hat{\tau}_{\text{OR}} = \log\{\hat{\mu}_1/(1-\hat{\mu}_1)\}/\{\hat{\mu}_0/(1-\hat{\mu}_0)\}$, respectively, with $\hat{\mu}_1$, $\hat{\mu}_0$ defined in (2.7).

2.3 Efficiency considerations and variance estimation

In this section we demonstrate that in randomized trials the OW estimator leads to increased large-sample efficiency in estimating the treatment effect compared to the unadjusted estimator. We further propose a consistent variance estimator for the OW estimator of both the additive and ratio estimands.

2.3.1 Continuous outcomes

Tsiatis et al. (Tsiatis et al., 2008) show that the family of regular and asymptotically linear estimators for the additive estimand τ is

$$\mathcal{I}: \frac{1}{N}\sum_{i=1}^{N}\left\{\frac{Z_i Y_i}{r} - \frac{(1-Z_i)Y_i}{1-r} - \frac{Z_i - r}{r(1-r)}\left\{r g_0(X_i) + (1-r) g_1(X_i)\right\}\right\} + o_p(N^{-1/2}), \tag{2.11}$$

where r is the randomization probability, and $g_0(X_i)$, $g_1(X_i)$ are scalar functions of the baseline covariates X_i. Several commonly used estimators for the treatment effect are members of the family $\mathcal{I}$, with different specifications of $g_0(X_i)$, $g_1(X_i)$. For example, setting $g_0(X_i) = g_1(X_i) = 0$, we obtain the unadjusted estimator $\hat{\tau}^{\text{UNADJ}}$. Setting $g_0(X_i) = g_1(X_i) = E(Y_i|X_i)$, we obtain the "ANCOVA I" estimator in Yang and Tsiatis (Yang and Tsiatis, 2001), which is the least-squares solution of the coefficient of Z_i in a linear regression of Y_i on Z_i and X_i. Further, setting $g_0(X_i) = E(Y_i|Z_i = 0, X_i)$ and $g_1(X_i) = E(Y_i|Z_i = 1, X_i)$, we obtain the "ANCOVA II" estimator (Yang and Tsiatis, 2001; Tsiatis et al., 2008; Lin, 2013), which is the least-squares solution of the coefficient of Z_i in a linear regression of Y_i on Z_i, X_i and their interaction terms. This estimator achieves the semiparametric variance lower bound within the family $\mathcal{I}$, when the conditional mean functions $g_0(X_i)$ and $g_1(X_i)$ are correctly specified in the ANCOVA model (Robins et al., 1994; Leon et al., 2003). Another member of $\mathcal{I}$ is the target maximum likelihood estimator (Moore and van der Laan, 2009; Moore et al., 2011; Colantuoni and Rosenblum, 2015), which is asymptotic efficient under correct outcome model specification. The IPW estimator $\hat{\tau}^{\text{IPW}}$ is also a member of $\mathcal{I}$. Specifically, Shen et al. (Shen et al., 2014) showed that if the logistic model (2.8) is used to estimate the propensity score $\hat{e}_i$, then the IPW estimator is asymptotically equivalent to the "ANCOVA II" estimator and becomes semiparametric efficient if the true $g_0(X_i)$ and $g_1(X_i)$ are linear functions of X_i.

In the following Proposition we show that the OW estimator is also a member of $\mathcal{I}$ and is asymptotically efficient under the linearity assumption. The proof of

Proposition 1 is provided in Section 8.1.1.

Proposition 1. *(Asymptotic efficiency of overlap weighting)*
(a) If the propensity score is estimated by a parametric model $e(X;\theta)$ with parameters θ that satisfies a set of mild regularity conditions (specified in Section 8.1.1), then $\hat{\tau}^{OW}$ belongs to the class of estimators $\mathcal{I}$.
(b) Suppose X^1 and X^2 are two nested sets of baseline covariates with $X^2 = (X^1, X^{*1})$, and $e(X^1;\theta_1)$, $e(X^2;\theta_2)$ are nested smooth parametric models. Write $\hat{\tau}_1^{OW}$ and $\hat{\tau}_2^{OW}$ as two OW estimators with the weights defined through $e(X^1;\hat{\theta}_1)$ and $e(X^2;\hat{\theta}_2)$, respectively. Then the asymptotic variance of $\hat{\tau}_2^{OW}$ is no larger than that of $\hat{\tau}_1^{OW}$.
(c) If the propensity score is estimated from the logistic regression (2.8)*, then $\hat{\tau}^{OW}$ is asymptotically equivalent to the "ANCOVA II" estimator, and becomes semiparametric efficient as long as the true $E(Y_i|X_i, Z_i = 1)$ and $E(Y_i|X_i, Z_i = 0)$ are linear in X_i.*

Proposition 1 summarizes the large-sample properties of the OW estimator in randomized trials, extending those demonstrated for IPW in Shen et al (Shen et al., 2014). In particular, adjusting for the baseline covariates using OW does not adversely affect efficiency in large samples than without adjustment. Further, the asymptotic equivalence between $\hat{\tau}^{\mathrm{OW}}$ and the "ANCOVA II" estimator indicates that OW becomes fully semiparametric efficient when the conditional outcome surface is a linear function of the covariates adjusted in the logistic propensity score model. In the special case where the randomization probability $r = 1/2$, we show in Section 8.1.3 that the limit of the large-sample variance of $\hat{\tau}^{\mathrm{OW}}$ is

$$\lim_{N\to\infty} N\mathrm{Var}(\hat{\tau}^{\mathrm{OW}}) = (1 - R^2_{\tilde{Y}\sim X}) \lim_{N\to\infty} N\mathrm{Var}(\hat{\tau}^{\mathrm{UNADJ}}) = 4(1 - R^2_{\tilde{Y}\sim X})\mathrm{Var}(\tilde{Y}_i), \quad (2.12)$$

where $\tilde{Y}_i = Z_i(Y_i - \mu_1) + (1 - Z_i)(Y_i - \mu_0)$ is the mean-centered outcome and $R^2_{\tilde{Y}\sim X}$ measures the proportion of explained variance after regressing $\tilde{Y}_i$ on X_i. Similar definition of R-squared was also used elsewhere when demonstrating efficiency gain with covariate adjustment (Moore and van der Laan, 2009; Moore et al., 2011; Wang et al.,

2019). The amount of variance reduction is also a direct result from the asymptotic equivalence between the OW, IPW, and "ANCOVA II" estimators. Equation (2.12) shows that incorporating additional covariates into the propensity score model will not reduce the asymptotic efficiency because $R^2_{\tilde{Y}\sim X}$ is non-decreasing when more covariates are considered. Although adding covariates does not hurt the asymptotic efficiency, in practice we recommend incorporating the covariates that exhibit baseline imbalance and that have large predictive power for the outcome (Williamson et al., 2014).

Perhaps more interestingly, the results in Proposition 1 apply more broadly to the family of balancing weights estimators, formalized in the following Proposition. The proof of Proposition 2 is presented in Section 8.1.1.

Proposition 2. *(Extension to balancing weights)*
Proposition 1 holds for the general family of estimators (2.5) *using balancing weights defined in* (2.4)*, as long as the tilting function $h(X)$ is a "smooth" function of the propensity score, where "smooth" is defined by satisfying a set of mild regularity conditions (specified in details in Section 8.1.1).*

2.3.2 Binary outcomes

For binary outcomes, the target estimand could be the causal risk difference, risk ratio and odds ratio, denoted as τ_{RD}, τ_{RR} and τ_{OR}, respectively. The discussions in Section 2.3.1 directly apply to the estimation of the additive estimand, τ_{RD}. When estimating the ratio estimands, one should proceed with caution in interpreting regression parameters for the ANCOVA-type generalized linear models due to the potential non-collapsibility issue. Additionally, it is well-known that the log-binomial model frequently fails to converge with a number of covariates, and therefore one may have to resort to less efficient regression methods such as the modified Poisson regression (Zou, 2004). Williamson et al. (Williamson et al., 2014) showed that IPW can be used to adjust for baseline covariates without changing the interpretation of

the marginal treatment effect estimands, τ_{RR} and τ_{OR}. Because of the asymptotic equivalence between the IPW and OW estimators (Proposition 1), OW shares the advantages of IPW in improving the asymptotic efficiency over the unadjusted estimators for risk ratio and odds ratio without compromising the interpretation of the marginal estimands. In addition, due to its ability to remove all chance imbalance associated with X_i, OW is likely to give higher efficiency than IPW in finite samples, which we will demonstrate in Section 2.4.

2.3.3 Variance estimation

To estimate the variance of the propensity score estimators, it is important to incorporate the uncertainty in estimating the propensity scores (Lunceford and Davidian, 2004a). Failing to do so leads to conservative variance estimates of the weighting estimator and therefore reduces power of the Wald test for treatment effect (Williamson et al., 2014). Below we use the M-estimation theory (Tsiatis, 2007) to derive a consistent variance estimator for OW. Specifically, we cast $\hat{\mu}_1, \hat{\mu}_0$ in equation (2.7), and $\hat{\theta}$ in the logistic model (2.8) as the solutions $\hat{\lambda} = (\hat{\mu}_1, \hat{\mu}_0, \hat{\theta}^T)^T$ to the following joint estimation equations $\sum_{i=1}^N U_i = \sum_{i=1}^N U(Y_i, X_i, Z_i; \hat{\lambda}) = 0$, where

$$\sum_{i=1}^{n} U(Y_i, X_i, Z_i, \lambda) = \sum_{i=1}^{N} \begin{bmatrix} Z_i(Y_i - \mu_1)(1 - e_i) \\ (1 - Z_i)(Y_i - \mu_0)e_i \\ \tilde{X}_i(Z_i - e_i) \end{bmatrix} = 0, \tag{2.13}$$

where $\tilde{X}_i = (1, X_i^T)^T$ is the augmented covariates with an intercept. Here, the first two rows represent the estimating functions for $\hat{\mu}_1$ and $\hat{\mu}_0$ and the last rows are the score functions of the logistic model with an intercept and main effects of X_i. If X_i is of p dimensions, equation (2.13) involves $p + 3$ scalar estimating equations for $p + 3$ parameters. Let $A = -E(\partial U_i/\partial\lambda)^T$,$B = E(U_i U_i^T)$, the asymptotic covariance matrix for $\hat{\lambda}$ can be written as $N^{-1}A^{-1}BA^{-T}$. Extracting the covariance matrix for the first two components in $\hat{\lambda}$, we can show that, as N goes to infinity,

$$\sqrt{N} \begin{bmatrix} \hat{\mu}_1 - \mu_1 \\ \hat{\mu}_0 - \mu_0 \end{bmatrix} \to \mathcal{N} \left\{ \mathbf{0}, \begin{bmatrix} \Sigma_{11}, \Sigma_{12} \\ \Sigma_{21}, \Sigma_{22} \end{bmatrix} \right\}, \tag{2.14}$$

where the covariance matrix is defined as the corresponding elements in $A^{-1}BA^{-T}$,

$$\Sigma_{11} = [A^{-1}BA^{-T}]_{1,1}, \Sigma_{22} = [A^{-1}BA^{-T}]_{2,2}, \Sigma_{12} = \Sigma_{21}^T = [A^{-1}BA^{-T}]_{1,2}. \tag{2.15}$$

where $[A^{-1}BA^{-T}]_{j,k}$ denotes the (j,k)th element of the matrix $A^{-1}BA^{-T}$. Using the delta method, we can obtain the asymptotic variance of $\hat{\tau}^{\text{OW}}_{\text{RD}}$, $\hat{\tau}^{\text{OW}}_{\text{RR}}$, $\hat{\tau}^{\text{OW}}_{\text{OR}}$ as a function of $\Sigma_{11}, \Sigma_{22}, \Sigma_{12}$. Consistent plug-in estimators can then be obtained by estimating the expectations in the "sandwich" matrix $A^{-1}BA^{-T}$ by their corresponding sample averages. We summarize the variance estimators for $\hat{\tau}^{\text{OW}}_{\text{RD}}, \hat{\tau}^{\text{OW}}_{\text{RR}}, \hat{\tau}^{\text{OW}}_{\text{OR}}$ in the following general equations,

$$\text{Var}(\hat{\tau}^{\text{OW}}) = \frac{1}{N}\left[\hat{V}^{\text{UNADJ}} - \hat{v}_1^T \left\{\frac{1}{N}\sum_{i=1}^N \hat{e}_i(1-\hat{e}_i)\tilde{X}_i^T\tilde{X}_i\right\}^{-1}(2\hat{v}_1 - \hat{v}_2)\right], \tag{2.16}$$

where

$$\hat{V}^{\text{UNADJ}} = \left\{\frac{1}{N}\sum_{i=1}^N \hat{e}_i(1-\hat{e}_i)\right\}^{-1}$$
$$\left(\frac{\hat{E}_1^2}{N_1}\sum_{i=1}^N Z_i\hat{e}_i(1-\hat{e}_i)^2(Y_i-\hat{\mu}_1)^2 + \frac{\hat{E}_0^2}{N_0}\sum_{i=1}^N (1-Z_i)\hat{e}_i^2(1-\hat{e}_i)(Y_i-\hat{\mu}_0)^2\right),$$
$$\hat{v}_1 = \left\{\frac{1}{N}\sum_{i=1}^N \hat{e}_i(1-\hat{e}_i)\right\}^{-1}$$
$$\left(\frac{\hat{E}_1}{N_1}\sum_{i=1}^N Z_i\hat{e}_i^2(1-\hat{e}_i)(Y_i-\hat{\mu}_1)^2\tilde{X}_i + \frac{\hat{E}_0}{N_0}\sum_{i=1}^N (1-Z_i)\hat{e}_i(1-\hat{e}_i)^2(Y_i-\hat{\mu}_0)^2\tilde{X}_i\right),$$
$$\hat{v}_2 = \left\{\frac{1}{N}\sum_{i=1}^N \hat{e}_i(1-\hat{e}_i)\right\}^{-1}$$
$$\left(\frac{\hat{E}_1}{N_1}\sum_{i=1}^N Z_i\hat{e}_i(1-\hat{e}_i)^2(Y_i-\hat{\mu}_1)^2\tilde{X}_i + \frac{\hat{E}_0}{N_0}\sum_{i=1}^N (1-Z_i)\hat{e}_i^2(1-\hat{e}_i)(Y_i-\hat{\mu}_0)^2\tilde{X}_i\right),$$

and $\hat{E}_k$ depends on the choice of estimands. For $\hat{\tau}^{\text{OW}}_{\text{RD}}$, we have $\hat{E}_k = 1$; for $\hat{\tau}^{\text{OW}}_{\text{RR}}$, we set $\hat{E}_k = \hat{\mu}_k^{-1}$; for $\hat{\tau}^{\text{OW}}_{\text{OR}}$, we use $\hat{E}_k = \hat{\mu}_k^{-1}(1-\hat{\mu}_k)^{-1}$ with $k = 0, 1$. Detailed derivation of the asymptotic variance and its consistent estimator can be found in Section 8.1.2.

These variance calculations are implemented in the R package **PSweight** (Zhou et al., 2020).

2.4 Simulation studies

We carry out extensive simulations to investigate the finite-sample operating characteristics of OW relative to IPW, direct regression adjustment and an augmented estimator that combined IPW and outcome regression. The main purpose of the simulation study is to empirically (i) illustrate that OW leads to marked finite-sample efficiency gain compared with IPW in estimating the treatment effect, and (ii) validate the sandwich variance estimator of OW developed in Section 2.3.3. Below we focus on the simulations with continuous outcomes. We have also conducted extensive simulations with binary outcomes, the details of which are presented in WSection 8.1.4.

2.4.1 Simulation design

We generate $p = 10$ baseline covariates from the standard normal distribution, $X_{ij} \sim \mathcal{N}(0,1)$, $j = 1, 2, \cdots, p$. Fixing the randomization probability r, the treatment indicator is randomly generated from a Bernoulli distribution, $Z_i \sim \text{Bern}(r)$. Given the baseline covariates $X_i = (X_{i1}, \ldots, X_{ip})^T$, we generate the potential outcomes from the following linear model (model 1): for $z = 0, 1$,

$$Y_i(z) \sim \mathcal{N}(z\alpha + X_i^T\beta_0 + zX_i^T\beta_1, \sigma_y^2), \quad i = 1, 2, \cdots, N \tag{2.17}$$

where α is the main effect of the treatment, and β_0, β_1 are the effects of the covariates and treatment-by-covariate interactions. The observed outcome is set to be $Y_i = Y_i(Z_i) = Z_iY_i(1) + (1 - Z_i)Y_i(0)$. In our data generating process, because the baseline covariates have mean zero, the true average treatment effect on the additive scale $\tau = \alpha$. For simplicity, we fix $\tau = 0$ and choose $\beta_0 = b_0 \times (1, 1, 2, 2, 4, 4, 8, 8, 16, 16)^T$, $\beta_1 = b_1 \times (1, 1, 1, 1, 1, 1, 1, 1, 1, 1)^T$. We specify the residual variance $\sigma_y^2 = 2$, and choose the

multiplication factor b_0 so that the signal-to-noise ratio (due to the main effects) is 1, namely, $\sum_{i=1}^{p} \beta_{0i}^2/\sigma_y^2 = 1$. This specification mimics a scenario where the baseline covariates can explain up to 50% of the variation in the outcome. We also assign different importance to each covariates. For example, the last two covariates, X_9, X_{10}, explain the majority of the variation, mimicking the scenario that one may have access to only a few strong prognostic risk factors. We additionally vary the value of $b_1 \in \{0, 0.25, 0.5, 0.75\}$ to control the strength of treatment-by-covariate interactions. A larger value of b_1 indicates a higher level of treatment effect heterogeneity so that the baseline covariates are more strongly associated with the individual-level treatment contrast, $Y_i(1) - Y_i(0)$. For brevity, we present the results with $b_1 = 0.25, 0.5$ to the Section 8.1.5 and focus here on the scenarios with homogeneous treatment effect ($b_1 = 0$) and with the strongest effect heterogeneity ($b_1 = 0.75$). For the randomization probability r, we consider two values: $r = 0.5$ represents a balanced design with one-to-one randomization, and $r = 0.7$ an unbalanced assignment where more patients are randomized to the treatment arm. We also vary the total sample sizes N from 50 to 500, with 50 and 500 mimicking a small and large sample scenario, respectively.

In each simulation scenario, we compare several different estimators for ATE, including the unadjusted estimator $\hat{\tau}^{\text{UNADJ}}$ (UNADJ), the IPW estimator $\hat{\tau}^{\text{IPW}}$, the estimator based on linear regression $\hat{\tau}^{\text{LR}}$ (LR), and the OW estimator $\hat{\tau}^{\text{OW}}$. For the IPW and OW estimators, we estimate the propensity score by logistic regression including all baseline covariates as linear terms, and the final estimator is given by the Hájek-type estimator (2.5) using the corresponding weights. For the LR estimator, we fit the correctly specified outcome model (2.17) (model 1). In addition, we also consider an augmented IPW (AIPW) estimator that augments IPW with an outcome regression (Lunceford and Davidian, 2004a), which is also a member of the class $\mathcal{I}$:

$$\hat{\tau}^{\text{AIPW}} = \hat{\mu}_1^{\text{AIPW}} - \hat{\mu}_0^{\text{AIPW}} = \frac{1}{N}\sum_{i=1}^{N}\left\{\frac{Z_i Y_i}{\hat{e}_i} - \frac{(Z_i - \hat{e}_i)\hat{\mu}_1(X_i)}{\hat{e}_i}\right\} - \left\{\frac{(1-Z_i)Y_i}{1-\hat{e}_i} + \frac{(Z_i - \hat{e}_i)\hat{\mu}_0(X_i)}{1-\hat{e}_i}\right\}, \tag{2.18}$$

where $\hat{\mu}_z(X_i) = \hat{E}[Y_i|X_i, Z_i = z]$ is the prediction from the outcome regression. In the context of observational studies, such an estimator is also known as the doubly-robust estimator. Because AIPW hybrids propensity score weighting and outcome regression, it does not retain the objectivity of the former. Nonetheless, the AIPW estimator is often perceived as an improved version of IPW (Bang and Robins, 2005); therefore, we also compare it in the simulations to understand its operating characteristics in randomized trials.

For each scenario, we simulate 2000 replicates, and calculate the bias, Monte Carlo variance and mean squared error for each estimator of τ. Across all scenarios, as expected we find that the bias of all estimators is negligible, and thus the Monte Carlo variance and the mean squared error are almost identical. For this reason, we focus on reporting the efficiency comparisons using the Monte Carlo variance. We define the *relative efficiency* of an estimator as the ratio between the Monte Carlo variance of that estimator and that of the unadjusted estimator. Relative efficiency larger than one indicates that estimator is more efficient than the unadjusted estimator. We also examine the empirical coverage rate of the associated 95% normality-based confidence intervals. Specifically, the confidence interval of $\hat{\tau}^{\text{LR}}$, $\hat{\tau}^{\text{IPW}}$, and $\hat{\tau}^{\text{OW}}$ is constructed based on the Huber-White estimator in Lin (Lin, 2013), the sandwich estimator in Williamson et al.(Williamson et al., 2014), and the sandwich estimator developed in Section 2.3.3, respectively. The confidence interval of $\hat{\tau}^{\text{AIPW}}$ is the based on the sandwich variance derived based on the M-estimation theory; the details are presented in Section 8.1.3.

To explore the performance of the estimators under model misspecification, we repeat the simulations by replacing the potential outcome generating process with

the following model (model 2)

$$Y_i(z) \sim \mathcal{N}(z\alpha + X_i^T\beta_0 + zX_i^T\beta_1 + X_{i,\text{int}}^T\gamma, \sigma_y^2), \tag{2.19}$$

where $X_{i,\text{int}} = (X_{i1}X_{i2}, X_{i2}X_{i3}, \cdots, X_{ip-1}X_{ip})$ represents $p-1$ interactions between pairs of covariates with consecutive indices and $\gamma = \sqrt{\sigma_y^2/p} \times (1, 1, \cdots, 1)^T$ represents the strength of this interaction effect. The LR estimator omitting these additional interactions is thus considered as misspecified. For IPW and OW, the propensity score model is technically correctly specified (because the true randomization probability is a constant) even though it does not adjust for the interaction term $X_{i,\text{int}}$. The AIPW estimator similarly omits $X_{i,\text{int}}$ in both the propensity score and outcome models. With a slight abuse of terminology, we refer to this scenario as "model misspecification."

2.4.2 Results on efficiency of point estimators

Figure 2.1 presents the relative efficiency of the different estimators in four typical scenarios. For a more clear presentation, we omit the results for $\hat{\tau}^{\text{AIPW}}$ as they become indistinguishable from the results for $\hat{\tau}^{\text{LR}}$ in these scenarios. Below, we discuss in order the relative efficiency results when the outcomes are generated under model 1 (panel (a) to (c)) and model 2 (panel (d)).

Panel (a) to (c) correspond to scenarios when the outcomes are simulated from model 1. When $r = 0.5$ and there is no treatment effect heterogeneity (panel (a)), it is evident that $\hat{\tau}^{\text{IPW}}$, $\hat{\tau}^{\text{LR}}$, and $\hat{\tau}^{\text{OW}}$ are consistently more efficient than the unadjusted estimator, and the relative efficiency increases with a larger sample size. However, when the sample size is no larger than 100, OW leads to higher efficiency compared to LR and IPW, with IPW being the least efficient among the adjusted estimators. With a strong treatment effect heterogeneity $b_1 = 0.75$ (panel (b)), $\hat{\tau}^{\text{LR}}$ becomes slightly more efficient than $\hat{\tau}^{\text{OW}}$; this is expected as the true outcome model is used and the design is balanced. The efficiency advantage decreases for $\hat{\tau}^{\text{LR}}$ and as b_1 moves closer

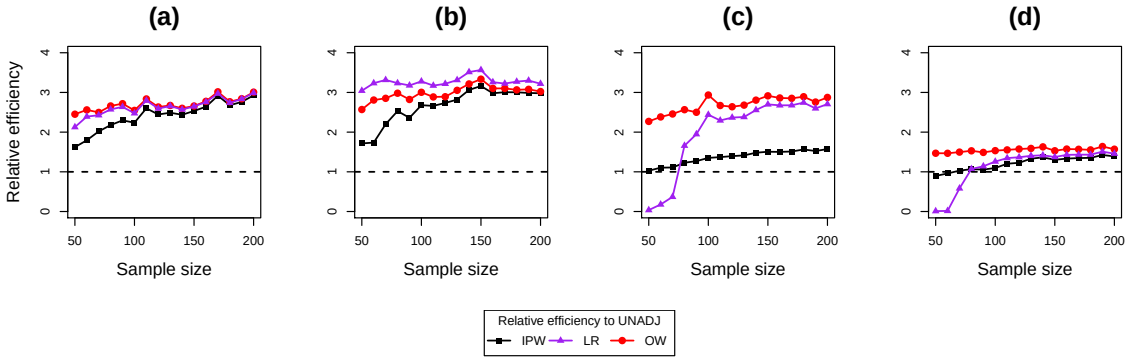

Figure 2.1: The relative efficiency of $\hat{\tau}^{\text{IPW}}$, $\hat{\tau}^{\text{AIPW}}$, $\hat{\tau}^{\text{LR}}$ and $\hat{\tau}^{\text{OW}}$ relative to $\hat{\tau}^{\text{UNADJ}}$ for estimating ATE when (a) $r = 0.5$, $b_1 = 0$ and the outcome model is correctly specified, (b) $r = 0.5, b_1 = 0.75$ and the outcome model is correctly specified, (c) $r = 0.7, b_1 = 0$ and the outcome model is correctly specified, (d) $r = 0.7, b_1 = 0$ and the outcome model is misspecified. A larger value of relative efficiency corresponds to a more efficient estimator.

to zero (see Table 8.1). On the other hand, $\hat{\tau}^{\text{OW}}$ becomes more efficient than $\hat{\tau}^{\text{LR}}$ when the randomization probability deviates from 0.5. For instance, in panel (c), with $r = 0.7$ and $N = 50$, $\hat{\tau}^{\text{LR}}$ becomes even less efficient than the unadjusted estimator, while OW demonstrates substantial efficiency gain over the unadjusted estimator. The deteriorating performance of $\hat{\tau}^{\text{LR}}$ under $r = 0.7$ also supports the findings in Freedman (Freedman, 2008). These results show that the relative performance between LR and OW is affected by the degree of treatment effect heterogeneity and the randomization probability. In the scenarios with a small degree of effect heterogeneity and/or with unbalanced design, OW tends to be more efficient than LR.

Overall, OW is generally comparable to LR with a correctly specified outcome model, both outperforming IPW. But OW becomes more efficient than LR when the outcome model is incorrectly specified. Namely, when the outcomes are generated from model 2, $\hat{\tau}^{\text{OW}}$ becomes the most efficient even if the propensity model omits important interaction terms in the true outcome model, as in panel (d) of Figure 2.1. The fact that LR and AIPW have almost identical finite-sample efficiency further confirms that the regression component dominates the AIPW estimator in random-

ized trials. Throughout, $\hat{\tau}^{\text{OW}}$ is consistently more efficient than $\hat{\tau}^{\text{IPW}}$, regardless of sample size, randomization probability and the degree of treatment effect heterogeneity. When the sample size increases to $N = 500$, the differences between methods become smaller as a result of Proposition 1. Additional results on relative efficiency are also provided in Table 2.1 and Table 8.1.

2.4.3 Results on variance and interval estimators

Table 2.1 summarizes the accuracy of the estimated variance and the empirical coverage rate of each interval estimator in four scenarios that match Figure 2.1. The former is measured by the ratio between the average estimated variance and the Monte Carlo variance of each estimator, and a ratio close to 1 indicates adequate performance. In general, we find that estimated variance is close to the truth for both IPW and OW, but less so for the LR and AIPW estimator, especially with small sample sizes such as $N = 50$ or 100. Specifically, when the outcomes are generated from model 1, the sandwich variances of IPW and OW estimators usually adequately quantify the uncertainty, even when the sample size is as small as $N = 50$. In the same settings, the Huber-White variance estimator for LR sometimes *substantially underestimates* the true variance, leading to under-coverage of the interval estimator. Also, in the case where LR has a slight efficiency advantage ($b_1 = 0.75$), the coverage of LR is only around 70% even when the true linear regression model is estimated. This result shows that the Huber-White sandwich variance, although known to be robust to heteroscedasticity in large samples, could be severely biased towards zero in finite samples when there is treatment effect heterogeneity. Further, the sandwich variance of AIPW also frequently underestimates the true variance when $N = 50$ and 100. On the other hand, when the outcomes are generated from model 2 and the randomization probability is $r = 0.7$, all variance estimators tend to underestimate the truth, and the coverage rate slightly deteriorates. However, the coverage of the IPW and OW estimators is still closer to nominal than LR and AIPW when $N = 50$ and 100.

Table 2.1: The relative efficiency of each estimator compared to the unadjusted estimator, the ratio between the average estimated variance over Monte Carlo variance ({Est Var}/{MC Var}), and 95% coverage rate of IPW, LR, AIPW and OW estimators. The results are based on 2000 simulations with a continuous outcome. In the "correct specification" scenario, data are generated from model 1; in the "misspecification" scenario, data are generated from model 2. For each estimator, the same analysis approach is used throughout, regardless of the data generating model.

Sample size	Relative efficiency				{Est Var}/{MC Var}				95% Coverage			
N	IPW	LR	AIPW	OW	IPW	LR	AIPW	OW	IPW	LR	AIPW	OW
$r = 0.5$, $b_1 = 0$, correct specification												
50	1.621	2.126	2.042	2.451	1.001	0.866	0.668	1.343	0.936	0.933	0.885	0.967
100	2.238	2.475	2.399	2.548	0.898	0.961	0.799	1.116	0.938	0.944	0.914	0.955
200	2.927	2.987	2.984	3.007	0.951	0.996	0.927	1.051	0.946	0.949	0.938	0.956
500	2.985	3.004	2.995	3.006	0.963	0.987	0.959	1.000	0.944	0.949	0.942	0.952
$r = 0.5$, $b_1 = 0.75$, correct specification												
50	1.715	3.043	2.972	2.570	0.991	0.286	0.816	1.383	0.935	0.712	0.918	0.967
100	2.679	3.279	3.253	3.003	0.931	0.280	0.917	1.168	0.942	0.710	0.934	0.966
200	2.979	3.220	3.215	3.023	0.967	0.278	0.995	1.075	0.951	0.697	0.949	0.964
500	3.337	3.425	3.426	3.338	0.995	0.273	1.013	1.037	0.943	0.696	0.945	0.954
$r = 0.7$, $b_1 = 0$, correct specification												
50	1.056	0.036	0.036	2.270	1.060	0.014	0.026	1.184	0.938	0.779	0.816	0.931
100	1.825	2.439	2.311	2.935	0.914	0.858	0.717	1.039	0.946	0.921	0.897	0.923
200	2.474	2.706	2.679	2.874	0.971	0.931	0.857	0.963	0.948	0.944	0.927	0.935
500	2.641	2.743	2.738	2.809	0.922	0.912	0.887	0.925	0.940	0.936	0.934	0.938
$r = 0.7$, $b_1 = 0$, misspecification												
50	0.896	0.009	0.009	1.468	0.843	0.005	0.009	0.857	0.904	0.777	0.808	0.906
100	1.096	1.258	1.152	1.533	0.724	0.754	0.637	0.837	0.911	0.903	0.878	0.917
200	1.390	1.457	1.398	1.570	0.861	0.894	0.816	0.898	0.929	0.938	0.920	0.933
500	1.591	1.632	1.612	1.648	0.980	1.003	0.976	0.981	0.948	0.949	0.948	0.949

2.4.4 Simulation studies with binary outcomes

We also perform a set of simulations with binary outcomes, generating from a logistic outcome model. Three estimands, $\tau_{\text{RD}}, \tau_{\text{RR}}$ and τ_{OR}, are considered in scenarios with different degree of treatment effect heterogeneity, prevalence of the outcome $\Pr(Y_i = 1)$, and randomization probability r. In these scenarios, we find that covariate adjustment improves efficiency of the unadjusted estimator most likely when the sample size is at least 100, except under large treatment effect heterogeneity where there is efficiency gain even with $N = 50$. Throughout, the OW estimator is uniformly more efficient than IPW and should be the preferred propensity score weighting estimator in randomized trials. Finally, although the correctly-specified outcome regression is slightly more efficient than OW in the ideal case with a non-rare outcome, in small samples regression adjustment is generally unstable when the prevalence of outcome also decreases. Similarly, the efficiency of AIPW is mainly driven by the outcome regression component, and the instability of the outcome model may also lead to an inefficient AIPW estimator in finite-samples. For brevity, we present full details of the simulation design in Section 8.1.4, and summarize all numerical results in Table 8.2 and 8.3.

2.5 Application to the Best Apnea Interventions for Research Trial

The Best Apnea Interventions for Research (BestAIR) trial is an individually randomized, parallel-group trial designed to evaluate the effect of continuous positive airway pressure (CPAP) treatment on the health outcomes of patients with high cardiovascular disease risk and obstructive sleep apnea but without severe sleepiness (Bakker et al., 2016). Patients were recruited from outpaient clinics at three medical centers in Boston, Massachusetts, and were randomized in a 1:1:1:1 ratio to receive conservative medical therapy (CMT), CMT plus sham CPAP (sham CPAP is a modified device that closely mimics the active CPAP and serves as the placebo for CPAP RCTs(Reid et al., 2019)), CMT plus CPAP, or CMT plus CPAP plus motivational

enhancement (ME). We follow the study protocol and pool two sub-arms into the combined control group (CMT, CMT plus sham CPAP) and the rest sub-arms into the combined CPAP or active intervention group. This results in 169 participants with 83 patients in the active CPAP group and 86 patients in the combined control arm. A set of patient-level covariates were measured at baseline and outcomes were measured at baseline, 6, and 12 months.

For illustration, we consider estimating the treatment effect of CPAP on two outcomes measured at 6 month. The objective outcome is the 24-hour systolic blood pressure (SBP), measured every 20 minutes during the daytime and every 30 minutes during the sleep. The subjective outcome includes the self-reported sleepiness in daytime, measured by Epworth Sleepiness Scale (ESS) (Zhao et al., 2017). We additionally consider dichotomizing SBP (high SBP if $\geq$130mmHg) to create a binary outcome, resistant hypertension. For covariate-adjusted analysis, we consider a total of 9 baseline covariates, including demographics (e.g. age, gender, ethnicity), body mass index, Apnea-Hypopnea Index (AHI), average seated radial pulse rate (SDP), site and baseline outcome measures (e.g. baseline blood pressure and ESS).

In Table 2.2, we provide the summary statistics for the covariates and compare between the treated and control groups at baseline. We measure the baseline imbalance of the covariates by the absolute standardized difference (ASD), which for the jth covariate is defined as, $\text{ASD}^{w} = |\sum_{i=1}^{N} w_i X_{ij} Z_i / \sum_{i=1}^{N} w_i Z_i - \sum_{i=1}^{N} w_i X_{ij}(1 - Z_i) / \sum_{i=1}^{N} w_i (1 - Z_i)| / S_j$, where w_i represents the weight for each patient and S_j^2 stands for the average variance, $S_j^2 = \{\text{Var}(X_{ij}|Z_i = 1) + \text{Var}(X_{ij}|Z_i = 0)\}/2$. The baseline imbalance is measured by $\text{ASD}^{\text{UNADJ}}$ with $w_i = 1$. Although the treatment is randomized, we still notice a considerable difference for some covariates between the treated and control group, such as BMI, baseline SBP and AHI. The $\text{ASD}^{\text{UNADJ}}$ for all three variables exceed 10%, which has been considered as a common threshold for balance (Austin and Stuart, 2015). In particular, the baseline SBP exhibits the largest imbalance ($\text{ASD}^{\text{UNADJ}} = 0.477$), and is expected to be highly correlated with

SBP measured at 6 months, the main outcome of interest. As we shall see later, failing to adjust for such a covariate leads to spurious conclusions of the treatment effect. Using the propensity scores estimated from a main-effects logistic model, IPW reduces the baseline imbalance as $\text{ASD}^{\text{IPW}} < 10\%$. As expected from the exact balance property (equation (2.9)), OW completely remove baseline imbalance such that $\text{ASD}^{\text{OW}} = 0$ for all covariates. In this regard, even before observing the 6-month outcome, applying OW mitigates the severe imbalance on prognostic baseline factors, and thus increases the face validity of the trial.

Table 2.2: Baseline characteristics of the BestAIR randomized trial by treatment groups, and absolute standardized difference (ASD) between the treatment and control groups before and after weighting. The ASD^{OW} is exactly zero due to the exact balance property of OW.

	All patients $N = 169$	CPAP group $N_1 = 83$	Control group $N_0 = 86$	$\text{ASD}^{\text{UNADJ}}$	ASD^{IPW}	ASD^{OW}
Baseline categorical covariates and number of units in each group.						
Gender (male)	107	54	53	0.046	0.002	0.000
Race & ethnicity						
White	152	75	77	0.051	0.015	0.000
Black	11	5	6	0.060	0.007	0.000
Other	5	2	3	0.086	0.034	0.000
Recruiting center						
Site 1	54	26	28	0.046	0.002	0.000
Site 2	10	5	5	0.065	0.024	0.000
Site 3	105	52	53	0.073	0.013	0.000
Baseline continuous covarites, mean and standard deviation (in parenthesis).						
Age (years)	64.4 (7.4)	64.4 (8.0)	64.3 (6.8)	0.020	0.017	0.000
BMI (kg/m^2)	31.7 (6.0)	31.0 (5.3)	32.4 (6.5)	0.261	0.042	0.000
Baseline SBP (mmHg)	124.3 (13.2)	121.6 (11.1)	127.0 (14.6)	0.477	0.020	0.000
Baseline SDP (beats/minute)	63.1 (10.7)	63.0 (10.4)	63.2 (10.9)	0.020	0.016	0.000
Baseline AHI (events/hr)	28.8 (15.4)	26.5 (13.0)	31.1 (17.2)	0.348	0.039	0.000
Baseline ESS	8.3 (4.5)	8.0 (4.5)	8.5 (4.6)	0.092	0.010	0.000

For the continuous outcomes (SBP and ESS), we estimate the ATE using $\hat{\tau}^{\text{UNADJ}}$, $\hat{\tau}^{\text{IPW}}$, $\hat{\tau}^{\text{AIPW}}$, $\hat{\tau}^{\text{LR}}$ and $\hat{\tau}^{\text{OW}}$. For IPW and OW, we estimate the propensity scores using a logistic regression with main effects of 9 baseline covariates mentioned above. For $\hat{\tau}^{\text{LR}}$, we fit the ANCOVA model with main effects of treatment and covariates as well as their interactions. For the binary SBP, we use these five approaches to estimate the causal risk difference, log risk ratio and log odds ratio due to the CPAP

treatment. For $\hat{\tau}^{\mathrm{LR}}$ with a binary outcome, we fit a logistic regression model for the outcome including both main effects of the treatment and covariates, as well as their interactions, and then obtain the marginal mean of each group via standardization. For each outcome, the corresponding propensity score and outcome model specifications are used to obtain the AIPW estimator. The variances and 95% CIs of the estimators are calculated in the same way as in the simulations. We present p-values for the associated hypothesis tests of no treatment effect and occasionally interpret statistical significance at the 0.05 level for illustrative purposes. We do acknowledge, however, that the interpretation of study results should not rely on a single dichotomy of a p-value that is great than or smaller than 0.05.

Table 2.3 presents the treatment effect estimates, standard errors (SEs), 95% confidence intervals (CI) and p-values for these five approaches across three outcomes. For the SBP continuous outcome, the treatment effect estimated by IPW, LR, AIPW and OW are substantially smaller than the unadjusted estimate. Specially, the ATE changes from approximately -5.0 to -2.7 after covariate adjustment. This difference is due to the fact that the control group has a higher average SBP at baseline and failing to adjust for this discrepancy leads to a biased estimate of the treatment effect of CPAP. In fact, one would falsely conclude a statistically significant treatment effect at the 0.05 level if the baseline imbalance is ignored. The treatment effect becomes no longer statistically significant at the 0.05 level using either one of the adjusted estimator. In terms of efficiency, IPW, LR, AIPW and OW provide a smaller SE compared with the unadjusted estimate and the difference among the adjusted estimators is negligible. For the ESS outcome, the treatment effect estimate changes from approximately -1.5 to -1.25 after covariate adjustment while the difference among IPW, LR, AIPW and OW remains small. Despite the change in the point estimates, the 95% confidence intervals for all five estimators exclude the null.

For the binary SBP outcome, the unadjusted method gives an estimate of -0.224 on risk difference scale, -0.698 on log risk ratio scale and -1.038 on log odds ratio

Table 2.3: Treatment effect estimates of CPAP intervention on blood pressure, day time sleepiness and resistant hypertension using data from the BestAIR study. The five approaches considered are: (a) UNADJ: the unadjusted estimator; (b) IPW: inverse probability weighting; (c) LR: linear regression (for continous outcomes, or ANCOVA) and logistic regression (for binary outcomes) for outcome; (d) AIPW: augmented IPW; (e) OW: overlap weighting.

Method	Estimate	Standard error	95% Confidence interval	p-value
Continuous outcomes				
Systolic blood pressure (continuous)				
UNADJ	-5.070	2.345	$(-9.667, -0.473)$	0.031
IPW	-2.638	1.634	$(-5.841, \ 0.566)$	0.107
LR	-2.790	1.724	$(-6.169, \ 0.588)$	0.106
AIPW	-2.839	1.642	$(-6.058, \ 0.380)$	0.084
OW	-2.777	1.689	$(-6.088, \ 0.534)$	0.100
Epworth Sleepiness Scale (continuous)				
UNADJ	-1.503	0.702	$(-2.878, -0.128)$	0.032
IPW	-1.232	0.486	$(-2.184, -0.279)$	0.011
LR	-1.260	0.519	$(-2.276, -0.243)$	0.015
AIPW	-1.255	0.479	$(-2.193, -0.317)$	0.009
OW	-1.251	0.491	$(-2.214, -0.288)$	0.011
Binary outcomes				
Resistant hypertension (SBP$\geq$130): risk difference				
UNADJ	-0.224	0.085	$(-0.391, -0.057)$	0.009
IPW	-0.145	0.082	$(-0.306, \ 0.015)$	0.077
LR	-0.131	0.074	$(-0.277, \ 0.014)$	0.076
AIPW	-0.133	0.071	$(-0.272, \ 0.006)$	0.061
OW	-0.149	0.083	$(-0.312, \ 0.013)$	0.071
Resistant hypertension (SBP$\geq$130): log risk ratio				
UNADJ	-0.698	0.281	$(-1.248, -0.147)$	0.013
IPW	-0.448	0.226	$(-0.892, -0.004)$	0.048
LR	-0.401	0.236	$(-0.864, \ 0.062)$	0.090
AIPW	-0.408	0.227	$(-0.854, \ 0.037)$	0.072
OW	-0.454	0.263	$(-0.970, \ 0.062)$	0.084
Resistant hypertension (SBP$\geq$130): log odds ratio				
UNADJ	-1.038	0.409	$(-1.838, -0.237)$	0.011
IPW	-0.665	0.324	$(-1.300, -0.030)$	0.040
LR	-0.598	0.346	$(-1.276, \ 0.080)$	0.084
AIPW	-0.607	0.331	$(-1.256, \ 0.041)$	0.067
OW	-0.680	0.387	$(-1.438, \ 0.079)$	0.079

scale. Due to baseline imbalance, the unadjusted confidence intervals for all three estimands exclude null. Similar to the analysis of the continuous SBP outcome, all four adjusted approaches move the point estimates closer to the null. This pattern further demonstrates that ignoring baseline imbalance may produce biased estimates. In terms of variance reduction, all four adjusted methods exhibit a decrease in the estimated standard error compared with the unadjusted one. Interestingly, although the 95% confidence intervals for LR, AIPW and OW all include zero, the confidence intervals for IPW excludes zero for the two ratio estimands (but not for the additive estimand). This result, however, needs to be interpreted with caution. As noticed in the simulation studies (panel (b), (c) and (d) in Figure 8.1), variance estimators of IPW and AIPW tend to underestimate the actual uncertainty when the sample size is modest and the outcome is not common. In our application, the resistant hypertension has a prevalence of around 12%, which is close to the most extreme scenario in our simulation. Because IPW likely underestimates the variability for ratio estimands, there could be a risk of inflated type I error. In contrast, the interval estimator of OW appears more robust in small samples.

2.6 Discussion

Through extensive simulation studies, we find the OW estimator is consistently more efficient than the IPW estimator in finite samples, particularly when the sample size is small (e.g. smaller than 150). This is largely due to the exact balance property that is unique to OW, which removes all chance imbalance in the baseline covariates adjusted for in a logistic propensity model. Our simulations also shed light on the performance of the regression adjustment method. With a continuous outcome, linear regression adjustment have similar efficiency to the OW and IPW estimators when the sample size is more than 150. With a limited sample size, say $N \leq 150$, the linear regression estimator is occasionally slightly more efficient than OW when correctly specified, while the OW estimator is more efficient when the linear model is

incorrectly specified. We find that when the sample size is smaller than 100, linear regression adjustment could even be less efficient than the unadjusted estimators when (i) the randomization probability deviates from 0.5, and/or (ii) the outcome model is incorrectly specified. In contrast, the OW estimator consistently leads to finite-sample efficiency gain over the unadjusted estimator in these scenarios. Although we generally believe the sample size is a major determining factor for efficiency comparison, our cutoff of N at 100 or 150 is specific to our simulation setting, and may not be generalizable to other scenarios we haven't considered. The findings for binary outcomes are slightly different from those for the continuous outcomes, especially in small samples (Section 8.1.4). In particular, OW generally performs similarly to the logistic regression estimator, and both approaches may lead to efficiency loss over the unadjusted estimator when the sample size is limited, e.g., $N < 100$. However, the efficiency loss generally does not exceed 10%. Throughout, the IPW estimator is the least efficient and could lead to over 20% efficiency loss compared to the unadjusted estimator in small samples. The findings for estimating the risk ratio and odds ratio are mostly concordant with those for estimating the risk difference. Of note, when the binary outcome is rare, regression adjustment frequently run into convergence issues and fails to provide an adjusted treatment effect, while the propensity score weighting estimators are not subject to such problems. Finally, because previous simulations (Moore and van der Laan, 2009; Moore et al., 2011; Colantuoni and Rosenblum, 2015) with binary outcomes have focused on trials with at least a sample size of $N = 200$, our simulations complement those previous reports by providing recommendations when the sample size falls below 200.

We also empirically evaluated the finite-sample performance of the AIPW estimator in randomized trials. The AIPW estimator is popular in observational studies due to its double robustness and local efficiency properties. In randomized trials, because the propensity score model is never misspecified, the finite-sample performance of AIPW is largely driven by the outcome model. In particular, we find that AIPW can

be less efficient than the unadjusted estimator under outcome model misspecification (Table 2.1). The sensitivity of AIPW to the outcome model specification was noted previously (Li et al., 2013; Li and Li, 2019a). AIPW could be slightly more efficient than OW with a correct outcome model and under substantial treatment effect heterogeneity, but it does not retain the objectivity of the simple weighting estimator and is subject to excessive variance when the outcome model is incorrect or fails to converge.

We further provide a consistent variance estimator for OW when estimating both additive and ratio estimands. Our simulation results confirm that the resulting OW interval estimator achieved close to nominal coverage for the additive estimand (ATE), except in a few challenging scenarios where the sample size is extremely small, e.g. $N = 50$. For example, with a continuous outcome, the empirical coverage of the OW interval estimator and the IPW interval estimator (Williamson et al., 2014) are both around 90% when the randomization is unbalanced and the propensity score model does not account for important covariate interaction terms. In this case, the Huber-White variance for linear regression has the worst performance and barely achieved 80% coverage. This is in sharp contrast to the findings of Raad et al.(Raad et al., 2020), who have demonstrated superior coverage of the linear regression interval estimator over the IPW interval estimator. However, Raad et al. (Raad et al., 2020) only considered the model-based variance (i.e. based on the information matrix) when the outcome regression is correctly specified. Assuming a correct model specification, it is expected that the model-based variance has more stable performance than the Huber-White variance in small samples, while the former may become biased under incorrect model specification when the randomization probability deviates from 0.5 (Wang et al., 2019). For robustness and practical considerations, we therefore focused on studying the operating characteristics of the commonly recommended Huber-White variance(Lin, 2013). On the other hand, the OW interval estimator maintains at worst over-coverage for estimating the risk ratios and odds ra-

tios when $N = 50$, while the IPW interval estimator exhibits under-coverage. When the outcome is rare, the logistic regression and AIPW interval estimators show severe under-coverage possibly due to constant non-convergence. Collectively, these results indicate the potential type I error inflation by using IPW, logistic regression and AIPW, and could favor the application of OW for covariate adjustment in trials with a limited sample size.

3

Propensity score weighting for survival outcome

3.1 Introduction

Survival or time-to-event outcomes are common in comparative effectiveness research and require unique handling because they are usually incompletely observed due to right-censoring. In observational studies, a popular approach to draw causal inference with survival outcomes is to combine standard survival estimators with propensity score methods (Rosenbaum and Rubin, 1983). For example, one can construct the Kaplan-Meier estimator on an inverse probability weighted sample to adjust for measured confounding (Robins and Finkelstein, 2000; Hubbard et al., 2000; Xie and Liu, 2005). Another common approach combines the Cox model with inverse probability weighting (IPW) to estimate the causal hazard ratio (Austin, 2014; Austin and Stuart, 2017) or the counterfactual survival curves (Cole and Hernán, 2004); this approach was also extended to accommodate time-varying treatments via the marginal structural models (Robins et al., 2000b). Coupling causal inference with the Cox model introduces two limitations. First, the Cox model assumes proportional hazards in the target population, violation to which would lead to biased causal estimates. Second, the target estimand is usually the causal hazard ratio, whose interpretation can be opaque due to the built-in selection bias (Hernán, 2010). In contrast, other estimands based on survival probability or restricted mean survival time are free of model assumptions and have natural causal interpretation (Mao et al., 2018).

To analyze observational studies with survival outcomes, an attractive alternative approach is to combine causal inference methods with the *pseudo-observations* (Andersen et al., 2003). Each pseudo-observation is constructed based on a jackknife

statistic and is interpreted as the individual contribution to the target estimate from a complete sample without censoring. The pseudo-observations approach addresses censoring in a "once for all" manner and allows standard methods to proceed as if the outcomes are completely observed (Andersen et al., 2004; Klein and Andersen, 2005; Klein et al., 2007). To this end, one can perform direct confounding adjustment using outcome regression with the pseudo-observations and derive casual estimators with the g-formula (Robins, 1986). Another approach is to combine propensity score weighting with the pseudo-observations. For example, Andersen et al. (2017) considered an IPW estimator to estimate the causal risk difference and difference in restricted mean survival time. Their approach was further extended to enable doubly robust estimation with survival and recurrent event outcomes (Wang, 2018; Su et al., 2020).

Despite its simplicity and versatility, several open questions in propensity score weighting with pseudo-observations remain to be addressed. First, pseudo-observations require computing a jackknife statistic for each unit, which poses computational challenges to resampling-based variance estimation under propensity score weighting (Andersen et al., 2017). On the other hand, failure to account for the uncertainty in estimating the propensity scores and jackknifing can lead to inaccurate and often conservative variance estimates. Second, the IPW estimator with pseudo-observations corresponds to a target population that is represented by the study sample, but the interpretation of such a population is often questionable in the case of a convenience sample (Li et al., 2019). Moreover, the inverse probability weights are prone to lack of covariate overlap and will engender causal estimates with excessive variance, even when combined with outcome regression (Mao et al., 2019). Li et al. (2018a) proposed a general class of balancing weights (which includes the IPW as a special case) to allow user-specified target estimands according to different target populations. In particular, the overlap weights emphasize a target population with the most covariate overlap and best clinical equipoise, and were theoretically shown to provide

the most efficient causal contrasts. However, the theory of overlap weights so far has focused on non-censored outcomes, and its optimality with survival outcomes is currently unclear. Third, contemporary healthcare registries such as the National Cancer Database (Ennis et al., 2018) necessitates comparative effectiveness evidence among multiple treatments, which can exacerbate the consequence of lack of overlap when only IPW is considered (Yang et al., 2016). While the overlap weights (Li and Li, 2019b) offered a promising solution to improve the bias and efficiency over IPW with non-censored outcomes, extensions to censored survival outcomes remain unexplored.

In this paper, we address all three open questions. We consider a general multiple treatment setup and extend the balancing weights in Li et al. (2018a) and Li and Li (2019b) to analyze survival outcomes in observational studies based on pseudo-observations. We develop new asymptotic variance expressions for causal effect estimators that properly account for the variability associated with estimating propensity scores as well as constructing pseudo-observations. Different from existing variance expressions developed for propensity score weighting estimators (Lunceford and Davidian, 2004a; Mao et al., 2018), our asymptotic variances are established additionally based on functional delta-method and the von Mises expansion of the pseudo-observations (Graw et al., 2009; Jacobsen and Martinussen, 2016; Overgaard et al., 2017), and enables computationally efficient inference without re-sampling. Under mild conditions, we prove that the overlap weights lead to the most efficient survival causal estimators, expanding the theoretical underpinnings of overlap weights to causal survival analysis. We carry out simulations to evaluate and compare a range of commonly used weighting estimators. Finally, we apply the proposed method to estimate the causal effects of three treatment options on mortality among patients with high-risk localized prostate cancer from the National Cancer Database.

3.2 Propensity score weighting with survival outcomes

3.2.1 Time-to-event outcomes, causal estimands and assumptions

We consider a sample of N units drawn from a population. Let $Z_i \in \mathcal{J} = \{1, 2, \cdots, J\}$, $J \geq 2$ denote the assigned treatment. Each unit has a set of potential outcomes $\{T_i(j), j \in \mathcal{J}\}$, measuring the counterfactual survival time mapped to each treatment. We similarly define $\{C_i(j), j \in \mathcal{J}\}$ as a set of potential censoring times. Under the Stable Unit Treatment Value Assumption, we have $T_i = \sum_{j \in \mathcal{J}} \mathbf{1}\{Z_i = j\} T_i(j)$ and $C_i = \sum_{j \in \mathcal{J}} \mathbf{1}\{Z_i = j\} C_i(j)$. Due to right-censoring, we might only observe the lower bound of the survival time for some units. We write the observed failure time, $\widetilde{T}_i = T_i \wedge C_i$, the censoring indicator, $\Delta_i = \mathbf{1}\{T_i \leq C_i\}$, and the p-dimensional time-invariant pre-treatment covariates, $\mathbf{X}_i = (X_{i1}, \ldots, X_{ip})' \in \mathcal{X}$. In summary, we observe the tuple $\mathcal{O}_i = (Z_i, \mathbf{X}_i, \widetilde{T}_i, \Delta_i)$ for each unit. With J treatments, we define the generalized propensity score, $e_j(\mathbf{X}_i) = \Pr(Z_i = j | \mathbf{X}_i)$, as the probability of receiving treatment j given baseline covariates (Imbens, 2000). Our results are presented for general, finite J, and include binary treatments as a special case when $J = 2$.

The causal estimands of interest are based on two typical transformations of the potential survival times: (i) the at-risk function, $\nu_1(T_i(j); t) = \mathbf{1}\{T_i(j) \geq t\}$, and (ii) the truncation function, $\nu_2(T_i(j); t) = T_i(j) \wedge t$, where t is a given time point of interest. The identity function is implied by $\nu_2(T_i(j); \infty) = T_i(j)$. To simplify the discussion, hereafter we use $k \in \{1, 2\}$ to index the choice of the transformation function v. We further define $m_j^k(\mathbf{X}; t) = \mathbb{E}\{\nu_k(T_i(j); t) | \mathbf{X}\}$ as the conditional expectation of the transformed potential survival outcome, and the pairwise conditional causal effect at time t as $\tau_{j,j'}^k(\mathbf{X}; t) = m_j^k(\mathbf{X}; t) - m_{j'}^k(\mathbf{X}; t)$ for $j \neq j' \in \mathcal{J}$). Our scientific interest lies in the pairwise conditional causal effect averaged over a *target population*. Following the formulation in Li and Li (2019b), we assume the study sample is drawn from the population with covariate density $f(\mathbf{X})$, and represent the target population by density $g(\mathbf{X})$. The ratio $h(\mathbf{X}) = g(\mathbf{X})/f(\mathbf{X})$ is called a tilting

function, which re-weights the observed sample to represent the target population. The *pairwise average causal effect* at time t in the target population is defined as

$$\tau_{j,j'}^{k,h}(t) = \frac{\int_{\mathcal{X}} \tau_{j,j'}^{k}(\mathbf{X};t) f(\mathbf{X}) h(\mathbf{X}) \mu(d\mathbf{X})}{\int_{\mathcal{X}} f(\mathbf{X}) h(\mathbf{X}) \mu(d\mathbf{X})}, \quad \forall \;\; j \neq j' \in \mathcal{J}. \tag{3.1}$$

The class of estimands (3.1) is transitive in the sense that $\tau_{j,j'}^{k,h}(t) = \tau_{j,j''}^{k,h}(t) + \tau_{j'',j'}^{k,h}(t)$. Different choices of function v_k lead to estimands on different scales. When $k = 1$, we refer to estimand (3.1) as the survival probability causal effect (SPCE). This estimand represents the causal risk difference and contrasts the potential survival probabilities at time t among the target population. When $k = 2$, estimand (3.1) is referred to as the restricted average causal effect (RACE), which compares the mean potential survival times restricted by t. When $t = \infty$, this estimand becomes the average survival causal effect (ASCE) comparing the unrestricted mean potential survival times. Of note, when $J = 2$, our pairwise estimands reduce to those introduced in Mao et al. (2018) for binary treatments.

To identify (3.1), we maintain the following assumptions. For each $j \in \mathcal{J}$, we assume (A1) weak unconfoundedness: $T_i(j) \perp\!\!\!\perp \mathbf{1}\{Z_i = j\}|\mathbf{X}_i$; (A2) overlap: $0 < e_j(\mathbf{X}) < 1$ for any $\mathbf{X} \in \mathcal{X}$; and (A3) completely independent censoring: $\{T_i(j), Z_i, \mathbf{X}_i\} \perp\!\!\!\perp C_i(j)$. Assumption (A1) and (A2) are the usual no unmeasured confounding and positivity conditions suitable for multiple treatments (Imbens, 2000), and allow us to identify $\tau_j^{k,h}(t)$ in the absence of censoring. Assumption (A3) assumes that censoring is independent of all remaining variables, and is introduced for now as a convenient technical device to establish our main results. We will relax this assumption in Section 3.3 and 3.4 to enable identification under a weaker condition, which assumes (A4) covariate-dependent censoring: $T_i(j) \perp\!\!\!\perp C_i(j)|\mathbf{X}_i, Z_i$.

3.2.2 Balancing weights with pseudo-observations

We now introduce balancing weights to estimate the causal estimands (3.1). Write $f_j(\mathbf{X}) = f(\mathbf{X}|Z = j)$ as the conditional density of covariates among treatment group

j over $\mathcal{X}$. It is immediate that $f_j(\mathbf{X}) \propto f(\mathbf{X})e_j(\mathbf{X})$. For any pre-specified tilting function $h(\mathbf{X})$, we weight the group-specific density to the target population density using the following balancing weights, up to a proportionality constant:

$$w_j^h(\mathbf{X}) \propto \frac{g(\mathbf{X})}{f_j(\mathbf{X})} \propto \frac{f(\mathbf{X})h(\mathbf{X})}{f(\mathbf{X})e_j(\mathbf{X})} = \frac{h(\mathbf{X})}{e_j(\mathbf{X})}, \quad \forall \ j \in \mathcal{J}. \tag{3.2}$$

The set of weights $\{w_j^h(\mathbf{X}) : j \in \mathcal{J}\}$ balance the weighted distributions of pre-treatment covariates towards the corresponding target population distribution, i.e., $f_j(\mathbf{X})w_j^h(\mathbf{X}) \propto g(\mathbf{X})$, for all $j \in \mathcal{J}$.

To apply the balancing weights to survival outcomes subject to right-censoring, we first construct the pseudo-observations (Andersen et al., 2003). For a given time t, define $\theta^k(t) = \mathbb{E}\{v_k(T_i; t)\}$ as a population parameter. The pseudo-observation for each unit is generically written as $\widehat{\theta}_i^k(t) = N\widehat{\theta}^k(t) - (N-1)\widehat{\theta}_{-i}^k(t)$, where $\widehat{\theta}^k(t)$ is the consistent estimator of $\theta^k(t)$, and $\widehat{\theta}_{-i}^k(t)$ is the corresponding estimator with unit i left out. For both transformation v_k with $k = 1, 2$, we consider the Kaplan–Meier estimator to construct $\theta^k(t)$, given by

$$\widehat{S}(t) = \prod_{\widetilde{T}_i \le t} \left\{ 1 - \frac{dN(\widetilde{T}_i)}{Y(\widetilde{T}_i)} \right\},$$

where $N(t) = \sum_{i=1}^N \mathbf{1}\{\widetilde{T}_i \le t, \Delta_i = 1\}$ is the counting process for the event of interest, and $Y(t) = \sum_{i=1}^N \mathbf{1}\{\widetilde{T}_i \ge t\}$ is the at-risk process. When the interest lies in the survival functions ($k = 1$), the ith pseudo-observation is estimated by

$$\widehat{\theta}_i^1(t) = N\widehat{S}(t) - (N-1)\widehat{S}_{-i}(t). \tag{3.3}$$

When the interest lies in the restricted mean survival times ($k = 2$), the ith pseudo-observation is estimated by

$$\widehat{\theta}_i^2(t) = N\int_0^t \widehat{S}(u)du - (N-1)\int_0^t \widehat{S}_{-i}(u)du = \int_0^t \widehat{\theta}_i^1(u)du. \tag{3.4}$$

The pseudo-observation is a leave-one-out jackknife approach to address right-censoring and provides a straightforward unbiased estimator of the functional of uncensored

data under the independent censoring assumption (A3). From Graw et al. (2009) and Andersen et al. (2017) and under the unconfoundedness assumption (A1), one can show that $\mathbb{E}\{\widehat{\theta}_i^k(t)|\mathbf{X}_i, Z_i = j\} = \mathbb{E}\{v_k(T_i;t)|\mathbf{X}_i, Z_i = j\} + o_p(1) = \mathbb{E}\{\nu_k(T_i(j);t)|\mathbf{X}_i\} + o_p(1)$, based on which the g-formula can be used to estimate the pairwise average causal effect among the combined population ($h(\mathbf{X}) = 1$). For the class of estimands (3.1), we propose the following Hájek-type estimator:

$$\hat{\tau}_{j,j'}^{k,h}(t) = \frac{\sum_{i=1}^N \mathbf{1}\{Z_i = j\}\hat{\theta}_i^k(t) w_j^h(\mathbf{X}_i)}{\sum_{i=1}^N \mathbf{1}\{Z_i = j\} w_j^h(\mathbf{X}_i)} - \frac{\sum_{i=1}^N \mathbf{1}\{Z_i = j'\}\hat{\theta}_i^k(t) w_{j'}^h(\mathbf{X}_i)}{\sum_{i=1}^N \mathbf{1}\{Z_i = j'\} w_{j'}^h(\mathbf{X}_i)}. \tag{3.5}$$

In implementation, it is crucial to normalize the weights so that the weights within each group are added up to 1, akin to the concept of stabilized weights (Robins et al., 2000b).

Estimator (3.5) essentially compares the weighted average pseudo-observations in each treatment group. First, without censoring, the ith pseudo-observation is simply the transformation of the observed outcome $\nu_k(T_i;t)$, and (3.5) is identical to the estimator in Li and Li (2019b) for complete outcomes. Second, a number of weighting schemes proposed for non-censored outcomes are applicable to (3.5). For example, the IPW estimator considers $h(\mathbf{X}) = 1$ and $w_j^h(\mathbf{X}) = 1/e_j(\mathbf{X})$, corresponding to a target population of the combination of all treatment groups represented by the study sample. In this case, when only $J = 2$ treatments are present, estimator (3.5) reduces to the IPW estimator in Andersen et al. (2017). When the target population is the group receiving treatment l, the balancing weights should specify $h(\mathbf{X}) = e_l(\mathbf{X})$ and $w_j^h = e_l(\mathbf{X})/e_j(\mathbf{X})$. The overlap weights (OW) specify $h(\mathbf{X}) = \left\{\sum_{l\in\mathcal{J}} e_l^{-1}(\mathbf{X})\right\}^{-1}$ and $w_j^h(\mathbf{X}) = e_j(\mathbf{X})\left\{\sum_{l\in\mathcal{J}} e_l^{-1}(\mathbf{X})\right\}^{-1}$, and correspond to the target population as an intersection of all treatment groups with optimal covariate overlap, or overlap population (Li and Li, 2019b). The overlap population mimics that enrolled in a randomized trial and emphasizes units whose treatment decisions are most ambiguous. When different groups have good covariate overlap, OW and IPW correspond to almost identical target population and estimands. The difference between OW

and IPW emerges with increasing regions of poor overlap. In the case of a complete outcome, OW has been proved to give the smallest total variance for pairwise comparisons among all balancing weights. The theory and optimality of OW, however, has not been explored with survival outcomes, and will be investigated below.

3.3 Theoretical properties

We present two main results on the theoretical properties of the proposed weighting estimator (3.5). The first result develops a new asymptotic variance expression for the weighted pairwise comparisons of the pseudo-observations, and the second result establishes the efficiency optimality of OW within the family of balancing weights based on the pseudo-observations.

Below we first outline the main steps of the asymptotic variance derivation before presenting the result. Let $(\Omega, \mathcal{F}, \mathcal{P})$ be a probability space and $(\mathbf{D}, \|\bullet\|)$ be a Banach space for distribution functions. We assume each tuple $\mathcal{O}_i = (Z_i, \mathbf{X}_i, \tilde{T}_i, \Delta_i)$ is an i.i.d draw from the sample space $\mathcal{S}$ in the probability space $(\Omega, \mathcal{F}, \mathcal{P})$. Define the Dirac measure $\delta_{(\bullet)} : \mathcal{S} \to \mathbf{D}$, we write the *empirical distribution function* as $F_n = N^{-1} \sum_{i=1}^{N} \delta_{\mathcal{O}_i}$ and its limit as F. Following Overgaard et al. (2017), we use functionals to represent different estimators for the transformed survival outcomes with pseudo-observations. Suppose $\phi_k(\bullet; t) : \mathbf{D} \to \mathcal{R}$ is the functional mapping a distribution to a real value, such as the Kaplan-Meier estimator, $\phi_1(F_N; t) = \widehat{S}(t)$, then each pseudo-observation is represented as $\widehat{\theta}_i^k(t) = N\phi_k(F_N; t) - (N-1)\phi_k(F_N^{-i}; t)$, where F_N^{-i} is the empirical distribution omitting $\mathcal{O}_i$.

To derive the asymptotic variance of estimator (3.5), we need to accommodate two sources of uncertainty. The first source stems from the calculation of the pseudo-observations. We consider the functional derivative of $\phi_k(\bullet; t)$ at $f \in \mathbf{D}$ along direction $s \in \mathbf{D}$ as $\phi'_{k,f}(s)$, which is a linear and continuous functional, $\{\phi_k(f + s; t) - \phi_k(f; t) - \phi'_{k,f}(s; t)\}^2 = o(||s||_{\mathbf{D}})$. Assuming $\phi_k(\bullet; t)$ is differentiable at the true distribution function F, we express the first-order influence function of $\mathcal{O}_i$

for the pseudo-observation estimator $\hat{\theta}^k(t)$ as the first-order derivative along the direction $\delta_{\mathcal{O}_i} - F$, denoted by $\phi'_{k,i}(t) \triangleq \phi'_{k,F}(\delta_{\mathcal{O}_i} - F; t)$. Similarly, the second-order derivative for the functional $\phi_k(\bullet; t)$ at f along direction (s, w) can be defined as $\phi''_{k,F}(s, w; t)$, and the second-order influence function for $(\mathcal{O}_i, \mathcal{O}_j)$ is given as $\phi''_{k,(l,i)}(t) \triangleq \phi''_{k,F}(\delta_{\mathcal{O}_l} - F, \delta_{\mathcal{O}_i} - F; t)$. To characterize the variability associated with jackknifing, we follow Graw et al. (2009) and Jacobsen and Martinussen (2016) to write the second-order von Mises expansion the pseudo-observations:

$$\widehat{\theta}_i^k(t) = \theta^k(t) + \phi'_{k,i}(t) + \frac{1}{N-1} \sum_{l \neq i} \phi''_{k,(l,i)}(t) + R_{N,i}, \tag{3.6}$$

where the first three terms dominate the asymptotic behaviour of $\widehat{\theta}_i^k(t)$ and the remainder $R_{N,i}$ vanishes asymptotically because $\lim_{N\to 0} \sqrt{N} \max_i |R_{N,i}| = 0$. The second source of uncertainty in estimator (3.5) comes from estimating the unknown propensity scores and hence the weights; such uncertainty is well studied in causal inference literature and is usually quantified using M-estimation (see, for example, Lunceford and Davidian (2004a)). Typically, the unknown propensity score model is parameterized as $e_j(\mathbf{X}_i; \boldsymbol{\gamma})$, where the finite-dimensional parameter $\boldsymbol{\gamma}$ is estimated by maximizing the multinomial likelihood.

Theorem 1. *Under suitable regularity conditions specified in Web Appendix A, for $k = 1, 2$, $j, j' \in \mathcal{J}$ and all continuously differentiable tilting function $h(\mathbf{X})$,*

1. *$\widehat{\tau}^{k,h}_{j,j'}(t)$ is a consistent estimator for $\tau^{k,h}_{j,j'}(t)$.*
2. *$\sqrt{N}\left\{\widehat{\tau}^{k,h}_{j,j'}(t) - \tau^{k,h}_{j,j'}(t)\right\}$ converges in distribution to a mean-zero normal random variate with variance $\mathbb{E}\{\Psi_j(\mathcal{O}_i; t) - \Psi_{j'}(\mathcal{O}_i; t)\}^2 / \{\mathbb{E}(h(\mathbf{X}_i))\}^2$, where the scaled influence function*

$$\begin{aligned}\Psi_j(\mathcal{O}_i; t) =& \mathbf{1}\{Z_i = j\} w_j^h(\mathbf{X}_i) \left\{ \left(\theta^k(t) + \phi'_{k,i}(t) - m_j^{k,h}(t) \right) + Q_N \right\} \\ &+ \mathbb{E}\left\{ \mathbf{1}\{Z_i = j\} \left(\theta^k(t) + \phi'_{k,i}(t) - m_j^{k,h}(t) \right) \frac{\partial}{\partial \gamma^T} w_j^h(\mathbf{X}_i) \right\} \mathbf{I}^{-1}_{\boldsymbol{\gamma}\boldsymbol{\gamma}} \mathbf{S}_{\boldsymbol{\gamma},i},\end{aligned} \tag{3.7}$$

$Q_N = (N-1)^{-1}\sum_{l\neq i}\phi''_{k,(l,i)}(t)\mathbf{1}\{Z_l = j\}w_j^h(\mathbf{X}_l)$, $\mathbf{S}_{\boldsymbol{\gamma},i}$ *and* $\mathbf{I}_{\boldsymbol{\gamma}}$ *are the score function and information matrix of* $\boldsymbol{\gamma}$*, respectively.*

Theorem 1 establishes consistency and asymptotic normality of the proposed weighting estimator (3.5). In particular, the influence function $\psi_j(\mathcal{O}_i;t)$ delineates two aforementioned sources of variability, with the first and second term characterizing the uncertainty due to estimating the pseudo-observations and the propensity scores, respectively. Because the jackknife pseudo-observation estimator for $\widehat{\theta}_i^k(t)$ includes information from the rest of $N-1$ observations and is no longer independent across units. Therefore, derivation of Equation (3.7) requires invoking the central limit theorem for U-statistics (cf. Chapter 12 in Van der Vaart, 1998), and leads to a second-order term, Q_N, that properly accommodates the correlation between the estimated pseudo-observations of different units. Theorem 1 immediately suggests the following consistent variance estimator for pairwise comparisons, $\widehat{\mathbb{V}}\{\hat{\tau}_{j,j'}^{k,h}(t)\} = \sum_{i=1}^N\{\widehat{\psi}_j(\mathcal{O}_i;t) - \widehat{\psi}_{j'}(\mathcal{O}_i;t)\}/\sum_{i=1}^N\widehat{h}(\mathbf{X}_i)^2$, where $\widehat{\psi}_j(\mathcal{O}_i;t)$ is defined explicitly in Section 8.2.1 for brevity. In Section 8.2.1, we also give explicit derivations of the functional derivatives for each transformation ν_k when the Kaplan-Meier estimator, $\widehat{S}(t)$, is used to construct the pseudo-observation as in Section 3.2.2.

Below we further provide several important remarks regarding expression (3.7).

Remark 1. *Without censoring, each pseudo-observation degenerates to the observed outcome, which implies* $\widehat{\theta}_i^k(t) = \theta^k(t) + \phi'_{k,i}(t)$ *and therefore* $Q_N = 0$*. In this case, formula* (3.7) *reduces to the usual influence function derived in Li and Li (2019b) for complete outcomes.*

Remark 2. *In the presence of censoring, we show in Section 8.2.1 that ignoring the uncertainty due to estimating pseudo-observations will overestimate the variance of* $\hat{\tau}_{j,j'}^{k,h}(t)$*. This insight for weighting estimator is in parallel to Jacobsen and Martinussen (2016), who suggested ignoring the uncertainty due to estimating the pseudo-observations leads to conservative inference for outcome regression parameters.*

Remark 3. *For $h(\mathbf{X}) = 1$ (and equivalently the IPW scheme), we show in Section 8.2.1 that treating the inverse probability weights as known will, somewhat counter-intuitively,* overestimate *the variance for pairwise comparisons; this extends the classic results of Hirano et al. (2003) to multiple treatments. The implications of ignoring the uncertainty in estimating the propensity scores, however, are generally uncertain for other choice of $h(\mathbf{X})$, which can lead to either conservative or anti-conservative inference, as explained in Haneuse and Rotnitzky (2013). An exception is when Z_i is completely randomized as in a randomized controlled trial (RCT), where the propensity score to any treatment group is a constant and thus any tilting function based on the propensity scores reduces to a constant, i.e. $h(\mathbf{X}) = \widetilde{h}(e_1(\mathbf{X}), \ldots, e_j(\mathbf{X})) \propto 1$. In this case, one can still estimate a "working" propensity score model and use the subsequent weighting estimator* (3.5) *to adjust for chance imbalance in covariates. Equation* (3.7) *shows that such a covariate adjustment approach in RCT leads to variance reduction for pairwise comparisons, extending the results developed in Zeng et al. (2020d) to multiple treatments and censored survival outcomes.*

Remark 4. *Estimator* (3.5) *and Theorem 1 can be extended to accommodate covariate-dependent censoring: $T_i(j) \perp\!\!\!\perp C_i(j)|\mathbf{X}_i, Z_i$. In this case, one can consider inverse probability of censoring weighted pseudo-observation (Robins and Finkelstein, 2000; Binder et al., 2014):*

$$\widehat{\theta}_i^k(t) = \frac{v_k(\widetilde{T}_i; t)\mathbf{1}\{C_i \geq \widetilde{T}_i \wedge t\}}{\widehat{G}(\widetilde{T}_i \wedge t|\mathbf{X}_i, Z_i)}, \tag{3.8}$$

where $\widehat{G}(u|\mathbf{X}_i, Z_i)$ is a consistent estimator of the censoring survival function $G(u|\mathbf{X}_i, Z_i) = \Pr(C_i \geq u|\mathbf{X}_i, Z_i)$. To show the asymptotic normality of the modified weighting estimator, we can similarly view (3.8) *as a functional mapping from the empirical distribution of data to a real value (Overgaard et al., 2019) and find the corresponding functional derivatives for asymptotic expansion. Details of these results are provided in Section 8.2.1.*

The following Theorem 2 shows that the overlap weights, similar to the case of

non-censored outcomes, lead to the smallest total asymptotic variance for all pairwise comparisons based on pseudo-observations among the family of balancing weights.

Theorem 2. *Under regularity conditions in Section 8.2.1 and assuming generalized homoscedasticity such that* $\lim_{N\to\infty} \mathbb{V}\{\widehat{\theta}_i^k(t)|Z_i, \mathbf{X}_i\} = \mathbb{V}\{\phi'_{k,i}(t)|Z_i, \mathbf{X}_i\}$ *is a constant across different levels of* $(Z_i, \mathbf{X}_i)$*, the harmonic mean function* $h(\mathbf{X}) = \left\{\sum_{l\in\mathcal{J}} e_l^{-1}(\mathbf{X})\right\}^{-1}$ *leads to the smallest total asymptotic variance for pairwise comparisons among all possible tilting functions.*

Theorem 2 generalizes the findings of Li et al. (2018a) and Li and Li (2019b) to provide new theoretical justification for the efficiency optimality of the overlap weights, $w_j^h(\mathbf{X}) = e_j(\mathbf{X})\left\{\sum_{l\in\mathcal{J}} e_l^{-1}(\mathbf{X})\right\}^{-1}$, when applied to censored survival outcomes. Technically this result relies on a generalized homoscedasticity assumption that requires the limiting variance of the estimated pseudo-observations to be constant within the strata defined by $(Z_i, \mathbf{X}_i)$. This condition includes the usual homoscedasticity for conditional outcome variance as a special case in the absence of censoring. Of note, the homoscedasticity condition may not hold in practice, but has been empirically shown to be not crucial for the efficiency property of OW, as exemplified in the simulations by Li et al. (2018a) and numerous applications. In Section 3.4, we carry out extensive simulations to verify that OW leads to improved efficiency over IPW when generalized homoscedasticity is violated.

We can further construct an augmented weighting estimator by augmenting estimator (3.5) with an outcome regression model for pseudo-observations. For any time t, we can posit treatment-specific outcome models $m_j^k(\mathbf{X}_i; \boldsymbol{\alpha}_j) = \mathbb{E}\{\widehat{\theta}_i^k(t)|\mathbf{X}_i, Z_i = j\}$,

and define an augmented weighting estimator

$$\begin{aligned}\hat{\tau}^{k,h}_{j,j',\mathrm{AUG}}(t) = &\frac{\sum_{i=1}^{N}\widehat{h}(\mathbf{X}_i)\{m_j(\mathbf{X}_i,\widehat{\boldsymbol{\alpha}}_j) - m_{j'}(\mathbf{X}_i,\widehat{\boldsymbol{\alpha}}_{j'})\}}{\sum_{i=1}^{N}\widehat{h}(\mathbf{X}_i)} \\ &+ \frac{\sum_{i=1}^{N}\mathbf{1}\{Z_i = j\}\{\widehat{\theta}^k_i(t) - m_j(\mathbf{X}_i,\widehat{\boldsymbol{\alpha}}_j)\}w^h_j(\mathbf{X}_i)}{\sum_{i=1}^{N}\mathbf{1}\{Z_i = j\}w^h_j(\mathbf{X}_i)} \\ &- \frac{\sum_{i=1}^{N}\mathbf{1}\{Z_i = j'\}\{\widehat{\theta}^k_i(t) - m_{j'}(\mathbf{X}_i,\widehat{\boldsymbol{\alpha}}_{j'})\}w^h_{j'}(\mathbf{X}_i)}{\sum_{i=1}^{N}\mathbf{1}\{Z_i = j'\}w^h_{j'}(\mathbf{X}_i)},\end{aligned} \tag{3.9}$$

where $\widehat{\boldsymbol{\alpha}}_j$ denotes the estimated regression parameters in the jth outcome model. Such an augmented estimator generalizes those developed in Mao et al. (2019) to multiple treatments and survival outcomes. When $h(\mathbf{X}) = 1$, i.e. with the IPW scheme, the augmented estimator becomes the doubly-robust estimator for pairwise comparisons. When only $J = 2$ treatments are compared, (3.9) reduces to the estimator of Wang (2018). For other choices of $h(\mathbf{X})$, the augmented estimator is not necessarily doubly-robust, but may be more efficient than weighting alone as long as the outcome model is correctly specified (Mao et al., 2019). For specifying an outcome regression model, Andersen and Pohar Perme (2010) reviewed a set of generalized linear models appropriate for pseudo-observations, and discussed residual-based diagnostic tools for checking model adequacy. One can follow their strategies and assume the outcome model as $m_j(\mathbf{X}_i;\boldsymbol{\alpha}_j) = g^{-1}(\mathbf{X}_i^T\boldsymbol{\alpha}_j)$, where g is a link function. The estimation of $\boldsymbol{\alpha}_j$ can proceed with conventional fitting algorithms for generalized linear models. For our estimands of interest, we can choose identity or log link for estimating the ASCE and RACE and the complementary log-log link (resembling a proportional hazards model) for the SPCE (Andersen et al., 2004; Klein et al., 2007). Compared to the Theorem 1 for the weighting estimator (3.5), derivation of the asymptotic variance of (3.9) requires considering a third source of uncertainty due to estimating $\boldsymbol{\alpha}_j$ in the outcome model. The resulting expression is rather complicated, thus we only sketch the key derivation steps in Section 8.2.1.

3.4 Simulation studies

We conduct simulation studies to evaluate the finite-sample performance of the propensity score weighting estimator (3.5), and to illustrate the efficiency property of the OW estimator.

3.4.1 Simulation design

We generate four pre-treatment covariates: $\mathbf{X}_i = (X_{1i}, X_{2i}, X_{3i}, X_{4i})^T$, where $(X_{1i}, X_{2i})^T$ are drawn from a mean-zero bivariate normal distribution with equal variance 2 and correlation 0.25, $X_{3i} \sim \text{Bern}(0.5)$, and $X_{4i} \sim \text{Bern}(0.4 + 0.2X_{3i})$. We consider $J = 3$ treatment groups, with the true propensity score model given by $\log\{e_j(\mathbf{X}_i)/e_1(\mathbf{X}_i)\} = \widetilde{\mathbf{X}}_i^T\boldsymbol{\beta}_j$, $j = 1, 2, 3$, where $\widetilde{\mathbf{X}}_i = (1, \mathbf{X}_i^T)^T$. We set $\boldsymbol{\beta}_1 = (0, 0, 0, 0, 0)^T$, $\boldsymbol{\beta}_2 = 0.2\boldsymbol{\beta}_3$; two sets of values for $\boldsymbol{\beta}_3$ are considered: (i) $\boldsymbol{\beta}_3 = \boldsymbol{\beta}_1$ and (ii) $\boldsymbol{\beta}_3 = (1.2, 1.5, 1, -1.5, -1)^T$, which represent good and poor covariate overlap between groups, respectively. Distribution of the true generalized propensity scores under each specification is presented in Figure 8.4.

Two outcome models are used to generate potential survival times. Model A is a Weibull proportional hazards model with hazard rate for $T_i(j)$ as $\lambda_j(t|\mathbf{X}_i) = \eta\nu t^{\nu-1}\exp\{L_i(j)\}$, and $L_i(j) = \mathbf{1}\{Z_i = 2\}\gamma_2 + \mathbf{1}\{Z_i = 3\}\gamma_3 + \mathbf{X}_i^T\boldsymbol{\alpha}$. We specify $\eta = 0.0001$, $\nu = 3$, $\boldsymbol{\alpha} = (0, 2, 1.5, -1, 1)^T$, and $\gamma_2 = \gamma_3 = 1$, implying worse survival experience due to treatments $j = 2$ and $j = 3$. The potential survival time $T_i(j)$ is then drawn using $T_i(j) = \left\{\frac{-\log(U_i)}{\eta\exp(L_i(j))}\right\}^{1/\nu}$, where $U_i \sim \text{Unif}(0, 1)$. Model B is an accelerated failure time (AFT) model that violates the proportional hazards assumption. Specifically, $T_i(j)$ is drawn from a log-normal distribution $\log\{T_i(j)\} \sim \mathcal{N}(\mu, \sigma^2 = 0.64)$, with $\mu = 3.5 - \gamma_2\mathbf{1}\{Z_i = 2\} - \gamma_3\mathbf{1}\{Z_i = 3\} - \mathbf{X}_i^T\boldsymbol{\alpha}$. For simplicity, we assume treatment has no causal effect on censoring time such that $C_i(j) = C_i$ for all $j \in \mathcal{J}$. Under completely independent censoring, $C_i \sim \text{Unif}(0, 115)$. Under covariate-dependent censoring, C_i is generated from a Weibull survival model with hazard rate $\lambda^c(t|\mathbf{X}_i) = \eta_c\nu_c t^{\nu_c-1}\exp(\mathbf{X}_i^T\boldsymbol{\alpha}_c)$, where $\boldsymbol{\alpha}_c = (1, 0.5, -0.5, 0.5)^T$,

$\eta_c = 0.0001$, $\nu_c = 2.7$. These parameters are specified so that the marginal censoring rate is roughly 50%.

Under each data generating process, we consider OW and IPW estimators based on (3.5), and focus our comparison here with two standard estimators: the g-formula estimator based on the confounder-adjusted Cox model, and the IPW-Cox model (Austin and Stuart, 2017). Details of these two and other alternative estimators are included in Section 8.2.2. While the IPW estimator (3.5) and the Cox model based estimators focus on the combined population with $h(\mathbf{X}) = 1$, the OW estimator focuses on the overlap population with the optimal tilting function suggested in Theorem 2. When comparing treatments $j = 2$ (or $j = 3$) with $j = 1$, the true values of target estimands can be different between OW and the other estimators (albeit very similar under good overlap), and are computed via Monte Carlo integration. Nonetheless, when we compare treatments $j = 2$ and $j = 3$, the true conditional average effect $\tau^k_{2,3}(\mathbf{X}; t) = 0$ for all k, and thus the true estimand $\tau^{k,h}_{2,3}(t)$ has the same value (zero) regardless of $h(\mathbf{X})$. This represents a natural scenario to compare the bias and efficiency between estimators without differences in true values of estimands. We vary the study sample size $N \in \{150, 300, 450, 600, 750\}$, and fix the evaluation point $t = 60$ for estimating SPCE ($k = 1$) and RACE ($k = 2$). We consider 1000 simulations and calculate the absolute bias, root mean squared error (RMSE) and empirical coverage corresponding to each estimator. To obtain the empirical coverage for OW and IPW, we construct 95% confidence intervals (CIs) based on the consistent variance estimators suggested by Theorem 1. Bootstrap CIs are used for Cox g-formula and IPW-Cox estimators. Additional simulations comparing OW with alternative regression estimators and the augmented weighting estimators (3.9) can be found in Section 8.2.3.

3.4.2 Simulation results

Under good overlap, Figure 8.5 presents the absolute bias, RMSE and coverage for OW, IPW estimators based on (3.5), Cox g-formula as well as IPW-Cox estimators, when survival outcomes are generated from model A and censoring is completely independent. Here we focus on comparing treatment $j = 2$ versus $j = 3$, and thus the true average causal effect among any target population is null. Across all three estimands (SPCE, RACE and ASCE), OW consistently outperforms the IPW with a smaller absolute bias and RMSE, and closer to nominal coverage across all levels of N. Due to correctly specified outcome model, the Cox g-formula estimator is, as expected, more efficient than the weighting estimators. However, its empirical coverage is not always close to nominal, especially for estimating ASCE. The IPW-Cox estimator has the largest bias, because the proportional hazards assumption does not marginally among any of the target population. Figure 3.1 represents the counterpart of Figure 8.4 but under poor overlap. The IPW estimator based on (3.5) is susceptible to lack of overlap due to extreme inverse probability weights, and has extremely large bias, variance and low coverage. The bias and under-coverage remain for IPW even after trimming units for whom $\max_j\{e_j(\mathbf{X}_i)\} > 0.97$ and $\min_j\{e_j(\mathbf{X}_i)\} < 0.03$ (Figure 8.5). Under poor overlap, OW is more efficient than IPW regardless of trimming, and becomes almost as efficient as the Cox g-formula estimator for estimating RACE and ASCE. Furthermore, the proposed OW interval estimator consistently carries close to nominal coverage for all three types of estimands. Figure 8.9 present the counterparts of Figure 8.4 and Figure 3.1, but focus on comparing treatments $j = 2$ and $j = 1$ where the true average causal effect is non-null. The patterns are qualitatively similar.

In Table 3.1, we summarize the performance metrics for different estimators when the proportional hazards assumption is violated and/or censoring depends on covariates. Similar to Figure 3.1, we focus on comparing treatment $j = 2$ versus $j = 3$ such that the true average causal effect is null among any target population. When

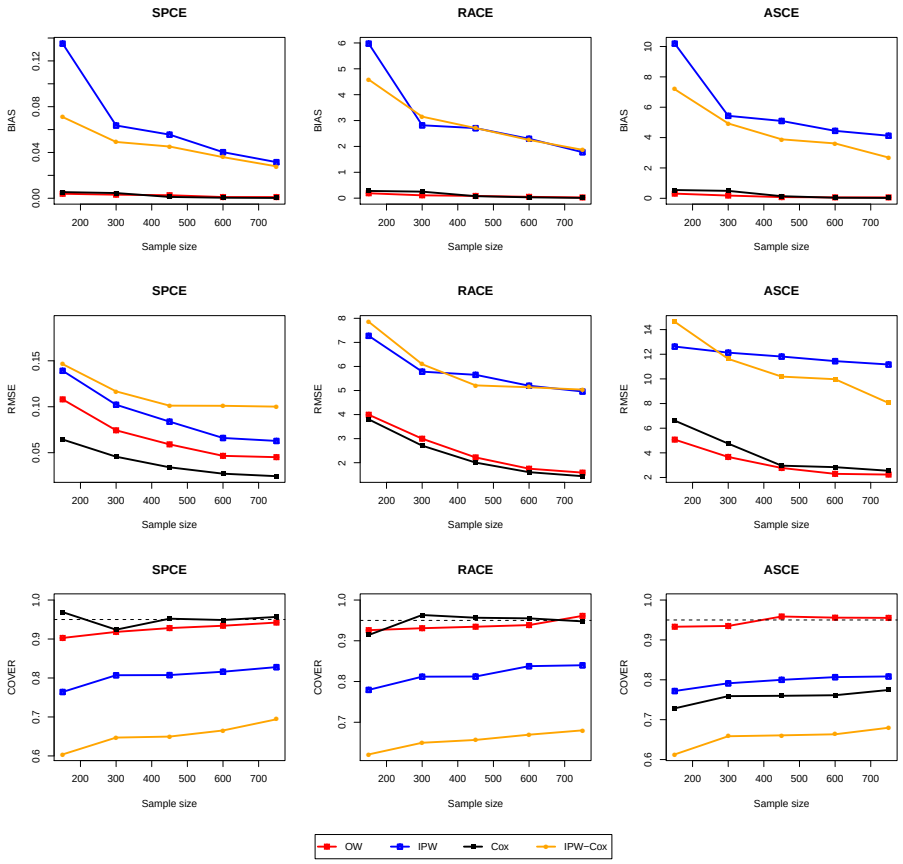

Figure 3.1: Absolute bias, root mean squared error (RMSE) and coverage for comparing treatment $j = 2$ versus $j = 3$ under poor overlap, when survival outcomes are generated from model A and censoring is completely independent.

survival outcomes are generated from model B and hence the proportional hazards assumption no longer holds, both the Cox g-formula and IPW-Cox estimators have the largest bias, especially under poor overlap. In those scenarios, OW maintains the largest efficiency, and consistently outperforms IPW in terms of bias and variance. While the empirical coverage of IPW estimator deteriorates under poor overlap, the coverage of OW estimator is robust to lack of overlap. When censoring further depends on covariates, we modify the OW and IPW estimators using (3.8) where the censoring survival functions are estimated by a Cox model. With the addition of inverse probability of censoring weights, only OW maintains the smallest bias, largest efficiency and closest to nominal coverage under poor overlap across all types of estimands. Results for comparing treatments $j = 2$ and $j = 1$ are similar and included in Table 8.5.

In Section 8.2.3, we have additionally compared OW with alternative outcome regression estimators similar to Mao et al. (2018), and the g-formula estimator based on pseudo-observations (Andersen et al., 2017; Tanaka et al., 2020). These estimators were originally developed with binary treatments, and we generalize them in Section 8.2.3 to multiple treatments for our purpose. Compared to OW estimator based on (3.5), these alternative regression estimators are frequently less efficient and have less than nominal coverage under poor overlap. An exception is the OW regression estimator generalizing the work of Mao et al. (2018), which has similar performance to the OW estimator based on (3.5). We have also carried out additional simulations in Section 8.2.3 to examine the performance of augmented OW and IPW estimators (3.9) relative to simple OW and IPW estimators (3.5). While including an outcome regression component can notably improve the efficiency of IPW with survival outcomes, the efficiency gain for OW estimator due to an additional outcome model is somewhat limited, which favors the use of the OW estimator based on (3.5) due to its simplicity. Finally, we replicate our simulations under a three-arm RCT similar to Zeng et al. (2020d) (see Remark 3 and Section 8.2.3 for details). We confirmed that

Table 3.1: Absolute bias, root mean squared error (RMSE) and coverage for comparing treatment $j = 2$ versus $j = 3$ under different degrees of overlap. In the "proportional hazards" scenario, the survival outcomes are generated from a Cox model (model A), and in the "non-proportional hazards" scenario, the survival outcomes are generated from an accelerated failure time model (model B). The sample size is fixed at $N = 300$.

	Degree of	RMSE				Absolute bias				95% Coverage			
	overlap	OW	IPW	Cox	IPW-Cox	OW	IPW	Cox	IPW-Cox	OW	IPW	Cox	IPW-Cox
Model A, completely random censoring													
SPCE	Good	0.002	0.002	0.001	0.003	0.052	0.055	0.011	0.029	0.943	0.947	0.952	0.968
	Poor	0.003	0.064	0.005	0.049	0.074	0.173	0.046	0.117	0.918	0.807	0.924	0.647
RACE	Good	0.056	0.080	0.047	0.137	1.570	1.523	0.651	1.413	0.945	0.954	0.941	0.969
	Poor	0.106	2.817	0.252	3.151	2.523	5.784	2.709	6.093	0.931	0.812	0.963	0.650
ASCE	Good	0.158	0.177	0.090	0.269	2.916	2.983	1.139	2.766	0.957	0.958	0.961	0.965
	Poor	0.213	5.433	0.490	4.930	4.305	12.131	4.750	11.625	0.935	0.791	0.749	0.658
Model B, completely random censoring													
SPCE	Good	0.002	0.003	0.002	0.006	0.069	0.075	0.042	0.081	0.947	0.945	0.854	0.841
	Poor	0.005	0.043	0.016	0.081	0.097	0.197	0.150	0.222	0.940	0.865	0.863	0.708
RACE	Good	0.087	0.127	0.137	0.314	2.432	2.701	2.400	4.096	0.955	0.946	0.844	0.839
	Poor	0.111	2.962	0.947	4.646	3.862	7.330	8.653	11.275	0.935	0.853	0.830	0.709
ASCE	Good	0.168	0.145	0.244	0.605	4.238	4.507	4.173	7.600	0.956	0.957	0.957	0.836
	Poor	0.223	4.307	1.661	7.562	6.274	13.157	15.027	20.920	0.941	0.862	0.731	0.702
Model A, conditionally independent censoring													
SPCE	Good	0.001	0.002	0.001	0.000	0.044	0.048	0.039	0.039	0.955	0.946	0.906	0.963
	Poor	0.005	0.047	0.009	0.089	0.060	0.154	0.056	0.149	0.910	0.792	0.871	0.641
RACE	Good	0.003	0.005	0.065	0.022	2.257	2.094	2.315	1.717	0.950	0.949	0.929	0.964
	Poor	0.168	3.167	0.532	4.603	2.974	6.264	3.334	7.159	0.936	0.858	0.900	0.635
ASCE	Good	0.008	0.276	0.163	0.188	4.447	9.351	4.899	10.564	0.952	0.950	0.950	0.974
	Poor	0.110	10.523	1.032	11.657	9.557	22.308	7.157	43.651	0.929	0.768	0.739	0.773
Model B, conditionally independent censoring													
SPCE	Good	0.000	0.001	0.001	0.000	0.037	0.055	0.055	0.059	0.952	0.906	0.772	0.902
	Poor	0.002	0.007	0.012	0.025	0.052	0.056	0.164	0.082	0.925	0.879	0.803	0.899
RACE	Good	0.005	0.003	0.064	0.136	4.733	4.738	2.944	5.310	0.951	0.953	0.794	0.855
	Poor	0.132	0.573	0.712	1.594	6.655	6.546	9.092	7.515	0.954	0.899	0.775	0.845
ASCE	Good	0.004	0.055	0.166	0.268	4.436	4.265	4.761	6.548	0.951	0.953	0.937	0.852
	Poor	0.179	0.428	1.339	1.973	6.516	7.589	13.039	8.835	0.957	0.908	0.747	0.846

OW and IPW estimators based on (3.5) are valid for covariate adjustment in RCTs since they lead to substantially improved efficiency over the unadjusted comparisons of pseudo-observations.

3.5 Application to National Cancer Database

We illustrate the proposed weighting estimators by comparing three treatment options for prostate cancer in an observational dataset with 44,551 high-risk, localized prostate cancer patients drawn from the National Cancer Database (NCDB). These patients were diagnosed between 2004 and 2013, and either underwent a surgical procedure – radical prostatectomy (RP), or were treated by one of two therapeutic procedures – external beam radiotherapy combined with androgen deprivation (EBRT+AD) or external beam radiotherapy plus brachytherapy with or without androgen deprivation (EBRT+brachy±AD). We focus on time to death since treatment initiation as the primary outcome, and pre-treatment confounders include age, clinical T stage, Charlson-Deyo score, biopsy Gleason score, prostate-specific antigen (PSA), year of diagnosis, insurance status, median income level, education, race, and ethnicity. A total of 2,434 patients died during the study period with their survival outcome observed, while other patients have right-censored outcomes. The median and maximum follow-up time is 21 and 115 months, respectively.

We used a multinomial logistic model to estimate the generalized propensity scores, and visualized the distribution of estimated scores in Figure 8.11. We model age and PSA by natural splines as in Ennis et al. (2018), and keep linear terms for all other covariates. We found good overlap across groups regarding the propensity of receiving EBRT+brachy±AD, but a slight lack of overlap regarding the propensity of receiving RP and EBRT+AD. We checked the weighted covariate balance under IPW and OW based on the maximum pairwise absolute standardized difference (MPASD) criteria, and present the balance statistics in Table 8.6. The MPASD for the pth covariate is defined as $\max_{j<j'}\{|\bar{X}_{p,j} - \bar{X}_{p,j'}|/S_p\}$, where

$\bar{X}_{p,j} = \sum_{i=1}^{N} \mathbf{1}\{Z_i = j\} X_{i,p} w_j^h(\mathbf{X}_i) / \sum_{i=1}^{N} \mathbf{1}\{Z_i = j\} w_j^h(\mathbf{X}_i)$ is the weighted covariate mean in group j, and $S_p^2 = J^{-1} \sum_{j=1}^{J} S_{p,j}^2$ is the unweighted sample variance averaged across all groups. Both IPW and OW improved covariate balance, with OW leading to consistently smaller MPASD, whose value is below the usual 0.1 threshold for all covariates.

Figure 3.2 presents the estimated causal survival curves for each treatment, $\mathbb{E}\{h(\mathbf{X}) \mathbf{1}\{T_i(j) \geq t\}\} / \mathbb{E}(h(\mathbf{X}))$, along with the 95% confidence bands in the combined population (corresponding to IPW) and the overlap population (corresponding to OW). We chose 220 grid points equally spaced by half a month for this evaluation. The estimated causal survival curves among the two target populations are generally similar, which is expected given there is only a slight lack of overlap (Figure 8.11). The surgical treatment, RP, shows the largest survival benefit, followed by the radiotherapeutic treatment, EBRT+brachy±AD, while EBRT+AD results in the worst survival outcomes during the first 80 months or so. Importantly, the estimated causal survival curves for the RP and EBRT+brachy±AD crossed after month 80, suggesting potential violations to the proportional hazards assumption commonly assumed in survival analysis. Figure 3.3a and 3.3b further characterized the the SPCE and RACE as a function of time t with the associated 95% confidence bands. Evidently, the SPCE results confirmed the largest causal survival benefit due to RP, followed by EBRT+brachy±AD. The associated confidence band of SPCE from OW is narrower than that from IPW and frequently excludes zero. While the analysis of the pairwise RACE yielded similar findings, the efficiency of OW over IPW became more relevant when comparing RP and EBRT+brachy±AD. Specifically, the confidence band of RACE from OW excludes zero until month 80, while the confidence band of RACE from IPW straddles zero across the entire follow-up period. This analysis shed new light on the significant causal survival benefit of RP over EBRT+brachy±AD at the 0.05 level in terms of the restricted mean survival time, which was not identified in previous analysis (Ennis et al., 2018).

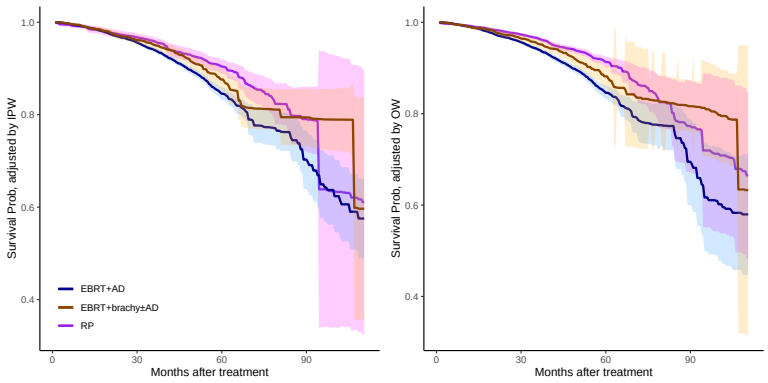

Figure 3.2: Survival curves of the three treatments of prostate cancer (Section 3.5) estimated from the pseudo-observations-based weighting estimator, using IPW (left) and OW (right).

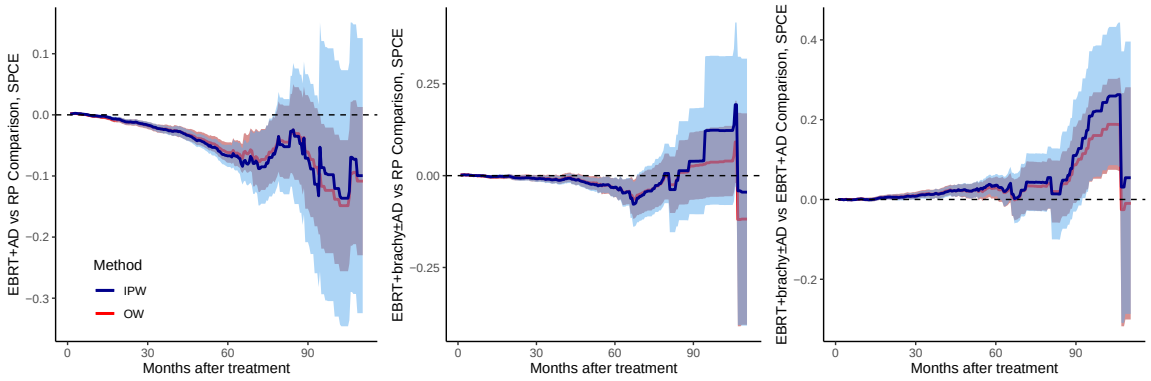

(a) Estimated survival probability as a function of time t in three treatment groups.

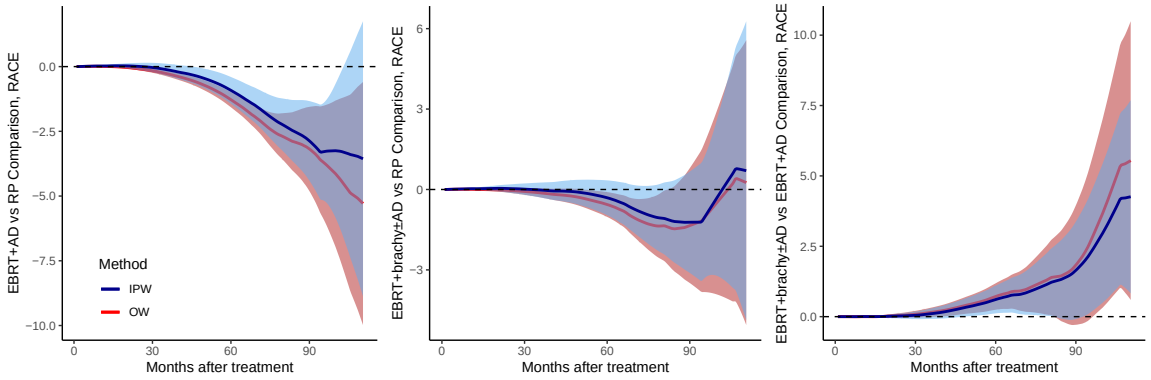

(b) Estimated restricted mean survival time as a function of time t in three treatment groups.

Figure 3.3: Point estimates and 95% confidence bands of SPCE and RACE as a function of time from the pseudo-observations-based IPW and OW estimator in the prostate cancer application in Section 3.5.

In Table 3.2, we also reported the SPCE and RACE using the IPW and OW estimators, as well as the Cox g-formula and IPW-Cox estimators at $t = 60$ months, i.e. the 80th quantile of the follow-up time. All methods conclude that RP leads to significantly lower mortality rate at 60 months than EBRT+AD. Compared to IPW, OW provides similar point estimates and no larger variance estimates. Consistently with Figure 3.3b, the smaller variance estimate due to OW (compared to IPW) leads to a change in conclusion when comparing EBRT+brachy±AD versus RP in terms of RACE at the 0.05 level and confirms the significant treatment benefit of RP. The Cox g-formula and IPW-Cox estimators sometimes provide considerably different results than weighting estimators based on (3.5), as they assumed proportional hazards which may not hold. Overall, we found that, compared to RP, the two radiotherapeutic treatments led to a shorter restricted mean survival time (1.2 months shorter with EBRT+AD and 0.5 month shorter with EBRT+brachy±AD) up to five years after treatment. The 5-year survival probability is also 6.7% lower under EBRT+AD and 3.1% lower under EBRT+brachy±AD compared to RP.

Table 3.2: Pairwise treatment effect estimates of the three treatments of prostate cancer (Section 3.5) using four methods, on the scale of restricted average causal effect (RACE) and survival probability causal effect (SPCE) at 60 months/5 years post-treatment.

Method	Estimate	Standard error	95% Confidence interval	p-value
EBRT-AD vs. RP comparison				
Restricted average causal effect				
OW	-1.277	0.150	(-1.524, -1.031)	0.000
IPW	-0.917	0.264	(-1.351, -0.484)	0.001
COX	-1.342	0.126	(-1.549, -1.136)	0.000
MSM	-0.931	0.220	(-1.294, -0.568)	0.000
Survival probability causal effect				
OW	-0.062	0.009	(-0.076, -0.048)	0.000
IPW	-0.067	0.009	(-0.083, -0.052)	0.000
COX	-0.059	0.006	(-0.068, -0.050)	0.000
MSM	-0.039	0.010	(-0.056, -0.023)	0.000
EBRT+brachy±AD vs. RP comparison				
Restricted average causal effect				
OW	-0.562	0.236	(-0.950, -0.174)	0.017
IPW	-0.309	0.331	(-0.855, 0.236)	0.350
COX	-0.802	0.214	(-1.155, -0.450)	0.000
MSM	-0.363	0.317	(-0.885, 0.158)	0.252
Survival probability causal effect				
OW	-0.032	0.013	(-0.054, -0.010)	0.016
IPW	-0.031	0.013	(-0.053, -0.009)	0.021
COX	-0.036	0.009	(-0.051, -0.020)	0.000
MSM	-0.015	0.014	(-0.038, 0.007)	0.256
EBRT+brachy±AD vs. EBRT+AD comparison				
Restricted average causal effect				
OW	0.715	0.240	(0.321, 1.109)	0.003
IPW	0.710	0.242	(0.195, 1.021)	0.015
COX	0.540	0.216	(0.184, 0.896)	0.012
MSM	0.568	0.246	(0.163, 0.973)	0.021
Survival probability causal effect				
OW	0.030	0.014	(0.006, 0.053)	0.036
IPW	0.036	0.014	(0.013, 0.059)	0.011
COX	0.024	0.009	(0.008, 0.039)	0.013
MSM	0.024	0.010	(0.007, 0.041)	0.021

4

Mediation analysis with sparse and irregular longitudinal data

4.1 Introduction

Mediation analysis seeks to understand the role of an intermediate variable (i.e. mediator) M that lies on the causal path between an exposure or treatment Z and an outcome Y. The most widely used mediation analysis method, proposed by Baron and Kenny (1986), fits two linear structural equation models (SEMs) between the three variables and interprets the model coefficients as causal effects. There is a vast literature on the Baron-Kenny framework across a variety of disciplines, including psychology, sociology, and epidemiology (see MacKinnon, 2012). A major advancement in recent years is the incorporation of the potential-outcome-based causal inference approach (Neyman, 1990; Rubin, 1974). This led to a formal definition of relevant causal estimands, clarification of identification assumptions, and new estimation strategies beyond linear SEMs (Robins and Greenland, 1992; Pearl, 2001; Sobel, 2008; Tchetgen Tchetgen and Shpitser, 2012; Daniels et al., 2012; VanderWeele, 2016). In particular, Imai et al. (2010b) proved that the Baron-Kenny estimator can be interpreted as a special case of a causal mediation estimator given additional assumptions. These methodological advancements opened up new application areas including imaging, neuroscience, and environmental health (Lindquist and Sobel, 2011; Lindquist, 2012; Zigler et al., 2012; Kim et al., 2019). Comprehensive reviews on causal mediation analysis are given in VanderWeele (2015); Nguyen et al. (2020).

In the traditional settings of mediation analysis, exposure Z, mediation M and outcome Y are all univariate variables at a single time point. Recent work has

extended to time-varying cases, where at least one of the triplet (Z, M, Y) is longitudinal. This line of research has primarily focused on cases with time-varying mediators or outcomes that are observed on sparse and regular time grids (van der Laan and Petersen, 2008; Roth and MacKinnon, 2012; Lin et al., 2017a). For example, VanderWeele and Tchetgen Tchetgen (2017) developed a method for identifying and estimating causal mediation effects with time-varying exposures and mediators based on marginal structural models (Robins et al., 2000a). Some researchers also investigated the case with time-varying exposure and mediator for the survival outcome (Zheng and van der Laan (2017); Lin et al. (2017b)). Another stream of research, motivated by applications in neuroimaging, focuses on cases where mediators or outcomes are densely recorded continuous functions, e.g. the blood-oxygen-level-dependent (BOLD) signal collected in a functional magnetic resonance imaging (fMRI) session. In particular, Lindquist (2012) introduced the concept of *functional mediation* in the presence of a functional mediator and extended causal SEMs to functional data analysis (Ramsay and Silverman, 2005). Zhao et al. (2018) further extended this approach to functional exposure, mediator and outcome.

Sparse and irregularly-spaced longitudinal data are increasingly available for causal studies. For example, in electronic health records (EHR) data, the number of observations usually varies between patients and the time grids are uneven. The same situation applies in animal behavior studies due to the inherent difficulties in observing wild animals. Such data structure poses challenges to existing causal mediation methods. First, one cannot simply treat the trajectories of mediators and outcomes as functions as in Lindquist (2012) because the sparse observations render the trajectories volatile and non-smooth. Second, with irregular time grids the dependence between consecutive observations changes over time, making the methods based on sparse and regular longitudinal data such as VanderWeele and Tchetgen Tchetgen (2017) not applicable. A further complication arises when the mediator and outcome are measured with different frequencies even within the same individual.

In this chapter, we propose a causal mediation analysis method for sparse and irregular longitudinal data that address the aforementioned challenges. Similar to Lindquist (2012) and Zhao et al. (2018), we adopt a functional data analysis perspective (Ramsay and Silverman, 2005), viewing the sparse and irregular longitudinal data as realizations of underlying smooth stochastic processes. We define causal estimands of direct and indirect effects accordingly and provide assumptions for nonparametric identification (Section 4.3). For estimation and inference, we proceed under the classical two-SEM mediation framework (Imai et al., 2010b) but diverge from the existing methods in modeling (Section 4.4). Specifically, we employ the functional principal component analysis (FPCA) approach (Yao et al., 2005; Jiang and Wang, 2010, 2011; Han et al., 2018) to project the mediator and outcome trajectories to a low-dimensional representation. We then use the first few functional principal components (instead of the whole trajectories) as predictors in the structural equation models. To accurately quantify the uncertainties, we employ a Bayesian FPCA model (Kowal and Bourgeois, 2020) to simultaneously estimate the functional principal components and the structural equation models. Though the Bayesian approach to mediation analysis has been discussed before (Daniels et al., 2012; Kim et al., 2017, 2018), it has not been developed for the setting of sparse and irregular longitudinal data.

Our motivating application is the evaluation of the causal relationships between early adversity, social bonds, and physiological stress in wild baboons (Section 4.2). Here the exposure is early adversity (e.g. drought, maternal death before reaching maturity), the mediators are the strength of adult social bonds, and the outcomes are adult glucocorticoid (GC) hormone concentrations, which is a measure of an animal's physiological stress level. The exposure, early adversity, is a binary variable measured at one time point, whereas both the mediators and outcomes are sparse and irregular longitudinal variables. We apply the proposed method to a prospective and longitudinal observational data set from the Amboseli Baboon Research Project

located in the Amboseli ecosystem, Kenya (Alberts and Altmann, 2012) (Section 4.5). We find that experiencing one or more sources of early adversity leads to significant direct effects (a 9-14% increase) on females' GC concentrations across adulthood, but find little evidence that these effects were mediated by weak social bonds. Though motivated from a specific application, the proposed method is readily applicable to other causal mediation studies with similar data structure, including EHR and ecology studies. Furthermore, our method is also applicable to regularly spaced longitudinal observations.

4.2 Motivating application: early adversity, social bond and stress

4.2.1 Biological background

Conditions in early life can have profound consequences for individual development, behavior, and physiology across the life course (Lindström, 1999; Gluckman et al., 2008; Bateson et al., 2004). These early life effects are important, in part, because they have major implications for human health. One leading explanation for how early life environments affect adult health is provided by the biological embedding hypothesis, which posits that early life stress causes developmental changes that create a "pro-inflammatory" phenotype and elevated risk for several diseases of aging (Miller et al., 2011). The biological embedding hypothesis proposes at least two, non-exclusive causal pathways that connect early adversity to poor health in adulthood. In the first pathway, early adversity leads to altered hormonal profiles that contribute to downstream inflammation and disease. Under this scenario, stress in early life leads to dysregulation of hormonal signals in the body's main stress response system, leading to the release of GC hormone, which engages the body's fight-or-flight response. Chronic activation is associated with inflammation and elevated disease risk (McEwen, 1998; Miller et al., 2002; McEwen, 2008). In the second causal pathway, early adversity hampers an individual's ability to form strong interpersonal relationships. Under this scenario, the social isolation contributes to both

altered GC profiles and inflammation.

Hence, the biological embedding hypothesis posits that early life adversity affects both GC profiles and social relationships in adulthood, and that poor social relationships partly mediate the connection between early adversity and GCs. Importantly, the second causal pathway—mediated through adult social relationships—suggests an opportunity to transmit the negative health effect of early adversity. Specifically, strong and supportive social relationships may dampen the stress response or reduce individual exposure to stressful events, which in turn reduces GCs and inflammation. For example, strong and supportive social relationships have repeatedly been linked to reduced morbidity and mortality in humans and other social animals (Holt-Lunstad et al., 2010; Silk, 2007). In addition to the biological embedding hypothesis, this idea of social mediation is central to several hypotheses that propose causal connections between adult social relationships and adult health, even independent of early life adversity; these hypotheses include the stress buffering and stress prevention hypotheses (Cohen and Wills, 1985; Landerman et al., 1989; Thorsteinsson and James, 1999) and the social causation hypothesis (Marmot et al., 1991; Anderson and Marmot, 2011).

Despite the aforementioned research, the causal relationships among early adversity, adult social relationships, and HPA (hypothalamic–pituitary–adrenal) axis dysregulation remain the subject of considerable debate. While social relationships might exert direct effects on stress and health, it is also possible that poor health and high stress limit an individual's ability to form strong and supportive relationships. As such, the causal arrow flows backwards, from stress to social relationships (Case and Paxson, 2011). In another causal scenario, early adversity exerts independent effects on social relationships and the HPA axis, and correlations between social relationships and GCs are spurious, arising solely as a result of their independent links to early adversity (Marmot et al., 1991).

4.2.2 Data

In this chapter, we test whether the links between early adversity, the strength of adult social bonds, and GCs are consistent with predictions derived from the biological embedding hypothesis and other related theories. Specifically, we use data from a well-studied population of savannah baboons in the Amboseli ecosystem in Kenya. Founded in 1971, the Amboseli Baboon Research Project has prospective longitudinal data on early life experiences, and fine-grained longitudinal data on adult social bonds and GC hormone concentrations, a measure of the physiological stress response (Alberts and Altmann, 2012).

Our study sample includes 192 female baboons. Each baboon entered the study after becoming mature at age 5, and we had information on its experience of six sources of early adversity (i.e., exposure) (Tung et al., 2016; Zipple et al., 2019): drought, maternal death, competing sibling, high group density, low maternal rank, and maternal social isolation. Table 4.1 presents the number of baboons that experienced each early adversity. Overall, while only a small proportion of subjects experienced any given source of early adversity, most subjects experienced at least one source of early adversity. Therefore, in our analysis we also create a cumulative exposure variable that summarizes whether a baboon experienced any source of the adversity.

Table 4.1: Sources of early adversity and the number of baboons experienced each type of early adversity. The last row summarizes the number of baboons had at least one of six individual adversity sources.

early adversity	no. subjects did not experience (control)	no. subjects did experience (exposure)
Drought	164	28
Competing Sibling	153	39
High group density	161	31
Maternal death	157	35
Low maternal rank	152	40
Maternal Social isolation	140	52
At least one	48	144

Each baboon's adult social bonds (i.e. mediators) and fecal GC hormone concentrations (i.e. outcomes) are measured repeatedly throughout its life on the same grid. Social bonds are measured using the dyadic sociality index with females (DSI-F) (Silk et al., 2006). The indices are calculated for each female baboon separately based on all visible observations for social interactions between the baboon and other members in the entire social group within a given period. Larger values mean stronger social bonds. We normalized the DSI-F measurements, and the normalized DSI-F values range from -1.47 to 3.31 with mean value at 1.04 and standard deviation 0.51. The fecal GC concentrations were collected opportunistically, and the values range from 7.51 to 982.87 with mean 74.13 and standard deviation 38.25. Age is used to index within-individual observations on both social bond and GC concentrations. Only about 20% baboons survive until age 18 and thus data on females older than 18 years are extremely sparse and volatile. Therefore, we truncated all trajectories at age 18, resulting in a final sample with 192 female baboons and 9878 observations.

For wild animals, the observations usually made on irregular or opportunistic basis. We have on average 51.4 observations of each baboon for both social bonds and GC concentrations, but the number of observations of a single baboon ranges from 3 to 113. Figure 4.1 shows the mediator and outcome trajectories as a function of age of two randomly selected baboons in the sample. We can see that the frequency of the observations and time grids of the mediator or outcome trajectories vary significantly between baboons.

We also have a set of static and time-varying covariates that are deemed important to wild baboons's physiology and behavior. These include reproductive state (i.e. cycling, pregnant, or lactating), density of the social group, max temperature in the last 30 days before the fecal sample was collected, whether the sample is collected in wet or dry season, the amount of rainfall, relative dominance rank of a baboon, and number of coresident adult maternal relatives.More information on the covariates, exposure, mediator, and outcomes can be found in Rosenbaum et al. (2020).

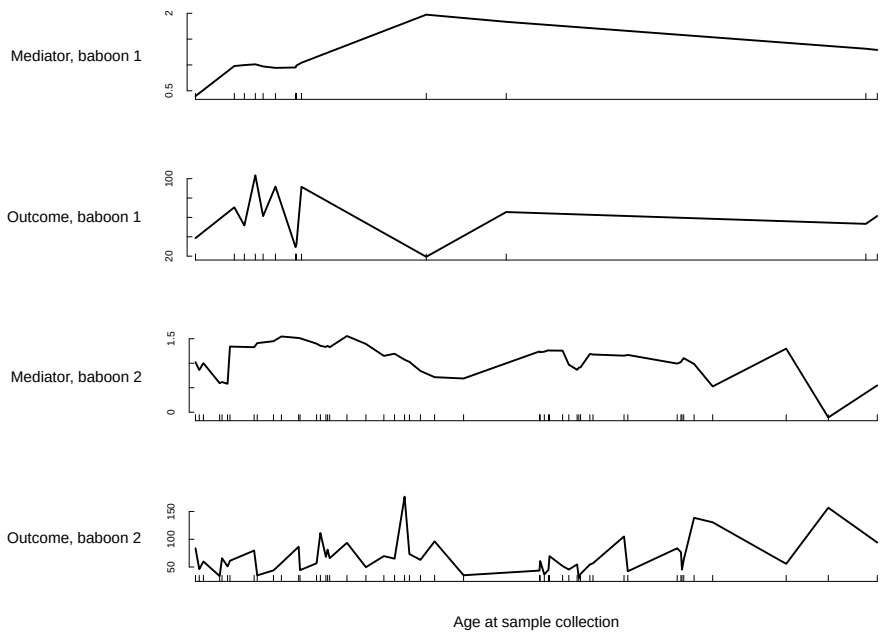

Figure 4.1: Observed trajectories of social bonds and GC hormone as a function of age of two randomly selected female baboons in the study sample.

4.3 Causal mediation framework

4.3.1 Setup and causal estimands

Suppose we have a sample of N units (in the use case described here, baboons); each unit i ($i = 1, 2, \cdots, N$) is assigned to a treatment ($Z_i = 1$) or a control ($Z_i = 0$) group. For each unit i, we make observations at T_i different time points $\{t_{ij} \in [0, T], j = 1, 2, \cdots, T_i\}$, and T_i can vary between units. At each time point t_{ij}, we measure an outcome Y_{ij} and a mediator M_{ij} prior to the outcome, and a vector of p time-varying covariates $\mathbf{X}_{ij} = (X_{ij,1}, \cdots, X_{ij,p})'$. For each unit, the observations points are sparse along the time span and irregularly spaced. For simplicity, we assume the observed time grids for the outcome and the mediator are the same within one unit. However, our method is directly applicable when the observation grids for the outcome and the mediator are different for a given individual.

A key to our method is to view the observed mediator and outcome values drawn from a smooth underlying process $M_i(t)$ and $Y_i(t)$, $t \in [0, T]$, with Normal measure-

ment errors, respectively:

$$M_{ij} = M_i(t_{ij}) + \varepsilon_{ij}, \quad \varepsilon_{ij} \sim \mathcal{N}(0, \sigma_m^2), \tag{4.1}$$

$$Y_{ij} = Y_i(t_{ij}) + \nu_{ij}, \quad \nu_{ij} \sim \mathcal{N}(0, \sigma_y^2). \tag{4.2}$$

Hence, instead of directly exploring the relationship between the treatment Z_i, mediators M_{ij} and outcomes Y_{ij}, we investigate the relationship between Z_i and the stochastic processes $M_i(t_{ij})$ and $Y_i(t_{ij})$. In particular, we wish to answer two questions: (a) how big is the causal impact of the treatment on the outcome process, and (b) how much of that impact is mediated through the mediator process?

To be consistent with the standard notation of potential outcomes in causal inference (Imbens and Rubin, 2015), from now on we move the time index of the mediator and outcome process to the superscript: $M_i(t) = M_i^t, Y_i(t) = Y_i^t$. Also, we use the following bold font notation to represent a process until time t: $\mathbf{M}_i^t \equiv \{M_i^s, s \leq t\} \in \mathcal{R}^{[0,t]}$, and $\mathbf{Y}_i^t \equiv \{Y_i^s, s \leq t\} \in \mathcal{R}^{[0,t]}$. Similarly, we denote covariates between the jth and $j+1$th time point for unit i as $\mathbf{X}_i^t = \{X_{i1}, X_{i2}, \cdots, X_{ij'}\}$ for $t_{ij'} \leq t < t_{ij'+1}$.

We extend the definition of potential outcomes to define the causal estimands. Specifically, let $\mathbf{M}_i^t(z) \in \mathcal{R}^{[0,t]}$ for $z = 0, 1, t \in [0, T]$, denote the potential values of the underlying mediator process for unit i until time t under the treatment status z; let $\mathbf{Y}_i^t(z, \mathbf{m}) \in \mathcal{R}^{[0,t]}$ be the potential outcome for unit i until time t under the treatment status z and the mediator process taking value of $\mathbf{M}_i^t = \mathbf{m}$ with $\mathbf{m} \in \mathcal{R}^{[0,t]}$. The above notation implicitly makes the stable unit treatment value assumption (SUTVA) (Rubin, 1980), which states that (i) there is no different version of the treatment, and (ii) there is no interference between the units, more specifically, the potential outcomes of one unit do not depend on the treatment and mediator values of other units. SUTVA is plausible in our application. First, there is unlikely different versions of the early adversities. Second, though baboons live in social groups, it is unlikely a baboon's long-term GC concentration (outcome) was much affected by the early adversities experienced by other cohabitant baboons in its social group,

particularly considering the fact that only a small proportion of baboons experienced any given early adversity. Moreover, the social bond index (mediator) summarizes the interaction between a focal baboon and other members in a social group, and thus we can view the impact from other baboons as constant while examining the variation of social bond for the focal baboon. The notation of $\mathbf{Y}_i^t(z, \mathbf{m})$ makes another implicit assumption that the potential outcomes are determined by the mediator values $\mathbf{m}$ before time t, but not after t. For each unit, we can only observe one realization from the potential mediator or outcome process:

$$\mathbf{M}_i^t = \mathbf{M}_i^t(Z_i) = Z_i \mathbf{M}_i^t(1) + (1 - Z_i)\mathbf{M}_i^t(0), \tag{4.3}$$

$$\mathbf{Y}_i^t = \mathbf{Y}_i^t(z, \mathbf{M}_i^t(Z_i)) = Z_i \mathbf{Y}_i^t(1, \mathbf{M}_i^t(1)) + (1 - Z_i)\mathbf{Y}_i^t(0, \mathbf{M}_i^t(0)). \tag{4.4}$$

We define the total effect (TE) of the treatment Z_i on the outcome process at time t as:

$$\tau_{\text{TE}}^t \quad = \quad E\{Y_i^t(1, \mathbf{M}_i^t(1)) - Y_i^t(0, \mathbf{M}_i^t(0))\}. \tag{4.5}$$

When there is a mediator, the TE can be decomposed into direct and indirect effects. Below we extend the framework of Imai et al. (2010b) to formally define these effects. First, we define the average causal mediation (or indirect) effect (ACME) under treatment z at time t by fixing the treatment status while altering the mediator process:

$$\tau_{\text{ACME}}^t(z) \quad \equiv \quad E\{Y_i^t(z, \mathbf{M}_i^t(1)) - Y_i^t(z, \mathbf{M}_i^t(0))\}, \quad z = 0, 1. \tag{4.6}$$

The ACME quantifies the difference between the potential outcomes, given a fixed treatment status z, corresponding to the potential mediator process under treatment $\mathbf{M}_i^t(1)$ and that under control $\mathbf{M}_i^t(0)$. In the previous literature, variants of the ACME are also called the *natural indirect effect* (Pearl, 2001), or the *pure indirect effect* for $\tau_{\text{ACME}}^t(0)$ and *total indirect effect* for $\tau_{\text{ACME}}^t(1)$ (Robins and Greenland, 1992)

Second, we define the average natural direct effect (ANDE) (Pearl, 2001; Imai et al., 2010b) of treatment on the outcome at time t by fixing the mediator process

while altering the treatment status:

$$\tau^t_{\text{ANDE}}(z) \equiv E\{Y_i^t(1, \mathbf{M}_i^t(z)) - Y_i^t(0, \mathbf{M}_i^t(z))\}. \tag{4.7}$$

The ANDE quantifies the portion in the TE that does not pass through the mediators.

It is easy to verify that the TE is the sum of ACME and ANDE:

$$\tau^t_{\text{TE}} = \tau^t_{\text{ACME}}(z) + \tau^t_{\text{ANDE}}(1-z), \quad z = 0, 1. \tag{4.8}$$

This implies we only need to identify two of the three quantities τ_{TE}, $\tau^t_{\text{ACME}}(z)$, $\tau^t_{\text{ANDE}}(z)$. In this chapter, we will focus on the estimation of τ_{TE} and $\tau^t_{\text{ACME}}(z)$. Because we only observe a portion of all the potential outcomes, we cannot directly identify these estimands from the observed data, which would require additional assumptions.

4.3.2 Identification assumptions

In this subsection, we list the causal assumptions necessary for identifying the ACME and ANDEs with sparse and irregular longitudinal data. There are several sets of identification assumptions in the literature (Robins and Greenland, 1992; Pearl, 2001; Imai et al., 2010a; Shpitser and VanderWeele, 2011) with subtle distinction (Ten Have and Joffe, 2012). Here we follow the similar set of assumptions in Imai et al. (2010b) and Forastiere et al. (2018).

The first assumption extends the standard ignorability assumption and rules out the unmeasured treatment-outcome confounding.

Assumption 1 (Ignorability)**.** *Conditional on the observed covariates, the treatment is unconfounded with respect to the potential mediator process and the potential outcomes process:*

$$\{\mathbf{Y}_i^t(1, \mathbf{m}), \mathbf{Y}_i^t(0, \mathbf{m}), \mathbf{M}_i^t(1), \mathbf{M}_i^t(0)\} \perp\!\!\!\perp Z_i \mid \mathbf{X}_i^t,$$

for any t and $\mathbf{m} \in \mathcal{R}^{[0,t]}$.

In our context, Assumption 1 indicates that there is no unmeasured confounding, besides the observed covariates, between the sources of early adversity and the processes of social bonds and GCs. In other words, early adversity is randomized among the baboons with the same covariates. This assumption is plausible given the early adversity events considered in this study are largely imposed by nature.

The second assumption extending the sequential ignorability assumption in Imai et al. (2010b); Forastiere et al. (2018) to the functional data setting.

Assumption 2 (Sequential Ignorability)**.** *There exists $\varepsilon > 0$, such that for any $0 < \Delta < \varepsilon$,the increment of the mediator process is independent of the increment of potential outcomes process from time t to $t+\Delta$, conditional on the observed treatment status, covariates and the mediator process up to time t:*

$$\{Y_i^{t+\Delta}(z, \mathbf{m}) - Y_i^t(z, \mathbf{m})\} \perp\!\!\!\perp \{M_i^{t+\Delta}(z') - M_i^t(z')\} \mid \{Z_i, \mathbf{X}_i^t, \mathbf{M}_i^t(z'')\},$$

for any $z, z', z'', 0 < \Delta < \varepsilon, t, t + \Delta \in [0, T], \mathbf{m} \in \mathcal{R}^{[0,T]}$.

In our application, Assumption 2 implies that conditioning on the early adversity status, covariates, and the potential social bond history up to a given time point, any change in the social bond values within a sufficiently small time interval Δ is randomized with respect to the change in the potential outcomes. Namely, there are no unobserved mediator-outcomes confounders in a sufficiently small time interval. Though it differs in the specific form, Assumption 2 is in essence the same sequential ignorability assumption used for the regularly spaced observations in Bind et al. (2015) and VanderWeele and Tchetgen Tchetgen (2017). This is a crucial assumption in mediation analysis, but is strong and generally untestable in practice because it is usually impossible to manipulate the mediator values, even in randomized trials.

Assumptions 1 and 2 are illustrated by the directed acyclic graphs (DAG) in Figure 4.2a, which condition on the covariates $\mathbf{X}_i^t$ and a window between two sufficiently close time points t and $t + \Delta$. The arrows between Z_i, M_i^t, Y_i^t represent a causal

relationship (i.e., nonparametric structural equation model), with solid and dashed lines representing measured and unmeasured relationships, respectively. Figure 4.2b and 4.2c depicts two possible scenarios where Assumptions 1 and 2 are violated, respectively, where U_i represents an unmeasured confounder.

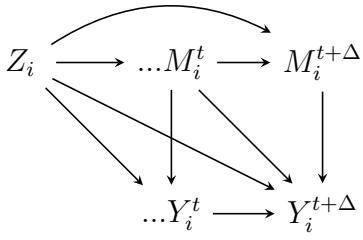

(a) DAG of Assumption 1 and 2

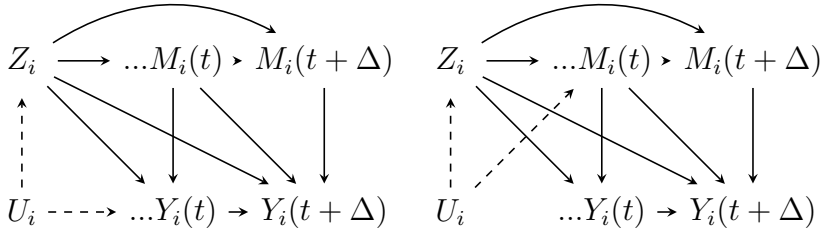

(b) DAG of two examples of violation to Assumption 1 (ignorability)

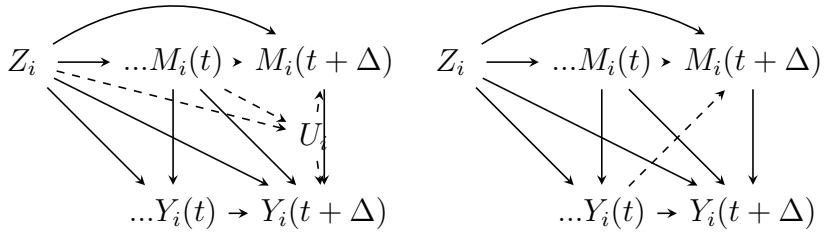

(c) DAG of two examples of violation to Assumption 2 (sequential ignorability)

Figure 4.2: Directed acyclic graphs (DAG) of Assumptions1,2 and examples of possible violations. The arrows between variables represent a causal relationship, with solid and dashed lines representing measured and unmeasured relationships, respectively.

Assumptions 1 and 2 allow nonparametric identification of the TE and ACME from the observed data, as summarized in the following theorem.

Theorem 3. *Under Assumption 1,2, and some regularity conditions (specified in the Section 8.3.1), the TE, ACME and ANDE can be identified nonparametrically from*

the observed data: for $z = 0, 1$, we have

$$\begin{aligned}
\tau_{TE} &= \int_X \{E(Y_i^t|Z_i = 1, \mathbf{X}_i^t = \mathbf{x}^t) - E(Y_i^t|Z_i = 0, \mathbf{X}_i^t = \mathbf{x}^t)\} \mathrm{dF}_{\mathbf{X}_i^t}(\mathbf{x}^t), \\
\tau_{ACME}^t(z) &= \int_{\mathcal{X}} \int_{R^{[0,t]}} E(Y_i^t|Z_i = z, \mathbf{X}_i^t = \mathbf{x}^t, \mathbf{M}_i^t = \mathbf{m}) \mathrm{dF}_{\mathbf{X}_i^t}(\mathbf{x}^t) \times \\
&\qquad \mathrm{d}\{\mathrm{F}_{\mathbf{M}_i^t|Z_i=1, \mathbf{X}_i^t=\mathbf{x}^t}(\mathbf{m}) - \mathrm{F}_{\mathbf{M}_i^t|Z_i=0, \mathbf{X}_i^t=\mathbf{x}^t}(\mathbf{m})\},
\end{aligned}$$

where $F_W(\cdot)$ and $F_{W|V}(\cdot)$ denotes the cumulative distribution of a random variable or a vector W and the conditional distribution given another random variable or vector V, respectively.

The proof of Theorem 3 is provided in the Section 8.3.1. Theorem 3 implies that estimating the causal effects requires modeling two components: (a) the conditional expectation of observed outcome process given the treatment, covariates, and the observed mediator process, $E(Y_i^t|Z_i, \mathbf{X}_i^t, \mathbf{M}_i^t)$, and (b) the distribution of the observed mediator process given the treatment and the covariates, $\mathrm{F}_{\mathbf{M}_i^t|Z_i, \mathbf{X}_i^t}(\cdot)$. These two components correspond to the two linear structural equations in the classic mediation framework of Baron and Kenny (1986). In the setting of functional data, we can employ more flexible models instead of linear regression models, and express the TE and ACME as functions of the model parameters. Theorem 3 can be readily extended to more general scenarios such as discrete (i.e., as opposed to continuous) mediators and time-to-event outcomes.

4.4 Modeling mediator and outcome via functional principal component analysis

In this section, we propose to employ the functional principal component analysis (FPCA) approach to infer the mediator and outcome processes from sparse and irregular observations (Yao et al., 2005; Jiang and Wang, 2010, 2011). In order to take into account the uncertainty due to estimating the functional principal components (Goldsmith et al., 2013), we adopt a Bayesian model to jointly estimate the principal

components and the structural equation models. Specifically, we impose a Bayesian FPCA model similar to that in Kowal and Bourgeois (2020) to project the observed mediator and outcome processes into lower-dimensional representations and then take the first few dominant principal components as the predictors in the structural equation models.

We assume the potential processes for mediators $\mathbf{M}_i^t(z)$ and outcomes $\mathbf{Y}_i^t(z, \mathbf{m})$ have the following Karhunen-Loeve decomposition,

$$M_i^t(z) = \mu_M(\mathbf{X}_i^t) + \sum_{r=1}^{\infty} \zeta_{i,z}^r \psi_r(t), \tag{4.9}$$

$$Y_i^t(z, \mathbf{m}) = \mu_Y(\mathbf{X}_i^t) + \int_0^t \gamma(s,t)\mathbf{m}(s)ds + \sum_{s=1}^{\infty} \theta_{i,z}^s \eta_s(t). \tag{4.10}$$

where $\mu_M(\cdot)$ and $\mu_Y(\cdot)$ are the mean functions of the mediator process $\mathbf{M}_i^t$ and outcome process $\mathbf{Y}_i^t$, respectively; $\psi_r(t)$ and $\eta_s(t)$ are the Normal orthogonal eigenfunctions for $\mathbf{M}_i^t$ and $\mathbf{Y}_i^t$, respectively, and $\zeta_{i,z}^r$ and $\theta_{i,z}^s$ are the corresponding principal scores of unit i. The above model assumes that the treatment affects the mediation and the outcome processes only through the principal scores. We represent the mediator and outcome process of each unit with its principal score $\zeta_{i,z}^r$ and $\theta_{i,z}^s$. Given the principal scores , we can transform back to the smooth process with a linear combination. As such, if we are interested in the differences in the process, it is equivalent to investigate the difference in the principal scores. Also, as we usually require only 3 or 4 components to explain most of the variation, we reduce the dimensions of the trajectories effectively by projecting the difference to the principal scores. With the model specification in (4.10), we make an implicit assumption that the ACME and ANDE are the same in the treatment and control groups in our application, $\tau_{\text{ACME}}^t(0) = \tau_{\text{ACME}}^t(1), \tau_{\text{ANDE}}^t(0) = \tau_{\text{ANDE}}^t(1)$, and thus there are no interactions between the treatment and the mediator. This assumption leads to a unique decomposition of the TE for simple interpretations (VanderWeele, 2014).

The underlying processes $\mathbf{M}_i^t$ and $\mathbf{Y}_i^t$ are not directly observed. Instead, we assume the observations M_{ij}'s and Y_{ij}'s are randomly sampled from the respective

underlying processes with errors. For the observed mediator trajectories, we posit the following model that truncates to the first R principal components of the mediator process:

$$M_{ij} = X'_{ij}\beta_M + \sum_{r=1}^{R} \zeta_i^r \psi_r(t_{ij}) + \varepsilon_{ij}, \quad \varepsilon_{ij} \sim \mathcal{N}(0, \sigma_m^2), \tag{4.11}$$

where $\psi_r(t)$ $(r = 1, ..., R)$ are the orthogonormal principal components, ζ_i^r $(r = 1, ..., R)$ are the corresponding principal scores, and ε_{ij} is the measurement error. With similar parametrization that used in Kowal and Bourgeois (2020), we express the principal components as a linear combination of the spline basis $\mathbf{b}(t) = (1, t, b_1(t), \cdots, b_L(t))'$ in $L + 2$ dimensions and choose the coefficients $\mathbf{p}_r \in \mathcal{R}^{L+2}$ to meet the normal orthogonality constraints of the rth principal component:

$$\psi_r(t) = \mathbf{b}(t)'\mathbf{p}_r, \text{ subject to } \int_0^T \psi_r^2(t)dt = 1, \int_0^T \psi_{r'}(t)\psi_{r''}(t)dt = 0, r' \neq r''. \tag{4.12}$$

We assume the principal scores ζ_i^r are randomly drawn from normal distributions with different means in the treatment and control groups, χ_1^r and χ_0^r, and diminishing variance as r increases:

$$\zeta_i^r \sim \mathcal{N}(\chi_{Z_i}^r, \lambda_r^2), \quad \lambda_1^2 \geq \lambda_2^2 \geq \cdots \lambda_R^2 \geq 0. \tag{4.13}$$

We select the truncation term R based on the fraction of explained variance (FEV), $\sum_{r=1}^{R} \lambda_r^2 / \sum_{r=1}^{\infty} \lambda_r^2$ being greater than 90%.

For the observed outcome trajectories, we posit a similar model that truncates to the first S principal components of the outcome process:

$$Y_{ij} = X_{ij}^T \beta_Y + \int_0^{t_{ij}} \gamma(u, t) M_i^u \mathrm{d}u + \sum_{s=1}^{S} \eta_s(t)\theta_i^s + \nu_{ij}, \quad \nu_{ij} \sim N(0, \sigma_y^2). \tag{4.14}$$

We express the principal components η_s as a linear combination of the spline basis $\mathbf{b}(t)$, with the normal orthogonality constraints:

$$\eta_s(t) = \mathbf{b}(t)'\mathbf{q}_s, \text{ subject to } \int_0^T \eta_s(t)^2 dt = 1, \int_0^T \eta_{s'}(t)\eta_{s''}(t)dt = 0, s' \neq s''. \tag{4.15}$$

Similarly, we assume that the principal scores of the outcome process for each unit come from two different normal distributions in the treatment and control group with means ξ_1^s and ξ_0^s respectively, and a shrinking variance ρ_s^2:

$$\theta_i^s \sim \mathcal{N}(\xi_{Z_i}^s, \rho_s^2), \quad \rho_1^2 \geq \rho_2^2 \geq \cdots \rho_S^2 \geq 0. \tag{4.16}$$

We select the truncation term S based on the FEV being greater than 90%, namely $\sum_{s=1}^{S} \rho_s^2 / \sum_{s=1}^{\infty} \rho_s^2 \geq 90\%$.

We assume the effect of the mediation process on the outcome is concurrent, namely the outcome process at time t does not depend on the past value of the mediation process. As such, $\gamma(u,t)$ can be shrunk to γ instead of the integral in Model (4.14),

$$Y_{ij} = X_{ij}^T \beta_Y + \gamma M_{ij} + \sum_{s=1}^{S} \eta_s(t)\theta_i^s + \nu_{ij}, \quad \nu_{ij} \sim N(0, \sigma_y^2). \tag{4.17}$$

The causal estimands, the TE and ACME, can be expressed as functions of the parameters in the above mediator and outcome models:

$$\tau_{\text{TE}}^t = \sum_{s=1}^{S} (\xi_1^s - \xi_0^s)\eta_s(t) + \gamma \sum_{r=1}^{R} (\chi_1^r - \chi_0^r)\psi_r(t), \tag{4.18}$$

$$\tau_{\text{ACME}}^t = \gamma(\chi_1^r - \chi_0^r)\psi_r(t). \tag{4.19}$$

To account for the uncertainty in estimating the above models, we adopt the Bayesian paradigm and impose prior distributions for the parameters (Kowal and Bourgeois, 2020). For the basis function $\mathbf{b}(t)$ to construct principal components, we choose the thin-plate spline which takes the form $\mathbf{b}(t) = (1, t, (|t-k_1|)^3, \cdots, |t-k_L|^3)' \in \mathcal{R}^{L+2}$, where the k_l $(l = 1, 2, \cdots, L)$ are the pre-defined knots on the time span. We set the values of knots k_l with the quantiles of observation time grids. For the parameters of the principal components, taking the mediator model as an example, we impose the following priors on the parameters in (4.12):

$$\mathbf{p}_r \sim N(0, h_r^{-1}\Omega^{-1}), h_r \sim \text{Uniform}(\lambda_r^2, 10^4),$$

where $\Omega \in \mathcal{R}^{(L+2)\times(L+2)}$ is the roughness penalty matrix and $h_r > 0$ is the smooth parameter. The implies a Gaussian Process prior on $\psi_r(t)$ with mean function zero and covariance function $\text{Cov}(\psi_r(t), \psi_r(s)) = h_r \mathbf{b}'(s)\Omega\mathbf{b}(t)$. We choose the Ω such that $[\Omega_r]_{l,l'} = (k_l - k_l)^2$,when $l, l' > 2$, and $[\Omega_r]_{l,l'} = 0$ when $l, l' \leq 2$. For the distribution of principal scores in (4.13), we specify a multiplicative Gamma prior (Bhattacharya and Dunson, 2011; Montagna et al., 2012) on the variance to encourage shrinkage as r increases,

$$\chi_0^r, \chi_1^r \sim N(0, \sigma^2_{\chi_r}), \quad \sigma^{-2}_{\chi_r} = \prod_{l \leq r} \delta_{\chi l}, \delta_{\chi_1} \sim \text{Ga}(a_{\chi_1}, 1), \delta_{\chi_l} \sim \text{Ga}(a_{\chi_2}, 1), l \geq 2,$$
$$\lambda_r^{-2} = \prod_{l \leq r} \delta_l, \quad \delta_1 \sim \text{Ga}(a_1, 1), \quad \delta_l \sim \text{Ga}(a_2, 1), l \geq 2,$$
$$a_1, a_{\chi_1} \sim \text{Ga}(2, 1), \quad a_2, a_{\chi_2} \sim \text{Ga}(3, 1).$$

Further details on the hyperparameters of the priors can be found in Bhattacharya and Dunson (2011) and Durante (2017). For the coefficients of covariates β_M, we specify a diffused normal prior $\beta_M \sim \mathcal{N}(0, 100^2 * \text{I}_{\dim(X)})$. We impose similar prior distributions for the parameters in the outcome model.

Posterior inference can be obtained by Gibbs sampling. The credible intervals of the causal effects τ^t_{TE} and τ^t_{ACME} can be easily constructed using the posterior sample of the parameters in the model. Details of the Gibbs sampler are provided in the Section 8.3.2.

4.5 Empirical application

4.5.1 Results of FPCA

We apply the method and models proposed in Section 4.3 and 4.4 to the data described in Section 4.2.2 to investigate the causal relationship between early adversity, social bonds and stress in wild baboons. Here we first summarize the results of FPCA of the observed trajectories. We posit model (4.11) for the social bonds and Model (4.17) for the GC concentrations, with some modifications. First, we added two

random effects, one for social group and one for hydrological year, in both models. Second, in the outcome model, we use the log transformed GC concentrations instead of the original scale as the outcome, which allows us to interpret the coefficient as the percent difference in GC concentrations between the treatment and control groups. For both the mediator and outcome processes, the first three functional principal components explain more than 90% of the total variation, and thus we use them in the structural equation model for mediation analysis. Figure 4.3 shows the first two principal components extracted from the mediator (left panel) and outcome (right panel) processes. For the social bond process, the first two principal components explain 53% and 31% of the total variation, respectively. The first component depicts a drastic change in the early stage of a baboon's life and stabilizes afterwards. The second component is relatively stable across the life span. For the GC process, the first two functional principal components explain 54% and 34% of the total variation, respectively. The first component depicts a stable trend throughout the life span. The second component shows a quick rise, then steady drop pattern across the lifespan.

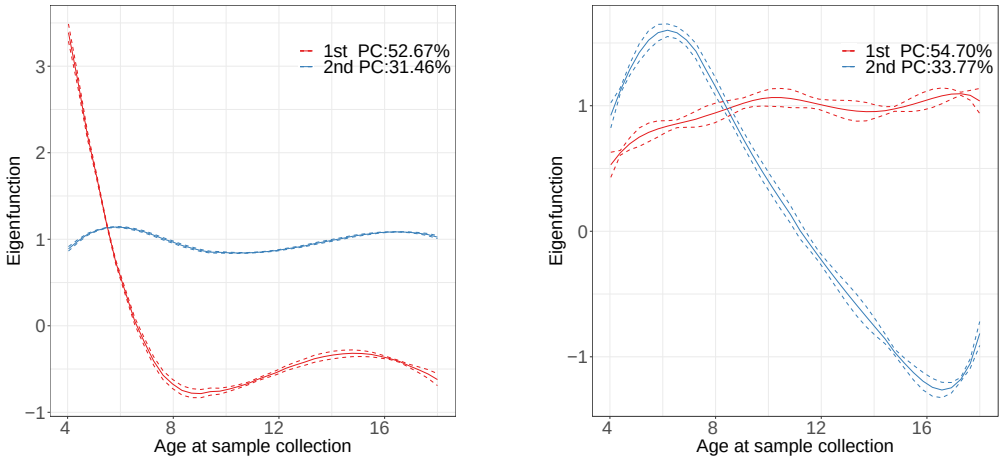

Figure 4.3: The first two functional principal components of the process of the mediator, i.e. social bonds (left panel) and the outcome, i.e., GC concentrations (right panel).

The left panel of Figure 4.4 displays the observed trajectory of GCs versus the

posterior mean of the imputed smooth process of three baboons who experienced zero (EAG), one (OCT), and two (GUI) sources of early adversity, respectively. We can see that the imputed smooth process generally captures the overall time trend of each subject while reducing the noise in the observations. The pattern is similar for the animals' social bonds, which is shown in Section 8.3.3 with a few more randomly selected subjects. Recall that each subject's observed trajectory is fully captured by its vector of principal scores, and thus the principal scores of the first few dominant principal components adequately summarize the whole trajectory. The right panel of Figure 4.4 shows the principal scores of the first (X-axis) versus second (Y-axis) principal component for the GC process of all subjects in the sample, plotted in clusters based on the number of early adversities experienced. We can see that significant differences exist in the distributions of the first two principal scores between the group who experienced no early adversity and the groups experienced one or more sources of adversity.

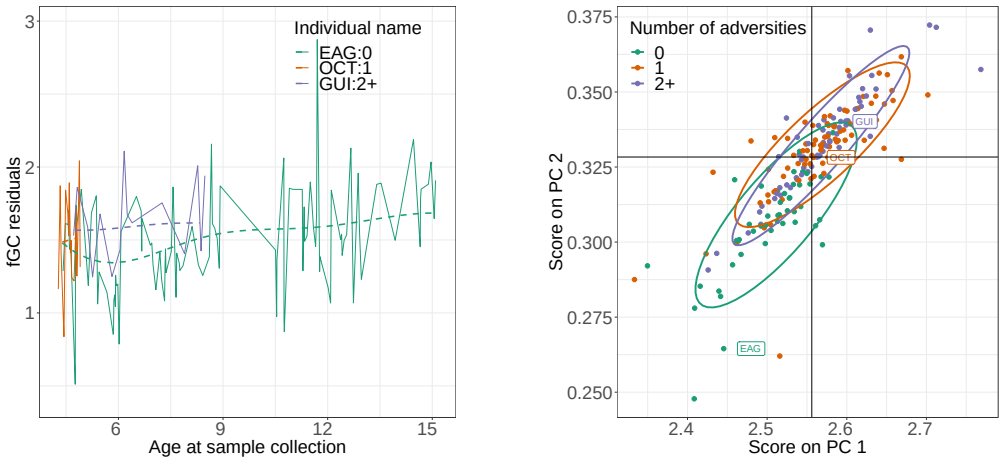

Figure 4.4: Left panel: Observed trajectory of GCs versus the posterior mean of its imputed smooth process of three baboons who experienced zero (EAG), one (OCT) and two (GUI) sources of early adversity, respectively. Right panel: Principal scores of the first (X-axis) versus second (Y-axis) principal component for the GC process of all subjects in the sample; plotted in clusters based on the number of early adversities experienced.

4.5.2 Results of causal mediation analysis

We perform a separate causal mediation analysis for each source of early adversity. Table 4.2 presents the posterior mean and 95% credible interval of the total effect (TE), direct effect (ANDE) and indirect effect mediated through social bonds (ACME) of each source of early adversity on adult GC concentrations, as well as the effects of early adversity on the mediator (social bonds). First, from the first column of Table 4.2 we can see that experiencing any source of early adversity would reduce the strength of a baboon's social bond strength with other baboons in adulthood. The negative effect is particularly severe for those who experienced drought, high group density, or maternal death in early life. For example, compared with the baboons who did not experience any early adversity, the baboons who experienced maternal death have a 0.221 unit decrease in social bonds, translating to a 0.4 standard deviation difference in social bond strength in this population. Overall, experiencing at least one source of early adversity corresponds to social bonds that are 0.2 standard deviations weaker in adulthood.

Second, from the second column of Table 4.2 we can see a strong total effect of early adversity on female baboon's GC concentrations across adulthood. Baboons who experienced at least one source of adversity had GC concentrations that were approximately 9% higher than their peers who did not experience any adversity. Although the range of total effect sizes across all individual adversity sources varies from 4% to 14%, the point estimates are consistently toward higher GC concentrations, even for the early adversity sources for which the credible interval includes zero. Among the individual sources of adversity, females who were born during a drought, into a high-density group, or to a low-ranking mother had particularly elevated GC concentrations (12-14%) in adulthood, although the credible interval of high group density includes zero.

Third, while female baboons who experienced harsh conditions in early life show higher GC concentrations in adulthood, we found no evidence that these effects were

Table 4.2: Total, direct and indirect causal effects of individual and cumulative sources of early adversity on social bonds and GC concentrations in adulthood in wild female baboons. 95% credible intervals are in the parenthesis.

Source of adversity	effect on mediator	τ_{TE}	τ_{ACME}	τ_{ANDE}
Drought	-0.164	0.124	0.009	0.114
	$(-0.314, -0.014)$	$(0.007, 0.241)$	$(0.000, 0.017)$	$(0.005, 0.222)$
Competing sibling	-0.106	0.084	0.006	0.078
	$(-0.249, 0.030)$	$(-0.008, 0.172)$	$(0.003, 0.009)$	$(-0.012, 0.163)$
High group density	-0.271	0.123	0.015	0.108
	$(-0.519, -0.023)$	$(-0.052, 0.281)$	$(0.000, 0.029)$	$(-0.053, 0.252)$
Maternal death	-0.221	0.061	0.011	0.049
	$(-0.423, -0.019)$	$(-0.006, 0.129)$	$(0.005, 0.014)$	$(-0.014, 0.113)$
Low maternal rank	-0.052	0.134	0.008	0.126
	$(-0.298, 0.001)$	$(0.011, 0.256)$	$(0.005, 0.011)$	$(0.008, 0.244)$
Maternal social isolation	-0.040	0.035	0.002	0.033
	$(-0.159, 0.095)$	$(-0.045, 0.116)$	$(0.000, 0.005)$	$(-0.044, 0.111)$
At least one	-0.102	0.092	0.007	0.084
	$(-0.195, -0.008)$	$(0.005, 0.178)$	$(0.002, 0.009)$	$(0.009, 0.159)$

significantly mediated by the absence of strong social bonds. Specifically, the mediation effect τ_{ACME} (third column in Table 4.2) is consistently small; the strength of females' social bonds with other females accounted for a difference in GCs of only 0.85% when averaged across the six individual adversity sources, even though the credible intervals did not include zero for five of the six individual adversity sources. On the other hand, the direct effects τ_{ANDE} (fourth column in Table 4.2) are much stronger than the mediation effects. When averaged across the six adversity sources, the direct effect of early adversity on GC concentrations was 11.6 times stronger than the mediation effect running through social bonds. For example, for females who experienced at least one source of early adversity, the direct effect explain an 8.4% difference in GC concentrations, while the mediation effect only takes up 0.7% for the difference in GCs.

We also assess the plausibility of the key causal assumptions in the application. One possible violation can be due to 'feedback' between the social bond and GC processes, as is shown in Figure 4.2c. We performed a sensitivity analysis by adding (a) the most recent prior observed GC value, or (b) the average of all past observed GC values, as a predictor in the mediation model, which led to little difference in

the results and thus bolsters sequential ignorability. Though we are not aware of the existence of other sequential confounders, we also cannot rule them out.

The above findings on the causal relationships among early adversity, social bonds, and GC concentrations in wild baboons are compatible with observations in many other species that early adversity and weak relationships both give rise to poor health, and that early adversity predicts various forms of social dysfunction, including weaker relationships. However, they call into question the notion that social bonds play a major role in mediating the effect of early adversity on poor health. In wild female baboons, any such effect appears to be functionally biologically irrelevant or minor.

4.6 Simulations

In this section, we conduct simulations to further evaluate the operating characteristics of the proposed method and compare it with two standard methods.

4.6.1 Simulation design

We generate 200 units to approximate the sample size in our application. For each unit, we make T_i observations at the time grid $\{t_{ij} \in [0,1], j = 1, 2, \cdots, T_i\}$. We draw T_i from a Poisson distribution with mean T and randomly pick t_{ij} uniformly:

$$T_i \sim \text{Poisson}(T), \quad t_{ij} \sim \text{Uniform}(0,1), \quad j = 1, 2, \cdots, T_i.$$

For each unit i and time j, we generate three covariates from a tri-variate Normal distribution, $\mathbf{X}_{ij} = (X_{ij1}, X_{ij2}, X_{ij3}) \sim \mathcal{N}([0,0,0]^T, \sigma_X^2 \mathrm{I}_3)$. We simulate the binary treatment indicator from $Z_i = \mathbf{1}\{c_{i1} > 0\}$, where $c_{i1} \sim \mathcal{N}(0,1)$. To simulate the sparse and irregular mediator trajectories, we first simulate a smooth underlying process $M_i^t(z)$ for the mediators:

$$M_i^t(z) = 0.2 + \{0.2 + 2t + \sin(2\pi t)\})(z+1) - X_{ij1} + 0.5X_{ij2} + \varepsilon_i^m(t) + c_{i2},$$

where the error term $\varepsilon_i^m(t) \sim \text{GP}(0, \sigma_m^2 \exp\{-8(s-t)^2\})$ is drawn from a Gaussian Process (GP) with an exponential kernel and σ_m^2 controlling the volatility of the realized curves, and $c_{i2} \sim \mathcal{N}(0, \sigma_m^2)$ to represent the individual random intercepts. The mean value of the mediator process depends on the covariates and time index t. The polynomial term and the trigonometric function of t introduce the long term growth trend and periodic fluctuations, respectively. Also, the coefficient of z evolves as the time changes, implying a time-varying treatment effect on the mediator. Similarly, we specify a GP model for the outcome process,

$$\begin{aligned} Y_i^t(z, \mathbf{m}) &= \mathbf{m}^t + \cos(2\pi t) + 0.1t^2 + 2t + \{\cos(2\pi t) + 0.2t^2 + 3t\}z - \\ &\quad 0.5X_{ij2} + X_{ij3} + \varepsilon_i^y(t) + c_{i3}, \end{aligned}$$

where the error term $\varepsilon_i^y(t) \sim \text{GP}(0, \sigma_y^2 \exp\{-8(s-t)^2\})$ is drawn from a GP, and $c_{i3} \sim \mathcal{N}(0, \sigma_y^2)$ controls the individual random effects for the outcome process.

The above settings imply non-linear true causal effects (τ_{TE}^t and τ_{ACME}^t) in time, which are shown as the dashed lines in Figure 4.5. Upon simulating the processes, we evaluate the potential values of the mediators and outcomes at the sampled time point t_{ij} to obtain the observed trajectories with measurement error:

$$M_{ij} \sim \mathcal{N}(\mathbf{M}_i^{t_{ij}}(Z_i), 1), \quad Y_{ij} \sim \mathcal{N}(\mathbf{Y}_i^{t_{ij}}(Z_i, \mathbf{M}_i^{t_{ij}}(Z_i)), 1).$$

We control the sparsity of the mediator and outcome trajectories by varying the value of T in the grid of $(15, 25, 50, 100)$, namely the average number of observations for each individual.

We compare the proposed method in Section 4.4 (abbreviated as MFPCA) with two standard methods in longitudinal data analysis: the random effects model (Laird and Ware, 1982) and the generalized estimating equations (GEE) (Liang and Zeger, 1986). To facilitate the comparisons, we aggregate the time-varying mediation effects into the following scalar values:

$$\tau_{\text{ACME}} = \int_0^T \tau_{\text{ACME}}^t \mathrm{d}t, \quad \tau_{\text{TE}} = \int_0^T \tau_{\text{TE}}^t \mathrm{d}t.$$

The true values for τ_{ACME} and τ_{TE} in the simulations are 1.20 and 2.77 respectively.

For the random effects approach, we fit the following two models:

$$M_{ij} = X_{ij}^T \beta_M + s_m(T_{ij}) + \tau_m Z_i + r_{ij}^m + \varepsilon_{ij}^m,$$
$$Y_{ij} = X_{ij}^T \beta_Y + s_y(T_{ij}) + \tau_y Z_i + \gamma M_{ij} + r_{ij}^y + \varepsilon_{ij}^y,$$

where r_{ij}^m and r_{im}^y are normally distributed random effects with zero means, $s_m(T_{ij})$ and $s_y(T_{ij})$ are thin plate splines to capture the nonlinear effect of time. To model the time dependency, we specify an AR(1) correlation structure for the random effects, thus $\text{Corr}(r_{ij}^m, r_{ij+1}^m) = p_1, \text{Corr}(r_{ij}^y, r_{ij+1}^y) = p_2$, namely the correlation decay exponentially within the observations of a given unit. Given the above random effects model, the mediation effect and TE can be calculated as: $\hat{\tau}_{\text{ACME}}^{\text{RD}} = \hat{\gamma}\hat{\tau}_m, \hat{\tau}_{\text{TE}}^{\text{RD}} = \hat{\gamma}\hat{\tau}_m + \hat{\tau}_y$.

For the GEE approach, we specify the following estimation equations:

$$E(M_{ij}|X_{ij}, Z_i) = X_{ij}^T \beta_M + \tau_m Z_i,$$
$$E(Y_{ij}|M_{ij}, X_{ij}, Z_i) = X_{ij}^T \beta_M + \tau_y Z_i + \gamma M_{ij}.$$

For the working correlation structure, we consider the AR(1) correlation for both the mediators and outcomes. Similarly, we obtain the estimations through $\hat{\tau}_{\text{ACME}}^{\text{GEE}} = \hat{\gamma}\hat{\tau}_m, \hat{\tau}_{\text{TE}}^{\text{GEE}} = \hat{\gamma}\hat{\tau}_m + \hat{\tau}_y$ with two different correlation structures.

It is worth noting that both the random effects model and the GEE model generally lack the flexibility to accommodate irregularly-spaced longitudinal data, which renders specifying the correlation between consecutive observations difficult. For example, though the AR(1) correlation takes into account the temporal structure of the data, it still requires the correlation between any two consecutive observations to be constant, which is unlikely to be the case in use cases with irregularly-spaced data. Nonetheless, we compare the proposed method with these two models as they are the standard methods in longitudinal data analysis.

4.6.2 Simulation results

We apply the proposed MFPCA method, the random effects model, and the GEE model in Section 4.6.1 to the simulated data $\{Z_i, \mathbf{X}_{ij}, M_{ij}, Y_{ij}\}$, to estimate the causal effects τ_{TE} and τ_{ACME}.

Figure 4.5 shows the causal effects and associated 95% credible interval estimated from MFPCA in one randomly selected simulated dataset under each of the four levels of sparsity T. Regardless of T, MFPCA appears to estimate the time-varying causal effects satisfactorily, with the 95% credible interval covering the true effects at any time. As expected, the accuracy of the estimation increases as the frequency of the observations increases.

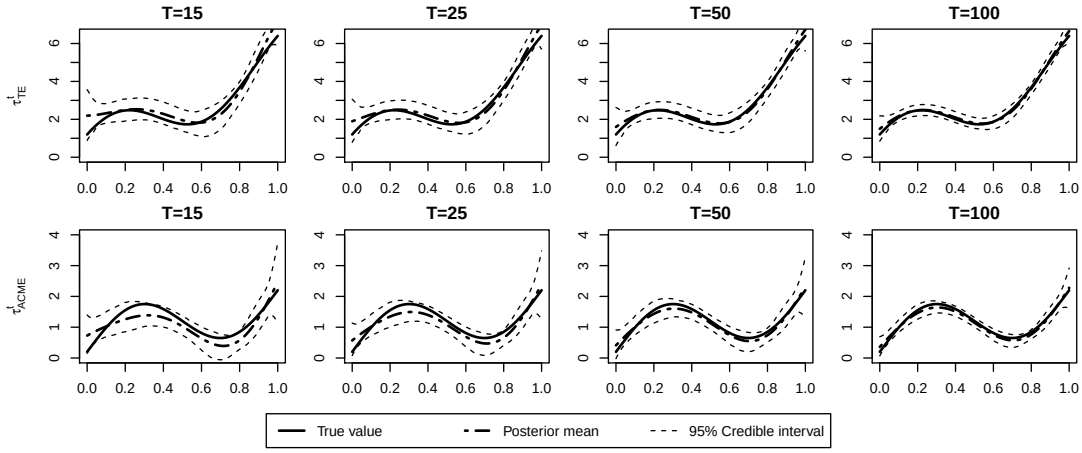

Figure 4.5: Posterior mean of τ^t_{TE},τ^t_{ACME} and 95% credible intervals in one simulated dataset under each level of sparsity with 200 units. The solid lines are the true surfaces for τ^t_{TE} and τ^t_{ACME}

Table 4.3 presents the absolute bias, root mean squared error (RMSE) and coverage rate of the 95% confidence interval of τ_{TE} and τ_{ACME} under the MFPCA, the random effects model and the GEE model based on 1000 simulated datasets for each level of sparsity T in $[15, 25, 50, 100]$. The performance of all three methods improves as the frequency of observations increases. With low frequency ($T < 100$), i.e. sparse observations, MFPCA consistently outperforms the random effects model, which in

turn outperforms GEE in all measures. The advantage of MFPCA over the other two methods diminishes as the frequency increases. In particular, with dense observations ($T = 100$), MFPCA leads to similar results as random effects, though both still outperform GEE. The simulation results bolster the use of our method in the case of sparse data.

We also conducted the same simulations with larger sample sizes, $N = 500, 1000$. MFPCA's advantage over the random effects and GEE models in terms of bias and RMSE increases as the sample size increases. With $N = 500$, MFPCA already achieves a coverage rate close to the nominal level. We leave the detailed results to Section 8.3.4.

Table 4.3: Absolute bias, RMSE and coverage rate of the 95% confidence interval of MFPCA, the random effects model and the generalized estimating equation (GEE) model under different frequency of observations in the simulations.

	τ_{TE}			τ_{ACME}		
Method	Bias	RMSE	Coverage	Bias	RMSE	Coverage
			T=15			
MFPCA	0.103	0.154	88.4%	0.134	0.273	86.4%
Random effects	0.165	0.208	78.2%	0.883	1.673	69.5%
GEE	0.183	0.304	77.6%	0.987	2.051	61.8%
			T=25			
MFPCA	0.092	0.123	92.3%	0.102	0.246	90.6%
Random effects	0.124	0.165	81.2%	0.679	1.263	72.3%
GEE	0.152	0.273	80.3%	0.860	1.753	64.4%
			T=50			
MFPCA	0.087	0.112	93.5%	0.094	0.195	92.3%
Random effects	0.109	0.134	90.3%	0.228	0.497	88.8%
GEE	0.121	0.175	83.5%	0.236	0.493	80.8%
			T=100			
MFPCA	0.053	0.089	94.3%	0.064	0.163	93.1%
Random effects	0.046	0.093	93.1%	0.053	0.154	92.8%
GEE	0.093	0.124	90.5%	0.098	0.161	90.3%

5

Double robust representation learning

5.1 Introduction

Causal inference is central to decision-making in healthcare, policy, online advertising and social sciences. The main hurdle to causal inference is confounding, *i.e.*, factors that affect both the outcome and the treatment assignment (VanderWeele and Shpitser, 2013). For example, a beneficial medical treatment may be more likely assigned to patients with worse health conditions; then directly comparing the clinical outcomes of the treated and control groups, without adjusting for the difference in the baseline characteristics, would severely bias the causal comparisons and mistakenly conclude the treatment is harmful. Therefore, a key in de-biasing causal estimators is to balance the confounding covariates or features.

This chapter focuses on using observational data to estimate treatment effects, defined as the contrasts between the counterfactual outcomes of the same study units under different treatment conditions (Neyman, 1990; Rubin, 1974). In observational studies, researchers do not have direct knowledge on how the treatment is assigned, and substantial imbalance in covariates between different treatment groups is prevalent. A classic approach for balancing covariates is to assign an importance weight to each unit so that the covariates are balanced after reweighting (Hirano et al., 2003; Hainmueller, 2012; Imai and Ratkovic, 2014; Li et al., 2018a; Kallus, 2018a). The weights usually involve the *propensity score* (Rosenbaum and Rubin, 1983) – a summary of the treatment assignment mechanism. Another stream of conventional causal methods directly model the outcome surface as a function of the covariates under treated and control condition to impute the missing counterfactual outcomes

(Rubin, 1979; Imbens et al., 2005; Hill, 2011).

Advances in machine learning bring new tools to causal reasoning. A popular direction employs the framework of representation learning and impose balance in the representation space (Johansson et al., 2016; Shalit et al., 2017; Zhang et al., 2020). These methods usually separate the tasks of propensity score estimation and outcome modeling. However, recent theoretical evidence reveals that good performance in predicting either the propensity score or the observed outcome alone does not necessarily translate into good performance in estimating the causal effects (Belloni et al., 2014). In particular, Chernozhukov et al. (2018) pointed out it is necessary to combine machine learning models for the propensity score and the outcome function to achieve $\sqrt{N}$ consistency in estimating the average treatment effect (ATE). A closely related concept is double-robustness (Scharfstein et al., 1999; Lunceford and Davidian, 2004b; Kang et al., 2007), in which an estimator is consistent if either the propensity score model or the outcome model, but not necessarily both, is correctly specified. A similar concept also appears in the field of reinforcement learning for policy evaluation (Dudík et al., 2011; Jiang and Li, 2016; Kallus and Uehara, 2019). Double-robust estimators are desirable because they give analysts two chances to "get it right" and guard against model misspecification.

This chapter highlights the following contributions: (i) We propose to regularize the representations with the entropy of an optimal weight for each unit, obtained via an entropy balancing procedure. (ii) We show that minimizing the entropy of balancing weights corresponds to a regularization on Jensen-Shannon divergence of the low-dimensional representation distributions between the treated and control groups, and more importantly, leads to a double-robust estimator of the ATE. (iii) We show that the entropy of balancing weights can bound the generalization error and therefore reduce ITE prediction error.

5.2 Background

5.2.1 Setup and assumptions

Assume we have a sample of N units, with N_0 in treatment group and N_1 in control group. Each unit i ($i = 1, 2, \cdots, N$) has a binary treatment indicator T_i ($T_i = 0$ for control and $T_i = 1$ for treated), p features or covariates $\mathbf{X}_i = (X_{1i}, \cdots, X_{ji}, \cdots, X_{pi}) \in \mathcal{R}^p$. Each unit has a pair of potential outcomes $\{Y_i(1), Y_i(0)\}$ corresponding to treatment and control, respectively, and causal effects are contrasts of the potential outcomes. We define individual treatment effect (ITE), also known as conditional average treatment effect (CATE) for context x as: $\tau(x) = E\{Y_i(1) - Y_i(0)|X_i = x\}$, and the average treatment effect (ATE) as: $\tau_{\text{ATE}} = E\{Y_i(1) - Y_i(0)\} = E_x\{\tau(x)\}$. The ITE quantifies the effect of the treatment for the unit(s) with a specific feature value, whereas ATE quantities the average effect over a target population. When the treatment effects are heterogeneous, the discrepancy between ITE for some context and ATE can be large. Despite the increasing attention on ITE in recent years, average estimands such as ATE remain the most important and commonly reported causal parameters in a wide range of disciplines. Our method is targeted at estimating ATE, but we will also examine its performance in estimating ITE.

For each unit, only the potential outcome corresponding to the observed treatment condition is observed, $Y_i = Y_i(T_i) = T_i Y_i(1) + (1 - T_i)Y_i(0)$, and the other is counterfactual. Therefore, additional assumptions are necessary for estimating the causal effects. Throughout the discussion, we maintain two standard assumptions:

Assumption 3 (Ignorabililty)**.** $\{Y_i(1), Y_i(0)\} \perp\!\!\!\perp T_i \mid X_i$

Assumption 4 (Overlap)**.** $0 < P(T_i = 1|X_i) < 1$.

Under Assumption 3 and 4, treatment effects can be identified from the observed data. In observational studies, there is often significant imbalance in the covariates distributions between the treated and control groups, and thus directly comparing

the average outcome between the groups may be lead to biased causal estimates. Therefore, an important step to de-bias the causal estimators is to balance the covariates distributions between the groups, which usually involves the propensity score $e(x) = P(T_i = 1|X_i = x)$, a summary of the treatment assignment mechanism. Once good balance is obtained, one can also build an outcome regression model $f_t(x) = E(Y(t)|X_i = x)$ for $t = 0, 1$ to impute the counterfactual outcomes and estimate ATE and ITE via the vanilla estimator $\hat{\tau}_{\text{ATE}} = \sum_{i=1}^{N}\{\hat{f}_1(X_i) - \hat{f}_0(X_i)\}/N$ and $\hat{\tau}(x) = \hat{f}_1(x) - \hat{f}_0(x)$.

5.2.2 Related work

Double robustness A *double-robust* (DR) estimator combines the propensity score and outcome model; a common example for ATE (Robins et al., 1994; Lunceford and Davidian, 2004b) is:

$$\hat{\tau}^{\text{DR}}_{\text{ATE}} = \sum_{i=1}^{N} \hat{w}_i^{\text{IPW}}(2T_i - 1)\{Y_i - \hat{f}_{T_i}(X_i)\} + \frac{1}{N}\sum_{i=1}^{N}\{\hat{f}_1(X_i) - \hat{f}_0(X_i)\}, \tag{5.1}$$

where $w_i^{\text{IPW}} = \frac{T_i}{e(X_i)} + \frac{(1-T_i)}{1-e(X_i)}$ is the inverse probability weights (IPW). DR estimator has two appealing benefits: (i) it is DR in the sense that it remains consistent if either propensity score model or outcome model is correctly specified, not necessarily both; (ii) it reaches the semiparametric efficiency bound of τ_{ATE} if both models are correctly specified (Hahn, 1998; Chernozhukov et al., 2018). However, the finite-sample variance for $\hat{\tau}^{\text{DR}}_{\text{ATE}}$ can be quite large when the IPW have extreme values, which is likely to happen with severe confoundings. Several variants of the DR estimator have been proposed to avoid extreme importance weights, such as clipping or truncation (Bottou et al., 2013; Wang et al., 2017; Su et al., 2019). We propose a new weighting scheme, combined with the representation learning, to calculate the weights with less extreme values and maintain the double robustness.

Representation learning with balance regularization For causal inference with high-dimensional or complex observational data, an important consideration is

dimension reduction. Specifically, we may wish to find a representations $\Phi(\cdot) = [\Phi_1(\cdot), \Phi_2(\cdot), \cdots, \Phi_m(\cdot)] : \mathbb{R}^p \to \mathbb{R}^m$ of the original space, and build the model based on the representations $\Phi(x)$ instead of directly on the features x, $f_t(\Phi(x))$. To this end, Johansson et al. (2016) and Shalit et al. (2017) proposed to combine predictive power and covariate balance to learn the representations, via minimizing the following type of loss function in the Counterfactual Regression (CFR) framework:

$$\arg\min_{f,\Phi}\{\sum_{i=1} L(f_{T_i}(\Phi(\mathbf{X}_i)), Y_i) + \kappa \cdot \mathbb{D}(\{\Phi(X_i)\}_{T_i=0}, \{\Phi(X_i)\}_{T_i=1})\}, \tag{5.2}$$

where the first term measures the predictive power the representation Φ, the second term measures the distance between the representation distribution in treated and control groups, and κ is a hyperparameter controlling the importance of distance. This type of loss function targets learning representations that are predictive of the outcome and well balanced between the groups. Choice of the distance measure $\mathbb{D}$ in (5.2) is crucial for the operating characteristics of the method; popular choices include the Integral Probability Measure (IPM) such as the Wasserstein (WASS) distance (Villani, 2008; Cuturi and Doucet, 2014) or Maximum Mean Discrepancy (MMD)(Gretton et al., 2009a).

Concerning related modifications of (5.2), in Zhang et al. (2020), the authors argue that balancing representations in (5.2) may over-penalize the model when domain overlap is satisfied and propose to use the counterfactual variance as a measure for imbalance, which can also address measure the "local" similarity in distribution. In Hassanpour and Greiner (2019) the authors reweight regression terms with inverse probability weights (IPW) estimated from the representations. In Johansson et al. (2018), the authors tackle the distributional shift problem, for which they alternately optimize a weighting function and outcome models for prediction jointly to reduce the generalization error.

The optimization problem (5.2) only involves the outcome model $f_t(x)$, misspecification of which would likely introduce biased causal estimates. In contrast, the class of causal estimators of DR estimators like (5.1) combine the propensity score model

with the outcome model to add robustness against model misspecifications. A number of DR causal estimators for high-dimensional data have been proposed (Belloni et al., 2014; Farrell, 2015; Antonelli et al., 2018), but none has incorporated representation learning. Below we propose the first DR representation learning method for counterfactual prediction. The key is the entropy balancing procedure, which we briefly review below.

Entropy balancing To mitigate the extreme weights problem of IPW in (5.1), one stream of weighting methods learn the weights by minimizing the variation of weights subject to a set of balancing constraints, bypassing estimating the propensity score. Among these, entropy balancing (EB) (Hainmueller, 2012) has received much interest in social science (Ferwerda, 2014; Marcus, 2013). EB was originally designed for estimating the average treatment effect on the treated (ATT), but is straightforward to adapt to other estimands. Specifically, the EB weights for ATE, are obtained via the following programming problem:

$$\begin{aligned} \boldsymbol{w}^{\text{EB}} &= \arg\,\max_w \left\{ -\sum_{i=1}^{N} w_i \log w_i, \right\}, \\ \text{s.t.} \quad & \begin{cases} \text{(i)} \sum_{T_i=0} w_i X_{ji} = \sum_{T_i=1} w_i X_{ji}, \forall j \in [1:p], \\ \text{(ii)} \sum_{T_i=0} w_i = \sum_{T_i=1} w_i = 1, w_i > 0. \end{cases} \end{aligned} \tag{5.3}$$

Covariate balancing is enforced by the the first constraint (i), also known as the moment constraint, that the weighted average for each covariate of respective treatment groups are equal. Generalizations to higher moments are straight forward although less considered in practice. The second constraint simply ensures the weights are normalized. This objective is an instantiation of the maximal-entropy learning principle (Jaynes, 1957a,b), a concept derived from statistical physics that stipulates the most plausible state of a constrained physical system is the one maximizes its entropy. Intuitively, EB weights penalizes the extreme weights while keeps balancing condition satisfied.

Though the construction of EB does not explicitly impose models for either $e(x)$

or $f_t(x)$, Zhao and Percival (2017) showed that EB implicitly fits a linear logistic regression model for the propensity score and a linear regression model for the outcome simultaneously, where the predictors are the covariates pr representations being balanced. Entropy balancing is DR in the sense that if only of the two models are correctly specified, the EB weighting estimator is consistent for the ATE. Note that the original EB procedure does not provide ITE estimation, which is explored in this work.

5.3 Methodology

5.3.1 Proposal: unifying covariate balance and representation learning

Based on the discussion above, we propose a novel method to learn DR representations for counterfactual predictions. Our development is motivated by an insightful heuristic: the entropy of balancing weight is a proxy measure of the covariate imbalance between the treatment groups. To understand the logic behind this intuition, recall the more dis-similar two distributions are, the more likely extreme weights are required to satisfy the matching criteria, and consequently resulting a bigger entropy for the balancing weight. See Figure 5.1 also for a graphical illustration of this. In Section 5.3.3, we will formalize this intuition based on information-theoretic arguments.

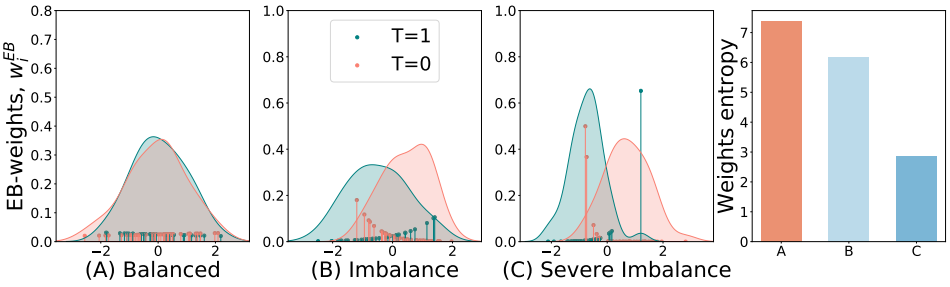

Figure 5.1: When covariates imbalance is more severe, the balance weights w_i^{EB} deviate more from uniform distribution, inducing a lower entropy

We adjust the constrained EB programming problem from (5.3) to (5.4), achieving the balance among the representations/transformed features. As we shall see later, this distance metric, entropy of balancing weights, leads to desirable theoretical properties in both ATE and ITE estimation.

$$\begin{aligned} \boldsymbol{w}^{\text{EB}} &= \arg\,\max_w \left\{ -\sum_{i=1}^{N} w_i \log w_i, \right\}, \\ \text{s.t.} \quad & \begin{cases} \text{(i)} \sum_{T_i=0} w_i \Phi(X_{ji}) = \sum_{T_i=1} w_i \Phi(X_{ji}), \\ \text{(ii)} \sum_{T_i=0} w_i = \sum_{T_i=1} w_i = 1, w_i > 0. \end{cases} \end{aligned} \tag{5.4}$$

Specifically, we propose to learn a low-dimensional representation of the feature space, $\Phi(\cdot)$, through minimizing the following loss function:

$$\arg\min_{f,\Phi} \overbrace{\{\sum_i (Y_i - f_{t=T_i}(\Phi(X_i)))^2}^{\text{prediction loss on observed outcomes}} + \underbrace{\kappa \sum_{i=1} w_i^{\text{EB}}(\Phi) \log w_i^{\text{EB}}(\Phi)\}}_{\text{distance metric, balance regularization}}, \tag{5.5}$$

where we replace the distance metrics in (5.2) with the entropy of $w_i^{\text{EB}}(\phi)$, function of the representation as implied in the notation, which is the solution to (5.4). At first sight, solving the system defined by (5.4) and (5.5) is challenging, because the gradient can not be back-propagated through the nested optimization (5.4). Another appealing property of EB is computational efficiency. We can solve the dual problem of (5.4):

$$\min_{\boldsymbol{\lambda}} \{\log \left(\sum_{T_i=0} \exp\left(\langle \boldsymbol{\lambda}_0, \Phi_i \rangle\right) \right) + \log \left(\sum_{T_i=1} \exp\left(\langle \boldsymbol{\lambda}_1, \Phi_i \rangle\right) \right) - \langle \boldsymbol{\lambda}_0 + \boldsymbol{\lambda}_1, \bar{\Phi} \rangle\}, \tag{5.6}$$

where $\boldsymbol{\lambda}_0, \boldsymbol{\lambda}_1 \in \mathbb{R}^m$ are the Lagrangian multipliers, $\bar{\Phi} \triangleq \sum_i \Phi_i$ is the unnormalized mean and $\langle \cdot, \cdot \rangle$ denote the inner product. Note that (5.6) is a convex problem wrt $\boldsymbol{\lambda}$, and therefore can be efficiently solved using standard convex optimization packages when the sample size is small. Via appealing to the Karush–Kuhn–Tucker (KKT) conditions, the optimal EB weights $\boldsymbol{w}^{\text{EB}}$ can be given in the following Softmax form

$$w_i^{\text{EB}}(\Phi) = \frac{\exp(\eta_i)}{\sum_{T_k=T_i}\exp(\eta_k)}, \eta_i \triangleq -(2T_i-1)\langle \boldsymbol{\lambda}_{T_i}^{\text{EB}}, \Phi_i\rangle, \tag{5.7}$$

where $\boldsymbol{\lambda}_t^{\text{EB}}, t \in \{0,1\}$ is the solution to the dual problem (5.6). Equation (5.7) shows how to explicitly express the entropy weights as a function of the representation Φ, thereby enabling efficient end-to-end training of the representation. Compared to the CFR framework, we have replaced the IPM matching term $\mathbb{D}_{\text{IPM}}(q_0 \parallel q_1)$ with the entropy term $\mathbb{H}(\boldsymbol{w}^{\text{EB}}) = \sum_i w_i^{\text{EB}} \log w_i^{\text{EB}}$. When applied to the ATE estimation, the commensurate learned entropy balancing weights $\boldsymbol{w}^{\text{EB}}$ guarantees the $\tau_{\text{ATE}}(\boldsymbol{w}^{\text{EB}})$ to be DR. For ITE estimation, $\mathbb{H}(\boldsymbol{w}^{\text{EB}})$, as a regularization term in (5.5), can bound the ITE prediction error.

A few remarks are in order. For reasons that will be clear in Section 5.3.3, we will restrict f_t to the family of linear functions, to ensure the nice theoretical properties of DRRL. Note that is not a restrictive assumption, as many schemes seek representations that can linearize the operations. For instance, outputs of a deep neural nets are typically given by a linear mapping of the penultimate layers. Many modern learning theories, such as reproducing kernel Hilbert space (RKHS), are formulated under inner product spaces (*i.e.*, generalized linear operations).

After obtaining the representation $\hat{\Phi}(x)$, the outcome function $\hat{f}_t$, and the EB weights $\hat{w}_i^{\text{EB}}$, we have the following estimators of τ_{ATE} and $\tau(x)$,

$$\hat{\tau}_{\text{ATE}}^{\text{EB}} = \sum_{i=1}^{N} \hat{w}_i^{\text{EB}}(2T_i-1)\{Y_i - \hat{f}_{T_i}(\hat{\Phi}(X_i))\} + \frac{1}{N}\sum_{i=1}^{N}\{\hat{f}_1(\hat{\Phi}(X_i)) - \hat{f}_0(\hat{\Phi}(X_i))\}, \tag{5.8}$$

$$\hat{\tau}^{\text{EB}}(x) = \hat{f}_1(\hat{\Phi}(x)) - \hat{f}_0(\hat{\Phi}(x)). \tag{5.9}$$

In practice, we can parameterize the representations by θ as $\Phi_\theta(\cdot)$ and the outcome function by $\gamma = (\gamma_0, \gamma_1)$ as $f_{t,\gamma}(\cdot) = f_{\gamma_t}(\cdot) = \langle \gamma_t, \Phi_\theta\rangle$ to learn the θ, γ instead.

5.3.2 Practical implementation

We now propose an algorithm – referred as *Double Robust Representations Learning* (DRRL) – to implement the proposed method when we parameterize the represen-

tations Φ_θ by neural networks. DRRL simultaneously learn the representations Φ_θ, the EB weights w_i^{EB} and the outcome function $f_{t,\gamma}$. The network consists of a representation layer performing non-linear transformation of the original feature space, an entropy-balancing layer solving the dual programming problem in (5.6) and a final layer learning the outcome function. We visualize the DRRL architecture in Figure 5.2.

We train the model by iteratively solving the programming problem in (5.4) given the representations Φ and minimizing the loss function in (5.5) given the optimized weights w_i^{EB}. As we have successfully expressed EB weights, and consequently the entropy term, directly through the learned representation Φ in (5.7), it enables efficient gradient-based learned schemes, such as stochastic gradient descent, for the training of DRRL using modern differential programming platforms (*e.g.*, tensorflow, pytorch). As an additional remark, we note although the Lagrangian multiplier $\boldsymbol{\lambda}$ is computed from the representation Φ, its gradient with respect to Φ is zero based on the Envelop theorem (Carter, 2001). This impliess we can safely treat $\boldsymbol{\lambda}$ as if it is a constant in our training objective.

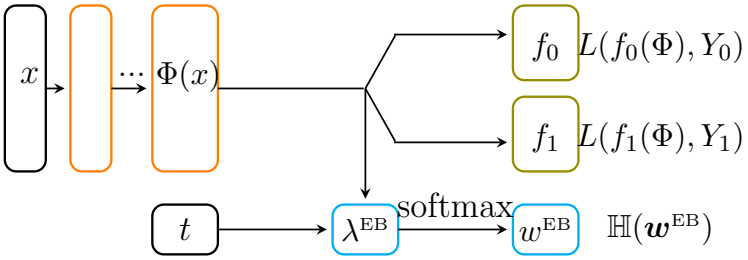

Figure 5.2: Architecture of the DRRL network

Adaptation to ATT estimand So far we have focused on DR representations for ATE; the proposed method can be easily modified to other estimands. For example, for the average treatment effect on the treated (ATT), we can modify the EB constraint to $\sum_{T_i=0} w_i \Phi_{ji} = \sum_{T_i=1} \Phi_{ji}/N_1$ and change the objective function to $-\sum_{T_i=0} w_i \log w_i$ in (5.4). For ATT, we only need to reweight the control group to match the distribution of the treated group, which remains the same. Thus we only

Algorithm 1: Double Robust Representation Learning

Input: data $\{Y_i, T_i, X_i\}_{i=1}^N$,
Hyperparameters: importance of balance κ, dimension of representations m, batch size B, learning rate η.
Initialize $\theta^0, \gamma^0, \boldsymbol{\lambda}^0$.
for $k = 1$ **to** K **do**
  Sample batch data $\{Y_i, X_i, T_i\}_{i=1}^B$
  Calculate $\Phi(X_i) = \Phi_{\theta^{k-1}}(X_i)$ for each i in the batch
  Entropy balance steps: Calculate the gradient of objective in (5.6) with respect to $\boldsymbol{\lambda}$, $\nabla_{\boldsymbol{\lambda}}$, update $\boldsymbol{\lambda}^k = \boldsymbol{\lambda}^{k-1} - \eta \nabla_{\boldsymbol{\lambda}}$.
  Learn representations and outcome function: calculate the gradient of loss (5.5) in the batch data with respect to θ and γ, $\nabla_\theta, \nabla_\gamma$. Update the parameters: $\theta^k = \theta^{k-1} - \eta \nabla_\theta$,$\gamma^k = \gamma^{k-1} - \eta \nabla_\gamma$.
end for
Calculate the weights w_i^{EB} with formula (5.7).
Output $\Phi_\theta(\cdot), f_{t,\gamma}, w_i^{\mathbf{EB}}$

impose balancing constraints on the weighted average of representations of the control units; the objective function only applies to the weights of the control units. In the Section 8.4.2, we also provide theoretical proofs for the double-robustness property of the ATT estimator.

Scalable generalization A bottleneck in scaling up our algorithm to large data is solving optimization problem (5.6) in the entropy balancing stage. Below we develop a scalable updating scheme with the idea of Fenchel mini-max learning in Tao et al. (2019). Specifically, let $g(d)$ be a proper convex, lower-semicontinuous function; then its convex conjugate function $g^*(v)$ is defined as $g^*(v) = \sup_{d \in \mathcal{D}(g)}\{dv - g(d)\}$, where $\mathcal{D}(g)$ denotes the domain of the function g (Hiriart-Urruty and Lemaréchal, 2012); g^* is also known as the Fenchel conjugate of g, which is again convex and lower-semicontinuous. The Fenchel conjugate pair (g, g^*) are dual to each other, in the sense that $g^{**} = g$, *i.e.*, $g(v) = \sup_{d \in \mathcal{D}(g^*}\{dv - g^*(d)\}$. As a concrete example, $(-\log(d), -1 - \log(-v))$ gives such a pair, which we exploit for our problem. Based on the Fenchel conjugacy, we can derive the mini-max training rule for the entropy-

balancing objective in (5.6), for $t = 0, 1$:

$$\min_{\boldsymbol{\lambda}_t}\{\max_{u_t}\{u_t - \exp(u_t)\sum_{T_i=t}\exp\left(\langle\boldsymbol{\lambda}_t, \Phi_i\rangle\right)\} - \langle\boldsymbol{\lambda}_t, \Phi_i\rangle\}. \tag{5.10}$$

5.3.3 Theoretical properties

In this section we establish the nice theoretical properties of the proposed DRRL framework. Limited by space, detailed technical derivations on Theorem 4, 5 and 6 are deferred to Section 8.4.1.

Our first theorem shows that, the entropy of the EB weights as defined in (5.5) asymptotically converges to a scaled α-Jensen-Shannon divergence (JSD) of the representation distribution between the treatment groups.

Theorem 4 (EB entropy as JSD)**.** *The Shannon entropy of the EB weights defined in* (5.4) *converges in probability to the following α-Jensen-Shannon divergence between the marginal representation distributions of the respective treatment groups:*

$$\begin{aligned}&\lim_{n\to\infty}\mathbb{H}_n^{EB}(\Phi) \triangleq \sum_i w_i^{EB}(\Phi)\log(w_i^{EB}(\Phi))\\ &\xrightarrow{p} c'\{\mathrm{KL}(p_\Phi^1(x)||p_\Phi(x)) + \mathrm{KL}(p_\Phi^0(x)||p_\Phi(x))\} + c'' = c'\mathrm{JSD}\alpha(p_\Phi^1, p_\Phi^0) + c''\end{aligned} \tag{5.11}$$

where $c' > 0, c''$ are non-zero constants, $p_\Phi^t(x) = P(\Phi(\mathbf{X}_i = x)|T_i = t)$ is representation distribution in group t ($t = 0, 1$), $p_\Phi(x)$ is the marginal density of the representations, α is the proportion of treated units $P(T_i = 1)$ and $\mathrm{KL}(\cdot||\cdot)$ is the Kullback–Leibler (KL) divergence.

An important insight from Theorem 4 is that entropy of EB weights is an endogenous measure of representation imbalance, validating the insight in Sec 5.3.1 theoretically. This theorem bridges the classical weighting strategies with the modern representation learning perspectives for causal inference, that representation learning and propensity score modeling are inherently connected and does not need to be modeled separately.

Theorem 5 (Double Robustness)**.** *Under the Assumption 3 and 4, the entropy balancing estimator* $\hat{\tau}_{ATE}^{EB}$ *is consistent for* τ_{ATE} *if either the true outcome models* $f_t(x), t \in \{0,1\}$ *or the true propensity score model logit*$\{e(x)\}$ *is linear in representation* $\Phi(x)$*.*

Theorem 5 establishes the DR property of the EB estimator $\hat{\tau}^{\text{EB}}$. Note that the double robustness property will not be compromised if we add regularization term in (5.5). Double robust setups require modeling both the outcome function and propensity score; in our formulation, the former is explicitly specified in the first component in (5.5), while the latter is implicitly specified via the EB constraints in (5.4). By M-estimation theory (Stefanski and Boos, 2002), we can show that λ^{EB} in (5.6) converges to the maximum likelihood estimate λ^* of a logistic propensity score model, which is equivalent to the solution of the following optimization problem,

$$\min_{\lambda} \quad \sum_{i=1}^{N} \log(1 + \exp(-(2T_i - 1) \sum_{j=1}^{m} \lambda_j \Phi_j(X_i))). \tag{5.12}$$

Jointly these two components constructs the double robustness property of estimator $\hat{\tau}_{\text{ATE}}^{\text{EB}}$. The linearity restriction on f_t is essential for double robustness, and may appear to be tight, but because the representations $\Phi(x)$ can be complex functions such as multi-layer neural networks (as in our implementation), both the outcome and propensity score models are flexible.

The third theorem shows that the objective function in (5.5) is an upper bound of the loss for the ITE. Before proceeding to the third theorem, we define a few estimation loss functions: Let $L(y, y')$ be the loss function on predicting the outcome, $l_{f,\Phi}(x,t)$ denote the expected loss for a specific covariates-treatment pair (x,t) given outcome function f and representation,

$$l_{f,\Phi}(x,t) = \int_y L(Y(t), f_t(\Phi_x)) P(Y(t)|x) dY(t). \tag{5.13}$$

Suppose the covariates follow $\mathbf{X}_i \in \mathcal{X}$ and we denote the distributions in treated and control group with $p_t(x) = p(X_i = x | T_i = t), t = 0, 1$. For a given f and Φ, the

expected factual loss over the distributions in the treated and control groups are,

$$\varepsilon_{\mathrm{F}}^{t}(f,\Phi) \;=\; \int_{\mathcal{X}} l_{f,\phi}(x,t)p_t(x)dx, t=0,1, \tag{5.14}$$

For the ITE estimation, we define the expected Precision in Estimation of Heterogeneous Effect (PEHE) (Hill, 2011),

$$\varepsilon_{\mathrm{PEHE}}(f,\Phi) = \int_{\mathcal{X}} (f_1(\Phi(x)) - f_0(\Phi(x)) - \tau(x))^2 p(x)dx. \tag{5.15}$$

Assessing $\varepsilon_{\mathrm{PEHE}}(f,\Phi)$ from the observational data is infeasible, as the countefactual labels are absent, but we can calculate the factual loss $\varepsilon_{\mathrm{F}}^{t}$. The next theorem illustrates we can bound $\varepsilon_{\mathrm{PEHE}}$ with $\varepsilon_{\mathrm{F}}^{t}$ and the α-JS divergence of $\Phi(x)$ between the treatment and control groups.

Theorem 6. *Suppose $\mathcal{X}$ is a compact space and $\Phi(\cdot)$ is a continuous and invertible function. For a given f,Φ, the expected loss for estimating the ITE, $\varepsilon_{\mathrm{PEHE}}$, is bounded by the sum of the prediction loss on the factual distribution $\varepsilon_{\mathrm{F}}^{t}$ and the α-JS divergence of the distribution of Φ between the treatment and control groups, up to some constants:*

$$\varepsilon_{PEHE}(f,\Phi) \leq 2\cdot(\varepsilon_{\mathrm{F}}^{0}(f,\Phi) + \varepsilon_{\mathrm{F}}^{1}(f,\Phi) + C_{\Phi,\alpha}\cdot \mathrm{JSD}_{\alpha}(p_{\Phi}^{1}, p_{\Phi}^{0}) - 2\sigma_{Y}^{2}), \tag{5.16}$$

where $C_{\Phi,\alpha} > 0$ is a constant depending on the representation Φ and α, and $\sigma_{Y}^{2} = \max_{t=0,1} E_X[\{(Y_i(t) - E(Y_i(t)|X))^2|X\}]$ is the expected conditional variance of $Y_i(t)$.

The third theorem shows that the objective function in (5.5) is an upper bound to the loss for the ITE estimation, which cannot be estimated based on the observed data. This theorem justifies the use of entropy as the distance metric in bounding the ITE prediction error.

5.4 Experiments

We evaluate the proposed DRRL on the fully synthetic or semi-synthetic benchmark datasets. The experiment validates the use of DRRL and reveals several crucial

properties of the representation learning for counterfactual prediction, such as the trade-off between balance and prediction power. The experimental details can be found in Section 8.4.3.

5.4.1 Experimental setups

Hyperparameter tuning, architecture As we only know one of the potential outcomes for each unit, we cannot perform hyperparameter selection on the validation data to minimize the loss. We tackle this problem in the same manner as Shalit et al. (2017). Specifically, we use the one-nearest-neighbor matching method (Abadie and Imbens, 2006) to estimate the ITE for each unit, which serves as the ground truth to approximate the prediction loss. We use fully-connected multi-layer perceptrons (MLP) with ReLU activations as the flexible learner. The hyperparameters to be selected in the algorithm include the architecture of the network (number of representation layer, number of nodes in layer), the importance of imbalance measure κ, batch size in each learning step. We provide detailed hyperparameter selection steps in section 8.4.3.

Datasets To explore the performance of the proposed method extensively, we select the following three datasets: (i) **IHDP** (Hill, 2011; Shalit et al., 2017): a semi-synthetic benchmark dataset with known ground-truth. The train/validation/test splits is 63/27/10 for 1000 realizations;(ii) **JOBS** (LaLonde, 1986): a real-world benchmark dataset with a randomized study and an observational study. The outcome for the Jobs dataset is binary, so we add a sigmoid function after the final layer to produce a probability prediction and use the cross-entropy loss in (5.5); (iii) high-dimensional dataset, **HDD**: a fully-synthetic dataset with high-dimensional covariates and varying levels of confoundings. We defer its generating mechanism to Section 5.4.4.

Evaluation metrics To measure the performance of different counterfactual predictions algorithms, we consider the following evaluation metrics for both average

causal estimands (including ATE and ATT) and ITE: (i) the absolute bias for ATE or ATT predictions $\varepsilon_{\text{ATE}} = |\hat{\tau}_{\text{ATE}} - \tau_{\text{ATE}}|, \varepsilon_{\text{ATT}} = |\hat{\tau}_{\text{ATT}} - \tau_{\text{ATT}}|$; (ii) the prediction loss for ITE, $\varepsilon_{\text{PEHE}}$; (iii) *policy risk*, quantifies the effectiveness of a policy depending on the outcome function $f_t(x)$, $R_{\text{POL}} \triangleq 1 - E(Y_i(1)|\pi_f(X_i) = 1)p(\pi_f = 1) - E(Y_i(1)|\pi_f(X_i) = 0)p(\pi_f = 0)$. It measures the risk of the policy π_f, which assigns treatment $\pi_f = 1$ if $f_1(x) - f_0(x) > \delta$ and remains as control otherwise.

Baselines We compare DRRL with the following state-of-the-art methods: ordinary least squares (OLS) with interactions, k-nearest neighbor (k-NN), Bayesian Additive Regression Trees (BART) (Hill, 2011), Causal Random Forests (Causal RF) (Wager and Athey, 2018a), Counterfactual Regression with Wasserstein distance (CFR-WASS) or Maximum Mean Discrepancy (CFR-MMD) and their variant without balance regularization, the Treatment-Agnostic Representation Network(TARNet) (Shalit et al., 2017). We also evaluate the models that separate the weighting and representation learning procedure. Specifically, we replace the distance metrics in (5.5) with other metrics like MMD or WASS, and perform entropy balancing on the learned representations (EB-MMD or EB-WASS).

5.4.2 Learned balanced representations

We first examine how DRRL extracts balanced representations to support counterfactual predictions. In Figure 5.3, we select one imbalanced case from IHDP dataset and perform t-SNE (t-Distributed Stochastic Neighbor Embedding) (Maaten and Hinton, 2008) to visualize the distribution of the original feature space and the representations learned from DRRL algorithm when $\kappa = 1, 1000$. While the original covariates are imbalanced, the learned representations or the transformed features have more similarity in distributions across two arms. Especially, a larger κ value leads the algorithm to emphasize on the balance of representations and gives rise to a nearly identical representations across two groups. However, an overly large κ may deteriorate the performance, because the balance is improved at the cost of predictive

power.

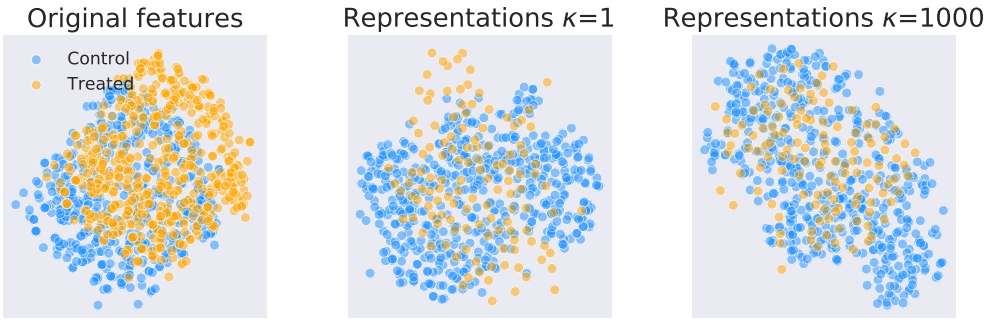

Figure 5.3: t-SNE visualization of original features, representations by DRRL when setting $\kappa = 1, 1000$.

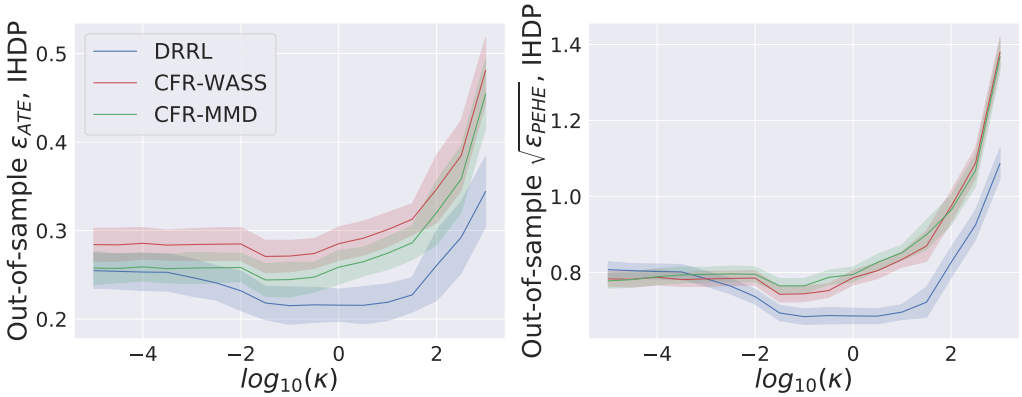

Figure 5.4: The sensitivity against the relative importance of balance κ of ε_{ATE} (left) and $\varepsilon_{\text{PEHE}}$ (right). Lower is better.

To see how the importance of balance constraint affects the prediction performance, we plot the ε_{ATE} and $\varepsilon_{\text{PEHE}}$ in IHDP dataset against the hyperparameter κ (on log scale) in Figure 5.4, for CFR-WASS, CFR-MMD and DRRL, which involve tuning κ in the algorithms. We obtain the lowest ε_{ATE} or $\varepsilon_{\text{PEHE}}$ at the moderate level of balance for the representations. This pattern makes sense as the perfect balance might compromise the prediction power of representations, while the poor balance

cannot adjust for the confoundings sufficiently. Also, the DRRL is less sensitive to the choice κ compared with CFR-WASS and CFR-MMD, with as the prediction loss has a smaller variation for different κ.

Table 5.1: Results on IHDP datasets with 1000 replications, JOBS data and HDD dataset with 100 replications, average performance and its standard deviations. The models parametrized by neural network are in bold fonts

	IHDP		**JOBS**		**HDD-A**		**HDD-B**		**HDD-C**	
	ε_{ATE}	$\sqrt{\varepsilon_{\text{PEHE}}}$	ε_{ATT}	R_{POL}	ε_{ATE}	$\sqrt{\varepsilon_{\text{PEHE}}}$	ε_{ATE}	$\sqrt{\varepsilon_{\text{PEHE}}}$	ε_{ATE}	$\sqrt{\varepsilon_{\text{PEHE}}}$
OLS	$0.96 \pm .06$	$6.6 \pm .32$	$0.08 \pm .04$	$0.27 \pm .03$	–	–	–	–	–	–
k-NN	$0.48 \pm .04$	$3.9 \pm .66$	$0.11 \pm .04$	$0.27 \pm .03$	$1.53 \pm .14$	$7.71 \pm .36$	$1.56 \pm .18$	$6.94 \pm .39$	$1.78 \pm .23$	$6.95 \pm .40$
BART	$0.36 \pm .04$	$3.2 \pm .39$	$0.08 \pm .03$	$0.28 \pm .03$	$0.97 \pm .03$	$5.63 \pm .28$	$0.98 \pm .06$	$4.31 \pm .28$	$0.94 \pm .08$	$3.94 \pm .31$
Causal RF	$0.36 \pm .03$	$4.0 \pm .44$	$0.09 \pm .03$	$0.24 \pm .03$	$0.85 \pm .05$	$5.52 \pm .16$	$0.93 \pm .05$	$4.14 \pm .20$	$0.87 \pm .06$	$3.17 \pm .27$
TARNet	$0.29 \pm .02$	$0.94 \pm .03$	$0.10 \pm .03$	$0.28 \pm .03$	$1.05 \pm .06$	$4.78 \pm .16$	$1.30 \pm .08$	$3.02 \pm .17$	$1.28 \pm .09$	$3.28 \pm .23$
CFR-MMD	$0.25 \pm .02$	$0.76 \pm .02$	$0.08 \pm .03$	$0.26 \pm .03$	$1.12 \pm .05$	$4.45 \pm .15$	$1.24 \pm .05$	$2.71 \pm .16$	$1.21 \pm .08$	$3.03 \pm .20$
CFR-WASS	$0.27 \pm .02$	$0.74 \pm .02$	$0.08 \pm .03$	$0.27 \pm .03$	$1.11 \pm .06$	$4.48 \pm .14$	$1.15 \pm .07$	$2.92 \pm .16$	$1.22 \pm .08$	$2.91 \pm .19$
EB-MMD	$0.30 \pm .02$	$0.76 \pm .03$	$0.04 \pm .01$	$0.26 \pm .03$	$1.07 \pm .05$	$4.45 \pm .15$	$0.98 \pm .05$	$2.71 \pm .16$	$1.00 \pm .08$	$3.03 \pm .20$
EB-WASS	$0.29 \pm .02$	$0.78 \pm .03$	$0.04 \pm .01$	$0.27 \pm .03$	$1.05 \pm .06$	$4.48 \pm .14$	$1.03 \pm .07$	$2.92 \pm .16$	$1.02 \pm .08$	$2.91 \pm .19$
DRRL	$\mathbf{0.21 \pm .03}$	$\mathbf{0.68 \pm .02}$	$\mathbf{0.03 \pm .02}$	$\mathbf{0.25 \pm .02}$	$\mathbf{1.01 \pm .04}$	$4.53 \pm .15$	$\mathbf{0.96 \pm .04}$	$\mathbf{2.70 \pm .16}$	$\mathbf{0.88 \pm .06}$	$\mathbf{2.57 \pm .17}$

5.4.3 Performance on semi-synthetic or real-world dataset

ATE estimation We can see a significant gain in ATE estimation of DRRL over most state-of-the-art algorithms in the IHDP data, as in Table 5.1; this is expected, as DRRL is designed to improve the inference of average estimands. The advantage remains even if we shift to binary outcome and the ATT estimand in the JOBS data, as in Table 5.1. Moreover, compared with EB-MMD or EB-WASS which separates out the weights learning and representation learning, the proposed DRRL also achieve a lower bias in estimating ATE. This demonstrates the benefits of learning the weights and representation jointly instead of separating them out.

ITE estimation The DRRL has a better performance compared with the state-of-the-art methods like CFR-MMD on the IHDP dataset for ITE prediction. For the binary outcome in the JOBS data, the DRRL gives a better R_{ROL} over most methods except for the Causal RF when setting threshold $\delta = 0$. In Figure 5.5, we plot the policy risk as a function of the inclusion rate $p(\pi_f = 1)$, through varying the threshold value δ. The straight dashed line is the random policy assigning treatment with probability π_f, serving as a baseline for the performance. The vertical line shows

the π_f when $\delta = 0$. The DRRL are persistently gives a lower R_{ROL} as we vary the inclusion rate of the policy

5.4.4 High-dimensional performance and double robustness

We generate HDD datasets from the following model:

$$X_i \sim \mathcal{N}(0, \sigma^2[(1-\rho)I_p + \rho 1_p 1_p^T])$$
$$||\beta_0||_0 = ||\beta_\tau||_0 = ||\gamma||_0 = p^*, \text{supp}(\beta_0) = \text{supp}(\beta_\tau)$$
$$P(T_i = 1) = \text{sigmoid}(X_i\gamma)$$
$$Y_i(t) = X_i\beta_0 + tX_i\beta_\tau + \varepsilon_i, \varepsilon_i \sim \mathcal{N}(0, \sigma_e^2), t = 0, 1,$$

where $\beta_0, \beta_\tau, \gamma$ are the parameters for outcome and treatment assignment model. We consider sparse cases where the number of nonzero elements in $\beta_0, \beta_\tau, \gamma$ is much smaller than the total feature size $p^* << p$. The support for β_0, β_τ is the same, for simplicity.

Three scenarios are considered, by varying the overlapping support of γ and β_0, β_τ: (i) scenario A (high confounding), the set of the variables determining the outcome and treatment assignment are identical, $||\text{supp}(\beta_0) \cap \text{supp}(\gamma)||_0 = p^*$; (ii) scenario B (moderate confounding), these two sets have 50% overlapping, $||\text{supp}(\beta_0) \cap \text{supp}(\gamma)||_0 = p^*/2$; scenario C (low confounding), these two sets do not overlap, $||\text{supp}(\beta_0) \cap \text{supp}(\gamma)||_0 = 0$. We set $p = 2000, p^* = 20, \rho = 0.3$ and generate the data of size $N = 800$ each time, with 54/21/25 train/validation/test splits. We report the ε_{ATE} and $\varepsilon_{\text{PEHE}}$ in Table 5.1[1]. The DRRL obtains the lowest error in estimating ATE, except for the Causal RF and BART, and achieve comparable performance in predicting ITE in all three scenarios.

This experiment also demonstrates the superiority of double robustness. The advantage of DRRL increases as the overlap between the predictors in the outcome

[1]We omit the OLS here as it is the true generating model.

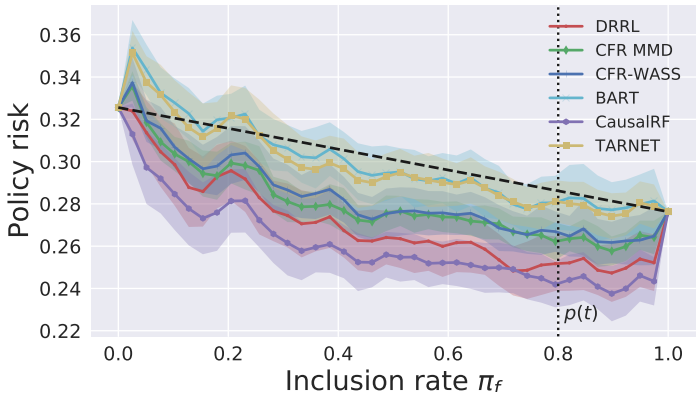

Figure 5.5: The policy risk curve for different methods, using the random policy as a benchmark (dashed line). Lower value is better.

function and those in the propensity score diminishes (from Scenario A to C), especially for ATE estimation. This illustrates the benefit of double robustness: when the representation learning fails to capture the predictive features of the outcomes, entropy balancing offers a second chance of correction via sample reweighting.

6

Causal transfer random forest

6.1 Introduction

A central assumption of the majority of machine learning algorithms is that training and testing data is collected independently and identically from an underlying distribution. Contrary to this assumption, in many scenarios training data is collected under different conditions than the deployed environment (Quionero-Candela et al., 2009). For example, online services commonly use counterfactual models of user behavior to evaluate system and policy changes prior to online deployment (Bayir et al., 2019). In these scenarios, models train on interaction data gathered from previously deployed versions of the system, yet must make predictions in the context of the new system (prior to deployment). Other domains with distribution or covariate shifts include text and image classification (Daume III and Marcu, 2006; Wang and Deng, 2018), information extraction (Ben-David et al., 2007), as well as prediction and now-casting (Lazer et al., 2014).

Conventional machine learning algorithms exploit all correlations to predict a target value. Many of these correlations, however, can shift when parts of the environment are unrelated to our task change. Viewed from a causal perspective, the challenge is to distinguish causal relationships from unstable spurious correlations, as well as to disentangle the influence of co-varying features with the target value (Peters et al., 2016; Rojas-Carulla et al., 2018; Arjovsky et al., 2019). For example, in the counterfactual click prediction task we may wish to predict whether a user would have clicked on a link if we change the page layout (Figure 6.1). Training a prediction model based on current click logged data will find many factors related

to an observation of a click (*e.g.*, display choices such as location and formatting, as well as factors related to ad quality and relevance). Yet, these factors are often entangled and co-vary due to platform policy, such as giving higher quality links more visual prominence through their location and formatting. In other cases, correlations may be unstable across environments as data generating mechanisms or the platform policy changes. A click prediction model based on this data may be unable to determine how much the likelihood of a click is due to relevant contextual features versus environmental factors. As long as the correlations among these features do not change, the prediction model will perform well. However, when the system is changed—perhaps a new page layout algorithm reassigns prominence or locations for links —the prediction model will fail to generalize. Moreover, such drastic system changes are very common in practice, which will be discussed in the real-application section.

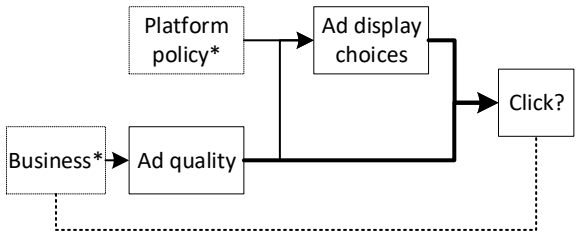

Figure 6.1: Challenges of robust prediction in a click prediction task: While click likelihood depends on display choices and ad quality, those two factors will co-vary in a way that changes as platform policy shifts. Other correlations (e.g,. business attributes) are unstable across environments.

One way to disentangle causal relationships from merely correlational ones is through experimentation (Cook et al., 2002; Kallus et al., 2018). For example, if we randomize the location of links on a page it will break the spurious correlations between page location and all other factors. This allows us to determine the true influence or the "causal effect" of page location on click likelihood. Unfortunately, randomizing all important aspects of a system and policy is often prohibitively ex-

pensive, as employing the random platform policy in the system generally induces revenue loss compared with the a well-tuned production system. Gathering the scale of randomization data necessary for building a good prediction model is frequently not possible. Therefore, it is desirable to efficiently combine the relatively small scale randomized data and the large scale logged data for robust predictions after the policy changes.

In this chapter, motivated by an offline evaluation application in the sponsored search engine, we describe a *causal transfer random forest* (CTRF). The proposed CTRF combines existing large-scale training data from past logs (**L-data**) with a small amount of data from a randomized experiment (**R-data**) to better learn the causal relationships for robust predictions. It uses a two-stage learning approach. First, we learn the CTRF tree structure from the **R-data**. This allows us to learn a decision structure that disentangles all the relevant randomized factors. Second, we calibrate each node (such as calculating the click probability) of the CTRF with both the **L-data** and the **R-data**. The calibration step allows us to achieve the high-precision predictions that are possible with large-scale data. Further, we complement our intuitions with theoretical foundations, showing that the model structure training on randomized data should provide a robust prediction across covariate shifts.

Our contributions in this chapter are 3-fold. Firstly, we introduce a new method for building robust prediction models that combine large-scale **L-data** with a small amount of **R-data**. Secondly, we provide a theoretical interpretation of the proposed method and its improved performance from the causal reasoning and invariant learning perspective. Lastly, we provide an empirical evaluation of the robustness improvements of this algorithm in both synthetic experiments and multiple experiments in a real-world, large-scale online system at Bing Ads.

6.2 Related work

6.2.1 Off-policy learning in online systems

This chapter is motivated from the task of performing offline policy evaluation in the online system (Bottou et al., 2013; Li et al., 2012). Occasionally, we would like to know the outcome of performing an unexplored tuning in the current system, which is also known as the counterfactual outcome. For example, we are interested in the change in users click probability after modifying the auction mechanism in the online ads system (Varian, 2007). Sometimes, the modifications can be drastic from the previous policy. Instead of running the costly online A/B testing (Xu et al., 2015), some offline methods are frequently used to predict the counterfactual outcomes based on the existing logged data from the current system. One novel solution is to build the model-based simulator. Specifically, we build the model simulating the users behaviour and measure the metrics change after implementing the proposed policy changes in the simulator (Bayir et al., 2019). We usually train the user-simulator model on the **L-data** generating under previous platform policy. As a result, the covariate shift problem happens if the proposed change is drastic.

6.2.2 Transfer learning and domain adaptation

The discrepancy across training (large scale logged data e.g.) and testing (data after policy change e.g.) distribution is a long-standing problem in the machine learning community. Classic supervised learning might suffer from the generalization problem when the training data has a different distribution with the data for testing, which is also referred to the covariate (or distribution or dataset) shift problem, or the domain adaptation task (Quionero-Candela et al., 2009; Bickel et al., 2009; Daume III and Marcu, 2006). Specifically, the model learned on a training data (source domain) is not necessarily minimizing the loss on the testing distribution (target domain). This hampers the ability of the model to transfer from one distribution or domain to

another one.

Some researchers propose to correct for the difference through sample reweighting (Neal, 2001; Huang et al., 2007). Ideally, we wish to weight each unit in the training set so that we can learn a model minimizing the loss averaged on the testing distribution after reweighting. However, this strand of approaches requires the knowledge of the testing distribution to estimate the density and is likely to fail when the testing distribution deviates a lot from the training distribution, with extreme values in the density ratio. Another type of methods is feature based. Some approaches aim at learning the features or representations that have predictive power while remaining a similar marginal distribution across source and target domain (Zhang et al., 2013; Ganin et al., 2016). However, the balance on marginal distributions does not ensure a similar performance on the target domain. We need to justify the predictive performance for the learnt features on the target domain.

6.2.3 Causality and invariant learning

Recently, some methods adapt the idea from causal inference to define the transfer learning with assumptions on the causality relationship among the features (Peters et al., 2016; Magliacane et al., 2018; Rojas-Carulla et al., 2018; Meinshausen, 2018; Kuang et al., 2018; Arjovsky et al., 2019; Huang et al., 2020). Specifically, researchers paraphrase the transfer difficulty as the confounding problem in causal inference literature (Pearl, 2009; Imbens and Rubin, 2015). The reason for poor generalization performance is that the model is learning some spurious correlation relationships on the source domain, which are not expected to hold on the target domain. The invariant features across the domains should be the direct causes of the outcome (suppose being not intervened), as the causality relationship is presumably to be stable across training and testing distribution (Pearl et al., 2009). Our work focus on utilizing the **R-data** generating from a random policy, which is formally defined later, to exploit the causal relationship with limited sample size. Within the same

causality framework, our model learns the invariant features that can transfer to the unknown target domain and be robust to severe covariate shifts.

6.3 Causal Transfer Random Forest

In this section, we formulate the covariate shift problem and the transfer task. First, we formalize the problem and illustrate its role in sponsored search. Second, we introduce our proposed causal transfer random forest method, which can efficiently extract causality information from randomized data and improve generalization for a new testing distribution. Third, we provide theoretical interpretation for the proposed algorithm with causal reasoning.

6.3.1 Problem setup

Let $y \in \mathcal{Y}$ be a binary outcome label given contextual features $x \in \mathcal{R}^p$ and intervenable features, $z \in \mathcal{R}^{p'}$. We desire a model to map from the feature space to a distribution over the outcome space, *i.e.* learning the conditional distribution $p(y|x, z)$. Taking our motivating application, sponsored search, as a concrete example, the contextual features x include user context and the query issued by the user; the features z encode aspects that the publishers can manipulate, for instance, the location or the quality of the ads; and y is whether or not a user clicked on the ad. In practice, an advertising system takes many steps to create the pages showing the ads.

The feature shift problem arises when there is a drastic change in the joint features distribution of $p(x, z)$. This shift might happen if the marginal distribution of contextual feature $p(x)$ varies. More commonly, the shift occurs when $p(z|x)$ changes to another distribution $p^*(z|x)$, namely, we change the data generating mechanism for z. This can happen when the platform policy change in the sponsored search system. In this case, the model learned from the training distribution $p(x, z) = p(x)p(z|x)$ might not generalize to the new distribution $p^*(x, z) = p(x)p^*(z|x)$. Therefore, we

wish to learn a model $p(y|x,z)$ that is robust to the feature distribution, which can be safely transferred from original feature distribution $p(x,z)$ to the new $p^*(x,z)$.

We factorize the data (x,z,y) in the following way(Bottou et al., 2013):

$$p(x,z,y) = p(x)p(z|x)p(y|x,z), \tag{6.1}$$

where $p(x)$ denotes the distribution of contextual variable, $p(z|x)$ represents how the platform manipulates certain features, such as the process of selecting ads and allocating each ad to the position on a page, which involves a complicated system including auction, filtering and ranking decisions (Varian, 2007). Here $p(y|x,z)$ is the user click model. One question of interest is how the click through rate $E(y)$ changes if we make modifications to the system, *i.e.*, replacing the usual mechanism $p(z|x)$ with a new one $p^*(z|x)$,

$$E^*(y) = \int\int\int p(x)p^*(z|x)p(y|x,z)\mathrm{d}x\mathrm{d}z. \tag{6.2}$$

Feature shifts happen if some radical modifications are proposed, namely $p(z|x)$ differs significantly from $p^*(z|x)$. The user click model $p(y|x,z)$ cannot produce a reliable estimate for the new click through rate $E^*(y)$ as we usually learn the click model based on $p(x,z)$ while the testing data for prediction is drawn from $p^*(x,z)$. As z depends on x differently under various policies, the correlation between z and y might change after policy changes from $p(z|x)$ to $p^*(z|x)$. In such a scenario, we wish to build a model that can transfer from training distribution $p(x,z)$ to the target distribution $p^*(x,z)$, allowing one to evaluate the impact of radical policy changes.

Currently, some publishers run experiments to randomize the features like the layout and advertisement in each impression shown to the user, which makes z independent of x. Now, we formally define the **R-data** as the data generated from $p(x)p(z)$, usually limited in size due to the low performance and revenue of a random policy. Meanwhile, we possess a large amount of past log data from the distribution $p(x)p(z|x)$, which we call **L-data**. This leads to the opportunity to more efficiently use **R-data** by pooling it with large-scale **L-data**.

Although our approach is motivated by the online advertising setting, it is not restricted to this domain or binary classification task. We aim at building a robust model $p(y|x,z)$ transferring from the smaller **R-data** and the large scale **L-data** to the targeting source $p^*(x,z)$. We focus on the case that $p^*(x,z)$ differs drastically from $p(x,z)$, which is either due to the change in the policy $p(z|x)$ or the variation in contextual features $p(x)$. Although in this application, we may know $p^*(x,z)$ in advance, the proposed method does not require any prior knowledge on the density of targeting source.

6.3.2 Proposed algorithm

We base our algorithm on the random forest method (Breiman, 2001), adapting prior work on the honesty principle for building causal trees and forests (Athey and Imbens, 2016; Wager and Athey, 2018b). Usually, the tree-based method is composed of two stages (Hastie et al., 2005): building decision boundary and calibrating each leaf value at the end of the branch to produce an estimate p_i. Furthermore, the random forest framework performs bagging on the training data and building decision tree on each bootstrap data to reduce variance. Advantages of random forests include their simplicity and ability to be paralleled.

To handle the feature shifts problem and use **R-data** efficiently, we propose the Causal Transfer Random Forest (CTRF) algorithm. The framework is shown in Figure 6.2. We propose to do bagging and build decision trees solely on the **R-data** and then calculate the predicted value (*e.g.*, click probability) on the nodes of each tree with pooled **R-data** and **L-data**. We make calibrations and aggregate over all trees with the simple average here, which can be extended to other approaches. In the first step, the model learn the structure of the tree or the decision boundary first with the **R-data**. In the next step, we transfer this structure learned to the whole data set. We take advantage of the pooled data, including both **L-data** and **R-data**, to calculate the predicted value at each node (calibrations). We describe

the detailed algorithm in Algorithm 2.

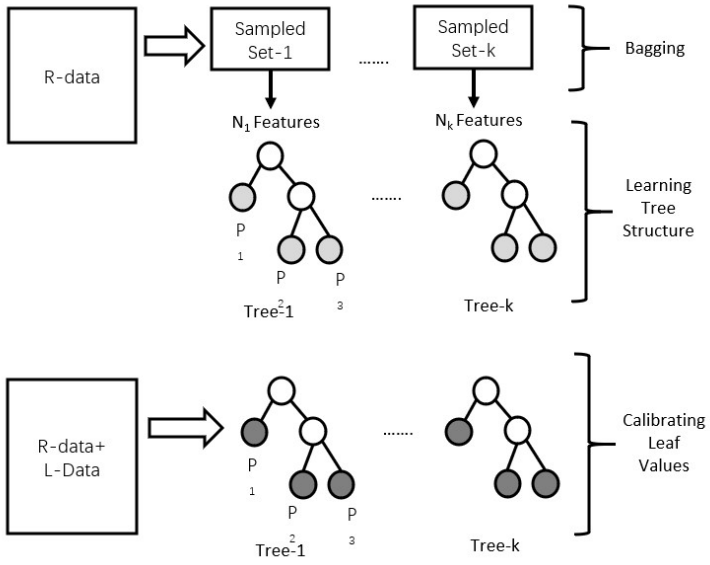

Figure 6.2: CTRF: building random forest from **R-data** and **L-data**

We design the algorithm with the intuition that the **R-data** reduces the problem of spurious correlation, one of the main reasons for the non-robustness of previous methods. Specifically, some of the correlations between z and the outcome y are influenced by the underlying generating mechanism, $p(z|x)$. In such cases, the correlation is spurious in the sense that it will disappear or change if we modify $p(z|x)$ to $p^*(z|x)$. The model trained on $p(x, z)$ will exploit those spurious correlations without the knowledge that the correlations will not hold on distribution $p^*(x, z)$. It is important to note that the spurious and non-spurious components of z's correlation with y are often not well-aligned with the raw feature representation of z. That is, this is not a feature selection problem.

Figure 6.3 demonstrates a spurious correlation instance in the ads system, depicting the relationships between ads relevance x, position z and the click outcome y. The solid lines represent the "stable" relationship or effect between the ads relevance or the position and the click, while the dashed line stands for the relationship we

Algorithm 2: Causal Transfer Random Forest

Input: R-data $\mathcal{D}^R = \{(x_i, z_i, y_i), i \in \mathcal{I}^R\}$, **L-data** $\mathcal{D}^L = \{(x_i, z_i, y_i), i \in \mathcal{I}^L\}$ and the prediction point (x^*, z^*).

Hyperparameters: bagging ratio: r_{bag}; feature subsampling ratio: r_{feature}; number of trees: n^{tree}.

Bagging: sample the data $\mathcal{D}^R$ with replacement for n^{tree} times with sampling ratio r_{bag} and sample on the feature set (x, z) for each bootstrap data with ratio r_{feature}.

for $b = 1$ **to** n^{tree} **do**

Learn decison tree For the bootstrapped data, $\{(x_i^b, z_i^b, y_i^b)\}$, build decision tree $\mathcal{T}_b$ and corresponding leaf nodes $\mathcal{L}_j^b \subset \mathcal{R}^{p+p'}, j = 1, 2, \cdots, L_b$, L_b is the number of nodes for $\mathcal{T}_b$ by maximizing the Information Gain (IG) or Gini Score.

Calibrations For each node $\mathcal{L}_j^b$, we calculate the predicted value by the mean value of samples in this node: $\hat{y_j}^b = \bar{y_i}, (x_i, z_i) \in \mathcal{L}_j^b, i \in \mathcal{I}^R \cup \mathcal{I}^L$.

end for

Predictions Collect the predicted value $\hat{y}^b$ for each $\mathcal{T}_b$ by examining the node that (x^*, z^*) belongs and produce a prediction after aggregation, such as $\hat{y} = \bar{\hat{y}}^b$.

Output Random forest $\{\mathcal{T}_b, b = 1, \cdots, n^{\text{tree}}\}$ and prediction $\hat{y^*}$.

can manipulate. In the **L-data**, the position is not randomly assigned but instead associated with other features like ads relevance(Bottou et al., 2013). We tend to allocate ads of higher relevance to the top of the page. However, the correlation between position and click changes if we alter the policy allocating the position based on the relevance, namely $p(z|x)$. Despite the correlation between position and click being partially spurious, there is still a causal connection as well—higher positioned ads do attract more clicks, all else being equal.

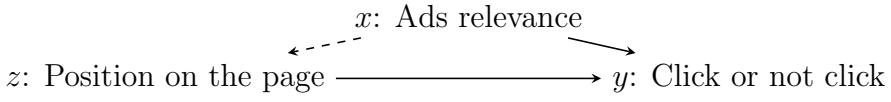

Figure 6.3: Causal Directed Acyclic Graph (DAG) for the online advertisement system

Suppose the tree algorithm makes a split on the position feature, subsequently it becomes hard to detect the importance of relevance in two sub-branches split by position. As a result, if we only train on **L-data**, the decision tree is likely to

underestimate the importance of ad relevance. We wish the decision tree structure we learn to disentangle the unstable or spurious aspects of the correlation among the features and only learn the "stable" relationships. This task can be accomplished with the **R-data** as it removes the spurious correlation. We formally define the "stable" relationship and prove why **R-data** can learn those relationships in the next section.

6.3.3 Interpretations from causal learning

In this section, we justify our intuitions in the previous sections theoretically based on the results in causal learning. Previous literature builds the connections between the capability to generalize and the conditional invariant property. Theorem 4 in Rojas-Carulla et al. (2018) demonstrates that if there is a subset of features S^* that are conditionally invariant, namely the conditional distribution $y|S^*$ remains unchanged across different distributions of $p(x, z, y)$, then the model built on those features S^* with pooling data, $E(y_i|S_i^*)$, gives the most robust performance. The robustness is measured by the worst performance with respect to all possible choices of the targeting distribution $p(x, z)$, which further ensures the model can transfer. This theorem indicates that we should build model on the set of features or the transformed features with conditional invariant property.

However, learning the stable features is not simple given we have only two types of distribution, The next theorem from Peters et al. (2016); Rojas-Carulla et al. (2018) states the relationship between conditional invariance and causality. Specifically, if we assume there are causal relationships or structural equation models (SEM) (Pearl, 2009), the direct causes of the outcome are the conditionally invariant features , $S^* = \mathrm{PA}_Y$, where PA_Y denotes the parents/direct causes for the outcome y.

With two well-established theorems above, we can look for the direct causes instead of the conditional invariant features. The following theorem shows that the **R-data** offers such opportunity.

Theorem 7 (Retain stable relationships with **R-data**). *Assume* (x_i, z_i, y_i) *can be expressed with a direct acyclic graph (DAG) or structural equation model (SEM). Then the model trained on* **R-data**, $p(x_i, z_i) = p(x_i^1)p(x_i^2)\cdots p(x_i^p)p(z_i^1)p(z_i^2)\cdots p(z_i^{p'})$ *is consistent for the most robust prediction:*

$$\hat{E}(y_i|x_i, z_i) \Rightarrow E(y_i|\boldsymbol{PA}^Y) = E(y_i|S_i^*) \tag{6.3}$$

The theorem assumes all the variables (x_i, z_i) are randomized and independent with each other in **R-data**, which has a gap to the **R-data** in practice as we cannot randomize the contextual features x. If the relationships between contextual features x and outcome y are unstable, it is hard to learn the stable relationships without randomizing on x. However, randomizing on the manipulable features z will suffice in practice as the correlation between x an y is likely to be stable. For instance, the relationship between the user preference or the ads quality itself and the intention to click is expected to remain unchanged even if we switch the platform policy on displaying ads. The theorem above suggests if the model is trained on **R-data**, it actually relies on the direct causes or robust features S_i^* to make prediction. The detailed theorem proof is provided in the Section 8.5.2.

Figure 6.4 demonstrates this idea. Compared with Figure 6.4 (a), **R-data** in Figure 6.4 (b) removes all the effects other than the direct causes of y (PA^Y is (X_1, X_2) here), which indicates that the model trained with **R-data** will pick up the features that are robust for predictions.

(a) **L-data** (b) **R-data**

Figure 6.4: Causal DAG in **L-data** and **R-data**, only direct causes or stable predictors (X_1, X_2) remain correlated with y in **R-data**

Likewise, CTRF firstly learns the structure of the model or identifies the stable

features for splitting the trees merely with the **R-data**. With our random forest method, the stable features are the leaves sliced in the decision tree, which can be viewed as a transformation of the raw features. This step serves as an analogy to search for the direct causes or extract robust features. The calibration step on the leaf values with pooled data corresponds to make predictions conditioning on all robust features. The second step will not be "contaminated" by the spurious correlation in **L-data** as the the decision tree structure has already identified a valid adjustment set with **R-data** and is conditioning on that. We also investigate whether the proposed method can pick up the stable features in the synthetic experiments to demonstrate its theoretical property.

6.4 Experiments on synthetic data

6.4.1 Setup and baselines

In this part, we evaluate the proposed method and compare with several baseline methods in the presence of covariate shifts. Given it is a novel scenario (small amount of **R-data** with large **L-data**), we design two synthetic experiments to create an artificial case that the data generating mechanism $p(z|x)$ changes. The first experiment specifies the causality relationship between variables explicitly. The second experiment is a simulated auction similar to the real-world online, in which the relationship between variables are specified implicitly. In both experiments, we have some parameters controlling the degree of covariate shift which allows us to evaluate the performance against different degree of distributional variation.

In our experiments, we compare the *causal transfer random forest* (CTRF) with the following methods: logistic regression (LR) (Menard, 2002), Gradient Boosting Decision Tree (GBDT) (Ke et al., 2017), logistic regression with sampling weighting (LR-IPW), Gradient Boosting Decision Tree with sample reweighting (GBDT-IPW), random forest model trained on **R-data** (RND-RF), random forest model trained on **L-data** (CNT-RF), random forest model trained with the **L-data** and **R-data** pool-

ing together (Combine-RF). Among all those methods, LR-IPW and GBDT-IPW are designed to handle distribution shifts with a proper weighting with ratio of densities (Bickel et al., 2009; Huang et al., 2007). Implementation details are included in the 8.5.1.

As our method is designed to handle extreme covariate shifts, we evaluate different methods in terms of the performance on the shifted testing data only. Although our method is not restricted to classification task, we only focus on the binary outcome to be coherent with our motivated application from ads click. For binary classification task, we focus on the following two metrics, AUC (area under curve) and the cumulative prediction bias, $|\bar{\hat{y}}_i - \bar{y}_i|/\bar{y}_i$, which is the adjusted difference in the mean value of predicted values and actual outcomes. AUC captures the prediction power of the model while the cumulative prediction bias captures how our method can predict the counterfactual change, such as the change in the overall click rate.

6.4.2 Synthetic data with explicit mechanism

We generate the data in a similar fashion with the experiments in Kuang et al. (2018). We generate two sets of features S, V for predictions. S represents the stable feature or the direct cause of the outcome while V represents the unstable factors that have spurious correlation with the outcome. We consider three possible scenarios for the relationships between (S, V): (a)$S \perp\!\!\!\perp V$, S and V are independent; (b) $S \to V$, S is the cause for V; (c) $V \to S$, V is the cause for S. Figure 6.5 demonstrates these three cases. In all cases, $S = (S_1, \cdots, S_{p_s})$ is the stable feature while $V = (V_1, \cdots, V_{p_v})$ is the possible unstable factors sharing spurious correlation with the outcome.

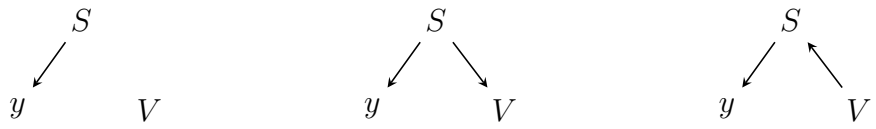

(a) $S \perp\!\!\!\perp V$ (b) $S \to V$ (c) $V \to S$

Figure 6.5: Three possible relationships among the variables

In case (a), we generate (S, V) from independent standard Normal distributions and transform them into the binary vectors,

$$\tilde{S}_j, \tilde{V}_k \sim \mathcal{N}(0,1), \quad S_j = \mathbf{1}_{\tilde{S}_j > 0}, V_k = \mathbf{1}_{\tilde{V}_k > 0}.$$

In case (b), we generate S from Normal distributions first and generate V as a function of S.

$$\tilde{S}_j \sim \mathcal{N}(0,1), \tilde{V}_k = \tilde{S}_k + \tilde{S}_{k+1} + \mathcal{N}(0,2), \quad S_j = \mathbf{1}_{\tilde{S}_j > 0}, V_k = \mathbf{1}_{\tilde{V}_k > 0}.$$

In case (c), we generate V first and simulate S as a function of V.

$$\tilde{V}_k \sim \mathcal{N}(0,1), \tilde{S}_j = \tilde{V}_j + \tilde{V}_{j+1} + \mathcal{N}(0,2), \quad S_j = \mathbf{1}_{\tilde{S}_j > 0}, V_k = \mathbf{1}_{\tilde{V}_k > 0}.$$

For the outcome, we keep the generating procedure same across three cases. The binary outcome y is generated solely as a function of S,

$$\tilde{y} = \text{sigmoid}(\sum_{j=1}^{p_s} \alpha_j S_j + \sum_{j=1}^{p_s - 1} \beta_j S_j S_{j+1}) + \mathcal{N}(0, 0.2), \quad y = \mathbf{1}_{\tilde{y} > 0.5},$$

where $\text{sigmoid}(x) = 1/(1 + \exp(-x))$. This specification includes both the linear and non-linear effect of S. The parameters take values as $\alpha_j = (-1)^j (j\%3 + 1) * p/3, \beta_j = p/2$.

In addition to different generating mechanisms, we introduce an additional spurious correlation with biased sample selection. Specifically, we set an inclusion rate $r = (0, 1)$ to create a spurious correlation between y and V. If the average value of $\bar{V}_i = \sum_{j=1}^{p_v} V_{ij}$ and $\tilde{y}_i$ exceed or fall below 0.5 together, we include sample i with probability r. Otherwise, we include the sample with probability $1 - r$. Namely, if $r > 0.5$, V and y share positive correlation and the correlation is negative if $r < 0.5$. The parameter r controls the degree of spurious correlation which induces the covariate shifts.

We generate a small amount of **R-data** following case (a) with size $n_r = 1000$, a large amount of **L-data** following case (b) $n_l = 5000$ and the testing data from

case (c) with size $n_t = 2000$ to mimic the policy change on testing data. We create a lower amount of **R-data** to mimic the real business scenario that randomizing the platform policy reduces the revenue and thus being expensive to collect. We keep a slightly larger proportion of **R-data** than the one in practice for fair comparisons (such as RND-RF) to demonstrate the essential advantage of the proposed method. Additionally, we set $r = 0.7$ on the **L-data** and let r vary from 0.1 to 0.9 on the testing data to create additional deviance in the distribution. We also vary the number of features in total $p \in [20, 40, 80]$ and keep $p_s = 0.4p$. Within each configuration, we perform the experiments 200 times and calculate the average AUC and cumulative bias.

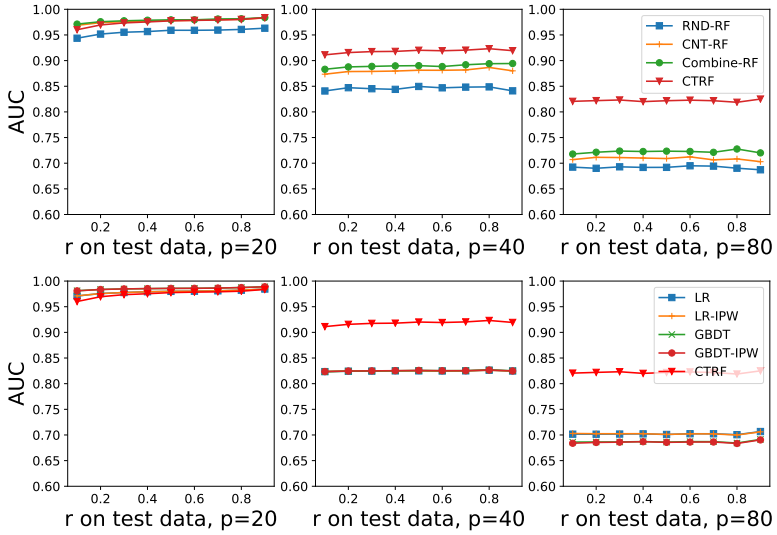

Figure 6.6: AUC comparison when $p = 20, 40, 80$. The top row compares with random forest based method and the bottom row compares other baselines. CTRF produces largest AUC in most cases.

Figure 6.6 shows the comparison of AUC against the variation on both p and r. The top row demonstrates the comparison within the domain of random forest. The CTRF (red lines) performs the best regardless of feature dimensions. The second row in Figure 6.6 shows the comparison with LR, LR-IPW, GBDT and GBDT-IPW. Although the performances are indistinguishable when $p = 20$, the advantage of CTRF emerges as we have more spurious correlations.

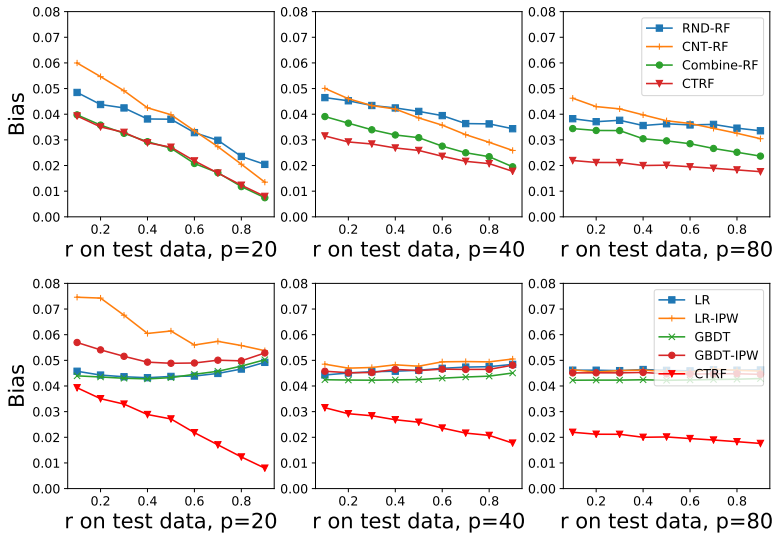

Figure 6.7: Bias comparison when $p = 20, 40, 80$, with top row comparing with random forest based method and bottom row comparing other baselines. CTRF achieves the lowest bias in all cases.

Figure 6.7 shows the comparison in terms of the bias. A lower value represents a better performance. The top row shows the comparison with other random forest based methods. Generally, the cumulative bias increases as r on the testing data decreases, which means the testing data deviates more from the **L-data**. However, the advantage of CTRF (red lines) increases slightly as r decreases, which demonstrates the robustness against covarites shifts. The comparison with LR or GBDT based methods at the bottom row shows a similar trend with the AUC. The CTRF achieves a lower bias among all the approaches and its advantage increases as we have more features.

In terms of the scalability, we find that the advantage of CTRF over other methods increases as the feature size p goes up, with a larger AUC and smaller bias. Additionally, the CTRF builds the decision tree solely on the **R-data** and the calibration stage on the pooled data is much less computationally intensive, which further demonstrates its advantage in scalability.

6.4.3 *Synthetic auction: implicit mechanism*

In this subsection, we setup a synthetic auction scenario with a single tuning parameter in the policy, demonstrating both how simple parameters can introduce bias into a domain and CTRF's ability to transfer between them. In a real-world setting, an organization can replay the observed control data under varying treatment settings, utilizing a probability of click model rather than actual clicks to estimate a variety of key performance indicators. We first generate synthetic samples of classification

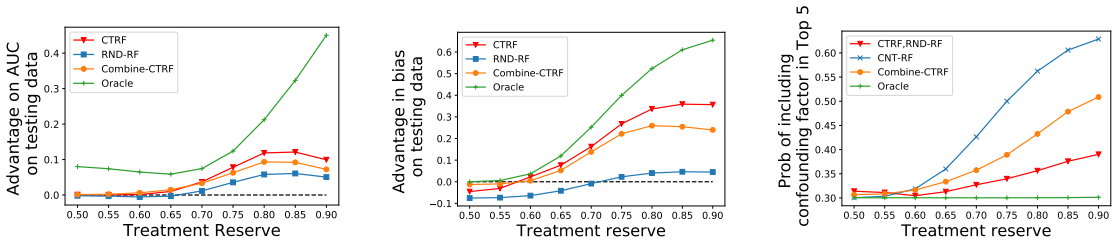

Figure 6.8: AUC (left graph), cumulative prediction bias (middle graph) and probability of including confounding factor "position" as Top 5 important features (right graph) versus treatment reserve r. Higher r represents a larger change in the testing distribution. CTRF performs the best among all random forest methods.

data, or a mapping from features to a true relevant/irrelevant binary label. From this data, we build a true relevance model with random forest to estimate the probability an item is relevant. Second, we build our **L-data** and testing auctions by sampling (20 per auction) from the underlying relevance features and assigning a relevance score. Per auction, the items are thresholded with the corresponding *relevance reserve* parameter and the remaining items are ranked. This provides layout and position information, in addition to the relevance score and relevance features. Third, Given the layout and items, a simulated user chooses a single ad as relevant uniformly at random to click, and leaves the others not clicked. The choice of click is uniform across positions, which means that *position* is purely a factor spuriously correlated with the relevance while not affecting the click. We provide the detailed generating mechanism in the Section 8.5.1.

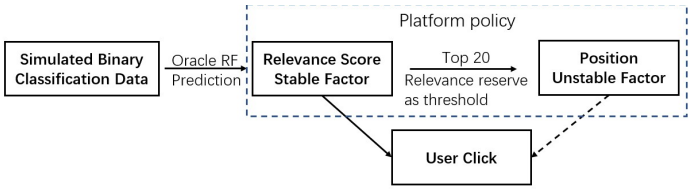

Figure 6.9: Procedures for simulating auctions. Position is an unstable factor for predicting click as the users pick ads uniformly on a page to click and its correlation with relevance score varies across policy, which is implicitly determined by the relevance reserve parameter.

The tuning parameter in the experiment is the *relevance reserve* parameter r, controlling the requirement that any item shown to a user meet a minimum relevance, which controls $p(z|x)$ implicitly. The mechanism to generate simulated auction is illustrated in Figure 6.9. This parameter affects the correlation between relevance and position, which can vary between **L-data** and testing data. Specifically, we generate the **L-data** with relevance reserve parameter $r = 0.5$ while the testing data with the relevance reserve varying in $r \in [0.5, 0.9]$, simulating a desire to increase the quality of items presented to a user (with a higher threshold). A larger value in $r > 0.5$ represents a higher deviation from the **L-data** with $r = 0.5$. For the **R-data**, we do not have the auction procedure and we pick up the advertisement uniformly random to display on the page. The size of **R-data** is approximately 20% of the **L-data**.

As we use the random forest model to generate the true relevance score, we compare the CTRF within the domain of random forest based methods only, including CNT-RF, RND-RF, Combine-RF and the oracle one training RF on the testing data. Figure 6.8 illustrates prediction performance of all method while setting CNT-RF as the baseline. To illustrate the advantage over the baseline method, CNT-RF, we minus the AUC of CNT-RF from that of all other methods and minus the bias of the corresponding model from the bias of CNT-RF. Therefore, a larger value in the graphs indicates a better performance of the corresponding method.

In Figure 6.8, we observe that when the reserve for testing data lies close to 0.5,

all models show similar performance. However, as we increase r on testing data and raise the degree of covariate shift, the CTRF method (red lines) greatly improves in both AUC and bias. Also, the CTRF demonstrates a better prediction power and lower bias compared with the RND-RF and Combine-RF. This illustrates CTRF's ability to transfer knowledge from one domain to a similar but distinct domain with unstable factor (in this case, an ad's position).

We calculate the probability of including the "position", which is a known spuriously correlated factor by design, in the top 5 factors ranking by feature importance (Genuer et al., 2010) evaluated on the training dataset. As shown in the right panel of Figure 6.8, the random forest learned on the **R-data** (RND-RF,CTRF are identical) has a lower probability of identifying the unstable or confounding factor as important predictors, compared with the one utilizing the **L-data** (CNT-RF, Combine-RF). This demonstrates that the first stage of structure learning or the decision boundary on **R-data** can reduce spurious correlation. This also validates utilizing the large amount of the **L-data** to calibrate the parameters in the structure or trees in the second stage as the prediction does not rely on the unstable factor.

6.5 Experiments on real-world data

In this section, we present experimental results in the real-world application with data collected from a sponsored search search platform (Bing Ads). First, we discuss how **R-data** is collected from real traffic. Next, we demonstrate the robustness of CTRF-trained click models against the distribution shifts. Finally, we show that CTRF-enabled holistic counterfactual policy estimation improves global marketplace optimization problem real business scenarios.

*6.5.1 Randomized experiment (**R-DATA**)*

Randomized data (**R-data**) collection is very important step to create CTRF since training requires **R-data** to learn the structure of trees. In order to collect **R-**

data, we used existing randomization policy on paid search engine which is triggered less than %1 of the live traffic. The existing randomization policy is triggered in typical sponsored search requests and there is no difference between randomized and mainstream traffic in terms of user and advertiser selection. For a given paid search request, if randomization is enabled, special uniform randomization policy is triggered. In this uniform randomization policy, all choices that depend on models are completely randomized. In particular, the ads are randomly permuted and the page layout (where ads are shown on the page) is chosen at random from the feasible layouts. The user cost (due to lower relevance) of such randomization is very high and consequently, limits the trigger rate for the randomized policy.

6.5.2 Robustness to real-world data shifts

We train the user click model on the data collected from the mainstream traffic and randomized traffic in the search engine, corresponding to the **L-data** and **R-data** respectively. We validate the proposed method on an exploration traffic with some radical experiments (layout template change, for example), which is the testing data with covariate shifts. We only compare the method with CNT-RF, Combine-RF and Oracle-RF, which trains a random forest on the testing data. The last one cannot be implemented in practice yet it serves to illustrate the capacity of the random forest method. We fix the total training size to be approximately 1 million with each method [1] and include the same feature set from production for a fair comparison. We focus on three metrics of interests: AUC (area under curve), RIG (Relative Information Gain) and cumulative prediction bias[2].

Table 6.1 shows that CTRF achieves the best performance among all the random

[1]The ratio of **R-data** and **L-data** is about 1:7, after down-sampling on the **L-data**. The proportion of **R-data** is upweighted for fair comparison. Otherwise, the performance of CNT-RF and Combined-RF will be very close.

[2]Relative information gain is defined as the RIG $= (H(\bar{y}) + L)/H(\bar{y})$, L is the log loss produced by the model and $H(p) = -p\log(p) - (1-p)\log(1-p)$ is the entropy function. Higher value indicates better performance.

Table 6.1: Performance comparison for different random forest based model, evaluated on some exploration flights with radical policy changes

Methods	AUC	RIG	Cumulative Bias
CNT-RF	0.9273	0.4424	3.87%
Combine-RF	0.9282	0.4460	3.39%
CTRF	**0.9285**	**0.4477**	**2.90**%
Oracle-RF	0.9287	0.4484	0.58%

forest candidates[3]. As for AUC and RIG, The CTRF shows a slightly better performance than other random forest candidates and is very close to Oracle-RF, which indicates its nearly-optimal prediction performance. In terms of the bias, although with a gap with the Oracle-RF, the CTRF reduces the cumulative bias for click rate prediction to a non-negligible degree, which is very essential to the publishers in decision making. As we are evaluating all the performance on a part of the traffic performing some radical changes, the results demonstrate that the CTRF improves the robustness of user click model in terms of prediction power.

6.5.3 End-to-end marketplace optimization

In addition to the prediction power of the model, we also evaluate how the usage of CTRF can advance the decision making procedure in real business optimization at Bing Ads.

Marketplace optimization in a nutshell

The goal of Marketplace Optimization for sponsored search is to find optimal operating points for each component of the search engine given all marketplace constraints. Marketplace optimization is very different from optimizing certain objective functions with a given machine learning model. While model training focuses on reducing prediction error for unobserved data, Ads Marketplace Optimization focuses

[3]We omit the standard error here for brevity and the reported difference here is considered as "significant" in practical application.

on improving global objectives like total clicks, revenue when new machine learning model is used as part of a bigger system. Due to data distribution shifts between components of a larger system, a locally optimized click model does not necessarily give best performances for global metrics. Therefore, whole components of the system may need to be tuned together by using more holistic approaches like A/B testing (Xu et al., 2015) or similar.

Experimental data selection and simulation setup

Robust click prediction plays a very crucial role in improving holistic Ads Marketplace Optimizer like an open box simulator (Bayir et al., 2019) which can easily have biased estimations due to data distribution shifts in counterfactual environments. In our problem context, we integrate CTRF to an open box offline simulator and show that a new simulator with CTRF will give better results for offline policy estimation scenarios when data distribution shift is significant.

For experimental runs, we use an open box simulator with two versions of random forest, CTRF and CNT-RF (typical RF used), along with the generalized linear Probit model (Graepel et al., 2010) for click prediction. Then, we run offline counterfactual policy estimation jobs with modified inputs over logs collected from real traffic. Finally, we compare predictions for marketplace level click metrics with different models against A/B testing by using same production data that is collected from A/B testing experiment.

To select experimental data, we checked the counterfactual vs factual feature distribution similarity of multiple real tuning scenarios in search engine traffic. We applied Jensen-Shannon (JS) divergence to compute the similarity of two distributions. Based on this distance metric, we selected 2 tuning use cases out of 10 candidate cases with significantly higher distribution shift, which fits the proposed approach. First use case belongs to capacity change for Text Ads blocks. Second use belongs to page layout change. This also demonstrates that drastic policy changes are common

in online advertisement tuning tasks. Details on this procedure are included in the Section 8.5.1.

Experiments on real case studies

In the first case, the capacity of the particular ad block that contains Textual Ads was increased on the traffic in May 2019 for 10 days time period during A/B testing. The change was expected to increase both overall click yield and click yield on textual ad slice for target ad block. For simulator runs, we used 4.6 million samples from control traffic (**L-data**) and 100K samples from the randomized traffic (**R-data**) that belongs to 3 weeks time period before end date of A/B testing. The randomized traffic corresponds to page view requests where the mechanisms in online system are randomized, as described in Section 6.5.1.

Table 6.2: Performance comparison in two cases with radical changes

Ad capacity change	ΔCY Error	ΔCY Error (Text Ads)
Probit Model	34.94%	17.13%
CNT-RF	12.11%	9.96%
CTRF	**2.07%**	**8.76%**
Layout change	ΔCY Error	ΔCY Error (Shopping Ads)
Probit Model	35.48%	45.08%
CNT-RF	58.06%	34.92%
CTRF	**22.58%**	**13.38%**

In simulator runs with CTRF, we train the forest and tree structures from **R-data** and combine the **L-data** and **R-data** to calibrate the leaves of trees in the forest. Each simulation job uses its trained model to score counterfactual page views that generated from replying control traffic logs in open box manner with the suggested input modification (capacity change of ad block). Table 6.2 presents the comparison of an open box simulator with generalized Probit model, with CTRF and the random forest trained on control traffic (CNT-RF) based on relative Click

Yield delta error [4] against A/B testing experiment that was active for 10 days in May 2019. To make a fair comparison, we use the same amount of training data for different variants of random forest models. We observe that click yield deltas coming from simulator results with CTRF is significantly better than other approaches since results from CTRF enabled simulator are closer to A/B Testing results from real traffic.

In the second scenario, the layout of product shopping ads was significantly updated in May 2019 for a week time period during A/B testing. The change was expected to increase both overall click yield and click yield on product shopping ads slice for target ad block. In this experiment, we used 15M samples from the control traffic in A/B testing and the same randomized traffic in the previous experiment. The bottom part in Table 6.2 presents the comparison of different model-based simulators in the relative error against the A/B testing experiment that was active for a week in May 2019. Since the modification for the second experiment yielded a radical shift in feature distribution of product shopping Ads. The difference with CTRF enabled simulator vs other approaches is more prominent. Thus, open box simulator with CTRF also outperforms other approaches in this scenario.

[4]Relative Click Yield delta error is defined as $—\Delta CY_{Method} - \Delta CY_{AB}|/|\Delta CY_{AB}—$. ΔCY_{Method} is the predicted change in click rate by the model. ΔCY_{AB} is the actual change in A/B testing.

7

Conclusions

In this thesis, I propose several methods to carry out causal inference for various proposes in different scenarios. The methodological and modeling advances can be summarized into the five categories: (i) propensity score weighting in randomized controlled trials (RCT) (ii) propensity score weighting for survival outcomes (iii) mediation analysis with sparse and longitudinal data (iv) enhancing counterfactual predictions with machine learning (v) robust prediction with a combination of randomized data and observational data. We will discuss the methods above and provide possible extension in this Chapter.

In Chapter 2, we advocate to use the overlap propensity score weighting (OW) method for covariate adjustment in RCT, especially when the sample size is small. Our simulation shows OW estimator is more efficient than other inverse probability weighting (IPW) in finite sample samples. Moreover, OW is very simple to implement in practice and only requires a one-line change of the programming code compared to the inverse probability weighting (IPW). We also implement the proposed estimatior and the closed form asymptotic variance estimator in R package **PSWeight** (Zhou et al., 2020). There are a number of possible extensions. First, subgroup analysis is routinely conducted in RCT to examine whether the treatment effect depends on certain sets of patient characteristics(Wang et al., 2007; Dong et al., 2020). Second, multi-arm randomized trials are common and the interest usually lies in determining the pairwise average treatment effect (Juszczak et al., 2019). Although the basic principle of improving efficiency via covariate adjustment still applies, there is a lack of empirical evaluation as to which adjustment approach works better in finite

samples. In particular, the performance of multi-group ANCOVA and propensity score weighting merits further study. Lastly, covariate adjustment is also relevant in cluster randomized controlled trials, where entire clusters of patients (such as hospitals or clinics) are randomized to intervention conditions (Turner et al., 2017). It remains an open question whether OW could similarly improve the performance of IPW for addressing challenges in the analysis of cluster randomized trials.

In Chapter 3, we propose a class of propensity score weighting estimator for time-to-event outcomes based on pseudo-observations. We established the theoretical properties of the weighting estimator and obtain a new closed-form variance estimator that takes into account of the uncertainty due to both pseudo-observations calculation and propensity score estimation; this allows valid and fast estimation of variance in big datasets, which is a main challenge for previous bootstrap-based methods (Andersen et al., 2017; Wang, 2018). The proposed weighting estimator is more robust than standard model-based approaches such as the popular Cox-model-based causal inference methods. We also established the optimal efficiency property of the overlap weights estimator within the class of balancing weights. This is confirmed in simulations and OW's advantage is particularly pronounced when the covariates between treatment are poorly overlapped and/or the sample size is small. The proposed method can be extended in several directions. First, in comparative effectiveness studies patients often receive treatments at multiple times and covariates information is repeatedly recorded during the follow up. The standard approach is to couple a marginal structural model with a Cox model for the survival outcomes (Robins et al., 2000b; Daniel et al., 2013; Keil et al., 2014); as discussed before, such an approach is susceptible to violation to the proportional hazards assumption. It is thus desirable to extend the pseudo-observations-based weighting method to the setting of sequential treatments with time-varying covariates. Second, subgroup analysis is common in comparative effectiveness research to study heterogeneous treatment effect (Green and Stuart, 2014; Dong et al., 2020). We can easily extend the pseudo-observations

approach to the propensity score weighting estimator for subgroup effects discussed in Yang et al. (2020). We implement the proposed propensity score weighting estimator in the function `PSW.pseudo` in the R package **PSWeight** (Zhou et al., 2020).

In Chapter 4, we proposed a framework for conducting causal mediation analysis with sparse and irregular longitudinal mediator and outcome data. We defined several causal estimands (total, direct and indirect effects) in such settings and specified structural assumptions to nonparametrically identify these effects. For estimation and inference, we combine functional principal component analysis (FPCA) techniques and the standard two structural-equation-model system. In particular, we use a Bayesian FPCA model to reduce the dimensions of the observed trajectories of mediators and outcomes. Identification of the causal effects in our method relies a set of structural assumptions. In particular, sequential ignorability plays a key role but it is untestable. Conducting a sensitivity analysis would shed light on the consequences of violating such assumptions (Imai et al., 2010b). However, it is a non-trivial task to design a sensitivity analysis in complex settings such as ours, which usually involves more untestable structural and modeling assumptions. An important extension of our method is to incorporate time-to-event outcomes, a common practice in longitudinal studies (Lange et al., 2012; VanderWeele, 2011). For example, it is of much scientific interest to extend our application to investigate the causal mechanisms among early adversity, social bonds, GC concentrations and length of lifespan. A common complication in the causal mediation analysis with time-to-event outcomes and time-varying mediators is that the mediators are not well-defined for the time period in which a unit was not observed (Didelez, 2019; Vansteelandt et al., 2019). Within our framework, which treats the time-varying observations as realizations from a process, we can bypass this problem by imputing the underlying smooth process of the mediators in an identical range for every unit.

In Chapter 5, we propose a novel framework to learn double-robust representations for counterfactual prediction with the high-dimensional data. By incorporating

an entropy balancing stage in the representation learning process and quantifying the balance of the representations between groups with the entropy of the resulting weights, we provide robust and efficient causal estimates. Important directions for future research include exploring other balancing weights methods (Deville and Särndal, 1992; Kallus, 2019; Zubizarreta, 2015) and generalizing into the learning problem with panel data (Abadie et al., 2010), sequential treatments (Robins et al., 2000b), and survival outcomes (Cox, 2018).

In Chapter 6, we present a novel method, causal transfer random forest, combining limited randomized data (**R-data**) and large scale observational or logged data (**L-data**) in the learning problem. We propose to learn the tree structure or the decision boundary with the **R-data** and calibrate the leaf value of each tree with the whole data (**R-data** and **L-data**). This approach overcomes the spurious correlation in **L-data** and the limitations on sample size for the **R-data** to provide robustness against covariate shifts. We evaluate the proposed model in the extensive synthetic data experiments and implement it in Bing ads system to train the user click model. The empirical results demonstrate its advantage over other baselines against the radical policy changes and robustness in real-world prediction tasks. For future work, there are some important research questions to explore, such as a better understanding of the relative importance of the **R-data** versus the **L-data**, how much **R-data** is needed and how this quantity related to the degree of distributional shift.

The thesis covers several important topics in causal inference and it is hard to wrap up every aspects of this thesis in a nutshell. However, I would like to highlight two main messages. First, from a modeling perspective, when dealing with the high dimensional data (e.g. Chapter 5) or the dataset of complex structure (e.g. Chapter 4), it is usually helpful to coupling the causal inference with some dimension reduction tools and build models on the parsimonious representation of the original data. Second, from a methodological perspective, the role of balance is highly essential for causal inference (e.g. Chapter 2,3). Intuitively, balanced data remove the confound-

ing bias and approximate a randomized trial, which in turn makes the estimation or prediction depend less on the models and therefore brings robustness (Chapter 5,6).

8

Appendix

8.1 Appendix for Chapter 2

8.1.1 Proofs of the propositions in Section 2.3

We proceed under a set of standard regularity conditions such as the expectations $E(Y_i|X_i, Z_i), E(Y_i^2|X_i, Z_i)$ are finite and well defined. We assume that the treatment Z is randomly assigned to patients, where $\Pr(Z_i = 1|X_i, Y_i(1), Y_i(0)) = \Pr(Z_i = 1) = r$, and $0 < r < 1$ is the randomization probability. We allow the joint distribution $\Pr(Z_1, Z_2, \cdots, Z_N)$ to be flexible as long as $\Pr(Z_i = 1) = r$ is fixed. This includes the case where we assign each unit treatment independently with probability r (N_1 and N_0 are random variables) or the case where we assign a fixed proportion into the treatment group (N_1 and N_0 are fixed). In the former case, we assume r is bounded away from 0 and 1 so that $\Pr(N_1 = 0)$ and $\Pr(N_0 = 0)$ are negligible (otherwise the weighting estimator may be undefined).

Proof for Proposition 1(a). Suppose the propensity score model $e_i = e(X_i; \theta)$ is a smooth function of θ, and the estimated parameter $\hat{\theta}$ is obtained by maximum likelihood, we derive the score function $S_{\theta,i}$ for each observation i, namely the first order derivative of the log likelihood with respect to θ,

$$\begin{aligned} S_{\theta,i} = \frac{\partial}{\partial\theta} l_i(\theta) &= \frac{\partial}{\partial\theta} \left\{ Z_i \log e(X_i;\theta) + (1 - Z_i) \log(1 - e(X_i;\theta)) \right\} \\ &= \frac{Z_i - e(X_i;\theta)}{e(X_i;\theta)(1 - e(X_i;\theta))} \frac{\partial e(X_i;\theta)}{\partial\theta}, \end{aligned}$$

where $\frac{\partial e(X_i;\theta)}{\partial\theta}$ is the derivative evaluated at θ. As the true probability of being treated is a constant r and the logistic model is always correctly specified as long as it includes

an intercept, there exists θ^* such that $e(X_i;\theta^*) = r$. When $\theta = \theta^*$, the score function is,

$$S_{\theta^*,i} = \frac{Z_i - r}{r(1-r)} \frac{\partial e(X_i;\theta^*)}{\partial \theta}.$$

Let $I_{\theta\theta}$ be the information matrix evaluated at θ, whose exact form is,

$$I_{\theta\theta} = E\left\{ \frac{\partial}{\partial\theta} l_i(\theta) \frac{\partial}{\partial\theta} l_i(\theta)^T \right\} = E\left\{ \frac{(Z_i - e(X_i;\theta))^2}{(e(X_i;\theta)(1-e(X_i;\theta)))^2} \frac{\partial e(X_i;\theta)}{\partial\theta} \frac{\partial e(X_i;\theta)}{\partial\theta}^T \right\}.$$

When $\theta = \theta^*$,

$$I_{\theta^*\theta^*} = \frac{1}{r(1-r)} E\left\{ \frac{\partial e(X_i;\theta^*)}{\partial\theta} \frac{\partial e(X_i;\theta^*)}{\partial\theta}^T \right\}.$$

Applying the Cramer-Rao theorem, assume the propensity score model $e(X_i;\theta)$ satisfies certain regularity conditions (Lehmann and Casella, 2006), the Taylor expansion $\hat{\theta}$ at true value is,

$$\sqrt{N}(\hat{\theta} - \theta^*) = I^{-1}_{\theta^*\theta^*} \frac{1}{\sqrt{N}} \sum_{i=1}^{N} S_{\theta^*,i} + o_p(1),$$

By the Weak Law of Large Numbers (WLLN), we can establish the consistency of $\hat{\theta}$,

$$\hat{\theta} - \theta^* \xrightarrow{p} I^{-1}_{\theta^*\theta^*} E(S_{\theta^*,i}) = I^{-1}_{\theta^*\theta^*} \frac{E(Z_i - r)}{r(1-r)} E\left\{ \frac{\partial e(X_i;\theta^*)}{\partial\theta} \right\} = 0.$$

With the consistency of $\hat{\theta}$, we also have,

$$\frac{1}{N}\sum_{i=1}^{N} Z_i(1 - e(X_i;\hat{\theta})) \xrightarrow{p} r(1-r), \frac{1}{N}\sum_{i=1}^{N}(1-Z_i)e(X_i;\hat{\theta}) \xrightarrow{p} r(1-r).$$

Next, we investigate the influence function of $\hat{\mu}_1^{\mathrm{OW}} - \hat{\mu}_0^{\mathrm{OW}}$,

$$\begin{aligned}
\sqrt{N}(\hat{\mu}_1^{\mathrm{OW}} - \hat{\mu}_0^{\mathrm{OW}}) =& \sqrt{N}\left(\frac{\sum_{i=1}^N Z_i Y_i (1 - e(X_i;\hat{\theta}))}{\sum_{i=1}^N Z_i(1 - e(X_i;\hat{\theta}))} - \frac{\sum_{i=1}^N (1-Z_i) Y_i e(X_i;\hat{\theta})}{\sum_{i=1}^N (1-Z_i) e(X_i;\hat{\theta})} \right), \\
=& \frac{1}{\sqrt{N}} \sum_{i=1}^{N} \{ \frac{Z_i Y_i (1 - e(X_i;\hat{\theta}))}{r(1-r)} - \frac{(1-Z_i) Y_i e(X_i;\hat{\theta})}{r(1-r)} \} + o_p(1).
\end{aligned}$$

We perform the Taylor expansion at the true value θ^*,

$$\begin{aligned}\sqrt{N}(\hat{\mu}_1^{\text{OW}} - \hat{\mu}_0^{\text{OW}}) =& \frac{1}{\sqrt{N}} \sum_{i=1}^{N} \{ \frac{Z_i Y_i (1 - e(X_i; \hat{\theta})) e(X_i; \hat{\theta})}{e(X_i; \hat{\theta}) r (1 - r)} \\ & - \frac{(1 - Z_i) Y_i (1 - e(X_i; \hat{\theta})) e(X_i; \hat{\theta})}{(1 - e(X_i; \hat{\theta})) r (1 - r)} \} + o_p(1)\end{aligned}$$

$$\begin{aligned}\sqrt{N}(\hat{\mu}_1^{\text{OW}} - \hat{\mu}_0^{\text{OW}}) =& \frac{1}{\sqrt{N}} \sum_{i=1}^{N} \{ \frac{Z_i Y_i (1 - e(X_i; \theta^*)) e(X_i; \theta^*)}{e(X_i; \theta^*) r (1 - r)} \\ & - \frac{(1 - Z_i) Y_i (1 - e(X_i; \theta^*)) e(X_i; \theta^*)}{(1 - e(X_i; \theta^*)) r (1 - r)} \} - \\ & \frac{1}{\sqrt{N}} \sum_{i=1}^{N} \{ \frac{Z_i Y_i (1 - e(X_i; \theta^*)) e(X_i; \theta^*)}{e(X_i; \theta^*) r (1 - r)} \\ & - \frac{(1 - Z_i) Y_i (1 - e(X_i; \theta^*)) e(X_i; \theta^*)}{(1 - e(X_i; \theta^*)) r (1 - r)} \} S_{\theta^*, i}^T (\hat{\theta} - \theta^*) + o_p(1), \\ =& \frac{1}{\sqrt{N}} \sum_{i=1}^{N} \left\{ \frac{Z_i Y_i}{r} - \frac{(1 - Z_i) Y_i}{1 - r} \right\} \\ & - \frac{1}{N} \left[\left\{ \frac{Z_i Y_i}{r} - \frac{(1 - Z_i) Y_i}{1 - r} \right\} S_{\theta^*, i}^T \right] \sqrt{N} (\hat{\theta} - \theta^*) + o_p(1), \\ =& \frac{1}{\sqrt{N}} \sum_{i=1}^{N} \left\{ \frac{Z_i Y_i}{r} - \frac{(1 - Z_i) Y_i}{1 - r} \right\} \\ & - E \left[\left\{ \frac{Z_i Y_i}{r} - \frac{(1 - Z_i) Y_i}{1 - r} \right\} S_{\theta^*, i}^T \right] I_{\theta^* \theta^*}^{-1} \frac{1}{\sqrt{N}} \sum_{i=1}^{N} S_{\theta^*, i} + o_p(1).\end{aligned}$$

After plugging in the value of $S_{\theta^*,i}$ and $I_{\theta^*\theta^*}$, we can show that,

$$\begin{aligned}\hat{\mu}_1^{\text{OW}} - \hat{\mu}_0^{\text{OW}} =& \frac{1}{N} \sum_{i=1}^{N} \left[\frac{Z_i Y_i}{r} - \frac{(1 - Z_i) Y_i}{1 - r} - \frac{Z_i - r}{r(1 - r)} \{ (1 - r) g_1(X_i) + r g_0(X_i) \} \right] \\ & + o_p(N^{-1/2}) \\ g_1(X_i) =& E \left[Y_i \frac{\partial e(X_i; \theta^*)}{\partial \theta} \middle| Z_i = 1 \right]^T E \left\{ \frac{\partial e(X_i; \theta^*)}{\partial \theta} \frac{\partial e(X_i; \theta^*)}{\partial \theta}^T \right\}^{-1} \frac{\partial e(X_i; \theta^*)}{\partial \theta}, \\ g_0(X_i) =& E \left[Y_i \frac{\partial e(X_i; \theta^*)}{\partial \theta} \middle| Z_i = 0 \right]^T E \left\{ \frac{\partial e(X_i; \theta^*)}{\partial \theta} \frac{\partial e(X_i; \theta^*)}{\partial \theta}^T \right\}^{-1} \frac{\partial e(X_i; \theta^*)}{\partial \theta}.\end{aligned}$$

Therefore, $\hat{\tau}^{\text{OW}}$ belongs to the augmented IPW estimator class $\mathcal{I}$ in the main text, which completes the proof of Proportion 1 (a).

Proof for Proposition 1(b): First, we build the relationship between the asymptotic variance of $\hat{\tau}^{\text{OW}}$ with the correpsonding information matrix $I_{\theta^*\theta^*}$ and score function $S_{\theta^*,i}$ evaluated at true value. Based on the results in Proposition 1(a), the asymptotic variance of $\hat{\tau}^{\text{OW}}$ depends on the following terms:

$$\begin{aligned}
\lim_{N\to\infty} N\text{Var}(\hat{\tau}^{\text{OW}}) =& \text{Var}(\frac{Z_iY_i}{r} - \frac{(1-Z_i)Y_i}{1-r} \\
&-E\left[\left\{\frac{Z_iY_i}{r} - \frac{(1-Z_i)Y_i}{1-r}\right\} S_{\theta^*,i}^T\right] I_{\theta^*\theta^*}^{-1} S_{\theta^*,i}), \\
=&\text{Var}\left(\frac{Z_iY_i}{r} - \frac{(1-Z_i)Y_i}{1-r}\right) \\
&+\text{Var}\left(E\left[\left\{\frac{Z_iY_i}{r} - \frac{(1-Z_i)Y_i}{1-r}\right\} S_{\theta^*,i}^T\right] I_{\theta^*\theta^*}^{-1} S_{\theta^*,i}\right) \\
&-2\text{Cov}\left(\left\{\frac{Z_iY_i}{r} - \frac{(1-Z_i)Y_i}{1-r}\right\}, E\left[\left\{\frac{Z_iY_i}{r} - \frac{(1-Z_i)Y_i}{1-r}\right\} S_{\theta^*,i}^T\right] I_{\theta^*\theta^*}^{-1} S_{\theta^*,i}\right).
\end{aligned}$$

Notice the facts that

$$\begin{aligned}
E\left(\frac{Z_iY_i}{r} - \frac{(1-Z_i)Y_i}{1-r}\right) = 0, E(S_{\theta^*,i}) = 0, \\
E(S_{\theta^*,i}S_{\theta^*,i}^T) = E\left\{\frac{(Z_i-r)^2}{r^2(1-r)^2}\right\} E\left\{\frac{\partial e(X_i;\theta^*)}{\partial\theta}\frac{\partial e(X_i;\theta^*)}{\partial\theta}^T\right\} \\
= \frac{1}{(1-r)r} E\left\{\frac{\partial e(X_i;\theta^*)}{\partial\theta}\frac{\partial e(X_i;\theta^*)}{\partial\theta}^T\right\} = I_{\theta^*\theta^*},
\end{aligned}$$

we have,

$$\begin{aligned}
&\text{Var}\left(E\left[\left\{\frac{Z_iY_i}{r} - \frac{(1-Z_i)Y_i}{1-r}\right\} S_{\theta^*,i}^T\right] I_{\theta^*\theta^*}^{-1} S_{\theta^*,i}\right) \\
=&E\left[\left\{\frac{Z_iY_i}{r} - \frac{(1-Z_i)Y_i}{1-r}\right\} S_{\theta^*,i}^T\right] I_{\theta^*\theta^*}^{-1} E\left[\left\{\frac{Z_iY_i}{r} - \frac{(1-Z_i)Y_i}{1-r}\right\} S_{\theta^*,i}\right], \\
=&\text{Cov}\left(\left\{\frac{Z_iY_i}{r} - \frac{(1-Z_i)Y_i}{1-r}\right\}, E\left[\left\{\frac{Z_iY_i}{r} - \frac{(1-Z_i)Y_i}{1-r}\right\} S_{\theta^*,i}^T\right] I_{\theta^*\theta^*}^{-1} S_{\theta^*,i}\right).
\end{aligned}$$

We can further reduce the asymptotic variance to,

$$\lim_{N\to\infty} N\text{Var}(\hat{\tau}^{\text{OW}}) = \text{Var}\left(\frac{Z_iY_i}{r} - \frac{(1-Z_i)Y_i}{1-r}\right) - \text{Var}\left(E\left[\left\{\frac{Z_iY_i}{r} - \frac{(1-Z_i)Y_i}{1-r}\right\} S^T_{\theta^*,i}\right] I^{-1}_{\theta^*\theta^*} S_{\theta^*,i}\right).$$

Recall that X^1 and X^2 denote two nested sets of covariates with $X^2 = (X^1, X^{*1})$, and $e(X^1_i;\theta_1)$, $e(X^2_i;\theta_2)$ are the nested smooth parametric propensity score models. Suppose $\hat{\tau}^{\text{OW}}_1$ and $\hat{\tau}^{\text{OW}}_2$ are two OW estimators derived from the fitted propensity score $e(X^1_i;\hat{\theta}_1)$ and $e(X^1_i;\hat{\theta}_2)$ respectively. Denote the true value of the nested propensity score models as θ^{*1},θ^{*2}, the score functions at true value as $S_{\theta^{*1},i}$,$S_{\theta^{*2},i}$ and the information matrix as $I_{\theta^{*1},\theta^{*1}}$ and $I_{\theta^{*2},\theta^{*2}}$. To prove $\lim_{N\to\infty} N\text{Var}(\hat{\tau}^{\text{OW}}_1) \geq \lim_{N\to\infty} N\text{Var}(\hat{\tau}^{\text{OW}}_2)$, it is equivalent to establish the following inequality,

$$\text{Var}\left(E\left[\left\{\frac{Z_iY_i}{r} - \frac{(1-Z_i)Y_i}{1-r}\right\} S^T_{\theta^{*2},i}\right] I^{-1}_{\theta^{*2}\theta^{*2}} S_{\theta^{*2},i}\right) \geq \text{Var}\left(E\left[\left\{\frac{Z_iY_i}{r} - \frac{(1-Z_i)Y_i}{1-r}\right\} S^T_{\theta^{*1},i}\right] I^{-1}_{\theta^{*1}\theta^{*1}} S_{\theta^{*1},i}\right).$$

Using the equivalent expression, this inequality becomes,

$$E\left[\left\{\frac{Z_iY_i}{r} - \frac{(1-Z_i)Y_i}{1-r}\right\} S^T_{\theta^{*2},i}\right] I^{-1}_{\theta^{*2}\theta^{*2}} E\left[\left\{\frac{Z_iY_i}{r} - \frac{(1-Z_i)Y_i}{1-r}\right\} S_{\theta^{*2},i}\right] \geq E\left[\left\{\frac{Z_iY_i}{r} - \frac{(1-Z_i)Y_i}{1-r}\right\} S^T_{\theta^{*1},i}\right] I^{-1}_{\theta^{*1}\theta^{*1}} E\left[\left\{\frac{Z_iY_i}{r} - \frac{(1-Z_i)Y_i}{1-r}\right\} S_{\theta^{*1},i}\right].$$

Additionally, as the two models are nested,

$$I_{\theta^{*2}\theta^{*2}} = \begin{bmatrix} I_{\theta^{*1}\theta^{*1}} & I^{12}_{\theta^{*2}\theta^{*2}} \\ I^{21}_{\theta^{*2}\theta^{*2}} & I^{22}_{\theta^{*2}\theta^{*2}} \end{bmatrix} \triangleq \begin{bmatrix} I_{11} & I_{12} \\ I_{21} & I_{22} \end{bmatrix},$$

$$E\left[\left\{\frac{Z_iY_i}{r} - \frac{(1-Z_i)Y_i}{1-r}\right\} S_{\theta^{*2},i}\right] = E\left[\begin{Bmatrix} \frac{Z_iY_i}{r} - \frac{(1-Z_i)Y_i}{1-r} \\ \frac{Z_iY_i}{r} - \frac{(1-Z_i)Y_i}{1-r} \end{Bmatrix} \begin{matrix} S_{\theta^{*1},i} \\ S^2_{\theta^{*1},i} \end{matrix}\right] \triangleq \begin{bmatrix} U_1 \\ U_2 \end{bmatrix}.$$

The inverse of the information matrix for the larger model is

$$I^{-1}_{\theta^{*2}\theta^{*2}} = \begin{bmatrix} I^{-1}_{11} + I^{-1}_{11} I_{12}(I_{22} - I_{21}I^{-1}_{11}I_{12})^{-1} I_{21} I^{-1}_{11} & -I^{-1}_{11} I_{12}(I_{22} - I_{21}I^{-1}_{11}I_{12})^{-1} \\ -(I_{22} - I_{21}I^{-1}_{11}I_{12})^{-1} I_{21} I^{-1}_{11} & (I_{22} - I_{21}I^{-1}_{11}I_{12})^{-1} \end{bmatrix}.$$

Hence we can calculate the difference of asymptotic variance,

$$\begin{aligned}\lim_{N\to\infty} N\mathrm{Var}(\hat{\tau}_1^{\mathrm{OW}}) - \lim_{N\to\infty} N\mathrm{Var}(\hat{\tau}_2^{\mathrm{OW}}) &= U_1^T\{I_{11}^{-1}I_{12}(I_{22}-I_{21}I_{11}^{-1}I_{12})^{-1}I_{21}I_{11}^{-1}\}U_1 \\ &-U_1^T I_{11}^{-1}I_{12}(I_{22}-I_{21}I_{11}^{-1}I_{12})^{-1}U_2 \\ &-U_2^T(I_{22}-I_{21}I_{11}^{-1}I_{12})^{-1}I_{21}I_{11}^{-1}U_1 + U_2^T(I_{22}-I_{21}I_{11}^{-1}I_{12})^{-1}U_2^T, \\ &=(I_{21}I_{11}^{-1}U_1-U_2)^T(I_{22}-I_{21}I_{11}^{-1}I_{12})^{-1}(I_{21}I_{11}^{-1}U_1-U_2)\geq 0.\end{aligned}$$

The last inequality follows from the fact that $(I_{22}-I_{21}I_{11}^{-1}I_{12})^{-1}$ is positive definite. Hence, we have proved the asymptotic variance of the $\hat{\tau}_2^{\mathrm{OW}}$ is no greater than the OW estimator $\hat{\tau}_1^{\mathrm{OW}}$ with fewer covariates, which completes the proof of Proposition 1(b).

Proof for Proposition 1(c): When we are using logistic regression to estimate the propensity score, we have $\frac{\partial e(X_i;\theta^*)}{\partial\theta} = r(1-r)\tilde{X}_i, \tilde{X}_i = (1, X_i^T)^T$. Plugging this quantity into the g_1, g_0, we have,

$$\begin{aligned}g_1(X_i) &= E(Y_i\tilde{X}_i|Z_i=1)^T E(\tilde{X}_i\tilde{X}_i^T)^{-1}\tilde{X}_i, \\ &= E(Y_i\tilde{X}_i|Z_i=1)^T E(\tilde{X}_i\tilde{X}_i^T|Z_i=1)^{-1}\tilde{X}_i, \\ g_0(X_i) &= E(Y_i\tilde{X}_i|Z_i=0)^T E(\tilde{X}_i\tilde{X}_i^T|Z_i=0)^{-1}\tilde{X}_i,\end{aligned}$$

where g_0 and g_1 correspond to linear projection of Y_i into the space of X_i (including a constant) in two arms. If the true outcome surface $E(Y_i|X_i, Z_i=1)$ and $E(Y_i|X_i, Z_i=0)$ are indeed linear functions of X_i, then the $g_1(X_i) = E(Y_i|X_i, Z_i=1)$,$g_0(X) = E(Y_i|X_i, Z_i=0)$, $\hat{\tau}^{\mathrm{OW}} = \hat{\mu_1}^{\mathrm{OW}} - \hat{\mu_0}^{\mathrm{OW}}$ is semiparametric efficient. As such, we complete the proof of Proposition 1(c).

Proof for Proposition 2: Since we require $h(x)$ to be a function of the propensity score, we denote the tilting function and the resulting balancing weights as $h(X_i;\theta), w_1(X_i;\theta), w_0(X_i;\theta)$ corresponding to each observation i. Also, we make the following assumptions:

(i) (Nonzero tilting function) There exists $\varepsilon > 0$ such that $P\{h(X_i;\theta^*) > \varepsilon\} = 1$.

(ii) (Smoothness) the first and second order derivatives of balancing weights with respect to the propensity score $\frac{d}{de}w_1(X_i;\theta)\}$, $\frac{d}{de}w_0(X_i;\theta)$,$\frac{d^2}{de^2}w_1(X_i;\theta)\}$, $\frac{d^2}{de^2}w_0(X_i;\theta)$ exists and are continuous in e.

(iii) (Bounded derivative in the neighborhood of θ^*) For the true value θ^*, there exists $c>0$ and $M_1>0, M_2>0$ such that

$$\left|\frac{d}{de}w_0(X_i;\theta^*)\right| \leq M_1, \left|\frac{d}{de}w_0(X_i;\theta^*)\right| \leq M_1$$
$$\left|\frac{d^2}{de^2}w_0(X_i;\theta)\right| \leq M_2, \left|\frac{d^2}{de^2}w_1(X_i;\theta)\right| \leq M_2,$$

almost surely for θ in the neighborhood of θ^*, i.e. $\theta \in \{\theta|\,||\theta-\theta^*||_1 \leq c\}$.

We do Taylor expansion at the true value θ^*,

$$\begin{aligned}
\sqrt{N}(\hat{\mu}_1^h-\hat{\mu}_0^h) =& \sqrt{N}\left(\frac{\sum_{i=1}^N Z_iY_iw_1(X_i;\hat{\theta})}{\sum_{i=1}^N Z_iw_1(X_i;\hat{\theta})}-\frac{\sum_{i=1}^N(1-Z_i)Y_iw_0(X_i;\hat{\theta})}{\sum_{i=1}^N(1-Z_i)w_0(X_i;\hat{\theta})}\right),\\
=&\frac{\frac{1}{\sqrt{N}}\sum_{i=1}^N Z_iY_iw_1(X_i;\hat{\theta})}{E\{h(X_i;\theta^*)\}}-\frac{\frac{1}{\sqrt{N}}\sum_{i=1}^N(1-Z_i)Y_iw_0(X_i;\hat{\theta})}{E\{h(X_i;\theta^*)\}}+o_p(1),\\
=&\frac{1}{\sqrt{N}}\sum_{i=1}^N\left\{\frac{Z_iY_iw_1(X_i;\theta^*)}{E\{h(X_i;\theta^*)\}}-\frac{(1-Z_i)Y_iw_0(X_i;\theta^*)}{E\{h(X_i;\theta^*)\}}\right.\\
&+\frac{\left\{Z_iY_i\frac{d}{de}w_1(X_i;\theta^*)-(1-Z_i)Y_i\frac{d}{de}w_0(X_i;\theta^*)\right\}\frac{\partial e(X_i;\theta^*)}{\partial\theta}^T(\hat{\theta}-\theta^*)}{E\{h(X_i;\theta^*)\}}\\
&+\{Z_iY_i\left[\frac{d^2}{de^2}w_1(X_i;\tilde{\theta})+\frac{d}{de}w_1(X_i;\tilde{\theta})\right]\\
&-(1-Z_i)Y_i\left[\frac{d^2}{de^2}w_0(X_i;\tilde{\theta})+\frac{d}{de}w_0(X_i;\tilde{\theta})\right]\}\\
&\left.(\hat{\theta}-\theta^*)^T\frac{\partial^2e(X_i;\tilde{\theta})}{\partial\theta^2}(\hat{\theta}-\theta^*)/E\{h(X_i;\theta^*)\}\right\}+o_p(1),
\end{aligned}$$

where $\tilde{\theta}$ lies in the line between θ^* and $\hat{\theta}$, such that $\tilde{\theta}=\theta^*+t(\hat{\theta}-\theta^*), t\in(0,1)$ (Taylor expansion with Lagrange remainder term). To see that the third term converges to zero in probability, we have $\sqrt{N}(\hat{\theta}-\theta^*)$ is asymptotic normal distributed with Cramer-Rao theorem and the asymptotic covariance is proportional to $E\left\{\frac{\partial^2e(X_i;\theta^*)}{\partial\theta^2}\right\}^{-1}$, which

means $N(\hat{\theta}-\theta^*)^T E\left\{\frac{\partial^2 e(X_i;\theta^*)}{\partial\theta^2}\right\}(\hat{\theta}-\theta^*)$ is tight, or equivalently

$$P\left\{N(\hat{\theta}-\theta^*)^T E\left\{\frac{\partial^2 e(X_i;\theta^*)}{\partial\theta^2}\right\}(\hat{\theta}-\theta^*)<\infty\right\}=1.$$

Secondly, as $\hat{\theta}\xrightarrow{p}\theta^*$, $\tilde{\theta}\xrightarrow{p}\theta^*$, when N is sufficiently large, $||\tilde{\theta}-\theta^*||_1\leq c$, the first and second order derivative is bounded almost surely, such that

$$\left|\frac{d^2}{de^2}w_1(X_i;\tilde{\theta})+\frac{d}{de}w_1(X_i;\tilde{\theta})\right|\leq M_1+M_2,\left|\frac{d^2}{de^2}w_0(X_i;\tilde{\theta})+\frac{d}{de}w_0(X_i;\tilde{\theta})\right|\leq M_1+M_2.$$

Therefore, by the WLLN,

$$\begin{aligned}&\frac{1}{N}\sum_{i=1}^{N}\{Z_iY_i\left[\frac{d^2}{de^2}w_1(X_i;\tilde{\theta})+\frac{d}{de}w_1(X_i;\tilde{\theta})\right]\\&-(1-Z_i)Y_i\left[\frac{d^2}{de^2}w_0(X_i;\tilde{\theta})+\frac{d}{de}w_0(X_i;\tilde{\theta})\right]\}\\\leq(M_1+M_2)&\frac{1}{N}\sum_{i=1}^{N}|Z_iY_i|+|(1-Z_i)Y_i)|\xrightarrow{p}E\{|Z_iY_i|+|(1-Z_i)Y_i)|\}<\infty.\end{aligned}$$

Also, as $\tilde{\theta}\xrightarrow{p}\theta^*$, and we assume $e(X_i;\theta)$ is smooth (so that $\frac{\partial^2 e(X_i;\tilde{\theta})}{\partial\theta^2}$ is continuous),

$$\frac{1}{N}\sum_{i=1}^{N}\frac{\partial^2 e(X_i;\tilde{\theta})}{\partial\theta^2}\xrightarrow{p}E\left\{\frac{\partial^2 e(X_i;\theta^*)}{\partial\theta^2}\right\}.$$

As such, we can conclude that the third term converges to zero in probability,

$$\begin{aligned}&\frac{1}{\sqrt{N}}\sum_{i=1}^{N}\{Z_iY_i\left[\frac{d^2}{de^2}w_1(X_i;\tilde{\theta})+\frac{d}{de}w_1(X_i;\tilde{\theta})\right]\\&-(1-Z_i)Y_i\left[\frac{d^2}{de^2}w_0(X_i;\tilde{\theta})+\frac{d}{de}w_0(X_i;\tilde{\theta})\right]\}\\&(\hat{\theta}-\theta^*)^T\frac{\partial^2 e(X_i;\tilde{\theta})}{\partial\theta^2}(\hat{\theta}-\theta^*)/E\{h(X_i;\theta^*)\}\\=O_p\left(\frac{1}{\sqrt{N}}\right.&\left.\frac{E\{|Z_iY_i|+|(1-Z_i)Y_i)|\}N(\hat{\theta}-\theta^*)^T E\left\{\frac{\partial^2 e(X_i;\theta^*)}{\partial\theta^2}\right\}(\hat{\theta}-\theta^*)}{E\{h(X_i;\theta^*)\}}\right)\xrightarrow{p}0.\end{aligned}$$

Hence, we have,

$$\begin{aligned}
\sqrt{N}(\hat{\mu}_1^h - \hat{\mu}_0^h) =& \frac{1}{\sqrt{N}} \sum_{i=1}^{N} \left\{ \frac{Z_i Y_i w_1(X_i;\theta^*)}{E\{h(X_i;\theta^*)\}} - \frac{(1-Z_i) Y_i w_0(X_i;\theta^*)}{E\{h(X_i;\theta^*)\}} \right. \\
& \left. + \frac{\left\{ Z_i Y_i \frac{d}{de} w_1(X_i;\theta^*) - (1-Z_i) Y_i \frac{d}{de} w_0(X_i;\theta^*) \right\} \frac{\partial e(X_i;\theta^*)}{\partial \theta} (\hat{\theta} - \theta^*)}{E\{h(X_i;\theta^*)\}} \right\} \\
& + o_p(1), \\
=& \frac{1}{\sqrt{N}} \sum_{i=1}^{N} \left\{ \frac{Z_i Y_i h(X_i;\theta^*)/r}{E\{h(X_i;\theta^*)\}} - \frac{(1-Z_i) Y_i h(X_i;\theta^*)/(1-r)}{E\{h(X_i;\theta^*)\}} \right. \\
& + \frac{E\left[\left\{ Z_i Y_i \frac{d}{de} w_1(X_i;\theta^*) - (1-Z_i) Y_i \frac{d}{de} w_0(X_i;\theta^*) \right\} \frac{\partial e(X_i;\theta^*)}{\partial \theta}^T \right]}{E\{h(X_i;\theta^*)\}} \\
& \left. I_{\theta^*\theta^*}^{-1} \frac{1}{\sqrt{N}} \sum_{i=1}^{N} S_{\theta^*,i} \right\} + o_p(1).
\end{aligned}$$

Since $h(X_i;\theta)$ is a function of propensity score, $h(X_i;\theta^*)$ is a function of r, which means $E\{h(X_i;\theta^*)\} = h(X_i;\theta^*)$. Applying this property and plugging in the value of $S_{\theta^*,i}, I_{\theta^*\theta^*}$, we have,

$$\begin{aligned}
\hat{\mu}_1^h - \hat{\mu}_0^h =& \frac{1}{N} \sum_{i=1}^{N} \left[\frac{Z_i Y_i}{r} - \frac{(1-Z_i) Y_i}{1-r} - \frac{Z_i - r}{r(1-r)} \left\{ (1-r) g_1^h(X_i) + r g_0^h(X_i) \right\} \right] \\
& + o_p(N^{-1/2}), \\
g_1^h(X_i) =& - \frac{r}{h(X_i;\theta^*)} E\left\{ Z_i Y_i \frac{d}{de} w_1(X_i;\theta^*) \right\} \frac{\partial e(X_i;\theta^*)}{\partial \theta}^T \\
& E\left\{ \frac{\partial e(X_i;\theta^*)}{\partial \theta} \frac{\partial e(X_i;\theta^*)}{\partial \theta}^T \right\}^{-1} \frac{\partial e(X_i;\theta^*)}{\partial \theta}, \\
g_0^h(X_i) =& \frac{1-r}{h(X_i;\theta^*)} E\left\{ (1-Z_i) Y_i \frac{d}{de} w_0(X_i;\theta^*) \right\} \frac{\partial e(X_i;\theta^*)}{\partial \theta}^T \\
& E\left\{ \frac{\partial e(X_i;\theta^*)}{\partial \theta} \frac{\partial e(X_i;\theta^*)}{\partial \theta}^T \right\}^{-1} \frac{\partial e(X_i;\theta^*)}{\partial \theta},
\end{aligned}$$

which completes the proof of Proposition 2.

8.1.2 Derivation of the asymptotic variance and its consistent estimator in Section 2.3

Asymptotic variance derivation. As we have shown in the main text (Section 3.3), the asymptotic variance of $\hat{\tau}^{\text{OW}}$ depends on the elements in the sandwich matrix $A^{-1}BA^{-T}$, where $A = -E(\partial U_i/\partial\lambda)$,$B = E(U_iU_i^T)$ evaluated at the true parameter value (μ_1, μ_0, θ^*). The exact form of the matrices A and B are as follows:

$$A = \begin{bmatrix} a_{11} & 0 & a_{13} \\ 0 & a_{22} & a_{23} \\ 0 & 0 & a_{33} \end{bmatrix}, A^{-1} = \begin{bmatrix} a_{11}^{-1} & 0 & -a_{11}^{-1}a_{13}a_{33}^{-1}, \\ 0 & a_{22}^{-1} & -a_{22}^{-1}a_{23}a_{33}^{-1} \\ 0 & 0 & a_{33}^{-1} \end{bmatrix}, B = \begin{bmatrix} b_{11} & 0 & b_{13} \\ 0 & b_{22} & b_{23} \\ b_{13}^T & b_{23}^T & b_{33} \end{bmatrix},$$

$$a_{11} = E\{Z_i(1-e_i)\}, a_{13} = E\{\tilde{X}_i^T(Y_i-\mu_1)Z_ie_i(1-e_i)\}, a_{22} = E\{(1-Z_i)e_i\},$$

$$a_{23} = -E(\tilde{X}_i^T(Y_i-\mu_0)(1-Z_i)e_i(1-e_i), a_{33} = E(e_i(1-e_i)\tilde{X}\tilde{X}^T],$$

$$b_{11} = E\{(Y_i-\mu_1)^2Z_i(1-e_i)^2\}, b_{13} = E\{\tilde{X}_i^T(Y_i-\mu_1)Z_i(Z_i-e_i)(1-e_i),$$

$$b_{23} = E\{\tilde{X}_i^T(Y_i-\mu_0)(1-Z_i)(Z_i-e_i)e_i\},$$

$$b_{22} = E\{(Y_i-\mu_0)^2(1-Z_i)e_i^2\}, b_{33} = E\{(Z_i-e_i)^2\tilde{X}_i\tilde{X}_i^T\}.$$

After multiplying $A^{-1}BA^{-T}$ and extracting the upper left 2×2 matrix, we have,

$$\Sigma_{11} = [A^{-1}BA^{-T}]_{1,1} = \frac{1}{a_{11}^{-2}}(b_{11} - 2a_{13}a_{33}^{-1}b_{13}^T + a_{13}a_{33}^{-1}b_{33}a_{33}^{-1}a_{13}^T),$$

$$\Sigma_{22} = [A^{-1}BA^{-T}]_{2,2} = \frac{1}{a_{22}^{-2}}(b_{22} - 2a_{23}a_{33}^{-1}b_{23}^T + a_{23}a_{33}^{-1}b_{33}a_{33}^{-1}a_{23}^T),$$

$$\Sigma_{12} = \Sigma_{21} = [A^{-1}BA^{-T}]_{1,2} = \frac{1}{a_{11}a_{22}}(-a_{13}a_{33}^{-1}b_{23}^T - a_{23}a_{33}^{-1}b_{13}^T + a_{13}a_{33}^{-1}b_{33}a_{33}^{-1}a_{23}^T).$$

With the delta method, we can express the asymptotic variance for $\hat{\tau}_{\text{RD}}^{\text{OW}}, \hat{\tau}_{\text{RR}}^{\text{OW}}, \hat{\tau}_{\text{OR}}^{\text{OW}}$,

$$\text{Var}(\hat{\tau}_{\text{RD}}^{\text{OW}}) = \frac{1}{N}\left(\Sigma_{11} + \Sigma_{22} - 2\Sigma_{12}\right),$$

$$\text{Var}(\hat{\tau}_{\text{RR}}^{\text{OW}}) = \frac{1}{N}\left(\frac{\Sigma_{11}}{\mu_1^2} + \frac{\Sigma_{22}}{\mu_0^2} - \frac{2\Sigma_{12}}{\mu_1\mu_0}\right),$$

$$\text{Var}(\hat{\tau}_{\text{OR}}^{\text{OW}}) = \frac{1}{N}\left\{\frac{\Sigma_{11}}{\mu_1^2(1-\mu_1)^2} + \frac{\Sigma_{22}}{\mu_0^2(1-\mu_0)^2} - \frac{2\Sigma_{12}}{\mu_1(1-\mu_1)\mu_0(1-\mu_0)}\right\}.$$

Specifically, we write out the exact form of large sample variance for the estimator on additive scale after exploiting the fact that $E(Z_i) = E(e_i) = r$,

$$NVar(\hat{\tau}^{\text{OW}}) \to \frac{\text{Var}(Y_i|Z_i=1)}{r} + \frac{\text{Var}(Y_i|Z_i=1)}{1-r} - \frac{\{rm_1 + (1-r)m_0\}E(\tilde{X}_i\tilde{X}_i^T)^{-1}\{(2-3r)m_1 + (3r-1)m_0\}}{r(1-r)},$$

where $m_1 = E(\tilde{X}_i(Y_i - \mu_1)|Z_i = 1), m_0 = E(\tilde{X}_i(Y_i - \mu_1)|Z_i = 1)$

Connection to R-squared: When $r = 0.5$, the large sample variance of $\hat{\tau}^{\text{OW}}$ is,

$$\begin{aligned}
N\text{Var}(\hat{\tau}^{\text{OW}}) \to & 2\left\{\text{Var}(Y_i|Z_i=1) + \text{Var}(Y_i|Z_i=0)\right\} \\
& -4(\frac{1}{2}m_1 + \frac{1}{2}m_0)E(\tilde{X}\tilde{X}^T)^{-1}(\frac{1}{2}m_1 + \frac{1}{2}m_0), \\
= & 2\left\{\text{Var}(Y_i|Z_i=1) + \text{Var}(Y_i|Z_i=0)\right\} - 4E(\tilde{X}_i\tilde{Y}_i)E(\tilde{X}_i\tilde{X}_i^T)^{-1}E(\tilde{X}_i\tilde{Y}_i), \\
= & 2\left\{\text{Var}(Y_i|Z_i=1) + \text{Var}(Y_i|Z_i=0)\right\} - 4R^2_{\tilde{Y}\sim X}\text{Var}(\tilde{Y}_i), \\
= & 2\left\{\text{Var}(Y_i|Z_i=1) + \text{Var}(Y_i|Z_i=0)\right\} \\
& -2R^2_{\tilde{Y}\sim X}\left\{\text{Var}(Y_i|Z_i=1) + \text{Var}(Y_i|Z_i=0)\right\}, \\
= & 4(1 - R^2_{\tilde{Y}\sim X})\text{Var}(\tilde{Y}_i), \\
= & \lim_{N\to\infty}(1 - R^2_{\tilde{Y}\sim X})N\text{Var}(\hat{\tau}^{\text{UNADJ}}).
\end{aligned}$$

where $\tilde{Y}_i = Z_i(Y_i - \mu_1) + (1 - Z_i)(Y_i - \mu_0)$. In the derivation, we use the fact that,

$$\begin{aligned}
\text{Var}(\tilde{Y}_i) = E(\tilde{Y}_i^2) - E(\tilde{Y}_i)^2 &= \frac{1}{2}E\left((Y_i - \mu_1)^2|Z_i = 1\right) + \frac{1}{2}E\left((Y_i - \mu_1)^2|Z_i = 1\right) \\
&= \frac{1}{2}\left\{\text{Var}(Y_i|Z_i=1) + \text{Var}(Y_i|Z_i=0)\right\}.
\end{aligned}$$

The efficiency gain is regardless of whether our model is correctly specified or not. Additionally, if we augment the covariate space from $\tilde{X}_i$ to X_i^*, the $R^2_{\tilde{Y}\sim X}$ is non-decreasing with $R^2_{\tilde{Y}\sim X} \leq R^2_{\tilde{Y}\sim X^*}$. Therefore, the asymptotic variance of OW estimator with additional covariates decreases, $\text{Var}(\hat{\tau}^{\text{OW}*}) \leq \text{Var}(\hat{\tau}^{\text{OW}})$. This provides a heuristic justification of Proposition 1(b) when $r = 0.5$.

Consistent variance estimator: We obtain the empirical estimator for the asymptotic variance by plugging in the finite sample estimate for the elements in the sandwich matrix $A^{-1}BA^{-T}$,

$$\hat{\Sigma}_{11} = \frac{1}{\hat{a}_{11}^2}(\hat{b}_{11} - 2\hat{a}_{13}\hat{a}_{33}^{-1}\hat{b}_{13}^T + \hat{a}_{13}\hat{a}_{33}^{-1}\hat{a}_{13}^T),$$
$$\hat{\Sigma}_{22} = \frac{1}{\hat{a}_{11}^2}(\hat{b}_{22} - 2\hat{a}_{23}\hat{a}_{33}^{-1}\hat{b}_{23}^T + \hat{a}_{23}\hat{a}_{33}^{-1}\hat{a}_{23}^T),$$
$$\hat{\Sigma}_{12} = -\frac{1}{\hat{a}_{11}^2}(\hat{a}_{13}\hat{a}_{33}^{-1}\hat{b}_{23}^T + \hat{a}_{23}\hat{a}_{33}^{-1}\hat{b}_{13}^T - \hat{a}_{13}\hat{a}_{33}^{-1}\hat{a}_{23}^T),$$

$$\hat{a}_{11} = \hat{a}_{22} = \frac{1}{N}\sum_{i=1}^{N}\{\hat{e}_i(1-\hat{e}_i)\}, \hat{a}_{33} = \hat{b}_{33} = \frac{1}{N}\sum_{i=1}^{N}\{\hat{e}_i(1-\hat{e}_i)\tilde{X}_i^T\tilde{X}_i\},$$
$$\hat{a}_{13} = \frac{1}{N_1}\sum_{i=1}^{N} Z_i\hat{e}_i^2(1-\hat{e}_i)(Y_i-\hat{\mu}_1)^2\tilde{X}_i, \hat{a}_{23} = \frac{1}{N_0}\sum_{i=1}^{N}(1-Z_i)\hat{e}_i(1-\hat{e}_i)^2(Y_i-\hat{\mu}_0)^2\tilde{X}_i,$$
$$\hat{b}_{11} = \frac{1}{N_1}\sum_{i=1}^{N} Z_i\hat{e}_i(1-\hat{e}_i)^2(Y_i-\hat{\mu}_1)^2, \hat{b}_{22} = \frac{1}{N_0}\sum_{i=1}^{N}(1-Z_i)\hat{e}_i^2(1-\hat{e}_i)(Y_i-\hat{\mu}_0)^2,$$
$$\hat{b}_{13} = \frac{1}{N_1}\sum_{i} Z_i\hat{e}_i(1-\hat{e}_i)^2(Y_i-\hat{\mu}_1)\tilde{X}_i, \hat{b}_{23} = \frac{1}{N_0}\sum_{i}(1-Z_i)\hat{e}_i^2(1-\hat{e}_i)(Y_i-\hat{\mu}_0)\tilde{X}_i.$$

Hence, we summarize the estimators for the asymptotic variance of $\hat{\tau}_{\text{RD}}^{\text{OW}}, \hat{\tau}_{\text{RR}}^{\text{OW}}, \hat{\tau}_{\text{OR}}^{\text{OW}}$ in the following equations,

$$\text{Var}(\hat{\tau}^{\text{OW}}) = \frac{1}{N}\left[\hat{V}^{\text{UNADJ}} - \hat{v}_1^T\left\{\frac{1}{N}\sum_{i=1}^{N}\hat{e}_i(1-\hat{e}_i)\tilde{X}_i^T\tilde{X}_i\right\}^{-1}(2\hat{v}_1 - \hat{v}_2)\right],$$

where

$$\hat{V}^{\text{UNADJ}} = \left\{ \frac{1}{N} \sum_{i=1}^{N} \hat{e}_i(1-\hat{e}_i) \right\}^{-1}$$
$$\left(\frac{\hat{E}_1^2}{N_1} \sum_{i=1}^{N} Z_i \hat{e}_i (1-\hat{e}_i)^2 (Y_i - \hat{\mu}_1)^2 + \frac{\hat{E}_0^2}{N_0} \sum_{i=1}^{N} (1-Z_i) \hat{e}_i^2 (1-\hat{e}_i)(Y_i - \hat{\mu}_0)^2 \right),$$
$$\hat{v}_1 = \left\{ \frac{1}{N} \sum_{i=1}^{N} \hat{e}_i(1-\hat{e}_i) \right\}^{-1}$$
$$\left(\frac{\hat{E}_1}{N_1} \sum_{i=1}^{N} Z_i \hat{e}_i^2 (1-\hat{e}_i)(Y_i - \hat{\mu}_1)^2 \tilde{X}_i + \frac{\hat{E}_0}{N_0} \sum_{i=1}^{N} (1-Z_i) \hat{e}_i (1-\hat{e}_i)^2 (Y_i - \hat{\mu}_0)^2 \tilde{X}_i \right),$$
$$\hat{v}_2 = \left\{ \frac{1}{N} \sum_{i=1}^{N} \hat{e}_i(1-\hat{e}_i) \right\}^{-1}$$
$$\left(\frac{\hat{E}_1}{N_1} \sum_{i=1}^{N} Z_i \hat{e}_i (1-\hat{e}_i)^2 (Y_i - \hat{\mu}_1)^2 \tilde{X}_i + \frac{\hat{E}_0}{N_0} \sum_{i=1}^{N} (1-Z_i) \hat{e}_i^2 (1-\hat{e}_i)(Y_i - \hat{\mu}_0)^2 \tilde{X}_i \right),$$

and $\hat{E}_k$ depends on the estimands. For $\hat{\tau}^{\text{OW}}_{\text{RD}}$, we have $\hat{E}_k = 1$; for $\hat{\tau}^{\text{OW}}_{\text{RR}}$, we set $\hat{E}_k = \hat{\mu}_k^{-1}$; for $\hat{\tau}^{\text{OW}}_{\text{OR}}$, we use $\hat{E}_k = \hat{\mu}_k^{-1}(1-\hat{\mu}_k)^{-1}$ with $k = 0, 1$.

8.1.3 Variance estimator for $\hat{\tau}^{AIPW}$

In this section, we provide the details on how to derive the variance estimator for $\hat{\tau}^{\text{AIPW}}$ in the main text. Let $\mu_1(X_i;\alpha_1)$, $\mu_0(X_i;\alpha_0)$ be the outcome surface for treated and control samples respectively, with α_1, α_0 being the regression parameters. Suppose $\hat{\alpha}_1$, $\hat{\alpha}_0$ are the MLEs that solve the score functions $\sum_{i=1}^{N} Z_i S_1(Y_i, X_i; \alpha_1) = 0$ and $\sum_{i=1}^{N} (1-Z_i) S_0(Y_i, X_i; \alpha_0) = 0$. We resume our notation and let $e(X_i;\theta)$ be the propensity score, $\hat{\theta}$ be the parameters and $S_\theta(X_i;\theta)$ be the corresponding score function. Recall that $\hat{\tau}^{\text{AIPW}}$ takes the following form:

$$\hat{\tau}^{\text{AIPW}} = \hat{\mu}_1^{\text{AIPW}} - \hat{\mu}_0^{\text{AIPW}} = \frac{1}{N} \sum_{i=1}^{N} \left\{ \frac{Z_i Y_i}{\hat{e}_i} - \frac{(Z_i - \hat{e}_i)\hat{\mu}_1(X_i)}{\hat{e}_i} \right\} - \left\{ \frac{(1-Z_i)Y_i}{1-\hat{e}_i} + \frac{(Z_i - \hat{e}_i)\hat{\mu}_0(X_i)}{1-\hat{e}_i} \right\},$$

Let $\lambda = (\nu_1, \nu_0, \alpha_0, \alpha_1, \theta)$ and $\hat{\lambda} = (\hat{\nu}_1, \hat{\nu}_0, \hat{\alpha}_0, \hat{\alpha}_1, \hat{\theta})$. Note that $\hat{\lambda}$ is the solution for λ in the equations below:

$$\sum_{i=1}^{N} \Psi_i = \sum_{i=1}^{N} \begin{bmatrix} \nu_1 - \{Z_i Y_i - (Z_i - e_i)\mu_1(X_i;\alpha_1)\}/e_i \\ \nu_0 - \{(1-Z_i)Y_i + (Z_i - e_i)\mu_0(X_i;\alpha_0)\}/(1-e_i) \\ Z_i S_1(Y_i, X_i; \alpha_1) \\ (1-Z_i) S_0(Y_i, X_i; \alpha_0) \\ S_\theta(X_i;\theta) \end{bmatrix} = 0.$$

The asymptotic covariance of $\hat{\lambda}$ can be obtained via M-estimation theory, which equals $A^{-1}BA^T$, with $A = -E(\partial\Psi_i/\partial\lambda), B = E(\Psi_i\Psi_i^T)$. In practice, we use plug-in method to estimate A, B. We can express $\hat{\tau}^{\text{AIPW}}$ with the solution $\hat{\lambda}$ as $\hat{\tau}^{\text{AIPW}} = \hat{\nu}_1 - \hat{\nu}_0$. Next, we can calculate the asymptotic variance of $\hat{\tau}^{\text{AIPW}}$ based on the asymptotic covariance of $\hat{\lambda}$ and the delta method. Similarly, it is straightforward to obtain the estimator for risk ratio estimator $\hat{\tau}^{\text{AIPW}}_{\text{RR}} = \log(\hat{\nu}_1/\hat{\nu}_0)$ and odds ratio estimator $\hat{\tau}^{\text{AIPW}}_{\text{OR}} = \log(\hat{\nu}_1/(1-\hat{\nu}_1)) - \log(\hat{\nu}_0/(1-\hat{\nu}_0))$, as in Appendix B.

8.1.4 Additional simulations with binary outcomes

Simulation design

We conduct a second set of simulations where the outcomes are generated from a generalized linear model. Specifically, we assume the potential outcome follows a logistic regression model (model 3): for $z = 0, 1$,

$$\text{logit}\{\Pr(Y_i(z) = 1)\} = \eta + z\alpha + X_i^T\beta_0 + zX_i^T\beta_1, \quad i = 1, 2, \ldots, N, \tag{8.1}$$

where X_i denotes the vector of $p = 10$ baseline covariates simulated as in Section 4.1 in the main manuscript, and the parameter η represents the prevalence of the outcomes in the control arm, i.e., $u \approx \Pr\{Y_i(0) = 1\} = 1/(1 + \exp(-\eta))$. We specify the main effects $\beta_0 = b_0 \times (1, 1, 2, 2, 4, 4, 8, 8, 16, 16)^T$, where b_0 is chosen to be the same value used in Section 4.1 for continuous outcomes. For the covariate-by-treatment interactions, we set $\beta_1 = b_1 \times (1, 1, 1, 1, 1, 1, 1, 1, 1, 1)^T$ and examine scenarios with $b_1 = 0$ and $b_1 = 0.75$, with the latter representing strong treatment

effect heterogeneity. Similarly, we set the true treatment effect to be zero $\tau = 0$. For the randomization probability r, we examine both balanced assignment with $r = 0.5$ and unbalanced assignment with $r = 0.7$. We vary the sample size N from 50 to 500 to represent both small and large sample sizes. We vary the value of η such that the baseline prevalence $u \in \{0.5, 0.3, 0.2, 0.1\}$, representing common to rare outcomes. It is expected that the regression adjustment becomes less stable with rare outcomes, while propensity score weighting estimators are less affected (Williamson et al., 2014).

Under each scenario, we simulate 2000 data replicates, and compare five estimators, $\hat{\tau}^{\text{UNADJ}}$, $\hat{\tau}^{\text{IPW}}$, $\hat{\tau}^{\text{LR}}$, $\hat{\tau}^{\text{AIPW}}$, $\hat{\tau}^{\text{OW}}$, for binary outcomes. The unadjusted estimator is the nonparametric difference-in-mean estimator. For the IPW and OW estimators, we fit a propensity score model by regressing the treatment on the main effects of the baseline covariates X_i. With a slight abuse of acronym, in this Section we will use the abbreviation 'LR' to represent logistic regression. For this estimator, we fit the logistic outcome model with main effects of treatment and covariates, along with their interactions, as in $\text{logit}\{\Pr(Y_i = 1)\} = \delta + Z_i\kappa + X_i^T\xi_0 + Z_iX_i^T\xi_1$. The group means μ_0, μ_1 are estimated by standardization (i.e. the basic form of the g-formula (Hernan and Robins, 2010)),

$$\hat{\mu}_0^{\text{LR}} = \frac{1}{N}\sum_{i=1}^{N} \frac{\exp(\hat{\delta} + X_i^T\hat{\xi}_0)}{1 + \exp(\hat{\delta} + X_i^T\hat{\xi}_0)}, \qquad \hat{\mu}_1^{\text{LR}} = \frac{1}{N}\sum_{i=1}^{N} \frac{\exp(\hat{\delta} + \hat{\kappa} + X_i^T\hat{\xi}_0 + X_i^T\hat{\xi}_1)}{1 + \exp(\hat{\delta} + \hat{\kappa} + X_i^T\hat{\xi}_0 + X_i^T\hat{\xi}_1)}. \tag{8.2}$$

The estimated group means are then used to calculate risk difference τ_{RD}, log risk ratio τ_{RR} and log odds ratio τ_{OR}. For the AIPW estimator, we estimate $\hat{\mu}_1^{\text{AIPW}}$ and $\hat{\mu}_0^{\text{AIPW}}$ as defined in equation (18) of the main text, except that $\hat{\mu}_z(X_i) = \hat{E}[Y_i|X_i, Z_i = z]$ is now the prediction from the above logistic outcome model. The ratio estimands are then estimated following equation (10) of the main text.

Because the bias of all these approaches is close to zero, we focus on the relative efficiency of the adjusted estimator compared to the unadjusted in estimating the three estimands. We also examine the performance of the variance and normality-based confidence interval estimators. For the LR estimator, we use the Huber-White

variance, and then derive the large-sample variance of $\hat{\tau}^{\text{LR}}_{\text{RD}}$, $\hat{\tau}^{\text{LR}}_{\text{RR}}$ and $\hat{\tau}^{\text{LR}}_{\text{OR}}$ using the delta method. For IPW, we use the sandwich variance of Williamson et al. (Williamson et al., 2014); for OW, we use the sandwich variance proposed in Section 3.3 of the main text. Details of the variance calculation for the AIPW estimator is given in Appendix C.

To explore the performance of estimators under model misspecification, we also repeat the simulations by considering a data generating process with additional covariate interaction terms (model 4): for $z = 0, 1$,

$$\text{logit}\{\Pr(Y_i(z) = 1)\} = \eta + z\alpha + X_i^T\beta_0 + zX_i\beta_1 + X_{i,\text{int}}^T\gamma, \quad i = 1, 2, \ldots, N, \quad (8.3)$$

which can be viewed as the binary analogy of model 2 defined in equation (19) of the main text. When the data are generated using model 4, we will examine the performance of a misspecified logistic regression ignoring the interaction terms $X_{i,\text{int}}$. Similarly, for IPW, OW and AIPW, the propensity score model will also ignore the interaction terms $X_{i,\text{int}}$.

Results on efficiency of point estimators

Within the range of sample sizes we considered, the potential efficiency gain using the covariate-adjusted estimators over the unadjusted estimator is *at most modest* for binary outcomes. Figure 8.1 presents the relative efficiency results. Because the finite-sample performance of AIPW is generally driven by the outcome regression component, we mainly focus on interpreting the comparisons between IPW, LR and OW. In column (a), where the outcome is common and the data are generated from model 3, $\hat{\tau}^{\text{IPW}}, \hat{\tau}^{\text{LR}}$ or $\hat{\tau}^{\text{OW}}$ become more efficient than $\hat{\tau}^{\text{UNADJ}}$ only when N is greater than 80. Because the true outcome model is used in model fitting, LR is slightly more efficient than OW and IPW but the difference quickly diminishes as N increases. The comparison results are similar when the outcome is generated from model 4 (column (b) and (d)). In addition, when the prevalence of the outcome decreases to

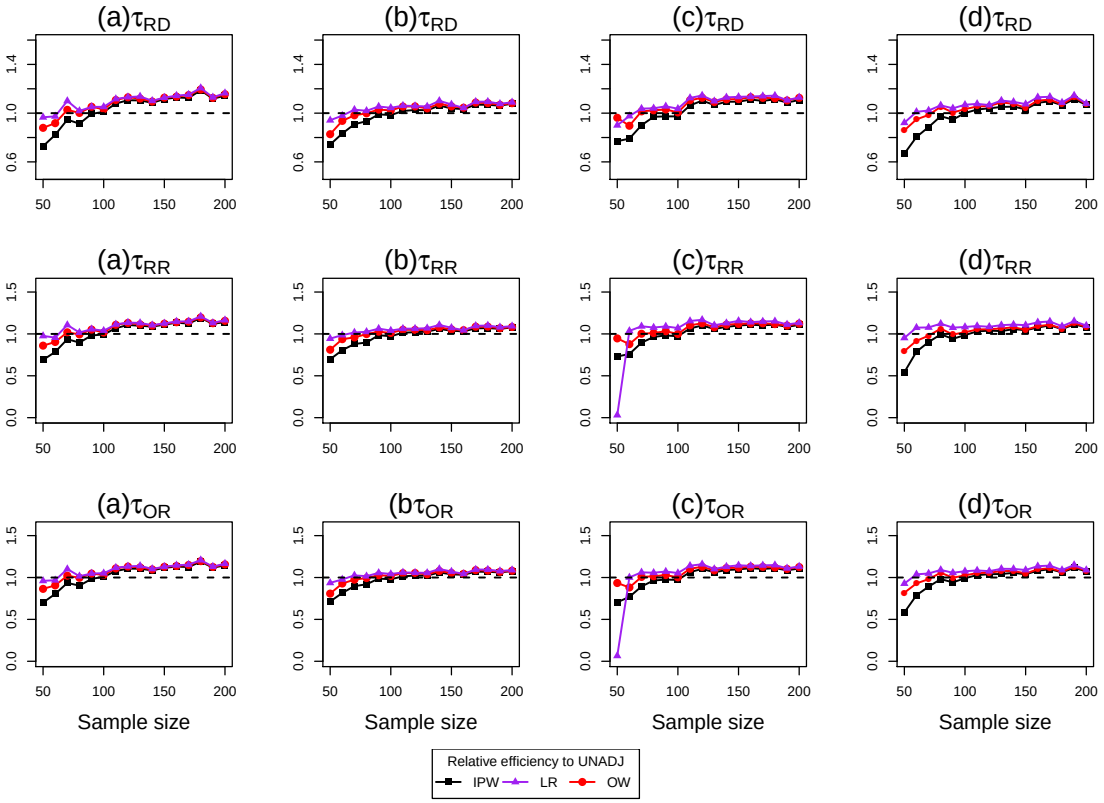

Figure 8.1: The relative efficiency of $\hat{\tau}^{\text{IPW}}$,$\hat{\tau}^{\text{LR}}$,$\hat{\tau}^{\text{AIPW}}$ and $\hat{\tau}^{\text{OW}}$ relative to $\hat{\tau}^{\text{UNADJ}}$ for estimating $\tau_{\text{RD}}, \tau_{\text{RR}}, \tau_{\text{OR}}$, when (a) $u = 0.5$ and the outcome model is correctly specified (b) $u = 0.5$ and the outcome model is misspecified (c) $u = 0.3$, and the outcome model is correctly specified (d) $u = 0.3$ and the outcome model is misspecified. A larger value of relative efficiency corresponds to a more efficient estimator.

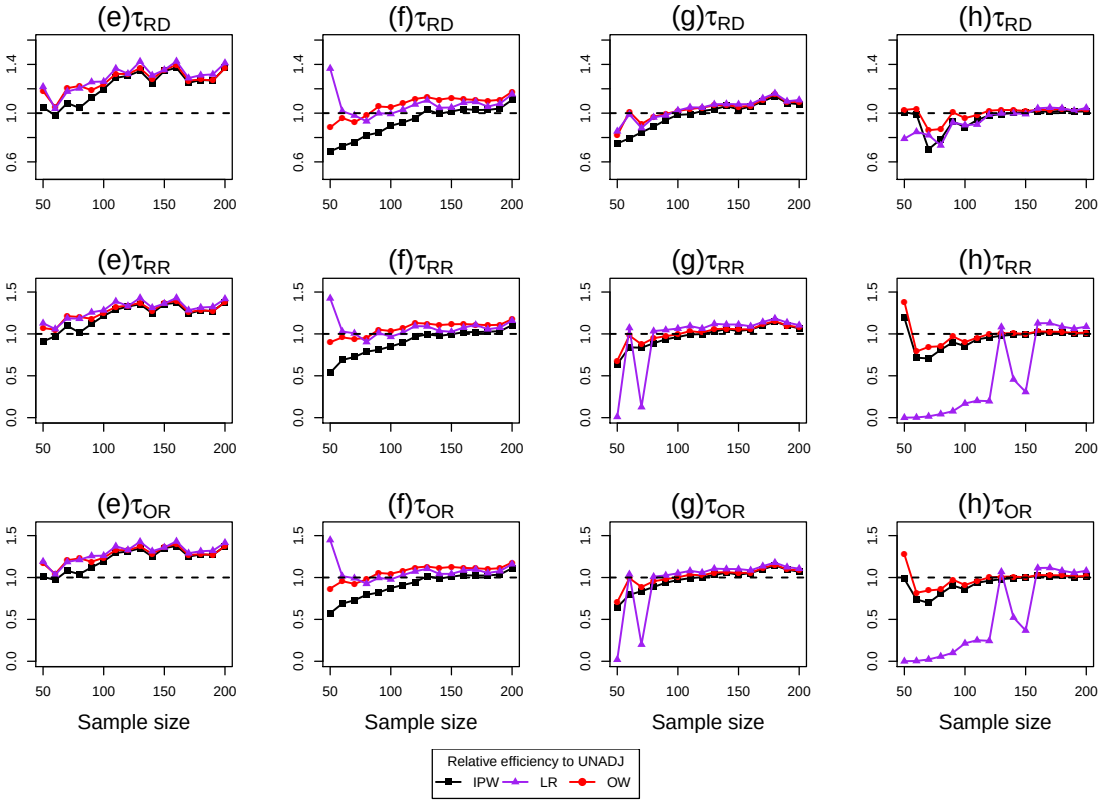

Figure 8.2: The relative efficiency of $\hat{\tau}^{\text{IPW}}$, $\hat{\tau}^{\text{LR}}$, $\hat{\tau}^{\text{AIPW}}$ and $\hat{\tau}^{\text{OW}}$ relative to $\hat{\tau}^{\text{UNADJ}}$ for estimating $\tau_{\text{RD}}, \tau_{\text{RR}}, \tau_{\text{OR}}$, when (e) $u = 0.5$, $b_1 = 0.75$, $r = 0.5$ and the outcome model is correctly specified (f) $u = 0.5$, $b_1 = 0$, $r = 0.7$ and the outcome model is misspecified (g) $u = 0.2$,$b_1 = 0$, $r = 0.5$, and the outcome model is correctly specified (h) $u = 0.1$, $b_1 = 0$,$r = 0.5$, and the outcome model is correctly specified.

around 30% (column (c)), the covariate-adjusted estimators become more efficient than the unadjusted estimator when $N > 100$. In this case, the correctly-specified LR estimator may become unstable in estimating the two ratio estimands when N is as small as 50, while both OW and IPW are not subject to such concerns because they do not attempt to estimate an outcome model.

Figure 8.2 presents the relative efficiency results in four additional scenarios. In the presence of strong treatment effect heterogeneity (column (e)), the covariate-adjusted estimators, LR and OW, improve over the unadjusted estimator even with a small sample size $N = 50$. In this case, the efficiency of LR and OW is almost identical across the range of sample size we examined. In contrast to the continuous outcome simulations, the LR estimator may become more efficient than OW and IPW with unbalanced randomization ($r = 0.7$) and $N \leq 80$ (column (f)). However, when the outcome becomes rare (column (g) and (h)), the OW and IPW estimators are more stable than LR. In these scenarios, the LR estimates can be quite variable, leading to dramatic efficiency loss even compared with the unadjusted estimator. With further investigation, we find that the LR estimator frequently run into numerical issues and fails to converge under rare outcomes. This non-convergence issue under rare outcomes also adversely affects the efficiency of the AIPW estimator. Table 8.4 summarizes the number of times that the logistic regression fails to converge as a function of sample size and prevalence of the outcome under the control condition. For instance, when the outcome is rare ($u = 0.1$), the logistic regression fails to converge more than half of the times even when $N = 100$. Finally, for binary outcomes, the difference in efficiency between the adjusted estimators is more pronounced when N does not exceed 200, and becomes trivial when $N = 500$.

To summarize, we conclude that for binary outcomes

(i) covariate adjustment improves efficiency most likely when the sample size is at least 100, except in the presence of large treatment effect heterogeneity where there is efficiency gain even with $N = 50$.

(ii) the OW estimator is uniformly more efficient in finite samples than IPW and should be the preferred propensity score weighting estimator in randomized trials.

(iii) although correctly-specified outcome regression is slightly more efficient than OW in the ideal case with a non-rare outcome, in small samples regression adjustment is generally unstable when the prevalence of outcome decreases.

(iv) the efficiency of AIPW is mainly driven by the outcome regression component, and the instability of the outcome model may also lead to an inefficient AIPW estimator in finite-samples.

Results on variance and interval estimators

For $N \in \{50, 100, 200, 500\}$, Table 8.2 and 8.3 further summarize the accuracy of the variance estimators and the empirical coverage rate of the corresponding interval estimator for each approach, in the scenarios presented in Figure 8.1 and 8.2. The Williamson's variance estimator for IPW and the sandwich variance for AIPW frequently underestimate the true variance for all three estimands, so that the associated confidence interval shows under-coverage, especially when the sample size does not exceed 100. From a hypothesis testing point of view, as we are setting the average causal effect to be null, the results suggest the risk of type I error inflation using IPW or AIPW. Both LR and OW generally improve upon IPW and AIPW by maintaining closer to nominal coverage rate, with a few exceptions. For example, we notice that the Huber-White variance for logistic regression can be unstable and biased towards zero, leading to under-coverage. On the other hand, the proposed sandwich variance for OW is always close to the true variance regardless of the target estimand. Likewise, the OW interval estimator demonstrates improved performance over IPW, LR and AIPW, and maintains close to nominal coverage even in small samples with rare outcomes, where outcome regression frequently fails to converge.

To summarize, we conclude that for binary outcomes

(i) the Williamson's variance estimator for IPW and the sandwich variance for AIPW frequently underestimate the true variance for all three estimands.

(ii) the Huber-White variance for logistic regression can be unstable, and may have large bias in small samples with rare outcomes.

(iii) the proposed sandwich variance for OW is always close to the true variance regardless of the target estimand, and the OW interval estimator demonstrates close to nominal coverage even in small samples with rare outcomes.

8.1.5 Additional tables

Table 8.1 summarizes the full simulation results with continuous outcomes. we consider the following scenarios:

1. $r = 0.5, b_1 = 0$, model is correctly specified, corresponding to scenario (a) in Figure 2.1.
2. $r = 0.5, b_1 = 0.25$, model is correctly specified.
3. $r = 0.5, b_1 = 0.5$, model is correctly specified.
4. $r = 0.5, b_1 = 0.75$, model is correctly specified, corresponding to scenario (b) in Figure 2.1 of the main text.
5. $r = 0.6, b_1 = 0$, model is correctly specified.
6. $r = 0.7, b_1 = 0$, model is correctly specified, corresponding to scenario (c) in Figure 2.1.
7. $r = 0.5, b_1 = 0$, model is misspecified.
8. $r = 0.7, b_1 = 0$, model is misspecified, corresponding to scenario (d) in Figure 2.1.

We include the additional numerical results for the simulations with binary outcomes in Table 8.2 and 8.3. For binary outcome, we consider the following scenarios,

1. $u = 0.5, r = 0.5, b_1 = 0$, model is correctly specified, corresponding to scenario (a) in Figure 8.1.

2. $u = 0.5, r = 0.5, b_1 = 0$, model is misspecified, corresponding to scenario (b) in Figure 8.1.

3. $u = 0.3, r = 0.5, b_1 = 0$, model is correctly specified, corresponding to scenario (c) in Figure 8.1.

4. $u = 0.3, r = 0.5, b_1 = 0$, model is misspecified, corresponding to scenario (d) in Figure 8.1.

5. $u = 0.5, r = 0.5, b_1 = 0.75$, model is correctly specified, corresponding to scenario (e) in Figure 8.2.

6. $u = 0.5, r = 0.7, b_1 = 0$, model is correctly specified, corresponding to scenario (f) in Figure 8.2.

7. $u = 0.2, r = 0.5, b_1 = 0$, model is correctly specified, corresponding to scenario (g) in Figure 8.2.

8. $u = 0.1, r = 0.5, b_1 = 0$, model is correctly specified, corresponding to scenario (h) in Figure 8.2.

For binary outcome, we also report in Table 8.4 the number of non-convergences for fitting logistic regression under different baseline outcome prevalence $u = 0.5, 0.3, 0.2, 0.1$.

Table 8.1: The relative efficiency of each estimator compared to the unadjusted estimator, the ratio between the average estimated variance over Monte Carlo variance ({Est Var}/{MC Var}), and 95% coverage rate of IPW, LR, AIPW and OW estimators. The results are based on 2000 simulations with a continuous outcome. In the "correct specification" scenario, data are generated from model 1; in the "misspecification" scenario, data are generated from model 2. For each estimator, the same specification is used throughout, regardless of the data generating model.

Sample size	Relative efficiency				{Est Var}/{MC Var}				95% Coverage			
N	IPW	LR	AIPW	OW	IPW	LR	AIPW	OW	IPW	LR	AIPW	OW
$r = 0.5$, $b_1 = 0$, correct specification												
50	1.621	2.126	2.042	2.451	1.001	0.866	0.668	1.343	0.936	0.933	0.885	0.967
100	2.238	2.475	2.399	2.548	0.898	0.961	0.799	1.116	0.938	0.944	0.914	0.955
200	2.927	2.987	2.984	3.007	0.951	0.996	0.927	1.051	0.946	0.949	0.938	0.956
500	2.985	3.004	2.995	3.006	0.963	0.987	0.959	1.000	0.944	0.949	0.942	0.952
$r = 0.5$, $b_1 = 0.25$, correct specification												
50	1.910	2.792	2.606	2.905	1.141	0.711	0.684	1.562	0.946	0.899	0.887	0.972
100	2.968	3.575	3.481	3.489	0.988	0.811	0.896	1.295	0.954	0.925	0.928	0.968
200	3.640	3.864	3.855	3.794	0.932	0.754	0.923	1.079	0.940	0.912	0.933	0.956
500	3.801	3.814	3.814	3.791	0.947	0.735	0.940	0.992	0.945	0.907	0.945	0.950
$r = 0.5$, $b_1 = 0.5$, correct specification												
50	1.635	2.894	2.781	2.755	1.021	0.463	0.769	1.530	0.936	0.822	0.910	0.970
100	3.084	3.917	3.835	3.546	0.984	0.510	0.977	1.291	0.942	0.840	0.944	0.968
200	3.187	3.410	3.406	3.287	0.924	0.446	0.936	1.061	0.944	0.802	0.942	0.956
500	3.730	3.809	3.810	3.717	1.037	0.477	1.049	1.085	0.957	0.818	0.960	0.962
$r = 0.5$, $b_1 = 0.75$, correct specification												
50	1.715	3.043	2.972	2.570	0.991	0.286	0.816	1.383	0.935	0.712	0.918	0.967
100	2.679	3.279	3.253	3.003	0.931	0.280	0.917	1.168	0.942	0.710	0.934	0.966
200	2.979	3.220	3.215	3.023	0.967	0.278	0.995	1.075	0.951	0.697	0.949	0.964
500	3.337	3.425	3.426	3.338	0.995	0.273	1.013	1.037	0.943	0.696	0.945	0.954
$r = 0.6$, $b_1 = 0$, correct specification												
50	1.415	1.686	1.605	2.418	1.041	0.745	0.617	1.377	0.938	0.913	0.883	0.959
100	2.042	2.378	2.290	2.521	0.889	0.942	0.784	1.104	0.944	0.941	0.915	0.956
200	2.777	2.926	2.896	2.981	0.987	1.027	0.947	1.078	0.949	0.950	0.940	0.953
500	2.898	2.939	2.939	2.950	0.976	0.994	0.969	1.003	0.953	0.953	0.949	0.953
$r = 0.7$, $b_1 = 0$, correct specification												
50	1.056	0.036	0.036	2.270	1.060	0.014	0.026	1.184	0.938	0.779	0.816	0.931
100	1.825	2.439	2.311	2.935	0.914	0.858	0.717	1.039	0.946	0.921	0.897	0.923
200	2.474	2.706	2.679	2.874	0.971	0.931	0.857	0.963	0.948	0.944	0.927	0.935
500	2.641	2.743	2.738	2.809	0.922	0.912	0.887	0.925	0.940	0.936	0.934	0.938
$r = 0.5$, $b_1 = 0$, misspecification												
50	1.009	1.093	0.986	1.299	0.773	0.768	0.598	0.900	0.908	0.915	0.870	0.933
100	1.371	1.502	1.379	1.549	0.805	0.954	0.779	0.924	0.924	0.946	0.921	0.942
200	1.526	1.567	1.516	1.592	0.897	0.965	0.888	0.925	0.938	0.953	0.936	0.944
500	1.576	1.587	1.569	1.595	0.913	0.937	0.911	0.912	0.943	0.949	0.944	0.941
$r = 0.7$, $b_1 = 0$, misspecification												
50	0.896	0.009	0.009	1.468	0.843	0.005	0.009	0.857	0.904	0.777	0.808	0.906
100	1.096	1.258	1.152	1.533	0.724	0.754	0.637	0.837	0.911	0.903	0.878	0.917
200	1.390	1.457	1.398	1.570	0.861	0.894	0.816	0.898	0.929	0.938	0.920	0.933
500	1.591	1.632	1.612	1.648	0.980	1.003	0.976	0.981	0.948	0.949	0.948	0.949

Table 8.2: The relative efficiency, the ratio between the average estimated variance over Monte Carlo variance and 95% coverage rate of IPW, LR, AIPW and OW estimators for binary outcomes. The scenarios correspond to Figure 8.1.

		Relative efficiency				{Est Var}/{MC Var}				95% Coverage			
	N	IPW	LR	AIPW	OW	IPW	LR	AIPW	OW	IPW	LR	AIPW	OW
$u = 0.5$, $b_1 = 0$, $r = 0.5$, correct specification **(a)**													
τ_{RD}	50	0.729	0.966	0.854	0.880	0.936	1.387	0.903	1.124	0.903	0.940	0.906	0.943
	100	1.034	1.100	1.061	1.083	0.796	0.924	0.763	0.972	0.914	0.934	0.905	0.945
	200	1.152	1.159	1.149	1.158	0.985	1.049	0.967	1.164	0.944	0.953	0.945	0.961
	500	1.186	1.191	1.191	1.184	0.969	0.995	0.969	1.151	0.946	0.948	0.947	0.962
τ_{RR}	50	0.690	0.976	0.832	0.860	0.910	1.372	0.870	1.097	0.924	0.966	0.926	0.964
	100	1.038	1.104	1.062	1.090	0.803	0.927	0.766	0.979	0.922	0.942	0.915	0.953
	200	1.154	1.160	1.150	1.160	0.987	1.050	0.969	1.165	0.948	0.957	0.947	0.964
	500	1.189	1.193	1.194	1.186	0.971	0.996	0.970	1.152	0.950	0.952	0.949	0.965
τ_{OR}	50	0.702	0.960	0.836	0.864	0.950	1.395	0.905	1.128	0.913	0.966	0.915	0.955
	100	1.031	1.101	1.060	1.082	0.795	0.925	0.763	0.973	0.920	0.938	0.910	0.950
	200	1.153	1.160	1.150	1.159	0.985	1.050	0.968	1.164	0.946	0.954	0.946	0.963
	500	1.187	1.191	1.192	1.184	0.969	0.994	0.968	1.150	0.948	0.951	0.948	0.964
$u = 0.5$, $b_1 = 0$, $r = 0.5$, misspecification **(b)**													
τ_{RD}	50	0.742	0.942	0.848	0.827	0.888	1.225	0.825	0.996	0.887	0.943	0.902	0.921
	100	0.971	1.057	1.002	1.033	0.813	0.996	0.799	0.976	0.913	0.945	0.911	0.937
	200	1.074	1.086	1.076	1.082	0.921	0.993	0.912	1.039	0.936	0.943	0.936	0.950
	500	1.100	1.106	1.105	1.100	0.962	0.993	0.963	1.088	0.948	0.950	0.948	0.957
τ_{RR}	50	0.697	0.944	0.824	0.811	0.869	1.244	0.834	1.000	0.909	0.943	0.914	0.948
	100	0.968	1.072	1.013	1.036	0.806	0.992	0.797	0.966	0.925	0.956	0.924	0.947
	200	1.071	1.084	1.075	1.078	0.913	0.983	0.903	1.029	0.940	0.948	0.940	0.955
	500	1.103	1.110	1.109	1.103	0.966	0.997	0.967	1.092	0.949	0.952	0.948	0.958
τ_{OR}	50	0.714	0.936	0.831	0.808	0.890	1.231	0.826	0.997	0.902	0.950	0.909	0.943
	100	0.966	1.058	1.001	1.031	0.810	0.995	0.797	0.973	0.919	0.951	0.920	0.944
	200	1.075	1.087	1.077	1.083	0.921	0.992	0.911	1.039	0.938	0.947	0.938	0.953
	500	1.100	1.107	1.106	1.101	0.962	0.993	0.963	1.088	0.949	0.951	0.948	0.958
$u = 0.3$, $b_1 = 0$, $r = 0.5$, correct specification **(c)**													
τ_{RD}	50	0.797	0.946	0.899	0.942	0.915	1.369	0.892	1.141	0.896	0.944	0.892	0.937
	100	1.002	1.044	1.021	1.043	0.852	1.138	0.814	1.015	0.925	0.951	0.914	0.945
	200	1.123	1.124	1.116	1.130	0.976	1.154	0.952	1.131	0.942	0.960	0.940	0.957
	500	1.187	1.201	1.198	1.188	1.014	1.147	1.014	1.185	0.951	0.964	0.951	0.966
τ_{RR}	50	0.758	0.034	0.004	0.938	1.004	0.051	0.004	1.241	0.919	0.964	0.917	0.971
	100	1.010	1.070	1.041	1.043	0.859	1.173	0.818	1.019	0.936	0.965	0.929	0.956
	200	1.124	1.132	1.122	1.129	0.962	1.148	0.939	1.114	0.949	0.968	0.945	0.962
	500	1.189	1.204	1.201	1.189	1.007	1.141	1.007	1.176	0.954	0.966	0.955	0.968
τ_{OR}	50	0.748	0.073	0.008	0.924	1.013	0.112	0.009	1.225	0.915	0.959	0.917	0.958
	100	1.005	1.057	1.031	1.043	0.855	1.158	0.816	1.019	0.931	0.961	0.922	0.952
	200	1.124	1.129	1.120	1.130	0.968	1.152	0.945	1.123	0.946	0.965	0.942	0.960
	500	1.188	1.203	1.200	1.189	1.011	1.144	1.010	1.181	0.952	0.964	0.953	0.967
$u = 0.3$, $b_1 = 0$, $r = 0.5$, misspecification **(d)**													
τ_{RD}	50	0.667	0.921	0.687	0.858	0.924	1.471	0.889	1.204	0.883	0.976	0.943	0.926
	100	0.950	1.021	0.977	0.989	0.859	1.196	0.837	1.019	0.918	0.958	0.912	0.948
	200	1.126	1.139	1.133	1.126	0.946	1.156	0.931	1.072	0.940	0.963	0.938	0.953
	500	1.116	1.137	1.132	1.118	1.031	1.209	1.029	1.183	0.951	0.966	0.952	0.962
τ_{RR}	50	0.543	0.952	0.630	0.795	0.885	1.515	1.039	1.189	0.905	0.986	0.953	0.959
	100	0.941	1.041	0.993	0.975	0.843	1.202	0.822	1.000	0.932	0.971	0.923	0.961
	200	1.127	1.147	1.142	1.123	0.949	1.170	0.934	1.074	0.946	0.969	0.939	0.958
	500	1.115	1.139	1.135	1.117	1.028	1.208	1.026	1.178	0.953	0.968	0.954	0.964
τ_{OR}	50	0.583	0.928	0.634	0.818	0.917	1.498	0.999	1.196	0.900	0.981	0.953	0.945
	100	0.944	1.031	0.985	0.981	0.851	1.201	0.829	1.010	0.926	0.965	0.920	0.953
	200	1.127	1.143	1.138	1.125	0.947	1.163	0.932	1.074	0.940	0.966	0.940	0.957
	500	1.116	1.138	1.134	1.118	1.029	1.209	1.027	1.181	0.952	0.967	0.954	0.963

Table 8.3: The relative efficiency of each estimator compared to the unadjusted, the ratio between the average estimated variance ({Est Var}) over Monte Carlo variance ({MC Var}) and 95% coverage rate of IPW, LR, AIPW and OW estimators for binary outcomes. The scenarios correspond to Figure 8.2.

		Relative efficiency				{Est Var}/{MC Var}				95% Coverage			
	N	IPW	LR	AIPW	OW	IPW	LR	AIPW	OW	IPW	LR	AIPW	OW
$u = 0.5$, $b_1 = 0.75$, $r = 0.5$, correct specification **(e)**													
τ_{RD}	50	1.046	1.217	1.129	1.181	0.905	1.151	0.707	1.066	0.895	0.857	0.829	0.944
	100	1.248	1.294	1.281	1.305	0.945	1.028	0.855	1.298	0.931	0.939	0.921	0.968
	200	1.365	1.420	1.411	1.367	0.988	1.014	0.966	1.353	0.945	0.947	0.941	0.976
	500	1.329	1.381	1.380	1.328	0.899	0.871	0.897	1.246	0.940	0.934	0.938	0.973
τ_{RR}	50	0.910	1.128	0.989	1.069	0.866	1.066	0.634	0.998	0.916	0.914	0.857	0.966
	100	1.257	1.283	1.272	1.305	0.959	1.022	0.855	1.306	0.938	0.940	0.933	0.976
	200	1.358	1.416	1.408	1.361	0.986	1.012	0.966	1.347	0.946	0.951	0.950	0.981
	500	1.330	1.384	1.383	1.329	0.899	0.871	0.898	1.244	0.940	0.936	0.940	0.974
τ_{OR}	50	1.009	1.191	1.107	1.168	0.912	1.136	0.704	1.089	0.909	0.857	0.857	0.957
	100	1.246	1.291	1.276	1.305	0.944	1.027	0.851	1.295	0.938	0.946	0.924	0.973
	200	1.368	1.425	1.416	1.371	0.988	1.015	0.966	1.353	0.945	0.948	0.944	0.979
	500	1.330	1.383	1.381	1.329	0.900	0.871	0.898	1.246	0.942	0.935	0.940	0.974
$u = 0.5$, $b_1 = 0$, $r = 0.7$, correct specification **(f)**													
τ_{RD}	50	0.619	1.379	1.328	0.882	0.871	18.187	0.560	0.803	0.848	0.917	0.836	0.901
	100	0.902	0.999	0.956	1.026	0.850	0.971	0.760	1.134	0.898	0.949	0.905	0.951
	200	1.017	1.047	1.033	1.081	0.849	0.898	0.808	1.122	0.920	0.935	0.913	0.960
	500	1.165	1.180	1.173	1.189	0.981	1.007	0.972	1.281	0.945	0.948	0.944	0.973
τ_{RR}	50	0.447	1.547	1.472	0.791	0.806	10.114	0.546	0.702	0.877	0.911	0.859	0.935
	100	0.872	0.987	0.938	1.025	0.843	0.963	0.757	1.136	0.916	0.954	0.922	0.961
	200	1.017	1.052	1.038	1.085	0.843	0.893	0.804	1.112	0.928	0.941	0.920	0.963
	500	1.166	1.180	1.174	1.190	0.977	1.002	0.968	1.274	0.952	0.952	0.949	0.974
τ_{OR}	50	0.489	1.512	1.450	0.816	0.881	5.454	0.545	0.728	0.892	0.915	0.842	0.928
	100	0.888	0.996	0.949	1.026	0.848	0.972	0.759	1.134	0.908	0.956	0.914	0.958
	200	1.015	1.046	1.032	1.081	0.848	0.897	0.807	1.120	0.929	0.941	0.919	0.962
	500	1.166	1.181	1.174	1.189	0.981	1.007	0.972	1.280	0.946	0.951	0.946	0.973
$u = 0.2$, $b_1 = 0$, $r = 0.5$, correct specification **(g)**													
τ_{RD}	50	0.755	0.806	0.758	0.807	0.738	1.093	0.689	0.863	0.887	0.915	0.851	0.917
	100	0.904	0.968	0.952	0.938	0.869	1.485	0.863	1.008	0.916	0.965	0.920	0.933
	200	1.103	1.129	1.120	1.114	0.925	1.296	0.918	1.048	0.938	0.973	0.933	0.955
	500	1.103	1.108	1.108	1.102	0.988	1.256	0.979	1.123	0.949	0.971	0.948	0.960
τ_{RR}	50	0.642	0.010	0.001	0.671	0.868	0.017	0.002	1.034	0.914	0.957	0.900	0.973
	100	0.908	1.028	1.004	0.933	0.860	1.532	0.856	0.997	0.925	0.977	0.939	0.952
	200	1.102	1.147	1.137	1.110	0.899	1.283	0.895	1.017	0.946	0.978	0.944	0.962
	500	1.097	1.104	1.104	1.096	0.983	1.253	0.973	1.116	0.949	0.977	0.949	0.964
τ_{OR}	50	0.649	0.020	0.003	0.698	0.861	0.033	0.003	1.030	0.906	0.957	0.900	0.960
	100	0.906	1.009	0.987	0.934	0.863	1.522	0.858	1.002	0.923	0.974	0.930	0.949
	200	1.103	1.142	1.133	1.112	0.907	1.289	0.903	1.028	0.943	0.976	0.938	0.960
	500	1.099	1.105	1.106	1.098	0.985	1.255	0.975	1.118	0.949	0.976	0.948	0.962
$u = 0.1$, $b_1 = 0$, $r = 0.5$, correct specification **(h)**													
τ_{RD}	50	0.995	0.800	0.785	1.032	0.238	0.255	0.193	0.277	0.888	0.440	0.417	0.912
	100	0.892	0.881	0.852	0.939	1.064	2.224	0.996	1.194	0.922	0.980	0.947	0.940
	200	1.038	1.056	1.044	1.054	0.958	1.878	0.948	1.042	0.938	0.991	0.942	0.947
	500	1.076	1.101	1.100	1.078	0.985	1.577	0.989	1.068	0.949	0.988	0.947	0.954
τ_{RR}	50	0.570	0.001	0.000	1.057	0.608	0.001	0.000	1.201	0.939	0.375	1.000	0.991
	100	0.868	0.979	0.940	0.893	1.089	2.348	1.024	1.232	0.944	0.994	0.952	0.972
	200	1.052	1.132	1.115	1.065	0.938	1.910	0.940	1.019	0.949	0.994	0.948	0.957
	500	1.073	1.101	1.098	1.074	0.976	1.565	0.975	1.058	0.951	0.990	0.951	0.960
τ_{OR}	50	0.610	0.002	0.000	1.078	0.685	0.002	0.000	1.335	0.928	0.375	1.000	0.985
	100	0.872	0.960	0.923	0.901	1.085	2.329	1.018	1.226	0.938	0.993	0.948	0.965
	200	1.050	1.121	1.105	1.063	0.941	1.909	0.941	1.024	0.948	0.993	0.945	0.954
	500	1.074	1.101	1.098	1.075	0.977	1.568	0.977	1.060	0.951	0.990	0.950	0.958

Table 8.4: Number of times that the logistic regression fails to converge given different outcome prevalence $u \in \{0.5, 0.3, 0.2, 0.1\}$ and sample sizes $N \in [50, 200]$.

N	$u = 0.5$	$u = 0.3$	$u = 0.2$	$u = 0.1$
50	1649	1802	1905	1975
60	1025	1320	1699	1947
70	525	823	1245	1829
80	207	433	834	1659
90	84	194	527	1393
100	34	89	307	1199
110	5	41	159	941
120	5	20	88	684
130	0	3	44	498
140	0	0	17	331
150	0	1	10	251
160	0	0	11	176
170	0	0	2	117
180	0	0	0	85
190	0	0	0	45
200	0	0	0	38

8.2 Appendix for Chapter 3

8.2.1 Proof of theoretical properties

Proof of Theorem 1 (i) We first list the regularity assumptions needed for Theorem 1.

- (R1) We only consider time point $t < \bar{t}$ such that $G(\bar{t}) > \epsilon > 0$, where G is the survival function for the censoring time C_i. Namely, any time point of interest has a strictly positive probability of not being censored.
- (R2) The generalized propensity score model (GPS), $e_j(\mathbf{X}_i; \boldsymbol{\gamma})$, satisfies the regularity conditions specified in Theorem 5.1 of Lehmann and Casella (2006).

Next, we establish the consistency of estimator (5) in the main text. Let $D_{ij} = \mathbf{1}\{Z_i = j\}$, we have

$$\begin{aligned}
\frac{\sum_{i=1}^N D_{ij}\widehat{\theta}_i^k(t) w_j^h(\mathbf{X}_i)}{\sum_{i=1}^N D_{ij} w_j^h(\mathbf{X}_i)} &= \frac{\mathbb{E}\{D_{ij}\widehat{\theta}_i^k(t) w_j^h(\mathbf{X}_i;\boldsymbol{\gamma})\}}{\mathbb{E}(h(\mathbf{X}_i)} + o_p(1) \\
&= \frac{\mathbb{E}[\{D_{ij}\widehat{\theta}_i^k(t) w_j^h(\mathbf{X}_i;\boldsymbol{\gamma})|\mathbf{X}_i\}]}{\mathbb{E}(h(\mathbf{X}_i))} + o_p(1) \\
&= \frac{\mathbb{E}\{w_j^h(\mathbf{X}_i;\boldsymbol{\gamma}) e_j(\mathbf{X}_i;\boldsymbol{\gamma})\, \mathbb{E}(v_k(T_i;t)|\mathbf{X}_i, D_{ij}=1)\}}{\mathbb{E}(h(\mathbf{X}_i))} + o_p(1) \\
&= \frac{\mathbb{E}\{w_j^h(\mathbf{X}_i;\boldsymbol{\gamma}) e_j(\mathbf{X}_i;\boldsymbol{\gamma})\, \mathbb{E}(v_k(T_i(j);t)|\mathbf{X}_i)\}}{\mathbb{E}(h(\mathbf{X}_i))} + o_p(1) \\
&= \frac{\mathbb{E}\{h(\mathbf{X}_i)\, \mathbb{E}(v_k(T_i(j);t)|\mathbf{X}_i)\}}{\mathbb{E}(h(\mathbf{X}_i))} + o_p(1) = m_j^{k,h}(t) + o_p(1)
\end{aligned}$$

where the third equality follows from the fact that $\mathbb{E}(\widehat{\theta}_i^k(t)|\ \mathbf{X}_i, D_{ij} = 1) = \mathbb{E}(v_k(T_i;t)|\mathbf{X}_i, D_{ij} = 1) + o_p(1)$ (Graw et al., 2009; Jacobsen and Martinussen, 2016) and the fourth equality follows from the unconfoundedness assumption (A1). Therefore, we can show that,

$$\frac{\sum_{i=1}^N D_{ij}\widehat{\theta}_i^k(t) w_j^h(\mathbf{X}_i)}{\sum_{i=1}^N D_{ij} w_j^h(\mathbf{X}_i)} - \frac{\sum_{i=1}^N D_{ij'}\widehat{\theta}_i^k(t) w_{j'}^h(\mathbf{X}_i)}{\sum_{i=1}^N D_{ij'} w_{j'}^h(\mathbf{X}_i)} \xrightarrow{p} m_j^{k,h}(t) - m_{j'}^{k,h}(t) = \tau_{j,j'}^{k,h}(t),$$

and thus prove the consistency of the weighting estimator (5).

(ii) Below we derive the asymptotic variance of estimator (5) using the von Mises expansion on the pseudo-observations (Jacobsen and Martinussen, 2016; Overgaard et al., 2017). Recall that estimator (5) is of the following form:

$$\hat{\tau}^{k,h}_{j,j'}(t) = \frac{\sum_{i=1}^N D_{ij}\widehat{\theta}^k_i(t)w^h_j(\mathbf{X}_i)}{\sum_{i=1}^N D_{ij}w^h_j(\mathbf{X}_i)} - \frac{\sum_{i=1}^N D_{ij'}\widehat{\theta}^k_i(t)w^h_{j'}(\mathbf{X}_i)}{\sum_{i=1}^N D_{ij'}w^h_{j'}(\mathbf{X}_i)} = \widehat{m}^{k,h}_j(t) - \widehat{m}^{k,h}_{j'}(t).$$

We can write the treatment-specific average potential outcome $\hat{m}^{k,h}_j(t)$ as the solution to the following estimating equation,

$$\sum_{i=1}^N D_{ij}\{\widehat{\theta}^k_i(t) - \widehat{m}^{k,h}_j(t)\}w^h_j(\mathbf{X}_i;\boldsymbol{\gamma}) = 0.$$

A first-order Taylor expansion at the true value of $(m^{k,h}_j(t), \boldsymbol{\gamma})$ yields,

$$\begin{aligned}\sqrt{N}\{\widehat{m}^{k,h}_j(t) - m^{k,h}_j(t)\} =& \bar{\omega}^{-1}\frac{1}{\sqrt{N}}\sum_{i=1}^N D_{ij}\{\widehat{\theta}^k_i(t) - m^{k,h}_j(t)\}w^h_j(\mathbf{X}_i;\boldsymbol{\gamma}) \\ &+ \mathbf{H}^T_j\sqrt{N}(\widehat{\boldsymbol{\gamma}} - \boldsymbol{\gamma}) + o_p(1),\end{aligned}$$

where $\bar{\omega} = \mathbb{E}(D_{ij}w^h_j(\mathbf{X}_i;\boldsymbol{\gamma})) = \mathbb{E}(h(\mathbf{X}_i))$ and

$$\begin{aligned}\mathbf{H}_j &= \mathbb{E}\left\{D_{ij}(\theta^k(t) + \phi'_{k,i}(t) - m^{k,h}_j(t))\frac{\partial}{\partial\boldsymbol{\gamma}}w^h_j(\mathbf{X}_i;\boldsymbol{\gamma})\right\} \\ &= \mathbb{E}\left\{D_{ij}(\theta^k(t) + \phi'_{k,i}(t) + \frac{1}{N-1}\sum_{l\neq i}\phi''_{k,(l,i)}(t) - m^{k,h}_j(t))\frac{\partial}{\partial\boldsymbol{\gamma}}w^h_j(\mathbf{X}_i;\boldsymbol{\gamma})\right\} \\ &= \mathbb{E}\left\{D_{ij}(\widehat{\theta}^k_i(t) - m^{k,h}_j(t))\frac{\partial}{\partial\boldsymbol{\gamma}}w^h_j(\mathbf{X}_i;\boldsymbol{\gamma})\right\} + o_p(1).\end{aligned}$$

The first line applies the centering property (equation 3.24 in Overgaard et al. (2017)) of the second order derivative $\mathbb{E}\{\phi''_{k,(l,i)}(t)|\mathcal{O}_i\} = 0$. The second line of the transformation for $\mathbf{H}_j$ follows from Von-Mises expansion of the pseudo-observations (equation (6) in the main text). Under the standard regularity conditions in Lehmann and Casella (2006), we have,

$$\sqrt{N}(\widehat{\boldsymbol{\gamma}} - \boldsymbol{\gamma}) = \frac{1}{N}\mathbf{I}^{-1}_{\boldsymbol{\gamma}\boldsymbol{\gamma}}\mathbf{S}_{\boldsymbol{\gamma},i} + o_p(1).$$

Then we have

$$\sqrt{N}\{\widehat{m}_j^{k,h}(t) - m_j^{k,h}(t)\} = \bar{\omega}^{-1}\frac{1}{\sqrt{N}}\sum_{i=1}^{N}\left\{D_{ij}(\widehat{\theta}_i^k(t) - m_j^{k,h}(t))w_j^h(\mathbf{X}_i;\boldsymbol{\gamma}) + \mathbf{H}_j^T\mathbf{I}_{\boldsymbol{\gamma}\boldsymbol{\gamma}}\mathbf{S}_{\boldsymbol{\gamma},i}\right\} + o_p(1).$$

Applying the von Mises expansion of the pseudo-observations as in Jacobsen and Martinussen (2016) and Overgaard et al. (2017), we have,

$$\begin{aligned}&\sqrt{N}\{\widehat{m}_j^{k,h}(t) - m_j^{k,h}(t)\}\\ =&\bar{\omega}^{-1}\frac{1}{\sqrt{N}}\sum_{i=1}^{N}\{D_{ij}\left\{\theta_k(t) + \phi'_{k,i}(t) + \frac{1}{N-1}\sum_{l\neq i}\phi''_{k,(l,i)}(t) - m_j^{k,h}(t)\right\}w_j^h(\mathbf{X}_i;\boldsymbol{\gamma})\\ &+ \mathbf{H}_j^T\mathbf{I}_{\boldsymbol{\gamma}\boldsymbol{\gamma}}\mathbf{S}_{\boldsymbol{\gamma},i}\} + o_p(1).\end{aligned}$$

Similar expansions also apply to $\widehat{m}_{j'}^{k,h}(t)$, and thus we have,

$$\sqrt{N}\{\widehat{\tau}_{j,j'}^{k,h}(t) - \tau_{j,j'}^{k,h}(t)\} = \bar{\omega}^{-1}\frac{1}{\sqrt{N}}\sum_{i=1}^{N}(\psi_{ij} - \psi_{ij'}) + o_p(1),$$

$$\psi_{ij} = D_{ij}\left\{\theta_k(t) + \phi'_{k,i}(t) + \frac{1}{N-1}\sum_{l\neq i}\phi''_{k,(l,i)}(t) - m_j^{k,h}(t)\right\}w_j^h(\mathbf{X}_i;\boldsymbol{\gamma}) + \mathbf{H}_j^T\mathbf{I}_{\boldsymbol{\gamma}\boldsymbol{\gamma}}\mathbf{S}_{\boldsymbol{\gamma},i}.$$

Recall that the ith estimated pseudo-observation depends on the observed outcomes for the rest of sample. Due to the correlation between the estimated pseudo-observations, the usual Central Limit Theorem does not directly apply. Instead we reorganize the above expression into a sum of U-statistics of order 2 as follows,

$$\sum_{i=1}^{N}(\psi_{ij} - \psi_{ij'}) = \frac{N}{\binom{N}{2}}\sum_{i=1}^{N}\sum_{l<i}\frac{1}{2}g_{il},$$

where

$$\begin{aligned}g_{il} =&D_{ij}\left\{\theta_k(t) + \phi'_i(t) - m_j^{k,h}(t)\right\}w_j^h(\mathbf{X}_i;\boldsymbol{\gamma}) + \mathbf{H}_j^T\mathbf{I}_{\boldsymbol{\gamma}\boldsymbol{\gamma}}^{-1}\mathbf{S}_{\boldsymbol{\gamma},i}\\ &- D_{ij'}\{\theta_k(t) + \phi'_i(t) - m_{j'}^{k,h}(t)\}w_{j'}^h(\mathbf{X}_i;\boldsymbol{\gamma}) + \mathbf{H}_{j'}^T\mathbf{I}_{\boldsymbol{\gamma}\boldsymbol{\gamma}}^{-1}\mathbf{S}_{\boldsymbol{\gamma},i}\\ &+ D_{lj}\{\theta_k(t) + \phi'_l(t) - m_j^{k,h}(t)\}w_j^h(\mathbf{X}_l;\boldsymbol{\gamma}) + \mathbf{H}_j^T\mathbf{I}_{\boldsymbol{\gamma}\boldsymbol{\gamma}}^{-1}\mathbf{S}_{\boldsymbol{\gamma},l}\\ &- D_{lj'}\{\theta_k(t) + \phi'_l(t) - m_{j'}^{k,h}(t)\}w_{j'}^h(\mathbf{X}_l;\boldsymbol{\gamma}) + \mathbf{H}_{j'}^T\mathbf{I}_{\boldsymbol{\gamma}\boldsymbol{\gamma}}^{-1}\mathbf{S}_{\boldsymbol{\gamma},l}\\ &+\phi''_{k,(l,i)}(t)\{D_{ij}w_j^h(\mathbf{X}_i;\boldsymbol{\gamma}) - D_{ij'}w_{j'}^h(\mathbf{X}_i;\boldsymbol{\gamma}) + D_{lj}w_j^h(\mathbf{X}_l;\boldsymbol{\gamma}) - D_{lj'}w_{j'}^h(\mathbf{X}_l;\boldsymbol{\gamma})\}.\end{aligned}$$

Applying Theorem 12.3 in Van der Vaart (1998), we can show that the asymptotic variance of $\widehat{\tau}^{k,h}_{j,j'}(t)$ is,

$$\sqrt{N}\{\widehat{\tau}^{k,h}_{j,j'}(t) - \tau^{k,h}_{j,j'}(t)\} \xrightarrow{d} \mathcal{N}(0, \sigma^2), \quad \sigma^2 = \bar{\omega}^{-2}\,\mathbb{E}(g_{il}g_{im}),$$

where $\mathbb{E}(g_{il}g_{im}) = \mathbb{V}\{\Psi_j(\mathcal{O}_i;t) - \Psi_{j'}(\mathcal{O}_i;t)\} = \mathbb{E}\{\Psi_j(\mathcal{O}_i;t) - \Psi_{j'}(\mathcal{O}_i;t)\}^2$, and the scaled influence function for treatment j is

$$\begin{aligned}\Psi_j(\mathcal{O}_i;t) =& D_{ij}\{\theta_k(t) + \phi'_{k,i}(t) - m^{k,h}_j(t)\}w^h_j(\mathbf{X}_i;\boldsymbol{\gamma}) \\ &+ \frac{1}{N-1}\sum_{l\neq i}\phi''_{k,(l,i)}(t)D_{lj}w^h_j(\mathbf{X}_l,\boldsymbol{\gamma}) + \mathbf{H}_j^T\mathbf{I}^{-1}_{\boldsymbol{\gamma}\boldsymbol{\gamma}}\mathbf{S}_{\boldsymbol{\gamma},i}.\end{aligned}$$

Hence, we have proved that the asymptotic variance of estimator (5) is $\mathbb{E}\{\Psi_j(\mathcal{O}_i;t) - \Psi_{j'}(\mathcal{O}_i;t)\}^2/\{\mathbb{E}(h(\mathbf{X}_i)\}^2$.

Explicit formulas for the functional derivatives We provide the explicit expression for the functional derivative $\phi'_{k,i}(t)$ and $\phi''_{k,(i,l)}(t)$ when the pseudo-observations are computed based on Kaplan-Meier estimator. We define three counting process in $\mathcal{E} : \mathcal{R} \to [0,1]$, that is, for each unit i: $Y_i(s) = \mathbf{1}\{\widetilde{T}_i \geq s\}, N_{i,0}(s) = \mathbf{1}\{\widetilde{T}_i \leq s, \Delta_i = 0\}$,$N_{i,1}(s) = \mathbf{1}\{\widetilde{T}_i \leq s, \Delta_i = 1\}$. Let $\widetilde{F}_N = N^{-1}\sum_{i=1}^N (Y_i, N_{i,0}, N_{i,1})$ be a vector of three step functions and its limit $\widetilde{F} = (H, H_0, H_1) \in \mathcal{E}^3$, where $H(s) = \Pr(\widetilde{T}_i \geq s), H_0(s) = \Pr(\widetilde{T}_i \leq s, \Delta_i = 0), H_1(s) = \Pr(\widetilde{T}_i \leq s, \Delta_i = 1)$ are the population analog of $(Y_i(s), N_{i,0}(s), N_{i,1}(s))$. Notice that for a given element in $\mathbf{D}$, the space of distribution, there is a unique image in $\mathcal{E}^3$. For example, $\delta_{\mathcal{O}_i}$ is mapped to $(Y_i, N_{i,0}, N_{i,1})$, F is mapped to $\widetilde{F}$, and F_N is mapped to $\widetilde{F}_N$.

We then introduce the Nelson-Aalen functional $\rho : \mathbf{D} \to \mathcal{R}$ at a fixed time point t as,

$$\rho(d;t) = \int_0^t \frac{\mathbf{1}\{h_* > 0\}}{h_*(s)} dh_1(s), \quad \widetilde{h} = (h_*, h_0, h_1) \in \mathcal{E}^3 \text{ is the unique image of } d \in \mathbf{D}$$

and the version using F and F_N as input,

$$\rho(F;t) = \int_0^t \frac{\mathbf{1}\{H(s) > 0\}}{H(s)} dH_1(s) = \Lambda_1(t), \rho(F_N;t) = \int_0^t \frac{\mathbf{1}\{Y(s) > 0\}}{Y(s)} dN_1(s) = \widehat{\Lambda}_1(t),$$

where $Y(s) = \sum_i Y_i(s), N_1(s) = \sum_i N_{1,i}(s)$. Also $\rho(F_N)$ actually corresponds to the Nelson-Aalen estimator of the cumulative hazard $\Lambda_1(t)$. Its first and second order derivative evaluated at F along the direction of sample i, l is given by James et al. (1997),

$$\rho_i'(t) = \int_0^t \frac{1}{H(s)} dM_{i,1}(s),$$
$$\rho_{i,l}''(t) = \int_0^t \frac{H(s) - Y_l(s)}{H(s)^2} dM_{i,1}(s) + \int_0^t \frac{H(s) - Y_i(s)}{H(s)^2} dM_{l,1}(s),$$

where $M_{i,1}(s) = N_{i,1}(s) - \int_0^s Y_i(u) d\Lambda_1(u)$ is a locally square integrable martingale for the counting process $N_{i,1}(s)$. The Kaplan-Meier estimator can then be represented as $\widehat{S}(t) = \phi_1(F_N; t)$, where $\phi_1(d; t)$ is defined as,

$$\phi_1(d; t) = \prod_0^t (1 - \rho(d; ds)), \quad d \in \mathbf{D}$$

where $\prod_0^{(\cdot)}$ is the product integral operator. Next, we fix the evaluation time point for the Kaplan-Meier functional and calculate its derivative along the direction of sample i at F,

$$\phi_{1,i}'(t) = -S(t)\rho_i'(t)$$

Similarly, we can take the second order derivative along the direction of sample (i, l) at F,

$$\phi_{1,(i,l)}''(t) = -S(t) \left\{ \rho_{(i,l)}''(t) - \rho_i'(t)\rho_l'(t) + \mathbf{1}\{i = l\} \int_0^t \frac{1}{H^2(s)} dN_{i,1}(s) \right\}.$$

Now we have the expression for $\phi_{1,i}'(t), \phi_{1,(i,l)}''(t)$. Notice that the functional for the restricted mean survival time is the integral of the Kaplan-Meier functional,

$$\phi_2(d; t) = \int_0^t \phi_1(d; u) du, \quad d \in \mathbf{D}.$$

Then the functional derivative are given by,

$$\phi_{2,i}'(t) = \int_0^s \phi_{1,i}'(s) ds, \qquad \phi_{2,(i,l)}''(t) = \int_0^s \phi_{1,(i,l)}''(s) ds.$$

Notice that the above equality holds only if $\phi_1(d;t)$ is differentiable at any order in the p-variation setting (Dudley and Norvaiša, 1999) and its composition with the integration operator is also differentiable at any order, which is indeed the case for the Kaplan-Meier functional (Overgaard et al., 2017).

Proof of Remark 1: Without censoring, each pseudo-observation becomes $\widehat{\theta}_i^k(t) = \theta^k(t) + \phi'_{k,i}(t) = v_k(T_i;t)$ and $Q_N = 0$. Plugging these into the formula of the asymptotic variance in Theorem 1, we obtain the asymptotic variance derived in Li and Li (2019b), replacing Y_i with $v_k(T_i;t)$.

Proof of Remark 2: In this part, we prove that ignoring the "correlation term" between the pseudo-observations of different units will over-estimate the variance of the weighting estimator.

Treating each pseudo-observation as an "observed response variable" and ignoring the uncertainty associated with jackknifing will induce the following asymptotic variance,

$$\begin{aligned}
\sigma^{*2} =& \bar{\omega}^{-2}\,\mathbb{E}[D_{ij}\{\widehat{\theta}_i^k(t) - m_j^{k,h}(t)\}w_j^h(\mathbf{X}_i;\boldsymbol{\gamma}) + \mathbf{H}_j^T\mathbf{I}_{\boldsymbol{\gamma}\boldsymbol{\gamma}}^{-1}\mathbf{S}_{\boldsymbol{\gamma},i} \\
& - D_{ij'}\{\widehat{\theta}_i^k(t) - m_{j'}^{k,h}(t)\}w_{j'}^h(\mathbf{X}_i;\boldsymbol{\gamma}) + \mathbf{H}_{j'}^T\mathbf{I}_{\boldsymbol{\gamma}\boldsymbol{\gamma}}^{-1}\mathbf{S}_{\boldsymbol{\gamma},i}]^2 \\
=& \bar{\omega}^{-2}\,\mathbb{E}[D_{ij}\{\theta_k(t) + \phi'_{k,i}(t) - m_j^{k,h}(t)\}w_j^h(\mathbf{X}_i;\boldsymbol{\gamma}) + \mathbf{H}_j^T\mathbf{I}_{\boldsymbol{\gamma}\boldsymbol{\gamma}}^{-1}\mathbf{S}_{\boldsymbol{\gamma},i} \\
& - D_{ij'}\{\theta_k(t) + \phi'_{k,i}(t) - m_{j'}^{k,h}(t)\}w_{j'}^h(\mathbf{X}_i;\boldsymbol{\gamma}) + \mathbf{H}_{j'}^T\mathbf{I}_{\boldsymbol{\gamma}\boldsymbol{\gamma}}^{-1}\mathbf{S}_{\boldsymbol{\gamma},i}]^2 \\
=& \bar{\omega}^{-2}\,\mathbb{E}\{\Psi_j^*(\mathcal{O}_i;t) - \Psi_{j'}^*(\mathcal{O}_i;t)\}^2,
\end{aligned}$$

where the first equality follows from Theorem 2 in Graw et al. (2009). We wish to show that,

$$\mathbb{E}\{\Psi_j^*(\mathcal{O}_i;t) - \Psi_{j'}^*(\mathcal{O}_i;t)\}^2 \geq \mathbb{E}\{\Psi_j(\mathcal{O}_i;t) - \Psi_{j'}(\mathcal{O}_i;t)\}^2,$$

and hence $\sigma^{*2} \geq \sigma^2$. Notice that,

$$\eta_i \triangleq \Psi_j^*(\mathcal{O}_i;t) - \Psi_{j'}^*(\mathcal{O}_i;t), \psi_i \triangleq \Psi_j(\mathcal{O}_i;t) - \Psi_{j'}(\mathcal{O}_i;t)$$
$$\psi_i = \eta_i + \frac{1}{N-1}\sum_{l\neq i} \phi''_{k,(l,i)}(t)[D_{lj}w_j^h(\mathbf{X}_l,\boldsymbol{\gamma}) - D_{lj'}w_{j'}^h(\mathbf{X}_l,\boldsymbol{\gamma})]$$

Next, we plug the exact formula of $\phi'_{k,i}(t)$ and $\phi''_{k,(i,l)}(t)$ into the above equation, and obtain

$$\begin{aligned}
&\mathbb{E}\{\eta_i(\psi_i - \eta_i)\} \\
=& -S^2(t)\,\mathbb{E}\left[\{D_{ij}w_j^h(\mathbf{X}_i,\boldsymbol{\gamma}) - D_{ij'}w_{j'}^h(\mathbf{X}_i,\boldsymbol{\gamma})\}\int_0^t \frac{1}{H(s)}dM(s)\right. \\
&\left.\left\{\int_0^t\int_0^s \frac{1}{H(u)}dM(u)d\mu(s) - \int_0^t\left(1-\frac{Y(s)}{H(s)}\right)d\mu(s)\right\}\right],
\end{aligned}$$

where $M(s) = N_1(s) - \int_0^s Y(t)d\Lambda_1(t)$, $d\mu(s) = \mathbb{E}\left\{\frac{D_{ij}w_j^h(\mathbf{X}_i,\boldsymbol{\gamma}) - D_{ij'}w_{j'}^h(\mathbf{X}_i,\boldsymbol{\gamma})}{H(s)}dM_{i,1}(s)\right\}$. With the results established in the proof of Theorem 2 in Jacobsen and Martinussen (2016) (equation (22) in their Appendix, treating $D_{ij}w_j^h(\mathbf{X}_i,\boldsymbol{\gamma}) - D_{ij'}w_{j'}^h(\mathbf{X}_i,\boldsymbol{\gamma})$ as the "$A(Z)$" in the equation), we can further simplify the above expression to,

$$\mathbb{E}\{\eta_i(\psi_i - \eta_i)\} = -S^2(t)\int_0^t\int_0^t\int_0^{s\wedge u}\frac{\lambda_c(v)}{H(v)}dvd\mu(u)d\mu(s),$$

where $\lambda_c(t)$ is the hazard function for the censoring time. Also, similar to equation (16) in the Appendix of Jacobsen and Martinussen (2016), we can show that,

$$\begin{aligned}
\mathbb{E}\{\psi_i - \eta_i\}^2 &= S^2(t)\int_0^t\int_0^t\int_0^{s\wedge u}\frac{\lambda_c(v)}{H(v)}dvd\mu(u)d\mu(s) \\
&= -\,\mathbb{E}\{\eta_i(\psi_i - \eta_i)\}
\end{aligned}$$

Combining the above results, we obtain

$$\begin{aligned}
\mathbb{E}\{\Psi_j(\mathcal{O}_i;t) - \Psi_{j'}(\mathcal{O}_i;t)\}^2 &= \mathbb{E}\{\psi_i\}^2 = \mathbb{E}\{\eta_i + \psi_i - \eta_i\}^2 \\
&= \mathbb{E}\{\eta_i\}^2 + \mathbb{E}\{\psi_i - \eta_i\}^2 + 2\,\mathbb{E}\{\eta_i(\psi_i - \eta_i)\} \\
&= \mathbb{E}\{\Psi_j^*(\mathcal{O}_i;t) - \Psi_{j'}^*(\mathcal{O}_i;t)\}^2 - \mathbb{E}\{\psi_i - \eta_i\}^2 \\
&\leq \mathbb{E}\{\Psi_j^*(\mathcal{O}_i;t) - \Psi_{j'}^*(\mathcal{O}_i;t)\}^2
\end{aligned}$$

which completes the proof of this remark.

Proof of Remark 3: Treating the generalized propensity score as known will remove the term $\mathbf{H}_{j'}^T \mathbf{I}_{\boldsymbol{\gamma}\boldsymbol{\gamma}} \mathbf{S}_{\boldsymbol{\gamma},i}$ in $\Psi_j(\mathcal{O}_i; t)$. When $h(\mathbf{X}) = 1$ or equivalently under the IPW scheme, the asymptotic variance based on the known or fixed GPS in estimator (5), $\widetilde{\sigma}^2$, becomes:

$$\begin{aligned}\widetilde{\sigma}^2 =& \mathbb{E}[D_{ij}\{\theta_k(t) + \phi'_{k,i}(t) - m_j^{k,h}(t)\}e_j(\mathbf{X}_i;\boldsymbol{\gamma})^{-1} \\ &- D_{ij'}\{\theta_k(t) + \phi'_{k,i}(t) - m_{j'}^{k,h}(t)\}e_{j'}(\mathbf{X}_i;\boldsymbol{\gamma})^{-1}. \\ &+ \frac{1}{N-1}\sum_{l\neq i}\phi''_{k,(l,i)}(t)\{D_{lj}e_j(\mathbf{X}_l;\boldsymbol{\gamma})^{-1} - D_{lj'}e_{j'}(\mathbf{X}_i;\boldsymbol{\gamma})^{-1}\}]^2.\end{aligned}$$

On the other hand, the asymptotic variance taking account of uncertainty in estimating the generalized propensity scores can be expressed as,

$$\begin{aligned}\sigma^2 =& \widetilde{\sigma}^2 + 2(\mathbf{H}_j - \mathbf{H}_{j'})^T \mathbf{I}_{\boldsymbol{\gamma}\boldsymbol{\gamma}}^{-1} \mathbb{E}\left[\left\{D_{ij}(\theta_k(t) + \phi'_{k,i}(t) - m_j^{k,h}(t))e_j(\mathbf{X}_i;\boldsymbol{\gamma})^{-1}\right.\right. \\ &\left. + \frac{1}{N-1}\sum_{l\neq i}\phi''_{k,(l,i)}(t)D_{lj}e_j(\mathbf{X}_l;\boldsymbol{\gamma})^{-1}\right\}\mathbf{S}_{\boldsymbol{\gamma},i} \\ &- \left\{D_{ij'}(\theta_k(t) + \phi'_{k,i}(t) - m_{j'}^{k,h}(t))e_{j'}(\mathbf{X}_i;\boldsymbol{\gamma})^{-1}\right. \\ &\left.\left. + \frac{1}{N-1}\sum_{l\neq i}\phi''_{k,(l,i)}(t)D_{lj'}e_{j'}(\mathbf{X}_l;\boldsymbol{\gamma})^{-1}\right\}\mathbf{S}_{\boldsymbol{\gamma},i}\right] + (\mathbf{H}_j - \mathbf{H}_{j'})^T \mathbf{I}_{\boldsymbol{\gamma}\boldsymbol{\gamma}}(\mathbf{H}_j - \mathbf{H}_{j'}) \\ =& \widetilde{\sigma}^2 + 2(\mathbf{H}_j - \mathbf{H}_{j'})^T \mathbf{I}_{\boldsymbol{\gamma}\boldsymbol{\gamma}}^{-1} \mathbb{E}\left[D_{ij}(\theta_k(t) + \phi'_{k,i}(t) - m_j^{k,h}(t))e_j(\mathbf{X}_i;\boldsymbol{\gamma})^{-1}\mathbf{S}_{\boldsymbol{\gamma},i}\right. \\ &+ \frac{1}{N-1}\sum_{l\neq i}\{\phi''_{k,(l,i)}(t)D_{lj}e_j(\mathbf{X}_l;\boldsymbol{\gamma})^{-1}\}\mathbf{S}_{\boldsymbol{\gamma},i} \\ &- D_{ij'}(\theta_k(t) + \phi'_{k,i}(t) - m_{j'}^{k,h}(t))e_{j'}(\mathbf{X}_i;\boldsymbol{\gamma})^{-1}\mathbf{S}_{\boldsymbol{\gamma},i} \\ &\left. - \frac{1}{N-1}\sum_{l\neq i}\{\phi''_{k,(l,i)}(t)D_{lj'}e_{j'}(\mathbf{X}_l;\boldsymbol{\gamma})^{-1}\}\mathbf{S}_{\boldsymbol{\gamma},i}\right] + (\mathbf{H}_j - \mathbf{H}_{j'})^T \mathbf{I}_{\boldsymbol{\gamma}\boldsymbol{\gamma}}(\mathbf{H}_j - \mathbf{H}_{j'}) \\ =& \tilde{\sigma}^2 + 2I + II,\end{aligned}$$

where we applied the facts that $E(\mathbf{S}_{\boldsymbol{\gamma},i}\mathbf{S}_{\boldsymbol{\gamma},i}^T) = \mathbf{I}_{\boldsymbol{\gamma}\boldsymbol{\gamma}}$. The score function $\mathbf{S}_{\boldsymbol{\gamma},i}$ can be expressed as,

$$D_{ij}\mathbf{S}_{\boldsymbol{\gamma},i} = D_{ij}\sum_{k=1}^{J}\left\{\frac{\partial}{\partial\boldsymbol{\gamma}}e_k(\mathbf{X}_i;\boldsymbol{\gamma})\right\}D_{ik}/e_k(\mathbf{X}_i;\boldsymbol{\gamma}) = \left\{\frac{\partial}{\partial\boldsymbol{\gamma}}e_j(\mathbf{X}_i;\boldsymbol{\gamma})\right\}D_{ij}/e_j(\mathbf{X}_i;\boldsymbol{\gamma}).$$

On the other hand, when $h(\mathbf{X}) = 1$, we have,

$$\frac{\partial}{\partial \boldsymbol{\gamma}} w_j^h(\mathbf{X}_i, \boldsymbol{\gamma}) = \frac{\partial}{\partial \boldsymbol{\gamma}} \left\{ e_j(\mathbf{X}_i; \boldsymbol{\gamma})^{-1} \right\} = -e_j(\mathbf{X}_i; \boldsymbol{\gamma})^{-2} \frac{\partial}{\partial \boldsymbol{\gamma}} e_j(\mathbf{X}_i; \boldsymbol{\gamma}) = -D_{ij} e_j(\mathbf{X}_i; \boldsymbol{\gamma})^{-1} \mathbf{S}_{\boldsymbol{\gamma},i}.$$

Notice that,

$$\begin{aligned}
\mathbb{E}\{\phi''_{k,(l,i)}(t) D_{lj} e_j(\mathbf{X}_l; \boldsymbol{\gamma})^{-1} \mathbf{S}_{\boldsymbol{\gamma},i}\} &= \mathbb{E}\{\mathbf{S}_{\boldsymbol{\gamma},i} \, \mathbb{E}\{\phi''_{k,(l,i)}(t) D_{lj} e_j(\mathbf{X}_l; \boldsymbol{\gamma})^{-1} | \mathcal{O}_i, \mathbf{X}_l\}\} \\
&= \mathbb{E}\{\mathbf{S}_{\boldsymbol{\gamma},i} \, \mathbb{E}\{D_{lj} | \mathbf{X}_l\} e_j(\mathbf{X}_l; \boldsymbol{\gamma})^{-1} \, \mathbb{E}\{\phi''_{k,(l,i)}(t) | \mathcal{O}_i, \mathbf{X}_l\}\} \\
&= \mathbb{E}\{\mathbf{S}_{\boldsymbol{\gamma},i} \, \mathbb{E}\{\phi''_{k,(l,i)}(t) | \mathcal{O}_i, \mathbf{X}_l\}\} \\
&= \mathbb{E}\{\phi''_{k,(l,i)}(t) \mathbf{S}_{\boldsymbol{\gamma},i}\} = \mathbb{E}\{\mathbf{S}_{\boldsymbol{\gamma},i} \, \mathbb{E}\{\phi''_{k,(l,i)}(t) | \mathcal{O}_i\}\} = 0,
\end{aligned}$$

where the second line follows from the weak unconfoundness assumption (A1), namely, $\phi''_{k,(l,i)}(t)$ is a function of $\widetilde{T}_l(j), \Delta_l(j)$ which independent of D_{lj} given $\mathbf{X}_l$. With the above equality, we can show,

$$\begin{aligned}
&\mathbb{E}\{D_{ij}(\theta^k(t) + \phi'_{k,i}(t) - m_j^{k,h}(t)) e_j(\mathbf{X}_i; \boldsymbol{\gamma})^{-1} \mathbf{S}_{\boldsymbol{\gamma},i} \\
&+ \frac{1}{N-1} \sum_{l \neq i} \{\phi''_{k,(l,i)}(t) D_{lj} e_j(\mathbf{X}_l; \boldsymbol{\gamma})^{-1}\} \mathbf{S}_{\boldsymbol{\gamma},i}\} \\
=& \, \mathbb{E}\{D_{ij}(\theta^k(t) + \phi'_{k,i}(t) - m_j^{k,h}(t)) e_j(\mathbf{X}_i; \boldsymbol{\gamma})^{-1} \mathbf{S}_{\boldsymbol{\gamma},i}\} \\
=& - \mathbb{E}\left\{ (\theta^k(t) + \phi'_{k,i}(t) - m_j^{k,h}(t)) \frac{\partial}{\partial \boldsymbol{\gamma}} w_j^h(\mathbf{X}_i, \boldsymbol{\gamma}) \right\} = -\mathbf{H}_j
\end{aligned}$$

Hence, we have $2I = -2II$, and $\sigma^2 - \tilde{\sigma}^2 = -(\mathbf{H}_j - \mathbf{H}_{j'})^T \mathbf{I}_{\boldsymbol{\gamma}\boldsymbol{\gamma}} (\mathbf{H}_j - \mathbf{H}_{j'}) \leq 0$ since $\mathbf{I}_{\boldsymbol{\gamma}\boldsymbol{\gamma}}$ is semi-positive definite. As such, we have proved Remark 3.

Proof of Remark 4: First we will prove the consistency of estimator (5) in the main text under covariate dependent (conditional independent) censoring specified in Assumption (A4). We define the functional G by

$$G(f; s|X, Z) = \prod_0^{s^-} (1 - \Lambda(f; du|X, Z)), \quad f \in \mathbf{D}$$

where Λ is the Nelson-Aalen functional for the cumulative hazard of censoring time C_i. And we define functional v as the $v_k(f; t) = v_k(\widetilde{T}; t) \mathbf{1}\{C \geq \widetilde{T} \wedge t\}$, for $f \in \mathbf{D}$.

Hence, we can view (5) using (8) in the main text as a functional from $\mathbf{D}$ to $\mathcal{R}$, which is given by,

$$\Theta_k(f) = \int \frac{v_k(f;t)}{G(f;\widetilde{T} \wedge t|\mathbf{X}, Z)} df.$$

According to Overgaard et al. (2019), functional Θ_k is measurable mapping and 2-times continuously differentiable with a Lipschitz continuous second-order derivative in a neighborhood of F. Assuming the censoring survival function G is consistently estimated, say, by a Cox proportional hazards model, we can establish a similar property as in the completely random censoring case that (Theorem 2 in Overgaard et al. (2019)),

$$\begin{aligned}
\mathbb{E}\{\widehat{\theta}_i^k(t)|\mathbf{X}_i, Z_i\} &= \mathbb{E}\left\{ \frac{v_k(\widetilde{T}_i;t)\mathbf{1}\{C_i \geq \widetilde{T}_i \wedge t\}}{G(\widetilde{T}_i \wedge t|\mathbf{X}_i, Z_i)} |\mathbf{X}_i, Z_i \right\} + o_p(1) \\
&= \frac{\mathbb{E}(v_k(\widetilde{T}_i;t)|\mathbf{X}_i, Z_i) G(\widetilde{T}_i \wedge t|\mathbf{X}_i, Z_i)}{G(\widetilde{T}_i \wedge t|\mathbf{X}_i, Z_i)} + o_p(1) \\
&= \mathbb{E}(v_k(\widetilde{T}_i;t)|\mathbf{X}_i, Z_i) + o_p(1).
\end{aligned}$$

Therefore, we can show the consistency of estimator (5) based on (8) in the main text follows the exact same procedure as in the proof for Theorem 1 (i).

Moreover, the asymptotic normality of estimator (5) using (8) follows the same proof in Theorem 2 (ii) where we replace the derivative $\phi'_{k,i}(t)$ and $\phi''_{k,(i,l)}(t)$ with the one corresponding to the functional Θ_k. We omit the detailed steps for brevity, but present the specific forms of the functional derivatives. The first-order derivative of Θ_k at F along the direction of sample i is given by,

$$\Theta'_{k,i} = \int \frac{v_k(\widetilde{T};t)\mathbf{1}\{C \geq \widetilde{T} \wedge t\}}{G(F;\widetilde{T} \wedge t|\mathbf{X}, Z)} d\delta_{\mathcal{O}_i} - \int \frac{v_k(\widetilde{T};t)\mathbf{1}\{C \geq \widetilde{T} \wedge t\}}{G(F|\widetilde{T} \wedge t|\mathbf{X}, Z)^2} G'_F(\delta_{\mathcal{O}_i}; \widetilde{T} \wedge t|\mathbf{X}, Z) dF.$$

Note that $G'_F(g;s|\mathbf{X}, Z)$ is the derivative of functional G at F along direction g, which is,

$$G'_F(g;s|\mathbf{X}, Z) = -G(F;s|\mathbf{X}, Z) \int_0^{s^-} \frac{1}{1 - d\Lambda(F;u|\mathbf{X}, Z)} \Lambda'_F(g;du|\mathbf{X}, Z),$$

where $\Lambda'_F(g; du|\mathbf{X}, Z)$ is the functional derivative of the cumulative hazard evaluated at F along direction g. For example, if the censoring survival function is estimated by Cox proportional hazards model, the above functional derivative can be obtained by viewing it as a solution to a set of estimating equations for the Cox model and employing the implicit function theorem. Detailed derivation is provided in the proof of Proposition 2 in Overgaard et al. (2019). The second order derivative of Θ_k at F along the direction of sample i, l is given by,

$$\begin{aligned}
\Theta''_{k,(i,l)} = &- \int \frac{v_k(\widetilde{T}; t)\mathbf{1}\{C \geq \widetilde{T} \wedge t\}}{G(F; \widetilde{T} \wedge t|\mathbf{X}, Z)^2} G'_F(\delta_{\mathcal{O}_l}; \widetilde{T} \wedge t|\mathbf{X}, Z) d\delta_{\mathcal{O}_i} \\
&- \int \frac{v_k(\widetilde{T}; t)\mathbf{1}\{C \geq \widetilde{T} \wedge t\}}{G(F; \widetilde{T} \wedge t|\mathbf{X}, Z)^2} G'_F(\delta_{\mathcal{O}_i}; \widetilde{T} \wedge t|\mathbf{X}, Z) d\delta_{\mathcal{O}_l} \\
&+ 2 \int \frac{v_k(\widetilde{T}; t)\mathbf{1}\{C \geq \widetilde{T} \wedge t\}}{G(F; \widetilde{T} \wedge t|\mathbf{X}, Z)^3} G'_F(\delta_{\mathcal{O}_i}; \widetilde{T} \wedge t|\mathbf{X}, Z) G'_F(\delta_{\mathcal{O}_l}; \widetilde{T} \wedge t|\mathbf{X}, Z) dF \\
&- \int \frac{v_k(\widetilde{T}; t)\mathbf{1}\{C \geq \widetilde{T} \wedge t\}}{G(F; \widetilde{T} \wedge t|\mathbf{X}, Z)^2} G''_F; (\delta_{\mathcal{O}_i}, \delta_{\mathcal{O}_l}; \widetilde{T} \wedge t|\mathbf{X}, Z) dF.
\end{aligned}$$

The second-order derivative of G at F along the direction of (g, h) is,

$$\begin{aligned}
G''_F(g, h; s|\mathbf{X}, Z) = &G(F; s|\mathbf{X}, Z) \int_0^{s^-} \frac{1}{1 - d\Lambda(F; u|\mathbf{X}, Z)} \Lambda'_F(g; du|\mathbf{X}, Z) \\
&\times \int_0^{s^-} \frac{1}{1 - d\Lambda(F; u|\mathbf{X}, Z)} \Lambda'_F(h; du|\mathbf{X}, Z) \\
&- G(F; s|\mathbf{X}, Z) \int_0^{s} \frac{d\Lambda'(g; |\mathbf{X}, Z) d\Lambda'(h; |\mathbf{X}, Z)}{(1 - d\Lambda(F; u|\mathbf{X}, Z))^2} \\
&- G(F; s|\mathbf{X}, Z) \int_0^{s^-} \frac{\Lambda''_F(g, h; du|\mathbf{X}, Z)}{1 - d\Lambda(F; u|\mathbf{X}, Z)}.
\end{aligned}$$

The second-order derivative of the cumulative hazard for using the proportional hazard model, $\Lambda''_F(g, h; du|\mathbf{X}, Z)$ is given in the Section 3 of the Appendix of Overgaard et al. (2019).

Proof of Theorem 2 We proceed under the regularity conditions specified in the proof of Theorem 1. Let $\mathbf{c} = (c_1, c_2, \cdots, c_J) \in \{-1, 0, 1\}^J$ and define,

$$\hat{\tau}(\mathbf{c}; t)^{k,h} = \sum_{j=1}^{J} c_j \left\{ \frac{\sum_{i=1}^{N} D_{ij} \widehat{\theta}_i^k(t) w_j^h(\mathbf{X}_i)}{\sum_{i=1}^{N} D_{ij} w_j^h(\mathbf{X}_i)} \right\}.$$

It is easy to show that when $c_j = 1, c_{j'} = -1, c_{j''} = 0, j'' \neq j, j'$, we have $\widehat{\tau}(\mathbf{c}; t)^{k,h} = \widehat{\tau}_{j,j'}^{k,h}(t)$. Conditional on the collection of design points $\underline{\mathbf{Z}} = \{Z_1, \ldots, Z_N\}$ and $\underline{\mathbf{X}} = \{\mathbf{X}_1, \ldots, \mathbf{X}_N\}$, the asymptotic variance of $\widehat{\tau}(\mathbf{c}; t)^{k,h}$ is,

$$\begin{aligned}
N\,\mathbb{V}(\widehat{\tau}(\mathbf{c}; t)^{k,h} | \underline{\mathbf{X}}, \underline{\mathbf{Z}}) =& N \sum_{j=1}^{J} c_j^2 \left[\frac{\sum_{i=1}^{N} D_{ij}\, \mathbb{V}\{\widehat{\theta}_i^k(t) | \underline{\mathbf{X}}, \underline{\mathbf{Z}}\} \{w_j^h(\mathbf{X}_i)\}^2}{\{\sum_{i=1}^{N} D_{ij} w_j^h(\mathbf{X}_i)\}^2} \right. \\
&\left. + \frac{\sum_{i \neq l} D_{ij} D_{lj} \mathrm{Cov}\{\widehat{\theta}_i^k(t), \widehat{\theta}_l^k(t) | \underline{\mathbf{X}}, \underline{\mathbf{Z}}\} w_j^h(\mathbf{X}_i) w_j^h(\mathbf{X}_l)}{\{\sum_{i=1}^{N} D_{ij} w_j^h(\mathbf{X}_i)\}^2} \right] \\
&+ N \sum_{j \neq j'} c_j c_{j'} \frac{\sum_{i \neq l} D_{ij} D_{lj'} \mathrm{Cov}\{\widehat{\theta}_i^k(t), \widehat{\theta}_l^k(t) | \underline{\mathbf{X}}, \underline{\mathbf{Z}}\} w_j^h(\mathbf{X}_i) w_{j'}^h(\mathbf{X}_l)}{\{\sum_{i=1}^{N} D_{ij} w_j^h(\mathbf{X}_i)\} \{\sum_{i=1}^{N} D_{ij'} w_{j'}^h(\mathbf{X}_i)\}} \\
=& A + B + C
\end{aligned}$$

First, we consider the asymptotic behaviour of term C. Notice that with von Mises expansion (equation (6) in the main text),

$$\begin{aligned}
\mathrm{Cov}\{\widehat{\theta}_i^k(t), \widehat{\theta}_l^k(t) | \underline{\mathbf{X}}, \underline{\mathbf{Z}}\} = \mathrm{Cov} \Bigg\{ & \theta^k(t) + \phi'_{k,i}(t) + \frac{1}{N-1} \sum_{m \neq i} \phi''_{k,(m,i)}, \\
& \theta^k(t) + \phi'_{k,l}(t) + \frac{1}{N-1} \sum_{n \neq l} \phi''_{k,(n,l)} | \underline{\mathbf{X}}, \underline{\mathbf{Z}} \Bigg\} + o_p(N^{-1/2}) \\
=& \mathrm{Cov}\{\phi'_{k,i}(t), \phi'_{k,l}(t) | \underline{\mathbf{X}}, \underline{\mathbf{Z}}\} + \frac{1}{N-1} \sum_{n \neq l} \mathrm{Cov}\{\phi'_{k,i}(t), \phi''_{k,(n,l)}(t) | \underline{\mathbf{X}}, \underline{\mathbf{Z}}\} \\
&+ \frac{1}{N-1} \sum_{m \neq i} \mathrm{Cov}\{\phi'_{k,l}(t), \phi''_{k,(m,i)}(t) | \underline{\mathbf{X}}, \underline{\mathbf{Z}}\} \\
&+ \frac{1}{(N-1)^2} \mathrm{Cov} \left\{ \sum_{m \neq i} \phi''_{k,(m,i)}(t), \sum_{n \neq l} \phi''_{k,(n,l)}(t) | \underline{\mathbf{X}}, \underline{\mathbf{Z}} \right\} + o_p(N^{-1/2}).
\end{aligned}$$

We view $\phi'_{k,i}(t)$ as a function of $(\widetilde{T}_i(j), \Delta_i(j))$ and $\phi''_{k,(i,l)}(t)$ as function of $(\widetilde{T}_i(j), \Delta_i(j), \widetilde{T}_l(j'), \Delta_l(j'))$ (since we have $D_{ij} D_{lj'}$ as the multiplier). Due to the independence

between $(\widetilde{T}_i(j), \Delta_i(j))$ and $(\widetilde{T}_l(j'), \Delta_l(j'))$ given $\underline{\mathbf{X}}, \underline{\mathbf{Z}}$, we can reduce the following covariance into zero,

$$\begin{aligned}
\mathrm{Cov}\{\phi'_{k,i}(t), \phi'_{k,l}(t)|\underline{\mathbf{X}}, \underline{\mathbf{Z}}\} &= 0, \text{when } i \neq l, \\
\mathrm{Cov}\{\phi'_{k,i}(t), \phi''_{k,(n,l)}(t)|\underline{\mathbf{X}}, \underline{\mathbf{Z}}\} &= 0, \text{when } i \neq n, \\
\mathrm{Cov}\{\phi'_{k,l}(t), \phi''_{k,(m,i)}(t)|\underline{\mathbf{X}}, \underline{\mathbf{Z}}\} &= 0, \text{when } l \neq m, \\
\mathrm{Cov}\{\phi''_{k,(m,i)}(t), \phi''_{k,(n,l)}(t)|\underline{\mathbf{X}}, \underline{\mathbf{Z}}\} &= 0, \text{when } m \neq n.
\end{aligned}$$

Therefore, we have

$$\begin{aligned}
\mathrm{Cov}\{\widehat{\theta}^k_i(t), \widehat{\theta}^k_l(t)|\underline{\mathbf{X}}, \underline{\mathbf{Z}}\} =& \frac{1}{N-1}\mathrm{Cov}\{\phi'_{k,i}(t), \phi''_{k,(i,l)}(t)|\underline{\mathbf{X}}, \underline{\mathbf{Z}}\} \\
&+ \frac{1}{N-1}\mathrm{Cov}\{\phi'_{k,l}(t), \phi''_{k,(l,i)}(t)|\underline{\mathbf{X}}, \underline{\mathbf{Z}}\} \\
&+ \frac{1}{(N-1)^2}\sum_{m\neq i, m\neq l}\mathrm{Cov}\{\phi''_{k,(m,i)}(t), \phi''_{k,(m,l)}(t)|\underline{\mathbf{X}}, \underline{\mathbf{Z}}\} \\
&+ o_p(N^{-1/2}).
\end{aligned}$$

Note that we have,

$$\frac{1}{N}\sum_{i=1}^{N} D_{ij} w^h_j(\mathbf{X}_i) \xrightarrow{p} \int_{\mathcal{X}} \mathbb{E}(D_{ij}|\mathbf{X})/e_j(\mathbf{X}) h(\mathbf{X}) f(\mathbf{X}) \mu(d\mathbf{X}) \triangleq C_h,$$

Then term C is asymptotically equals to,

$$\begin{aligned}
&N\sum_{j\neq j'} c_j c_{j'} \frac{\sum_{i\neq l} D_{ij} D_{lj'} \mathrm{Cov}\{\widehat{\theta}^k_i(t), \widehat{\theta}^k_l(t)|\underline{\mathbf{X}}, \underline{\mathbf{Z}}\} w^h_j(\mathbf{X}_i) w^h_{j'}(\mathbf{X}_l)}{\{\sum_{i=1}^N D_{ij} w^h_j(\mathbf{X}_i)\}\{\sum_{i=1}^N D_{ij'} w^h_{j'}(\mathbf{X}_i)\}} \\
&= \sum_{j\neq j'} c_j c_{j'} \frac{\sum_{i\neq l} D_{ij} D_{lj'} \mathrm{Cov}\{\widehat{\theta}^k_i(t), \widehat{\theta}^k_l(t)|\underline{\mathbf{X}}, \underline{\mathbf{Z}}\} w^h_j(\mathbf{X}_i) w^h_{j'}(\mathbf{X}_l)/N}{\{\sum_{i=1}^N D_{ij} w^h_j(\mathbf{X}_i)/N\}\{\sum_{i=1}^N D_{ij'} w^h_{j'}(\mathbf{X}_i)/N\}} \\
&= \sum_{j\neq j'} c_j c_{j'} \frac{\sum_{i\neq l} D_{ij} D_{lj'} \frac{1}{N-1}\mathrm{Cov}\{\phi'_{k,i}(t), \phi''_{k,(i,l)}(t)|\underline{\mathbf{X}}, \underline{\mathbf{Z}}\} w^h_j(\mathbf{X}_i) w^h_{j'}(\mathbf{X}_l)/N}{\{\sum_{i=1}^N D_{ij} w^h_j(\mathbf{X}_i)/N\}\{\sum_{i=1}^N D_{ij'} w^h_{j'}(\mathbf{X}_i)/N\}} \\
&+ \sum_{j\neq j'} c_j c_{j'} \frac{\sum_{i\neq l} D_{ij} D_{lj'} \frac{1}{N-1}\mathrm{Cov}\{\phi'_{k,l}(t), \phi''_{k,(l,i)}(t)|\underline{\mathbf{X}}, \underline{\mathbf{Z}}\} w^h_j(\mathbf{X}_i) w^h_{j'}(\mathbf{X}_l)/N}{\{\sum_{i=1}^N D_{ij} w^h_j(\mathbf{X}_i)/N\}\{\sum_{i=1}^N D_{ij'} w^h_{j'}(\mathbf{X}_i)/N\}} \\
&+ \sum_{j\neq j'} c_j c_{j'} \frac{\sum_{i\neq l} D_{ij} D_{lj'} \frac{1}{(N-1)^2}\sum_{m\neq i, m\neq l}\mathrm{Cov}\{\phi''_{k,(m,i)}(t), \phi''_{k,(m,l)}(t)|\underline{\mathbf{X}}, \underline{\mathbf{Z}}\} w^h_j(\mathbf{X}_i) w^h_{j'}(\mathbf{X}_l)/N}{\{\sum_{i=1}^N D_{ij} w^h_j(\mathbf{X}_i)/N\}\{\sum_{i=1}^N D_{ij'} w^h_{j'}(\mathbf{X}_i)/N\}} \\
&+ o_p(1) = o_p(1)
\end{aligned}$$

Next, we consider term B. Similarly, we have

$$\begin{aligned}
&\mathrm{Cov}\{\widehat{\theta}_i^k(t), \widehat{\theta}_l^k(t)|\underline{\mathbf{X}}, \underline{\mathbf{Z}}\} = \mathrm{Cov}\{\phi'_{k,i}(t), \phi'_{k,l}(t)|\underline{\mathbf{X}}, \underline{\mathbf{Z}}\} \\
&+ \frac{1}{N-1}\sum_{n\neq l}\mathrm{Cov}\{\phi'_{k,i}(t), \phi''_{k,(n,l)}(t)|\underline{\mathbf{X}}, \underline{\mathbf{Z}}\} + \frac{1}{N-1}\sum_{m\neq i}\mathrm{Cov}\{\phi''_{k,(m,i)}(t), \phi'_{k,l}(t)|\underline{\mathbf{X}}, \underline{\mathbf{Z}}\} \\
&+ \frac{1}{(N-1)^2}\sum_{m\neq i, n\neq l}\mathrm{Cov}\{\phi'_{k,(m,i)}(t), \phi''_{k,(n,l)}(t)|\underline{\mathbf{X}}, \underline{\mathbf{Z}}\} + o_p(N^{-1/2}) \\
&= \frac{1}{N-1}\mathrm{Cov}\{\phi'_{k,i}(t), \phi''_{k,(i,l)}(t)|\underline{\mathbf{X}}, \underline{\mathbf{Z}}\} + \frac{1}{N-1}\mathrm{Cov}\{\phi'_{k,l}(t), \phi''_{k,(i,l)}(t)|\underline{\mathbf{X}}, \underline{\mathbf{Z}}\} \\
&+ \frac{1}{(N-1)^2}\sum_{m\neq i, m\neq l}\mathrm{Cov}\{\phi'_{k,(m,i)}(t), \phi''_{k,(m,l)}(t)|\underline{\mathbf{X}}, \underline{\mathbf{Z}}\} + o_p(N^{-1/2}).
\end{aligned}$$

Then the term B asymptotically equals,

$$\begin{aligned}
&N\frac{\sum_{i\neq l} D_{ij}D_{lj}\mathrm{Cov}\{\widehat{\theta}_i^k(t), \widehat{\theta}_l^k(t)|\underline{\mathbf{X}}, \underline{\mathbf{Z}}\}w_j^h(\mathbf{X}_i)w_j^h(\mathbf{X}_l)}{\{\sum_{i=1}^N D_{ij}w_j^h(\mathbf{X}_i)\}^2} \\
&= \frac{\sum_{i\neq l} D_{ij}D_{lj}\frac{1}{N-1}\mathrm{Cov}\{\phi'_{k,i}(t), \phi''_{k,(i,l)}(t)|\underline{\mathbf{X}}, \underline{\mathbf{Z}}\}w_j^h(\mathbf{X}_i)w_j^h(\mathbf{X}_l)/N}{\{\sum_{i=1}^N D_{ij}w_j^h(\mathbf{X}_i)/N\}^2} \\
&+ \frac{\sum_{i\neq l} D_{ij}D_{lj}\frac{1}{N-1}\mathrm{Cov}\{\phi'_{k,l}(t), \phi''_{k,(i,l)}(t)|\underline{\mathbf{X}}, \underline{\mathbf{Z}}\}w_j^h(\mathbf{X}_i)w_j^h(\mathbf{X}_l)/N}{\{\sum_{i=1}^N D_{ij}w_j^h(\mathbf{X}_i)/N\}^2} \\
&+ \frac{\sum_{i\neq l} D_{ij}D_{lj}\frac{1}{(N-1)^2}\sum_{m\neq i, m\neq l}\mathrm{Cov}\{\phi'_{k,(m,i)}(t), \phi''_{k,(m,l)}(t)|\underline{\mathbf{X}}, \underline{\mathbf{Z}}\}w_j^h(\mathbf{X}_i)w_j^h(\mathbf{X}_l)/N}{\{\sum_{i=1}^N D_{ij}w_j^h(\mathbf{X}_i)/N\}^2} \\
&+ o_p(1) = o_p(1)
\end{aligned}$$

Lastly, for term A, Note that we have,

$$\begin{aligned}
\mathbb{V}\{\widehat{\theta}_i^k(t)|\underline{\mathbf{X}}, \underline{\mathbf{Z}}\} = \mathrm{Cov}\{\widehat{\theta}_i^k(t), \widehat{\theta}_i^k(t)|\underline{\mathbf{X}}, \underline{\mathbf{Z}}\} = \mathrm{Cov}\Bigg\{&\theta^k(t) + \phi'_{k,i}(t) + \frac{1}{N-1}\sum_{m\neq i}\phi''_{k,(m,i)}, \\
&\theta^k(t) + \phi'_{k,i}(t) + \frac{1}{N-1}\sum_{m\neq i}\phi''_{k,(m,i)}|\underline{\mathbf{X}}, \underline{\mathbf{Z}}\Bigg\} + o_p(N^{-1/2}) \\
= \mathbb{V}\{\phi'_{k,i}(t)|\underline{\mathbf{X}}, \underline{\mathbf{Z}}\} &+ \frac{1}{(N-1)^2}\sum_{m\neq i}\mathrm{Cov}\{\phi''_{k,(m,i)}(t)^2|\underline{\mathbf{X}}, \underline{\mathbf{Z}}\} + o_p(N^{-1/2}).
\end{aligned}$$

Further observe that

$$N\frac{\sum_{i=1}^N D_{ij}\,\mathbb{V}\{\widehat{\theta}_i^k(t)|\underline{\mathbf{X}},\underline{\mathbf{Z}}\}\{w_j^h(\mathbf{X}_i)\}^2}{\{\sum_{i=1}^N D_{ij}w_j^h(\mathbf{X}_i)\}^2} = \frac{\sum_{i=1}^N D_{ij}\,\mathbb{V}\{\phi'_{k,i}(t)|\underline{\mathbf{X}},\underline{\mathbf{Z}}\}\{w_j^h(\mathbf{X}_i)\}^2/N}{\{\sum_{i=1}^N D_{ij}w_j^h(\mathbf{X}_i)/N\}^2}$$
$$+\frac{\sum_{i=1}^N D_{ij}\sum_{m\neq i}\mathrm{Cov}\{\phi''_{k,(m,i)}(t)^2|\underline{\mathbf{X}},\underline{\mathbf{Z}}\}\{w_j^h(\mathbf{X}_i)\}^2/(N(N-1)^2)}{\{\sum_{i=1}^N D_{ij}w_j^h(\mathbf{X}_i)/N\}^2}+o_p(1)$$
$$=\frac{\sum_{i=1}^N D_{ij}\,\mathbb{V}\{\phi'_{k,i}(t)|\underline{\mathbf{X}},\underline{\mathbf{Z}}\}\{w_j^h(\mathbf{X}_i)\}^2/N}{\{\sum_{i=1}^N D_{ij}w_j^h(\mathbf{X}_i)/N\}^2}+o_p(1).$$

Also, we have

$$\sum_{i=1}^N D_{ij}\,\mathbb{V}\{\phi'_{k,i}(t)|\underline{\mathbf{X}},\underline{\mathbf{Z}}\}\{w_j^h(\mathbf{X}_i)\}^2/N \underset{p}{\to} \int_{\mathcal{X}}\{\mathbb{V}\{\phi'_{k,i}(t)|\underline{\mathbf{X}},\underline{\mathbf{Z}}\}/e_j(\mathbf{X})\}h(\mathbf{X})^2 f(\mathbf{X})\mu(d\mathbf{X}).$$

Therefore, assuming the generalized homoscedasticity condition such that $\mathbb{V}\{\phi'_{k,i}(t)|\underline{\mathbf{X}},\underline{\mathbf{Z}}\} = \mathbb{V}\{\phi'_{k,i}(t)|\mathbf{X}_i,Z_i\} = v$, the conditional asymptotic variance of $\widehat{\tau}(\mathbf{c};t)^{k,h}$ is,

$$\begin{aligned}\lim_{N\to\infty} N\,\mathbb{V}\{\widehat{\tau}(\mathbf{c};t)^{k,h}|\underline{\mathbf{X}},\underline{\mathbf{Z}}\} =& \int_{\mathcal{X}}\sum_{j=1}^J c_j^2\{v/e_j(\mathbf{X})\}h(\mathbf{X})^2 f(\mathbf{X})\mu(d\mathbf{X})/C_h^2\\ =&\frac{\mathbb{E}_{\mathcal{X}}\{h^2(\mathbf{X})\sum_{j=1}^J c_j^2/e_j(\mathbf{X})\}}{C_h^2}v\\ =&\frac{\mathbb{E}_{\mathcal{X}}\{h^2(\mathbf{X})\sum_{j=1}^J c_j^2/e_j(\mathbf{X})\}}{\mathbb{E}_{\mathcal{X}}[h(\mathbf{X})]^2}v\\ \geq&\frac{\mathbb{E}_{\mathcal{X}}\{h^2(\mathbf{X})\sum_{j=1}^J c_j^2/e_j(\mathbf{X})\}}{\mathbb{E}_{\mathcal{X}}\{h^2(\mathbf{X})\sum_{j=1}^J c_j^2/e_j(\mathbf{X})\}\,\mathbb{E}_{\mathcal{X}}\{(\sum_{j=1}^J c_j^2/e_j(\mathbf{X}))^{-1}\}}.\end{aligned}$$

The inequality follows from the Cauchy-Schwarz inequality and the equality is attained when $h(\mathbf{X}) \propto \{\sum_{j=1}^J c_j^2/e_j(\mathbf{X})\}^{-1}$. Consequently, the sum of the asymptotic variance of all pairwise comparisons is,

$$\sum_{j<j'}\lim_{N\to\infty} N\,\mathbb{V}(\hat{\tau}_{j,j'}(t)^{k,h}|\underline{\mathbf{X}},\underline{\mathbf{Z}}) =(J-1)\sum_{j=1}^J\frac{\mathbb{E}_{\mathcal{X}}\{h^2(\mathbf{X})/e_j(\mathbf{X})\}}{\mathbb{E}_{\mathcal{X}}[h(\mathbf{X})]^2}v$$

We consider the variance of $\widehat{\tau}(\bar{\mathbf{c}};t)^{k,h}$ where $\bar{\mathbf{c}} = (1,1,1,\cdots,1)$. We can show that,

$$\lim_{N\to\infty} N\widehat{\tau}(\bar{\mathbf{c}};t)^{k,h} = \sum_{j=1}^J\frac{\mathbb{E}_{\mathcal{X}}\{h^2(\mathbf{X})/e_j(\mathbf{X})\}}{\mathbb{E}_{\mathcal{X}}[h(\mathbf{X})]^2}v$$

Therefore, $\sum_{j<j'} \lim_{N\to\infty} N\, \mathbb{V}(\widehat{\tau}_{j,j'}(t)^{k,h}|\underline{\mathbf{X}}, \underline{\mathbf{Z}})$ attains its minimum when $\lim_{N\to\infty} N\, \widehat{\tau}(\bar{\mathbf{c}}; t)^{k,h}$ are minimized. Notice that $c_j^2 = 1$ in $\bar{\mathbf{c}}$. Hence, when $h(\mathbf{X}) \propto \{\sum_{j=1}^{J} 1/e_j(\mathbf{X})\}^{-1}$, the sum of the conditional asymptotic variance of all pairwise comparison is minimized, which completes the proof of Theorem 2.

Details on augmented weighting estimator In this part, we provide the outline on how to derive the variance estimator of the augmented weighting estimator using the pseudo-observations. Suppose the estimated parameter of the outcome model $\widehat{\boldsymbol{\alpha}}_j$ are the MLEs that solve the score functions $\sum_{i=1}^{N} \mathbf{1}\{Z_i = j\} S_j(\mathbf{X}_i, \widehat{\theta}_i^k; \boldsymbol{\alpha}_j) = 0$, then we can express the augmented weighting estimator based on the solution $(\widehat{\nu}_0, \widehat{\nu}_j, \widehat{\nu}_{j'}, \widehat{\boldsymbol{\alpha}}_j^T, \widehat{\boldsymbol{\gamma}})^T$ to the following estimation equations $\sum_{i=1}^{N} U_i = 0$,

$$\sum_{i=1}^{N} U_i(\widehat{\nu}_0, \widehat{\nu}_j, \widehat{\nu}_{j'}, \widehat{\boldsymbol{\alpha}}_j^T, \widehat{\boldsymbol{\gamma}}) = \sum_{i=1}^{N} \begin{bmatrix} h(\mathbf{X}_i; \boldsymbol{\gamma})\{m_j^k(\mathbf{X}_i; \boldsymbol{\alpha}_j) - m_{j'}^k(\mathbf{X}_i; \boldsymbol{\alpha}_j) - \nu_0\} \\ \mathbf{1}\{Z_i = j\}\{\widehat{\theta}_i^k - m_j^k(\mathbf{X}_i; \boldsymbol{\alpha}_j) - \nu_j\} w_j^h(\mathbf{X}_i) \\ \mathbf{1}\{Z_i = j'\}\{\widehat{\theta}_i^k - m_{j'}^k(\mathbf{X}_i; \boldsymbol{\alpha}_{j'}) - \nu_{j'}\} w_{j'}^h(\mathbf{X}_i) \\ \mathbf{1}\{Z_i = 1\} S_1(\mathbf{X}_i, \widehat{\theta}_i^k; \boldsymbol{\alpha}_1) \\ \cdots \\ \mathbf{1}\{Z_i = J\} S_J(\mathbf{X}_i, \widehat{\theta}_i^k; \boldsymbol{\alpha}_J) \\ \mathbf{S}_{\boldsymbol{\gamma}}(\mathbf{X}_i, Z_i; \boldsymbol{\gamma}) \end{bmatrix} = 0.$$

The augmented weighting estimator is $\widehat{\nu}_0 + \widehat{\nu}_j - \widehat{\nu}_{j'}$. The corresponding variance estimator can be obtained by applying Theorem 3.4 in Overgaard et al. (2017), which offers the asymptotic variance of the estimated parameters based on the estimating equations involving the pseudo-observations.

8.2.2 Details on simulation design

Figure 8.3 illustrates the distribution of the true generalized propensity score (GPS) in the simulations that approximate (i) randomized controlled trials (RCT), (ii) observational study with good covariate overlap between groups, and (iii) observational study with poor covariate overlap between groups. In the simulated RCT, the propensity for being assigned to three arms are the same (1/3) for each unit. In the simulated

observational study, the GPS for three arms differ; the distributions of the GPS to each arm exhibit a larger difference when the overlap is poor.

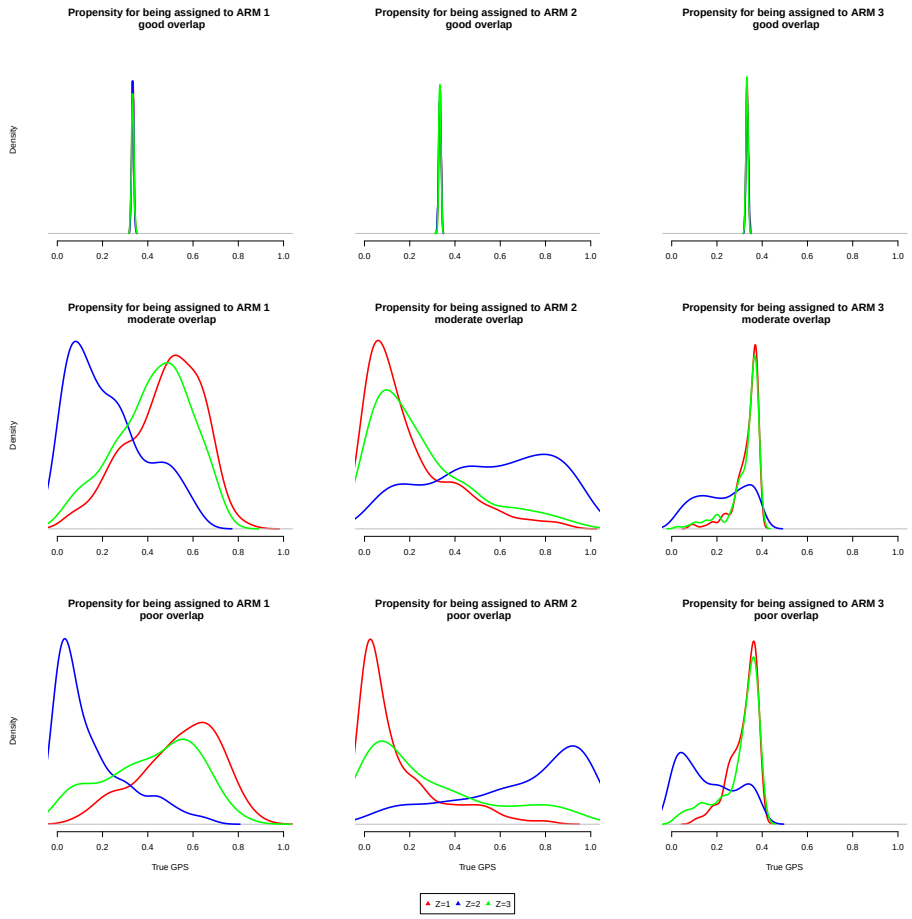

Figure 8.3: Generalized propensity score distribution under different overlap conditions across three arms in the simulation studies. First row: randomized controlled trials (RCT); second row: observational study with good covariate overlap; third row: observational study with poor covariate overlap.

Below, we describe the details of the alternative estimators considered in the simulation studies.

1. Cox model with g-formula (Cox): We fit the cox proportional hazard model with the hazard rate $\lambda(t|\mathbf{X}_i, Z_i)$,

$$\lambda(t|\mathbf{X}_i, Z_i) = \lambda_0(t) \exp(\mathbf{X}_i \alpha^T + \sum_{j \in \mathcal{J}} \boldsymbol{\gamma}_j \mathbf{1}_{Z_i = j}).$$

Based on the hazard rate, we can calculate the conditional survival probability function $\hat{S}(t|X_i, Z_i)$ and estimate $\hat{\tau}^{k,h}_{j,j'}(t)$ when $h(x) = 1$ with the g-formula,

$$\hat{\tau}^1_{j,j'}(t) = \left\{ \sum_{i=1}^{N} \hat{S}(t|X_i, Z_i = j) - \sum_{i=1}^{N} \hat{S}(t|X_i, Z_i = j') \right\} /N,$$
$$\hat{\tau}^2_{j,j'}(t) = \left\{ \int_0^t \sum_{i=1}^{N} \hat{S}(u|X_i, Z_i = j) - \sum_{i=1}^{N} \hat{S}(u|X_i, Z_i = j')du \right\} /N.$$

2. Cox with IPW (Cox-IPW): We first fit a multinomial logistic regression model for the GPS and construct the IPW, i.e. we assign weights $w_i = 1/\Pr(Z_i|\mathbf{X}_i)$ for each unit. Next, we fit a Cox proportional hazard model on the weighted sample with a hazard rate,

$$\lambda(t|\mathbf{X}_i, Z_i) = \lambda_0(t) \exp(\mathbf{X}_i \alpha^T + \sum_{j \in \mathcal{J}} \boldsymbol{\gamma}_j \mathbf{1}_{Z_i = j}).$$

We then calculate the survival probability $\hat{S}(t|Z_i)$ in each arm and estimate $\hat{\tau}^{k,h}_{j,j'}(t)$ when $h(x) = 1$ using,

$$\hat{\tau}^1_{j,j'}(t) = \hat{S}(t|Z_i = j) - \hat{S}(t|Z_i = j'),$$
$$\hat{\tau}^2_{j,j'}(t) = \int_0^t \hat{S}(u|Z_i = j) - \hat{S}(u|Z_i = j')du.$$

3. Trimmed IPW-PO (T-IPW): this is the propensity score weighting estimator (3.5) with $h(x) = 1$, and trim the units with $\max_j\{e_j(\mathbf{X}_i)\} > 0.97$ and $\min_j\{e_j(\mathbf{X}_i)\} < 0.03$. We select this threshold so that the proportion of the sample being trimmed does not exceed 20%.

4. Unadjusted estimator based on pseudo-observations (PO-UNADJ): we take the mean difference of the pseudo-observations between two arms.

$$\tau^k_{j,j'}(t) = \sum_{i=1}^{N} \widehat{\theta}^k_i(t) \mathbf{1}_{Z_i = j} / \sum_{i=1}^{N} \mathbf{1}_{Z_i = j} - \sum_{i=1}^{N} \widehat{\theta}^k_i(t) \mathbf{1}_{Z_i = j'} / \sum_{i=1}^{N} \mathbf{1}_{Z_i = j'}.$$

5. Regression model using the pseudo-observations with the g-formula (PO-G): we fit the following regression model between the pseudo-observations and $\mathbf{X}_i$ and Z_i,

$$E(\widehat{\theta}_i^k(t)|\mathbf{X}_i, Z_i) = g(\mathbf{X}_i\alpha^T + \sum_{j\in\mathcal{J}} \boldsymbol{\gamma}_j \mathbf{1}_{Z_i=j}),$$

where $g(\cdot)$ is the link function (we use log-link for RACE/ASCE and complementary log-log link and construct the estimator for $\hat{\tau}_{j,j'}^{k,h}(t)$ with $h(x) = 1$ using the g-formula,

$$\hat{\tau}_{j,j'}^k(t) = \sum_{i=1}^{N} \{E(\widehat{\theta}_i^k(t)|\mathbf{X}_i, Z_i = j) - E(\widehat{\theta}_i^k(t)|\mathbf{X}_i, Z_i = j')\}/N.$$

6. Augmented weighting estimator (AIPW, OW): we use equation (9) in the main text using IPW or OW.

7. Propensity score weighted Cox model estimator in Mao et al. (2018) (IPW-MAO,OW-MAO): we employ the estimator proposed in Mao et al. (2018) combining IPW or OW in fitting the Cox model.

8.2.3 Additional simulation results

Additional comparisons under poor covariate overlap Figure 8.4 shows the comparison of different estimators in the simulated data with good covariate overlap between treatment arms. The OW estimator achieves lower bias and RMSE compared with other estimators (except for comparing with the Cox estimator) in most cases. Moreover, coverage of the 95% confidence interval of the OW estimator is close to the nominal level while the other estimators exhibit poor coverage especially in estimating the ASCE.

Comparison with trimmed IPW In Figure 8.5, we compare the performance of the trimmed IPW estimator (T-IPW) in the case of good overlap. Firstly, we

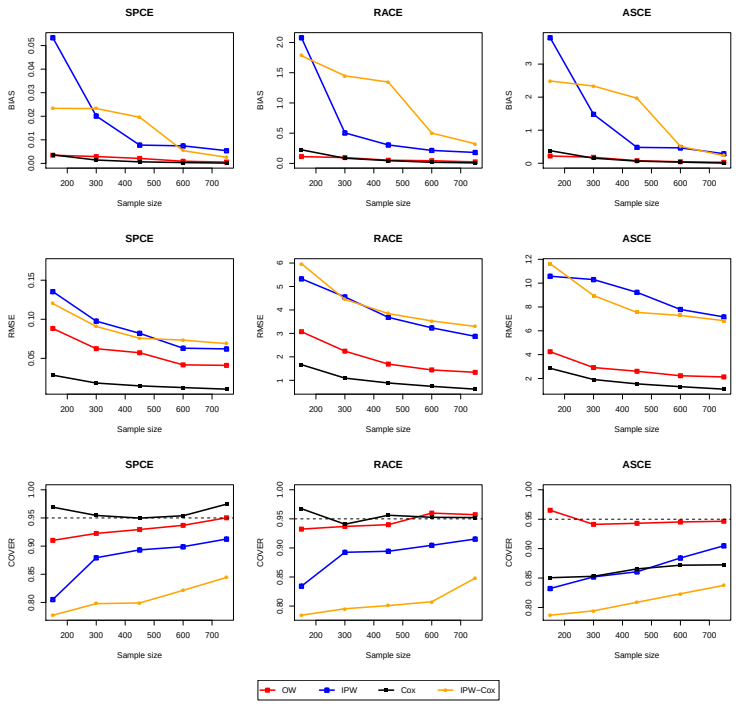

Figure 8.4: Absolute bias, root mean squared error (RMSE) and coverage of the 95% confidence interval for comparing treatment $j = 2$ versus $j = 3$ under good overlap, when the survival outcomes are generated from Model A and censoring is completely independent.

notice that trimming greatly reduces RMSE and absolute bias compared to the untrimmed IPW estimator in Figure 8.4. Moreover, coverage rate of the trimmed IPW estimator become closer to the nominal level. Nonetheless, IPW with trimming is still consistently worse than OW under poor overlap.

Comparison with regression on pseudo-observations Figure 8.6 shows the comparison with the estimators using regression on pseudo-observations. When we have a good overlap, the regression adjusted estimator PO-G achieves a similar RMSE and bias with the IPW estimator and being slightly better when we target at the ASCE. However, the coverage of the PO-G is relatively poor compared with the weighting estimators, which might be due to the misspecifications of the regression models. The performance of PO-G deteriorates when the covariates overlap is poor,

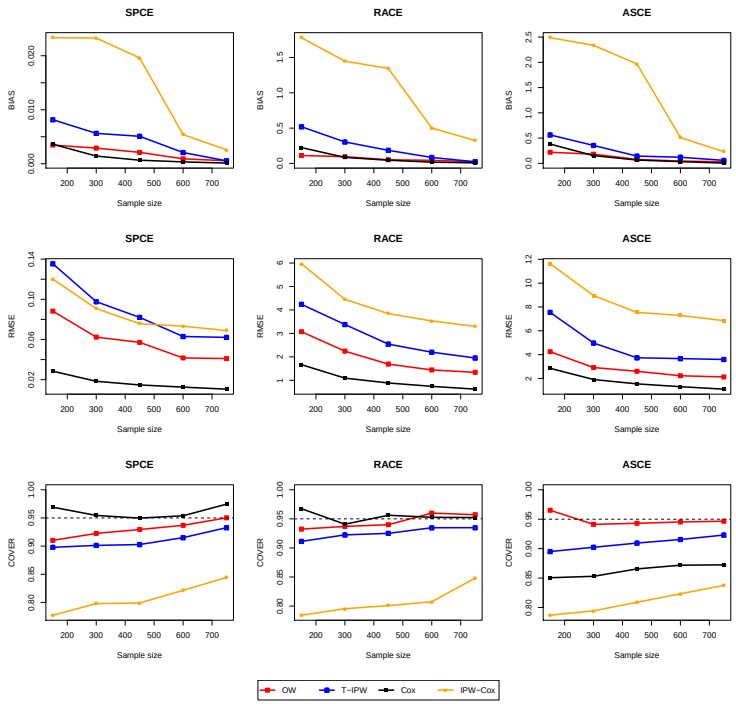

Figure 8.5: Absolute bias, root mean squared error (RMSE) and coverage for comparing treatment $j = 2$ versus $j = 3$ under poor overlap, when survival outcomes are generated from model A and censoring is completely independent. Additional comparison with T-IPW.

with a larger bias, RMSE and lower coverage rate.

Comparison with augmented weighting estimator In Figure 8.7, we compare the proposed estimators with two augmented weighting estimators, AIPW and AOW, under a good or poor overlap respectively. The AOW achieves a lower bias and RMSE than the AIPW. Also, the AIPW brings much efficiency gain and reduces the bias drastically compared to the IPW estimator. The improvement of augmenting IPW estimator with an outcome model is more pronounced under a poor overlap. On the other hand, the difference between AOW and OW is almost indistinguishable under a good or poor overlap.

Comparison with the estimators in Mao et al. (2018) Figure 8.8 compares with the estimator proposed in Mao et al. (2018) in the simulations. OW-MAO exhibits a lower bias and RMSE in both cases with good or poor overlap except for the estimation on ASCE. The IPW-MAO estimator has a smaller bias and RMSE than the IPW estimator yet not comparable to the OW estimator in all cases. However, the coverage of both estimators, especially the IPW-MAO, is lower than the nominal level. The under-coverage is severe when we have a poor overlap or the target estimand is the ASCE.

Simulation results with non-zero treatment effect Figure 8.9 draws the comparison among estimators when the true treatment effect is not zero ($j = 1, j' = 2$). For a fair comparison, we scale the bias and RMSE by the absolute value of the true estimand $\tau_{1,2}(t)^{k,h}$ for different choices of h. The pattern under good or poor overlap is similar to the one with zero treatment effect. The OW has a lower RMSE and bias in most cases except when comparing with the Cox estimator if targeting at SPCE. Additionally, we find that the coverage rate of the Cox and IPW-Cox estimator using the bootstrap method is extremely low for ASCE, which is similar to our findings under zero treatment effect. In Table 8.5, we report the performance of different estimators under conditionally independent censoring or when the proportional hazards assumption is violated. The pattern is similar to Table 1 in the main text with OW performs the best under dependent censoring or with the violation of proportional hazards assumption.

Results with for simulated RCT In Figure 8.10, we show the results in the simulated RCT. The bias and RMSE of different estimators becomes similar except that the Cox achieves the smallest RMSE among all estimators considered. More importantly, we can see that the weighting estimators using IPW and OW show a similar bias yet a lower RMSE compared to the PO-UNADJ. This demonstrates the efficiency gain from covariates adjustment through weighting in RCT, which

Table 8.5: Absolute bias, root mean squared error (RMSE) and coverage for comparing treatment $j = 1$ versus $j' = 2$ under different degrees of overlap. In the "proportional hazards" scenario, the survival outcomes are generated from a Cox model (model A), and in the "non-proportional hazards" scenario, the survival outcomes are generated from an accelerated failure time model (model B). The sample size is fixed at $N = 300$.

	Degree of	RMSE				Absolute bias				95% Coverage			
	overlap	OW	IPW	Cox	Cox-IPW	OW	IPW	Cox	MSM	OW	IPW	Cox	Cox-IPW
Model A, completely random censoring													
SPCE	Good	0.002	0.004	0.001	0.005	0.054	0.054	0.013	0.030	0.948	0.951	0.947	0.930
	Poor	0.004	0.081	0.003	0.078	0.083	0.176	0.048	0.145	0.913	0.790	0.939	0.561
RACE	Good	0.026	0.090	0.037	0.132	1.383	1.500	0.697	1.417	0.945	0.956	0.964	0.968
	Poor	0.071	3.645	0.140	4.049	1.953	6.681	2.762	7.213	0.933	0.798	0.919	0.599
ASCE	Good	0.530	1.339	7.309	2.146	4.982	4.775	3.887	4.413	0.942	0.923	0.061	0.886
	Poor	2.432	3.353	21.485	3.726	9.413	12.230	12.852	12.540	0.888	0.847	0.012	0.674
Model B, completely random censoring													
SPCE	Good	0.001	0.001	0.003	0.017	0.071	0.077	0.046	0.094	0.955	0.943	0.752	0.837
	Poor	0.004	0.055	0.021	0.130	0.086	0.201	0.198	0.250	0.942	0.862	0.733	0.650
RACE	Good	0.073	0.065	0.148	0.501	2.234	2.844	2.496	4.441	0.956	0.939	0.755	0.842
	Poor	0.112	3.800	1.883	5.573	2.948	8.242	10.762	11.610	0.940	0.837	0.735	0.687
ASCE	Good	1.643	3.743	5.538	3.293	5.838	7.934	7.245	12.613	0.935	0.931	0.539	0.820
	Poor	3.549	5.817	19.251	8.771	8.595	13.510	26.296	19.850	0.860	0.850	0.475	0.626
Model A, conditionally independent censoring													
SPCE	Good	0.001	0.003	0.000	0.036	0.045	0.045	0.049	0.060	0.950	0.947	0.886	0.934
	Poor	0.005	0.056	0.006	0.144	0.069	0.157	0.060	0.194	0.955	0.790	0.908	0.533
RACE	Good	0.014	0.074	0.197	0.999	1.895	2.410	2.715	2.206	0.953	0.952	0.912	0.951
	Poor	0.204	3.339	0.300	6.250	2.505	7.396	3.407	8.536	0.956	0.848	0.887	0.562
ASCE	Good	0.402	0.412	20.575	11.066	9.203	10.636	12.305	21.736	0.950	0.942	0.701	0.956
	Poor	0.989	9.342	21.787	26.463	16.998	22.016	12.859	48.089	0.951	0.790	0.636	0.596
Model B, conditionally independent censoring													
SPCE	Good	0.018	0.029	0.000	0.006	0.062	0.070	0.053	0.078	0.830	0.842	0.722	0.869
	Poor	0.028	0.046	0.018	0.036	0.084	0.074	0.241	0.161	0.685	0.429	0.712	0.833
RACE	Good	0.287	1.337	0.072	0.075	4.707	5.168	2.805	5.512	0.944	0.940	0.731	0.858
	Poor	1.129	4.045	0.585	3.511	6.286	7.240	11.919	10.292	0.924	0.756	0.707	0.805
ASCE	Good	3.743	6.095	6.892	6.848	9.481	11.344	8.277	14.402	0.798	0.769	0.534	0.733
	Poor	6.111	15.916	19.178	12.482	12.905	13.447	27.745	15.250	0.753	0.387	0.522	0.532

generalizes the findings in Zeng et al. (2020d) to the censoring outcomes setting. Moreover, all estimators include the simple PO-UNADJ achieve the coverage rates close to the nominal level.

8.2.4 Additional information of the application

Table 8.6 reports the summary statistics of covariates in the application on prostate cancer (Section 6) and demonstrates that the balance is improved after weighting. The $\text{MPASD}^{\text{IPW}}$ and MPASD^{OW} is smaller than the unadjusted difference $\text{MPASD}^{\text{UNADJ}}$. Please refer to Ennis et al. (2018) for the details of the variable used. Figure 8.11 illustrates the estimated generalized propensity scores, which indicates a good overlap.

Table 8.6: Descriptive statistics of baseline covariates in the comparative effectiveness study on prostate cancer described in Section 5 and maximized pairwise absolute standardized difference (MPASD) of each covariate across three arms before and after weighting.

	Overall	RP	EBRT+AD	EBRT+brachy±AD	$\text{MPASD}^{\text{UNADJ}}$	$\text{MPASD}^{\text{IPW}}$	MPASD^{OW}
No (%)	44551(100)	26474 (59.42)	15435 (34.65)	2642(5.93)			
Continuous covariates, mean and standard deviation (in parenthesis).							
Age	65.32 (8.19)	62.61 (7.02)	69.66 (8.19)	67.15 (7.72)	0.919	0.105	0.096
PSA	201.89 (223.42)	189.20 (214.84)	225.77 (238.08)	189.577 (207.46)	0.166	0.055	0.029
Categorial covariates, number of units in each class.							
Race							
Black	7127	3632	3000	495	0.151	0.032	0.036
Other	1524	903	522	99	0.020	0.012	0.004
Spanish or Hispanic	1963	1135	703	125	0.021	0.020	0.013
Insure type ($)							
Not insured	986	555	402	29	0.110	0.004	0.009
Private insurance	19522	14608	3925	989	0.629	0.014	0.015
Medicaid	1284	598	612	74	0.100	0.030	0.033
Medicare	1026	436	553	37	0.149	0.013	0.006
Government	482	235	211	36	0.044	0.020	0.006
Income level ($)							
<30000	5533	2954	2234	345	0.099	0.034	0.018
30000-34999	7628	4330	2858	440	0.057	0.024	0.013
35000-45999	12436	7317	4458	661	0.087	0.003	0.009
Education level >29	6776	3719	2651	406	0.086	0.024	0.021
20-28.9	9707	5461	3690	556	0.079	0.005	0.004
14-19.9	10706	6299	3806	601	0.045	0.014	0.005
Charlson Comorbidity Index							
1	7008	4575	2101	332	0.134	0.002	0.011
≥ 2	1211	631	517	63	0.060	0.003	0.003
Gleason score							
≤ 6	3493	2769	553	171	0.274	0.030	0.007
7	9347	5964	2837	546	0.103	0.023	0.016
9	11781	6130	4968	683	0.204	0.012	0.007
10	932	348	532	52	0.144	0.008	0.004
Clinical T stage							
$\leq$ cT3	5723	2785	2529	409	0.169	0.008	0.025
Year of diagnosis							
2004-2007	330	127	167	36	0.090	0.012	0.013
2008-2010	11582	6665	4082	835	0.144	0.009	0.005

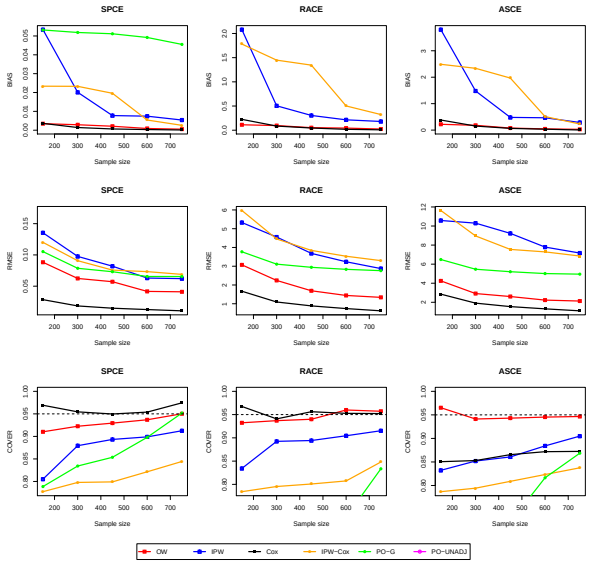

(a) Comparison under good overlap

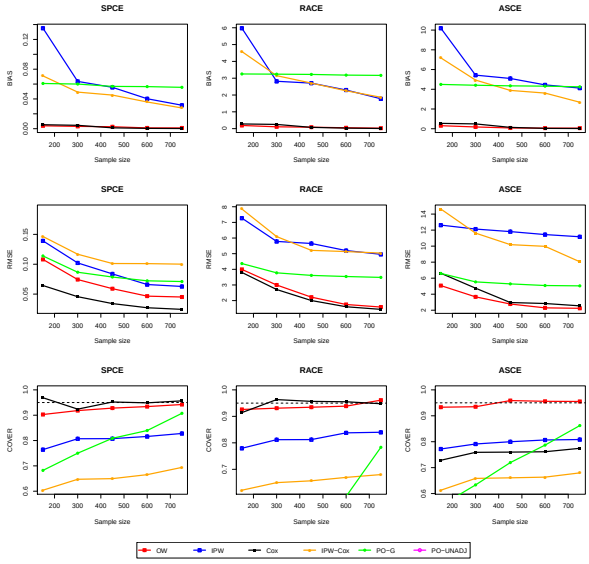

(b) Comparison under poor overlap

Figure 8.6: Absolute bias, root mean squared error (RMSE) and coverage for comparing treatment $j = 2$ versus $j = 3$, when survival outcomes are generated from model A and censoring is completely independent. Additional comparison with PO-G and PO-UNADJ.

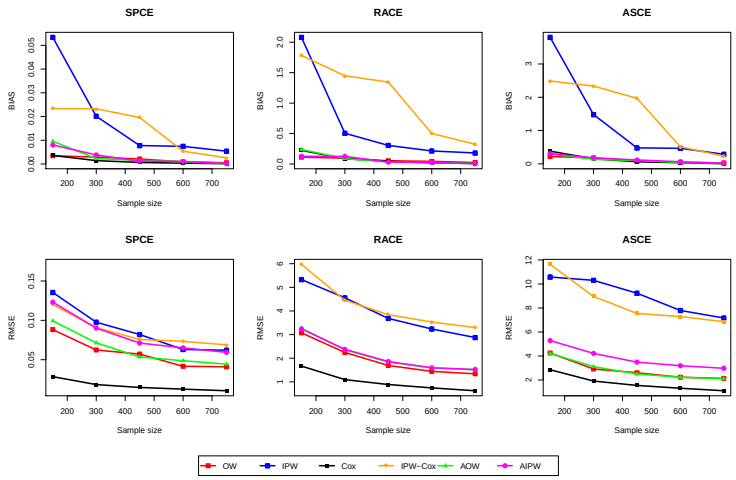

(a) Comparison under good overlap

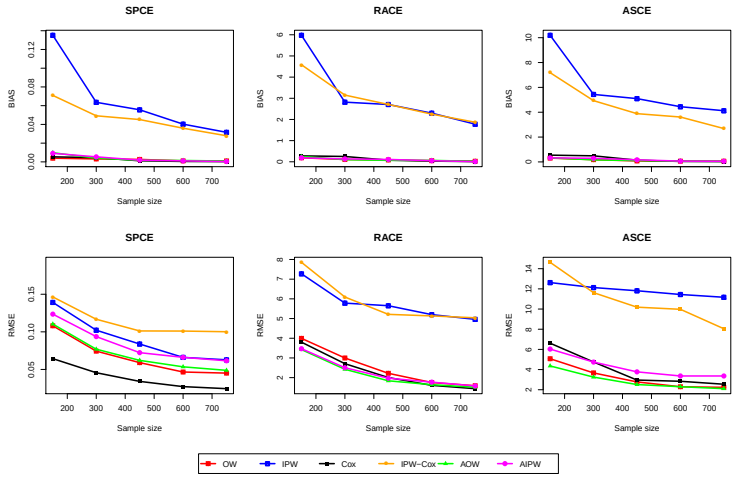

(b) Comparison under poor overlap

Figure 8.7: Absolute bias, root mean squared error (RMSE) and coverage for comparing treatment $j = 2$ versus $j = 3$, when survival outcomes are generated from model A and censoring is completely independent. Additional comparison with augmented weighting estimators.

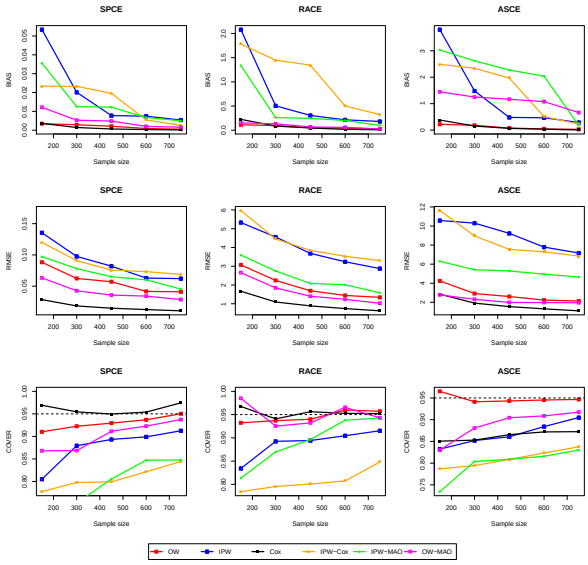

(a) Comparison under good overlap

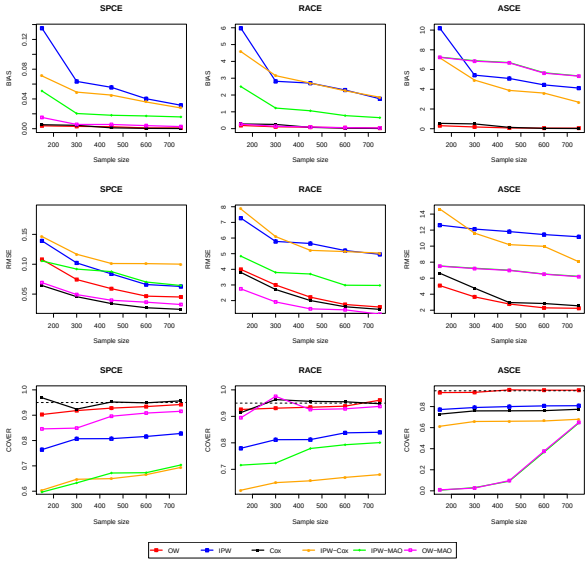

(b) Comparison under poor overlap

Figure 8.8: Absolute bias, root mean squared error (RMSE) and coverage for comparing treatment $j = 2$ versus $j = 3$, when survival outcomes are generated from model A and censoring is completely independent. Additional comparison with IPW-MAO,OW-MAO.

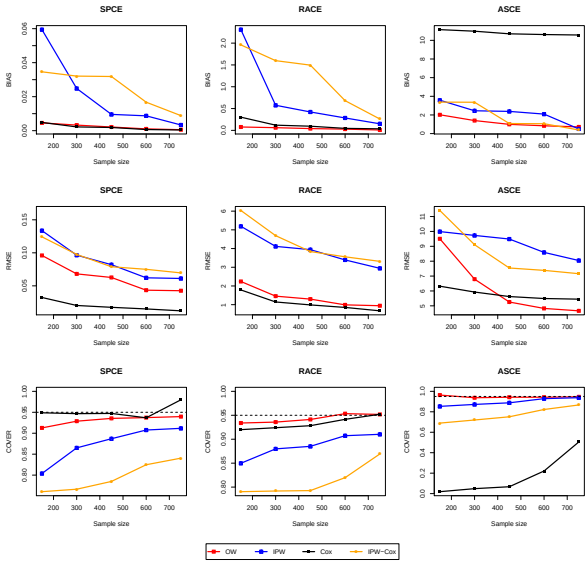

(a) Comparison under good overlap

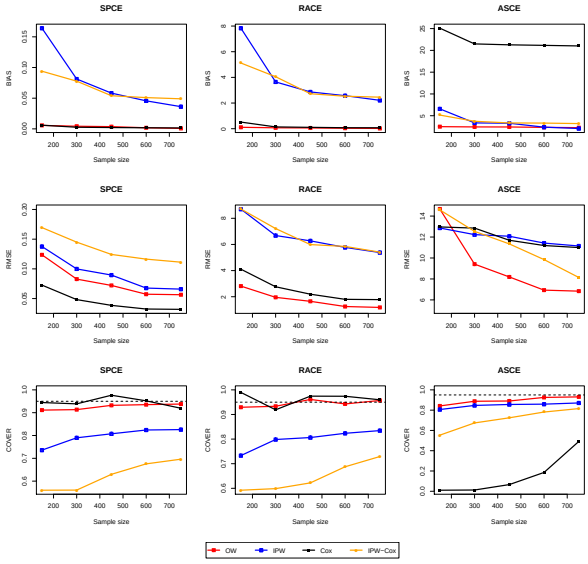

(b) Comparison under poor overlap

Figure 8.9: Absolute bias, root mean squared error (RMSE) and coverage for comparing treatment $j = 1$ versus $j = 2$, when survival outcomes are generated from model A and censoring is completely independent.

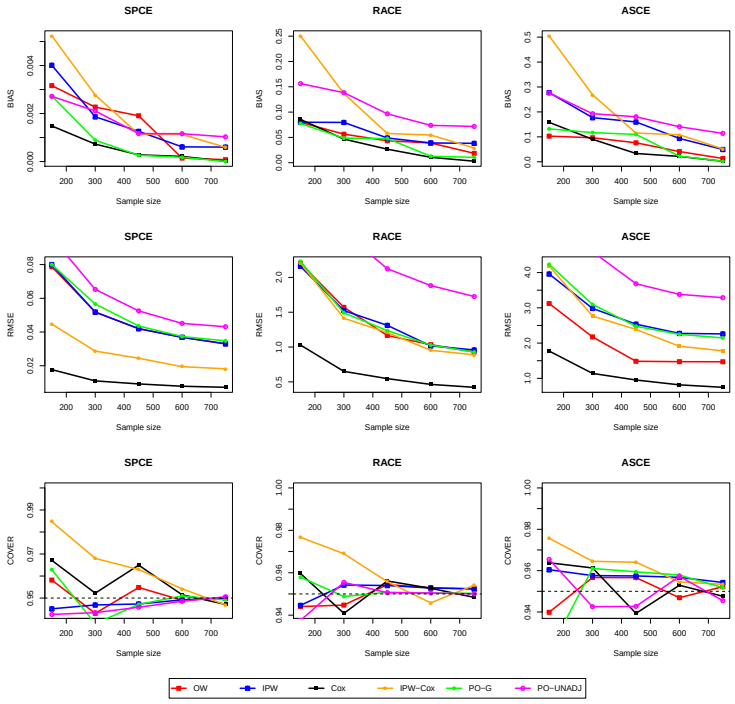

Figure 8.10: Absolute bias, root mean squared error (RMSE) and coverage for comparing treatment $j = 2$ versus $j = 3$ in simulate RCT, when survival outcomes are generated from model A and censoring is completely independent. Additional comparison with PO-G and PO-UNADJ.

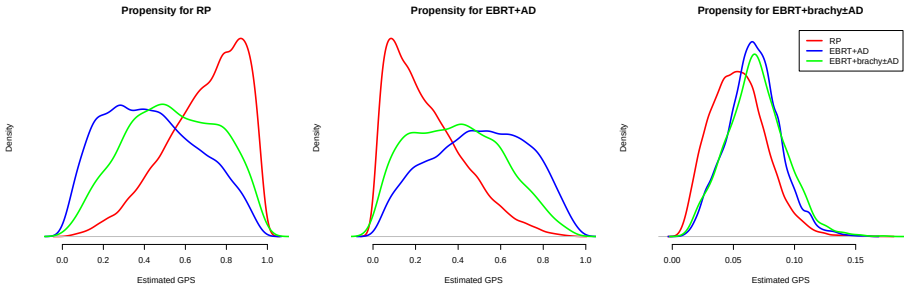

Figure 8.11: Marginal distributions of the estimated generalized propensity scores for three arms from a multinomial logistic regression in the prostate cancer application.

8.3 Appendix for Chapter 4

8.3.1 Proof of Theorem 3

We provide the mathematical proof for Theorem 3. For the first part of Theorem 3, identification of total effect, for any $z \in \{0,1\}$ we have

$$E(Y_i^t|Z_i = z, \mathbf{X}_i^t) = E(Y_i^t(z, \mathbf{M}_i(z))|Z_i = z, \mathbf{X}_i^t) = E(Y_i^t(z, \mathbf{M}_i(z))|\mathbf{X}_i^t).$$

The second equality follows from Assumption 1. Therefore, we prove the identification of τ_{TE}^t,

$$\begin{aligned}\tau_{\text{TE}}^t &= \int_{\mathcal{X}} \{E(Y_i^t(1, \mathbf{M}_i(1))|\mathbf{X}_i^t) - E(Y_i^t(0, \mathbf{M}_i(0))|\mathbf{X}_i^t)\} \mathrm{dF}_{\mathbf{X}_i^t}(\mathbf{x}^t), \\ &= \int_{\mathcal{X}} \{E(Y_i^t|Z_i = 1, \mathbf{X}_i^t = \mathbf{x}^t) - E(Y_i^t|Z_i = 0, \mathbf{X}_i^t = \mathbf{x}^t)\} \mathrm{dF}_{\mathbf{X}_i^t}(\mathbf{x}^t),\end{aligned}$$

For the second part, identification of τ_{ACME}^t, we make the following regularity assumptions. Suppose the potential outcomes $Y_i^t(z, \mathbf{m})$ as a function of $\mathbf{m}$ is Lipschitz continuous on $[0, T]$ with probability one. There exists $A < \infty$, $|Y_i^t(z, \mathbf{m}) - Y_i^t(z, \mathbf{m}')| \leq A||\mathbf{m} - \mathbf{m}'||_2$, for any $z, t, \mathbf{m}, \mathbf{m}'$ almost surely.

For any $z, z' \in \{0,1\}$, we have

$$\begin{aligned}&\int_{\mathcal{X}} \int_{R^{[0,t]}} E(Y_i^t|Z_i = z, \mathbf{X}_i^t = \mathbf{x}^t, \mathbf{M}_i^t = \mathbf{m}) \mathrm{dF}_{\mathbf{X}_i^t}(\mathbf{x}^t) \times \mathrm{d}\{\mathrm{F}_{\mathbf{M}_i^t|Z_i=z', \mathbf{X}_i^t=\mathbf{x}^t}(\mathbf{m})\} \\ &= \int_{\mathcal{X}} \int_{R^{[0,t]}} E(Y_i^t(z, \mathbf{m})|Z_i = z, \mathbf{X}_i^t = \mathbf{x}^t, \mathbf{M}_i^t = \mathbf{m}) \times \mathrm{d}\{\mathrm{F}_{\mathbf{M}_i^t|Z_i=z', \mathbf{X}_i^t=\mathbf{x}^t}(\mathbf{m})\}.\end{aligned}$$

For any path $\mathbf{m}$ on the time span $[0, t]$, we make a finite partition into H pieces at points $\mathcal{M}_H = \{t_0 = 0, t_1 = t/H, t_2 = 2t/H, \cdots, t_H = t\}$. Now we consider using a step function with jumps at points $\mathcal{M}_H$. Denote the step function as $\mathbf{m}_H$, which is:

$$\mathbf{m}_H(x) = \begin{cases} \mathbf{m}(0) = m_0 & 0 \leq x < t/H, \\ \mathbf{m}(t/H) = m_1 & t/H \leq x < 2t/H, \\ \cdots & \\ \mathbf{m}((H-1)t/H) = m_H & (H-1)t/H \leq x \leq t. \end{cases}$$

We wish to use this step function $\mathbf{m}_H(x)$ to approximate function $\mathbf{m}$. First, given $\mathbf{m}$ is Lipschitz continuous, there exists $B > 0$ such that $|m(x_1) - m(x_2)| \leq B|x_1 - x_2|$.

Therefore, the step functions $\mathbf{m}_H$ approximates the original function $\mathbf{m}$ well in the sense that,

$$||\mathbf{m}_H - \mathbf{m}||_2 \leq \sum_{i=1}^{H} \frac{t}{H} B^2 \frac{t^2}{H^2} \asymp O(H^{-2}).$$

As such we can approximate the expectation over a continuous process with expectation on a vector with values on the jumps, $(m_0, m_1, \cdots, m_H)$. That is,

$$\begin{aligned}\int_{\mathcal{X}} \int_{R^{[0,t]}} & E(Y_i^t(z, \mathbf{m}) | Z_i = z, \mathbf{X}_i^t = \mathbf{x}^t, \mathbf{M}_i^t = \mathbf{m}) \times \mathrm{d}\{\mathrm{F}_{\mathbf{M}_i^t | Z_i = z', \mathbf{X}_i^t = \mathbf{x}^t}(\mathbf{m})\} \\ & \asymp \int_{\mathcal{X}} \int_{R^{[0,t]}} E(Y_i^t(z, \mathbf{m}_H) | Z_i = z, \mathbf{X}_i^t = \mathbf{x}^t, \mathbf{M}_i^t = \mathbf{m}_H) \\ & \times \mathrm{d}\{\mathrm{F}_{\mathbf{M}_i^t | Z_i = z', \mathbf{X}_i^t = \mathbf{x}^t}(\mathbf{m}_H)\} + O(H^{-2}).\end{aligned}$$

This equivalence follows from the regularity condition that the potential outcome $Y_i^t(z, \mathbf{m})$ as a function of $\mathbf{m}$ is continuous with the L_2 metrics of $\mathbf{m}$. As the values of steps function $\mathbf{m}_H$ are completely determined by the values on finite jumps, we can further reduce to,

$$\begin{aligned}\asymp & \int_{\mathcal{X}} \int_{R^H} E(Y_i^t(z, \mathbf{m}_H) | Z_i = z, \mathbf{X}_i^t = \mathbf{x}^t, m_0, m_1, m_2, \cdots m_H) \\ & \times \mathrm{d}\{\mathrm{F}_{m_0, m_1, \cdots, m_H | Z_i = z', \mathbf{X}_i^t = \mathbf{x}^t}(m_0, m_1, m_2, \cdots m_H)\} + O(H^{-2}).\end{aligned}$$

With Assumption 1, we can show that

$$\begin{aligned}& \mathrm{d}\{\mathrm{F}_{m_0, m_1, \cdots, m_H | Z_i = z', \mathbf{X}_i^t = \mathbf{x}^t}(m_0, m_1, m_2, \cdots m_H)\} \\ & = \mathrm{d}\{\mathrm{F}_{m_0(z'), m_1(z'), \cdots, m_H(z') | \mathbf{X}_i^t = \mathbf{x}^t}(m_0, m_1, m_2, \cdots m_H)\}, \\ & = \mathrm{d}\{\mathrm{F}_{\mathbf{m}_H(z') | \mathbf{X}_i^t = \mathbf{x}^t}(\mathbf{m}_H)\}.\end{aligned}$$

With a slightly abuse of notations, we use $\mathbf{m}_H(z)$ to denote the potential process induced by the original potential process $\mathbf{M}_i^t(z)$ and $m_i(z)$ to denote potential values of $\mathbf{M}_i^t(z)$ evaluated at point $x_i = it/H$. Also, with the Assumption 2, we can choose a large H such that $t/H \leq \varepsilon$. Then we have the following conditional independence

conditions,

$$
\begin{aligned}
Y_i^0(z, \mathbf{m}_H) &\perp\!\!\!\perp m_0 | Z_i, \mathbf{X}_i^t, \\
\{Y_i^{t/H}(z, \mathbf{m}_H) - Y_i^0(z, \mathbf{m}_H)\} &\perp\!\!\!\perp (m_1 - m_0) | Z_i, \mathbf{X}_i^t, \mathbf{m}_H^0, \\
\{Y_i^{2t/H}(z, \mathbf{m}_H) - Y_i^{t/H}(z, \mathbf{m}_H)\} &\perp\!\!\!\perp (m_2 - m_1) | Z_i, \mathbf{X}_i^t, \mathbf{m}_H^{t/H}, \\
&\cdots \\
\{Y_i^{t}(z, \mathbf{m}_H) - Y_i^{t(H-1)/H}(z, \mathbf{m}_H)\} &\perp\!\!\!\perp (m_H - m_{H-1}) | Z_i, \mathbf{X}_i^t, \mathbf{m}_H^{t(H-1)/H},
\end{aligned}
$$

where are equivalent to,

$$
\begin{aligned}
Y_i^0(z, \mathbf{m}_H) &\perp\!\!\!\perp m_0 | Z_i, \mathbf{X}_i^t, \\
\{Y_i^{t/H}(z, \mathbf{m}_H) - Y_i^0(z, \mathbf{m}_H)\} &\perp\!\!\!\perp (m_1 - m_0) | Z_i, \mathbf{X}_i^t, m_0, \\
\{Y_i^{2t/H}(z, \mathbf{m}_H) - Y_i^{t/H}(z, \mathbf{m}_H)\} &\perp\!\!\!\perp (m_2 - m_1) | Z_i, \mathbf{X}_i^t, m_0, m_1, \\
&\cdots \\
\{Y_i^{t}(z, \mathbf{m}_H) - Y_i^{t(H-1)/H}(z, \mathbf{m}_H)\} &\perp\!\!\!\perp (m_H - m_{H-1}) | Z_i, \mathbf{X}_i^t, m_0, m_1 \cdots, m_{H-1},
\end{aligned}
$$

as the step function $m_H^{it/H}$ is completely determined by values $m_0, \cdots, m_i$. With the above conditional independence, we have,

$$
\begin{aligned}
&E(Y_i^t(z, \mathbf{m}_H) | Z_i = z, \mathbf{X}_i^t = \mathbf{x}^t, m_0, m_1, m_2, \cdots m_H) \\
&\qquad = E(Y_i^t(z, \mathbf{m}_H) | Z_i = z, \mathbf{X}_i^t = \mathbf{x}^t).
\end{aligned}
$$

With similar arguments, it also equals:

$$
\begin{aligned}
&E(Y_i^t(z, \mathbf{m}_H) | Z_i = z, \mathbf{X}_i^t = \mathbf{x}^t) = E(Y_i^t(z, \mathbf{m}_H) | Z_i = z', \mathbf{X}_i^t = \mathbf{x}^t), \\
&= E(Y_i^t(z, \mathbf{m}_H) | Z_i = z, \mathbf{X}_i^t = \mathbf{x}^t, m_0 = m_0(z'), \cdots m_H = m_H(z')), \\
&= E(Y_i^t(z, \mathbf{m}_H) | Z_i = z, \mathbf{X}_i^t = \mathbf{x}^t, \mathbf{m}_H(z') = \mathbf{m}_H), \\
&= E(Y_i^t(z, \mathbf{m}_H) | \mathbf{X}_i^t = \mathbf{x}^t, \mathbf{m}_H(z') = \mathbf{m}_H).
\end{aligned}
$$

As a conclusion, we have shown that,

$$\begin{aligned}
&\int_{\mathcal{X}}\int_{R^{[0,t]}} E(Y_i^t(z,\mathbf{m})|Z_i=z,\mathbf{X}_i^t=\mathbf{x}^t,\mathbf{M}_i^t=\mathbf{m})\times \mathrm{d}\{\mathrm{F}_{\mathbf{M}_i^t|Z_i=z',\mathbf{X}_i^t=\mathbf{x}^t}(\mathbf{m})\},\\
&\asymp \int_{\mathcal{X}}\int_{R^{[0,t]}} E(Y_i^t(z,\mathbf{m}_H)|\mathbf{X}_i^t=\mathbf{x}^t,\mathbf{m}_H(z')=\mathbf{m}_H)\times \mathrm{d}\{\mathrm{F}_{\mathbf{m}_H(z')|\mathbf{X}_i^t=\mathbf{x}^t}(\mathbf{m}_H)\}+O(H^{-2}),\\
&\asymp \int_{\mathcal{X}} E(Y_i^t(z,\mathbf{m}_H(z'))|\mathbf{X}_i^t=\mathbf{x}^t)+O(H^{-2}),\asymp \int_{\mathcal{X}} E(Y_i^t(z,\mathbf{m}(z'))|\mathbf{X}_i^t=\mathbf{x}^t)+O(H^{-2}).
\end{aligned}$$

The last equivalence comes from the regularity condition of $Y_i^t(z,\mathbf{m}(z'))$ as a function of $\mathbf{m}(z')$. Let H goes to infinity, we have,

$$\begin{aligned}
\int_{\mathcal{X}}\int_{R^{[0,t]}} E(Y_i^t|Z_i=z,\mathbf{X}_i^t=\mathbf{x}^t,\mathbf{M}_i^t=\mathbf{m})\mathrm{dF}_{\mathbf{X}_i^t}(\mathbf{x}^t)\times \mathrm{d}\{\mathrm{F}_{\mathbf{M}_i^t|Z_i=z',\mathbf{X}_i^t=\mathbf{x}^t}(\mathbf{m})\}&\\
=\int_{\mathcal{X}} E(Y_i^t(z,\mathbf{m}(z'))|\mathbf{X}_i^t=\mathbf{x}^t)\mathrm{dF}_{\mathbf{X}_i^t}(\mathbf{x}^t).&
\end{aligned}$$

With this relationship established, it is straightforward to show that,

$$\begin{aligned}
\tau^t_{\mathrm{ACME}}(z)&=\int_{\mathcal{X}}\{E(Y_i^t(z,\mathbf{m}(1))|\mathbf{X}_i^t=\mathbf{x}^t)-E(Y_i^t(z,\mathbf{m}(0))|\mathbf{X}_i^t=\mathbf{x}^t)\}\mathrm{dF}_{\mathbf{X}_i^t}(\mathbf{x}^t),\\
&=\int_{\mathcal{X}}\int_{R^{[0,t]}} E(Y_i^t|Z_i=z,\mathbf{X}_i^t=\mathbf{x}^t,\mathbf{M}_i^t=\mathbf{m})\mathrm{dF}_{\mathbf{X}_i^t}(\mathbf{x}^t)\times\\
&\qquad \mathrm{d}\{\mathrm{F}_{\mathbf{M}_i^t|Z_i=1,\mathbf{X}_i^t=\mathbf{x}^t}(\mathbf{m})-\mathrm{F}_{\mathbf{M}_i^t|Z_i=0,\mathbf{X}_i^t=\mathbf{x}^t}(\mathbf{m})\},
\end{aligned}$$

which completes the proof of Theorem 3.

8.3.2 Gibbs sampler

In this section, we provide detailed descriptions on the Gibbs sampler for the model in Section 4.4. We only include the sampler for mediator process as the sampling procedure is essentially identical for the outcome process. For simplicity, we introduce some notations to represent vector values, $M_i = (M_{i1}, M_{i2}, \cdots, M_{in_i}) \in \mathcal{R}^{T_i}$,$X_i = [X_{i1}, X_{i2}, \cdots, X_{in_i}]' \in \mathcal{R}^{T_i \times p}$, $\psi_r(\mathbf{t}_i) = [\psi_r(t_{i1}), \cdots, \psi_r(t_{in_i})] \in \mathcal{R}^{T_i}$

1. **Sample the eigen function** $\psi_r(t), r = 1, 2 \cdots, R$**.**

   - (a)$\mathbf{p}_r| \cdots \sim N(Q_{\psi_r}^{-1} l_{\psi_r}, Q_{\psi_r}^{-1})$ conditional on $C_r \psi_r = 0$,

   $$\begin{aligned} C_r &= [\psi_1, \psi_2, \cdots, \psi_{r-1}, \psi_{r+1}, \cdots, \psi_R]' B_G \\ &= [\mathbf{p}_1, \cdots, \mathbf{p}_{r-1}, \mathbf{p}_{r+1}, \cdots, \mathbf{p}_R] B_G' B_G, \end{aligned}$$

   where B_G is the basis functions evaluated at a equal spaced grids on [0,1],$\{t_1, t_2, \cdots, t_G\}$, $G = 50$ for example, $B_G = [\mathbf{b}(t_1), \cdots, \mathbf{b}(t_G)]' \in R^{G \times (L+2)}$. The corresponding mean and covariance functions are,

   $$\begin{aligned} Q_{\psi_r} &= \frac{\sum_{i=1}^N B_i' B_i \zeta_{r,i}^2}{\sigma_m^2} + h_k \Omega, \\ l_{\psi_r} &= \frac{\sum_{i=1}^N B_i' \zeta_{i,r} (M_i - X_i \beta_M^T - \sum_{r' \neq r}^R \psi_r(\mathbf{t_i}) \zeta_{r',i})}{\sigma_m^2}. \end{aligned}$$

   Update the $\mathbf{p}_r \leftarrow \mathbf{p}_r / \sqrt{\mathbf{p}_r' B_G' B_G \mathbf{p}_r} = \mathbf{p}_r / ||\psi_r(t)||_2$ to ensure $||\psi_r(t)||_2 = 1$ and $\psi_r(t) = \mathbf{b}(t)\psi_r$ and update $\zeta_{r,i} =\rightarrow \zeta_{r,i} * ||\psi_r(t)||_2$ to maintain likelihood function.

   - (b)$h_k| \cdots \sim \text{Ga}((L+1)/2, \psi_r' \Omega \psi_r)$ truncated on $[\lambda_r^2, 10^4]$.

2. **Sample the principal score** $\zeta_{r,i}.\zeta_{r,i}| \cdots \sim N(\mu_r/\lambda_r^2, \lambda_r^2)$

   $$\begin{aligned} \sigma_r^2 &= (||\psi_r(\mathbf{t}_i)||_2^2 / \sigma_m^2 + \xi_{i,r} / \lambda_r^2)^{-1}, \\ \mu_r &= \frac{(M_i - X_i \beta_M^T - (\sum_{r' \neq r} \psi_{r'}(\mathbf{t}_i) \zeta_{r',i}))' \psi_r(\mathbf{t_i})}{\sigma_\varepsilon^2} + \frac{(\tau_{0,r}(1 - Z_i) + \tau_{1,r} Z_i) \xi_{i,r}}{\lambda_r^2}. \end{aligned}$$

3. **Sample the causal parameters** χ_0^r, χ_1^r. Let $\chi_z = (\chi_z^r, \cdots, \chi_z^R), z = 0, 1, \chi_z^r|\cdots \sim N(Q_{z,r}^{-1} l_{z,r}, Q_{z,r}^{-1})$.

$$Q_{z,r} = (\sum_{i=1}^{N} \xi_{r,i} \mathbf{1}_{Z_i=z}/\lambda_r^2 + 1/\sigma_{\chi_r}^2)^{-1},$$
$$l_{z,r} = \sum_{i=1}^{N} \zeta_{r,i} \xi_{r,i} \mathbf{1}_{Z_i=z}/\lambda_r^2.$$

4. **Sample the coefficients** β_M. The coefficients for covariates are $\beta_M|\cdots \sim N(Q_\beta^{-1}\mu_\beta, Q_\beta^{-1})$,

$$Q_\beta = X'X/\sigma_m^2 + 100^2 I_{\dim(X)},$$
$$\mu_\beta = \sum_{i=1}^{N} X_i'(M_i - \sum_{r=1}^{R} \psi_r(\mathbf{t_i})\zeta_{i,r})/\sigma_m^2.$$

5. **Sample the precision/variance parameters**.

- (a) $\sigma_m^{-2}|\cdots \sim \text{Ga}(\sum_{i=1}^{N} T_i/2, \sum_{i=1}^{N} ||M_i - X_i\beta_M' - \sum_{r=1}^{R} \psi_r(\mathbf{t_i})\zeta_{i,r}||_2^2/2)$
- (b) $\sigma_{\chi_r}^2|\cdots$,

$$\delta_{\chi_1}|\cdots \sim \text{Ga}(a_{\chi_1} + R, 1 + \frac{1}{2}\sum_{r=1}^{R} \chi_1^{(r)}(\chi_0^{r2} + \chi_1^{r2})), \chi_l^{(r)} = \prod_{i=l+1}^{r} \delta_{\chi_i}$$
$$\delta_{\chi_r}|\cdots \sim \text{Ga}(a_{\chi_2} + R + 1 - r, 1 + \frac{1}{2}\sum_{r'=r}^{R} \chi_{r'}^{(r)}(\tau_0^{r'2} + \chi_1^{r'2})), r \geq 2,$$
$$\sigma_{\chi_r}^{-2} = \prod_{r'=1}^{r} \delta_{\chi_{r'}}.$$

- (c)$\lambda_r^2|\cdots$,

$$\delta_1|\cdots \sim \text{Ga}(a_1 + RN/2, 1 + \frac{1}{2}\sum_{r=1}^{R} \chi_1^{(r)'} \xi_{i,r}(\zeta_{i,r} - (1 - Z_i)\chi_0^r - Z_i\chi_1^r)^2,$$
$$\chi_l^{(r)'} = \prod_{i=l+1}^{r} \delta_i,$$

$$\delta_r|\cdots \mathrm{Ga}(a_2+(R-r+1)N/2,$$
$$1+\frac{1}{2}\sum_{r'=r}^{R}\chi_{r'}^{(r)'}\xi_{i,r'}(\zeta_{i,r'}-(1-Z_i)\chi_0^{r'}-Z_i\chi_1^{r'})^2), r\geq 2,$$
$$\lambda_r^{-2}=\prod_{r'=1}^{r}\delta_{r'}.$$

- (d) $\xi_{i,r}|\cdots \sim \mathrm{Ga}(\frac{v+1}{2}, \frac{1}{2}(v+(\zeta_{i,r'}-(1-Z_i)\chi_0^{r'}-Z_i\chi_1^{r'})^2/\lambda_r^2))$.
- (e) $a_1, a_2, a_{\chi_1}, a_{\chi_2}$ can be sampled with Metropolis-Hasting algorithm.

The sampling for the outcomes model Y_{ij} is similar to that for the mediator model except that we added the imputed value of the mediator process $M(t_{ij})$ as a covariate.

8.3.3 Individual imputed process

Figure 8.12 shows the posterior means of the imputed smooth processes of the mediators and the outcomes against their respective observed trajectories of eight randomly selected subjects in the sample. For social bonds (left panel of Figure 8.12), the imputed smooth process adequately captures the overall time trend of each subject while reduce the noise in the observations, evident in the subjects with code name HOK, DUI and LOC.

For the subjects with few observations or observations concentrating in a short time span, such as subject NEA, the imputed process matches the trend of the observations while extrapolating to the rest of the time span with little information. FPCA achieves this by borrowing information from other units when learning the principal component on the population level. Compared with social bonds, variation of the adult GC concentrations across the lifespan is much smaller. In the right panel in Figure 8.12, we can see the imputed processes for the GC concentrations are much flatter than those for social bonds. It appears that most variation in the GCs trajectories is due to noise rather than intrinsic developmental trend.

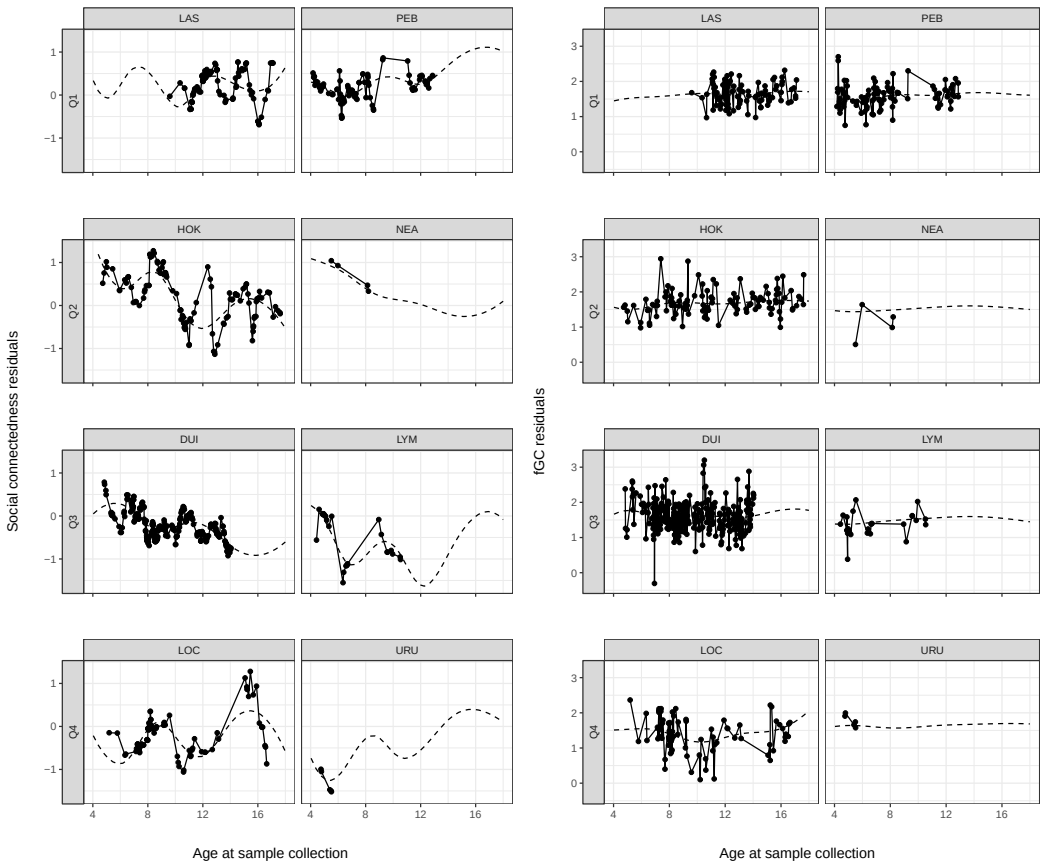

Figure 8.12: The imputed underlying smooth process against the observed trajectories for social bonds (left panel) and GC concentrations (right panel).

8.3.4 Simulation results for sample size $N = 500, 1000$

We provide the detailed simulation results on the performance of MFPCA when sample size N equals $300, 500$ here. In Figure 8.13, we draw the posterior mean and the 95% credible intervals for MFPCA of τ^t_{TE},τ^t_{ACME} across different levels of sparsity. The MFPCA produces the point estimations that are close to the true values and the credible intervals covering the true process. In Table 8.7, we compare the bias, RMSE and coverage rate of the proposed method with random effects and GEE approaches. Across different levels of sparsity, the MFPCA shows a lower bias and the RMSE compared with the other methods. Also, the coverage rate of the MFPCA for τ^t_{TE},τ^t_{ACME} becomes close to the nominal level 95% when the sample size N and

the observations per unit T is larger.

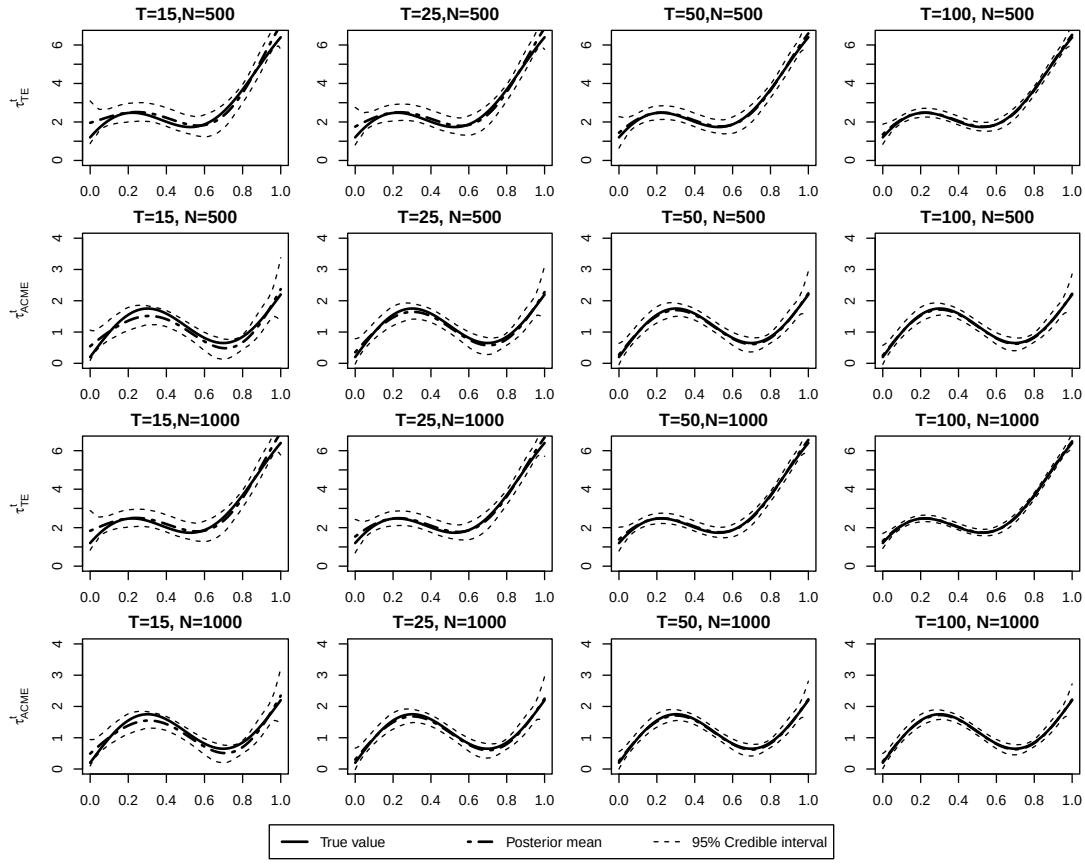

Figure 8.13: Posterior mean of τ^t_{TE},τ^t_{ACME} and 95% credible intervals in one simulated dataset under each level of sparsity. The top two rows are the ones when setting $N = 300$ and the bottom two rows are the case when $N = 500$. The solid lines are the true surfaces for τ^t_{TE} and τ^t_{ACME}

Table 8.7: Absolute bias, RMSE and coverage rate of the 95% confidence interval of MFPCA, the random effects model and the generalized estimating equation (GEE) model under different sparsity levels with $N = 500, 1000$.

	τ_{TE}			τ_{ACME}		
Method	Bias	RMSE	Coverage	Bias	RMSE	Coverage
			T=15, N=500			
MFPCA	0.079	0.109	91.4%	0.104	0.196	90.8%
Random effects	0.103	0.132	87.4%	0.424	0.967	84.2%
GEE	0.117	0.163	87.1%	0.531	1.421	79.5%
			T=25, N=500			
MFPCA	0.076	0.102	93.8%	0.096	0.189	92.0%
Random effects	0.092	0.118	91.5%	0.397	0.894	88.4%
GEE	0.095	0.134	90.7%	0.523	1.032	89.1%
			T=50, N=500			
MFPCA	0.061	0.095	94.3%	0.073	0.176	92.4%
Random effects	0.068	0.097	93.7%	0.078	0.170	92.8%
GEE	0.073	0.104	93.2%	0.089	0.323	92.5%
			T=100, N=500			
MFPCA	0.035	0.068	95.2%	0.046	0.123	94.8%
Random effects	0.033	0.061	95.1%	0.045	0.129	94.3%
GEE	0.035	0.067	94.5%	0.051	0.130	94.2%
			T=15, N=1000			
MFPCA	0.065	0.097	91.9%	0.097	0.164	91.3%
Random effects	0.085	0.123	90.7%	0.387	0.885	89.6%
GEE	0.093	0.145	90.4%	0.489	1.103	84.6%
			T=25, N=1000			
MFPCA	0.053	0.081	93.9%	0.088	0.185	93.1%
Random effects	0.058	0.097	93.0%	0.230	0.526	91.7%
GEE	0.068	0.115	92.4%	0.297	0.611	91.5%
			T=50, N=1000			
MFPCA	0.036	0.063	94.2%	0.054	0.221	93.6%
Random effects	0.035	0.068	94.2%	0.052	0.203	93.2%
GEE	0.040	0.073	93.9%	0.057	0.214	93.1%
			T=100, N=1000			
MFPCA	0.020	0.053	95.1%	0.023	0.087	94.8%
Random effects	0.023	0.050	94.8%	0.021	0.097	94.4%
GEE	0.021	0.054	94.6%	0.027	0.098	94.5%

8.4 Appendix for Chapter 5

8.4.1 Theorem proofs

In this section, we present the detailed proofs for the theoretical properties in Section 5.3.3 in the main text,

Lemma 1. *The optimal value of dual variable $\boldsymbol{\lambda}^{EB}$ converges to maximum likelihood estimator $\boldsymbol{\lambda}^{\star}$ in (5.7) in probability.*

Proof: The following proposition is based on a given representation, therefore we treat $\Phi(\cdot)$ as a fixed function. With Karush-Kuhn-Tucker (KKT) conditions, we derive the first order optimiality condition of (5.6):

$$\sum_{i=1}^{n}(1-T_i)e^{\sum_{j=1}^{m}\boldsymbol{\lambda}_m\Phi_j(X_i)}(\Phi_j(X_j)-\bar{\Phi}_j)=0$$
$$\sum_{i=1}^{n}T_ie^{-\sum_{j=1}^{m}\boldsymbol{\lambda}_m\Phi_j(X_i)}(\Phi_j(X_j)-\bar{\Phi}_j)=0,$$

for $j=1,2,\cdots,m$. We rewrite the above conditions as estimating equations, let $a_j(X,T,r,\boldsymbol{\lambda})=(1-T)e^{\sum_{j=1}^{m}\boldsymbol{\lambda}_j\Phi_j(X)}(\Phi_j(X)-r_j), b_j(X,T,m,\boldsymbol{\lambda})=Te^{\sum_{j=1}^{m}\boldsymbol{\lambda}_j\Phi_j(X)}(\Phi_j-r_j)$. Then (8.4.1) is the same as:

$$\sum_{i}^{n}a_j(X_i,T_i,r,\boldsymbol{\lambda})=0, j=1,2,\cdots,m$$
$$\sum_{i}^{n}b_j(X_i,T_i,r,\boldsymbol{\lambda})=0, j=1,2,\cdots,m.$$

We can verify that $r_j=E(\Phi_j(X))$ and $\boldsymbol{\lambda}^*$ is the solution to the population version of (8.4.1). First, set $r_j=E(\Phi_j(X))$ and taking the conditional expectation of a_j, b_j given X is:

$$E(a_j(X,T,\boldsymbol{\lambda},r)|X)=(1-e(X))e^{\sum_{j=1}^{m}\boldsymbol{\lambda}_j\Phi_j(X)}(\Phi_j(X)-E(\Phi_j(X)),$$
$$E(b_j(X,T,\boldsymbol{\lambda},r)|X)=e(X)e^{\sum_{j=1}^{m}-\boldsymbol{\lambda}_j\Phi_j(X)}(\Phi_j(X)-E(\Phi_j(X)).$$

Suppose we are fitting the propensity score model with the log likelihood in (13), let $\boldsymbol{\lambda}^* = (\boldsymbol{\lambda}_1^*, \cdots \boldsymbol{\lambda}_m^*)$ be the MLE solution in (8.2) and plug into the $e(X)$, we have:

$$E(a_j(X,T,\boldsymbol{\lambda},r)|X) = \frac{e^{\sum_{j=1}^m \boldsymbol{\lambda}_j \Phi_j(x)}}{e^{\sum_{j=1}^m \boldsymbol{\lambda}_j^* \Phi_j(X)}}(\Phi_j(X) - E(\Phi_j(X)),$$
$$E(b_j(X,T,\boldsymbol{\lambda},r)|X) = \frac{e^{\sum_{j=1}^m -\boldsymbol{\lambda}_j \Phi_j(x)}}{e^{\sum_{j=1}^m -\boldsymbol{\lambda}_j^* \Phi_j(x)}}(\Phi_j(X) - E(\Phi_j(X)).$$

The only way to make the follow quantify to be zero is to set $\boldsymbol{\lambda}_j = \boldsymbol{\lambda}_j^*$. So far we have verified $\boldsymbol{\lambda}^*$ is the solution to the population version of (8.4.1), whose sample version is the KKT condition. Therefore, according to the M-estimation theory, we show that $\boldsymbol{\lambda}^{\text{EB}}$ to $\boldsymbol{\lambda}^*$, which is the MLE solution for (8.2).

Proof for Theorem 4: According to Lemma 1, we have $\boldsymbol{\lambda}^{\text{EB}} \to \boldsymbol{\lambda}^*$. Therefore, with $w_i^{\text{EB}} = \frac{\exp(-(2T_i-1)\sum_{j=1}^m \boldsymbol{\lambda}_j^{\text{EB}} \Phi_j(X_i))}{\sum_{T_i=0} \exp(-(2T_i-1)\sum_{j=1}^m \lambda_j^{\text{EB}} \Phi_j(X_i))}$, $w_i \propto \frac{1}{e(x_i)}$ for $T_i = 1$ and $w_i \propto \frac{1}{1-e(x_i)}$ (up to a normalized constant) for $T_i = 0$. Also, we have,

$$\frac{1}{e(x_i)} = \frac{1}{p(T_i = 1|\Phi(X_i))} = \frac{p(\Phi(X_i))}{p(\Phi(X_i)|T_i = 1)p(T_i = 1)},$$
$$\frac{1}{1-e(x_i)} = \frac{1}{p(T_i = 0|\Phi(X_i))} = \frac{p(\Phi(X_i))}{p(\Phi(X_i)|T_i = 0)p(T_i = 0)}.$$

Also, we can derive,

$$N_1 w_i^{\text{EB}} \to \frac{1/e(x_i)}{\sum_{T_i=1} \frac{1}{e(x_i)}/N_1} = \frac{1}{e(x_i)}/E(1/e(x_i)|T_i = 1).$$

Notice that,

$$E(1/e(x_i)|T_i = 1) = \int_{\mathcal{X}} \frac{1}{e(x)} p(x|T = 1)dx = \int_{\mathcal{X}} \frac{p(\Phi(X_i))}{p(T = 1)}dx = p(T_i = 1).$$

Therefore, we have,

$$N_1 w_i^{\text{EB}} \to \frac{p(\Phi(X_i))}{p(\Phi(X_i)|T_i = 1)},$$

where N_1 is the number of treated. For the entropy of the EB weights,

$$
\begin{aligned}
-\sum_{T_i=1} w_i^{\text{EB}} \log w_i^{\text{EB}} &= \frac{\sum_{T_i=1} N_1 w_i^{\text{EB}} \log N_1 w_i^{\text{EB}}}{N_i} + c_1'' \\
&= E_{x_i|T_i=1}(N_1 w_i^{\text{EB}} \log N_1 w_i^{\text{EB}})) + c_1'' \\
&= -\int_{\mathcal{X}} \log \frac{p(\Phi(x))}{p(\Phi(x)|T_i=1)} p(\Phi(x)|T=1)dx + c_1'' \\
&= \int_{\mathcal{X}} \log \frac{p(\Phi(x)|T=1)}{p(x)} p(\Phi(x)|T=1)dx + c_1'' \\
&= \text{KL}(p(\Phi(x)|T=1)||p(\Phi(x))) + c_1''.
\end{aligned}
$$

Similarly, we have,

$$
-\sum_{T_i=0} w_i^{\text{EB}} \log w_i^{\text{EB}} \to \text{KL}(p(\Phi(x)|T=0)||p(\Phi(x))) + c_0''.
$$

Therefore, we can conclude that

$$
-\sum_i w_i{}^{\text{EB}} \log w_i^{\text{EB}} \to c'[\text{KL}(p_\Phi^0(x)||p_\Phi(x)) + \text{KL}(p_\Phi^1(x)||p_\Phi(x))] + c''.
$$

Specifically, with $p_\Phi(x) = \alpha p_\Phi^1(x) + (1-\alpha)p_\Phi^0(x)$, with $\alpha = p(T_i = 1)$ we can conclude that

$$
-\sum_i w_i^{\text{EB}} \log w_i^{\text{EB}} \to c' \text{JSD}_\alpha(p_\Phi^1(x), p_\Phi^0(x)) + c''.
$$

Therefore, we show that the max entropy is a linear transformation of $\text{JSD}_\alpha(p_\Phi^1(x)|p_\Phi^0(x))$. We can use its negative value $\sum_i w_i^{\text{EB}} log w_i^{\text{EB}}$ as a measure of balance.

Proof for Theorem 5:(a) Correctly specified propensity score model Suppose $\text{logit}\{e(x)\}$ is linear in $\Phi(x)$, which means fitting a logistic regression between T_i and $\Phi(x)$ is a correctly specified model for the propensity score. Therefore, according to Lemma 1, we have $\hat{w}_i^{\text{EB}} \to \frac{1}{e(x_i)}$ for $T_i = 1$ and $\hat{w}_i^{\text{EB}} \to \frac{1}{1-e(x_i)}$ for $T_i = 0$. The estimator in (8) can be expressed as,

$$
\begin{aligned}
\hat{\tau}_{\text{ATE}}^{\text{EB}} = &\sum_{T_i=1} \hat{w}_i^{\text{EB}} Y_i - \sum_{T_i=0} \hat{w}_i^{\text{EB}} Y_i + \frac{1}{N} \sum_{i=1}^{N} (T_i \hat{w}_i^{\text{EB}} N - 1) \hat{f}_1(\hat{\Phi}(X_i)) \\
&- \frac{1}{N} \sum_{i=1}^{N} ((1-T_i) \hat{w}_i^{\text{EB}} N - 1) \hat{f}_0(\hat{\Phi}(X_i)),
\end{aligned}
$$

where we $\sum_{T_i=1} \hat{w}_i^{\text{EB}} Y_i - \sum_{T_i=0} \hat{w}_i^{\text{EB}} Y_i$ converges to τ^{ATE}, which is the usual IPW estimator when the propensity score model is correctly specified. For the last two terms in (8.4.1),

$$\begin{aligned}\sum_{i=1}^{N}(T_i\hat{w}_i^{\text{EB}}N-1)\hat{f}_1(\hat{\Phi}(X_i)) &= N\sum_{T_i=1}\hat{w}_i^{\text{EB}}\hat{\gamma}_1'\hat{\Phi}(X_i) - N\sum_{i=1}^{N}\hat{\gamma}_1'\hat{\Phi}(X_i)/N \\ &= N\sum_{T_i=1}\sum_{j=1}^{m}\hat{\gamma}_{1j}(\hat{w}_i^{\text{EB}}\hat{\Phi}_j(X_i) - \bar{\Phi}_j(X_i)) = 0.\end{aligned}$$

The second equality follows from the balance constraint in (7). Similarly, we can show that $\frac{1}{N}\sum_{i=1}^{N}((1-T_i)\hat{w}_i^{\text{EB}}N-1)\hat{f}_0(\hat{\Phi}(X_i)) = 0$. Therefore, we have shown that $\hat{\tau}_{\text{ATE}}^{\text{EB}}$ converges to τ^{ATE} when propensity score model is correctly specified.

(b)Correctly specified outocme model Suppose the true outcome function is linear in representation $\Phi(x)$, thus $f(x,0) = \gamma_0'\Phi(x)$, $f(x,1) = \gamma_1'\Phi(x)$, which means $\hat{f}_1(\hat{\Phi}(X_i)) \to f_1(\Phi(X_i))$, $\hat{f}_0(\hat{\Phi}(X_i)) \to f_0(\Phi(X_i))$. Then we have,

$$\begin{aligned}\sum_{T_i=1}\hat{w}_i^{\text{EB}}\{Y_i - \hat{f}_1(\hat{\Phi}(X_i))\} \to & E\{N_1\hat{w}_i^{\text{EB}}(Y_i - f_1(\Phi(X_i)))|T_i=1\} \\ &= E\{N_1\hat{w}_i^{\text{EB}}(E(Y_i|X_i,T_i=1) - f_1(\Phi(X_i)))\} \qquad (8.4) \\ &= E\{N_1\hat{w}_i^{\text{EB}}(E(Y_i(1)|X_i) - f_1(\Phi(X_i)))\} \qquad (8.5) \\ &= E\{N_1\hat{w}_i^{\text{EB}}(f_1(\Phi(X_i)) - f_1(\Phi(X_i)))\} = 0. \qquad (8.6)\end{aligned}$$

The first equality (8.4) follows from the law of iterated expectation. The second equality (8.5) follows from the ignorability Assumption 3. Similarly, we can prove that,

$$\sum_{T_i=0}\hat{w}_i^{\text{EB}}\{Y_i - \hat{f}_0(\hat{\Phi}(X_i))\} \to 0.$$

Therefore, the first term in (8), $\sum_{i=1}^{N}\hat{w}_i^{\text{EB}}(2T_i-1)\{Y_i - \hat{f}_{T_i}(\hat{\Phi}(X_i))\} = \sum_{T_i=1}\hat{w}_i^{\text{EB}}\{Y_i - \hat{f}_1(\hat{\Phi}(X_i))\} + \sum_{T_i=0}\hat{w}_i^{\text{EB}}\{Y_i - \hat{f}_0(\hat{\Phi}(X_i))\} \to 0$. Also, the second term in (8) converges

to the true τ^{ATE},

$$\begin{aligned}\frac{1}{N}\sum_{i=1}^{N}\{\hat{f}_1(\hat{\Phi}(X_i)) - \hat{f}_0(\hat{\Phi}(X_i))\} &\to E(f_1(\Phi(X_i)) - f_0(\Phi(X_i)) \\ &= E\{E(Y_i(1)|X_i) - E(Y_i(0)|X_i)\} \\ &= E\{E((Y_i(1) - Y_i(0))|X_i)\} \\ &= E(Y_i(1) - Y_i(0)) = \tau^{\text{ATE}}\end{aligned}$$

Based on the consistency under condition (a) and (b), we can conclude estimator in (8) is doubly robust for τ^{ATE}.

We list two lemmas required for the proof of Theorem 6. Lemma 2 defines the counterfactual loss and show that the expected loss of estimating ITE can be bounded by the sum of factual loss and counterfactual loss.

Lemma 2. *For given outcome function f and representation Φ, define the counterfactual loss for treatment arm t as,*

$$\varepsilon^t_{\text{CF}}(f, \Phi) = \int_{\mathcal{X}} l_{f,\Phi}(x, t) p_{1-t}(x) dx.$$

Then, we can bound the expected loss in estimating ε_{PEHE} by the factual loss $\varepsilon^t_{\text{F}}(f, \Phi)$ and counterfactual loss $\varepsilon^t_{\text{CF}}(f, \Phi)$,

$$\begin{aligned}\varepsilon_{PEHE}(f, \Phi) &\leq 2(\varepsilon_{\text{F}}(f, \Phi) + \varepsilon_{\text{CF}}(f, \Phi) - 2\sigma^2_Y), \\ \varepsilon_{\text{F}}(f, \Phi) &= \alpha\varepsilon^1_{\text{F}}(f, \Phi) + (1-\alpha)\varepsilon^0_{\text{F}}(f, \Phi), \\ \varepsilon_{\text{CF}}(f, \Phi) &= (1-\alpha)\varepsilon^1_{\text{CF}}(f, \Phi) + \alpha\varepsilon^0_{\text{CF}}(f, \Phi),\end{aligned}$$

where $\sigma^2_Y = \max_{t=0,1} E_X[\{(Y_i(t) - E(Y_i(t)|X))^2|X\}]$ is the expected conditional variance of $Y_i(t)$ over the covariate space $\mathcal{X}$.

Proof: This lemma is exactly the same as the proof for the first inequality of Theorem 1 in Shalit et al. (2017). We refer readers to that part for conciseness.

Lemma 3 below outlines the connection between the total variation distance and α-JS divergence.

Lemma 3. *The total variational distance between distributions p and q can be bounded by the α-JS divergence,*

$$TV(p,q) = \int |p(x) - q(x)|dx \leq \frac{2}{\alpha}\sqrt{(1 - e^{-\mathrm{JSD}_\alpha(p,q)})} \leq \frac{2}{\alpha}\sqrt{\mathrm{JSD}_\alpha(p,q)}.$$

Proof: Define $r_\alpha(x) = (1-\alpha)p(x) + \alpha q(x)$, we evaluate $\mathrm{KL}(p(x)||r_\alpha(x))$,

$$\begin{aligned}
\mathrm{KL}(p(x)||r_\alpha(x)) &= -\int p(x)\log\frac{r_\alpha(x)}{p(x)} \\
&= -\int p(x)[\log\min(\frac{r_\alpha(x)}{p(x)}, 1) + \log\max(\frac{r_\alpha(x)}{p(x)}, 1)]dx && (8.7)\\
&\geq -\log\int p(x)\min(\frac{r_\alpha(x)}{p(x)}, 1)dx - \log\int p(x)\max(\frac{r_\alpha(x)}{p(x)}, 1)dx && (8.8)\\
&= -\log\int \min(r_\alpha(x), p(x))dx - \log\int \max(r_\alpha(x), p(x))dx && (8.9)\\
&= -\log\int(\frac{p(x) + r_\alpha(x)}{2} - \frac{|p(x) - r_\alpha(x)|}{2})dx \\
&\quad -\log\int(\frac{p(x) + r_\alpha(x)}{2} + \frac{|p(x) - r_\alpha(x)|}{2})dx && (8.10)\\
&= -\log(1 - \frac{\alpha}{2}\int|p(x) - q(x)|dx) + \log(1 + \frac{\alpha}{2}\int|p(x) - q(x)|dx) \\
&= -\log(1 - \frac{\alpha^2}{4}TV^2(p,q)).
\end{aligned}$$

The second equality (8.7) follows from the fact that $x = \min(x,1)\max(x,1)$. The first inequality (8.8) follows from Jensen inequality. The fourth equality (8.10) follows from the fact that $\min(a,b) = \frac{a+b}{2} - \frac{|a-b|}{2}, \max(a,b)\frac{a+b}{2} + \frac{|a-b|}{2}$. which indicates,

$$\mathrm{JSD}_\alpha(p,q) = \frac{1}{2}[\mathrm{KL}(p(x)||r_\alpha(x)) + \mathrm{KL}(q(x)||r_\alpha(x))] \geq -\log(1 - \frac{\alpha^2}{4}TV^2(p,q)), \tag{8.11}$$

$$TV(p,q) \leq \frac{2}{\alpha}\sqrt{(1 - e^{-\mathrm{JSD}_\alpha(p,q)})} \leq \frac{2}{\alpha}\sqrt{\mathrm{JSD}_\alpha(p,q)}. \tag{8.12}$$

The second inequality in (8.12) follows from the fact that $1 - e^{-x} \leq x$.

With Lemma 2 and 3, we proceed to prove Theorem 6. The strategy is to bound by the counterfactual loss by the factual loss and total variation distance. Next step, we replace total variation distance with α-JS divergence. In the final, we bound the loss of estimating ITE by the counterfactual loss an factual loss with Lemma 2.

Proof for Theorem 6 Let $\Psi(\cdot) : \mathcal{R}^m \to \mathcal{X}$ denote the inverse mapping of $\Phi(X)$. First, we bound the counterfactual loss $\varepsilon_{\text{CF}}(f, \Phi)$ with the factual loss $\varepsilon_{\text{F}}(f, \Phi)$ and α-JS divergence,

$$\begin{aligned}
|\varepsilon^0_{\text{CF}}(f, \Phi) - \varepsilon^0_{\text{F}}(f, \Phi)| &= |\int_{\mathcal{X}} l_{f,\Phi}(x, 0)p_1(x)dx - \int_{\mathcal{X}} l_{f,\Phi}(x, 0)p_0(x)dx| \\
&\leq \int_{\mathcal{X}} l_{f,\Phi}(x, 0)|p_1(x) - p_0(x)|dx \\
&= \int_{\mathcal{R}^m} l_{f,\Phi}(\Psi(s), 0)|p^1_\Phi(s) - p^0_\Phi(s)|ds \qquad (8.13) \\
&\leq B_\Phi \int_{\mathcal{R}^m} |p^1_\Phi(s) - p^0_\Phi(s)|ds = B_\Phi TV(p^1_\Phi, p^0_\Phi) \qquad (8.14) \\
&\leq \frac{2B_\Phi}{\alpha}\sqrt{\text{JSD}_\alpha(p^1_\Phi, p^0_\Phi)}. \qquad (8.15)
\end{aligned}$$

The equality (8.13) follows from the change of variable formula, the second inequality (8.14) from the fact that $l_{f,\Phi}(\Psi(s), 0)$ is a continuous function on a compact space. The third inequality (8.15) follow from Lemma 3. With similar argument, we can derive that,

$$|\varepsilon^1_{\text{CF}}(f, \Phi) - \varepsilon^1_{\text{F}}(f, \Phi)| \leq \frac{2B'_\Phi}{\alpha}\sqrt{\text{JSD}_\alpha(p^1_\Phi, p^0_\Phi)}.$$

Therefore, we have,

$$\begin{aligned}
&|\varepsilon_{\text{CF}}(f, \Phi) - \alpha\varepsilon^0_{\text{F}}(f, \Phi) + (1 - \alpha)\varepsilon^1_{\text{F}}(f, \Phi)| \\
&\quad = \alpha|\varepsilon^0_{\text{CF}}(f, \Phi) - \varepsilon^0_{\text{F}}(f, \Phi)| + (1 - \alpha)|\varepsilon^1_{\text{CF}}(f, \Phi) - \varepsilon^1_{\text{F}}(f, \Phi)| \\
&\quad \leq 2\frac{(1 - \alpha)B_\Phi + \alpha B'_\Phi}{\alpha}\sqrt{\text{JSD}_\alpha(p^1_\Phi, p^0_\Phi)} \leq C_{\Phi,\alpha}\sqrt{\text{JSD}_\alpha(p^1_\Phi, p^0_\Phi)}
\end{aligned}$$

.

With Lemma 2, we have

$$\begin{aligned}
\varepsilon_{\text{PEHE}}(f, \Phi) &\leq 2(\varepsilon_{\text{F}}(f, \Phi) + \varepsilon_{\text{CF}}(f, \Phi) - 2\sigma^2_Y) \\
&\leq 2(\alpha\varepsilon^1_{\text{F}}(f, \Phi) + (1 - \alpha)\varepsilon^0_{\text{F}}(f, \Phi) + \varepsilon_{\text{CF}}(f, \Phi) - 2\sigma^2_Y) \\
&\leq 2(\alpha\varepsilon^1_{\text{F}}(f, \Phi) + (1 - \alpha)\varepsilon^0_{\text{F}}(f, \Phi) + \alpha\varepsilon^0_{\text{F}}(f, \Phi) \\
&+ (1 - \alpha)\varepsilon^1_{\text{F}}(f, \Phi) + C_{\Phi,\alpha}\sqrt{\text{JSD}_\alpha(p^1_\Phi, p^0_\Phi)} - 2\sigma^2_Y) \\
&= 2(\varepsilon^0_{\text{F}}(f, \Phi) + \varepsilon^1_{\text{F}}(f, \Phi) + C_{\Phi,\alpha}\sqrt{\text{JSD}_\alpha(p^1_\Phi, p^0_\Phi)} - 2\sigma^2_Y),
\end{aligned}$$

which proves the inequality in Theorem 6 (typo correction: missing squared root in the main text on $\mathrm{JSD}_\alpha(p^1_\Phi, p^0_\Phi)$).

8.4.2 Generalization to other estimands

In this section, we use τ^{ATT} an example of how to generalize to other estimands. If we are interested in estimating τ^{ATT}, we can solve the following optimization problem,

$$\begin{aligned} \max_{w} \quad & -\sum_{T_i=0}^{N} w_i \log w_i, \\ \text{s.t} \quad & \sum_{T_i=0} w_i \Phi_{ji} = \sum_{T_i=1} \Phi_{ji}/N_1 = \bar{\Phi}_j(1), j = 1, 2 \cdots, m, \\ & \sum_{T_i=0} w_i = 1, w_i > 0. \end{aligned}$$

And our estimator for τ^{ATT} is

$$\hat{\tau}^{\mathrm{EB}}_{\mathrm{ATT}} = \sum_{T_i=1} Y_i/N_1 - \sum_{T_i=0} \hat{w}^{\mathrm{EB}}_i Y_i.$$

We prove its double robustness in Theorem 8.

Theorem 8 (Double Robustness for ATT)**.** *Under Assumptions 3 and 4, the entropy balancing estimator $\hat{\tau}^{EB}_{ATT}$ with the weights $w^{EB}_i(\Phi)$ solved from Problem (6) and* (8.4.2) *is doubly robust in the sense that: If either the true outcome model $f(x,0)1$ or the true propensity score model $logit\{e(x)\}$ is linear in the representations $\Phi(x)$, then $\hat{\tau}^{EB}_{ATT}$ is consistent for τ_{ATT}.*

Proof: The dual problem for the optimization problem is

$$\min_{\boldsymbol{\lambda}} \quad \log(\sum_{T_i=0} exp(\sum_{j=1}^{m} \boldsymbol{\lambda}_j \Phi_j(X_i))) - \sum_{j=1}^{m} \boldsymbol{\lambda}_j \bar{\Phi}_j(1)$$

where $\boldsymbol{\lambda}_j$ is the Lagrangian multiplier. With KKT condition, the optimal weights are

$$w^{\mathrm{EB}}_i = \frac{exp(\sum_{j=1}^{m} \boldsymbol{\lambda}^{\mathrm{EB}}_j \Phi_j(X_i))}{\sum_{T_i=0} exp(\sum_{j=1}^{m} \boldsymbol{\lambda}^{\mathrm{EB}}_j \Phi_j(X_i))}$$

where $\boldsymbol{\lambda}^{\text{EB}}$ is the solution to the dual problem (8.4.2). **(a)Correctly specified propensity score model** If the logit of true propensity score value, $\log(\frac{e(X_i)}{1-e(X_i)})$ is linear in $\Phi_j(X_i)$, then we can show that $\boldsymbol{\lambda}^{\text{EB}}$ converges to the solution $\boldsymbol{\lambda}^*$ to the following optimization problem by Lemma 1.

$$\min_{\boldsymbol{\lambda}} \quad \sum_{T_i=0} \log(1 + exp(-(2T_i - 1)\sum_{j=1}^{m} \boldsymbol{\lambda}_j \Phi_j(X_i)))$$

which is maximizing the log likelihood when fitting a logistic regression between T_i and $\Phi_j(X_i)$. As long as we have $\boldsymbol{\lambda}^{\text{EB}}$ converges to $\boldsymbol{\lambda}^*$, we can claim that $N_0 w_i^{\text{EB}} \to c\frac{e(X_i)}{1-e(X_i)}$(Zhao and Percival, 2017), c is some normalized constant, which proves the consistency of the estimator.

(b)Correctly specified outcome model If outcome model $f(x, 0)$ is linear in $\Phi_j(X_i)$, then we can expand $E(Y_i(0)|X_i = x) = f(x, 0) = \sum_{j=1}^{m} \gamma_{0j}\Phi_j(x)$.

$$\begin{aligned} E(Y_i(0)|T_i = 1) &= \int_{\mathcal{X}} E(Y_i(0)|X_i = x, T_i = 1)p_1(x)dx, \\ &= \int_{\mathcal{X}} E(Y_i(0)|X_i = x)p_1(x)dx, \\ &= \sum_{j=1}^{m} \gamma_{0j} \int \Phi_j(x)p_1(x)dx. \end{aligned}$$

We also have,

$$\begin{aligned} \sum_{T_i=0} w_i^{\text{EB}} Y_i &= \sum_{T_i=0} w_i^{\text{EB}'} Y_i/N_0 \to E\{w_i^{\text{EB}'} Y_i(0)|T_i = 0\} \\ &= \int w_i^{\text{EB}'} E(Y_i(0)|X_i)p_0(x)dx \\ &= \sum_{j=1}^{m} \gamma_{0j} \int w_i^{\text{EB}'} \Phi_j(x)p_0(x)dx. \end{aligned}$$

where $w_i^{\text{EB}'}$ is the normalized w_i^{EB} with $w_i^{\text{EB}'} = N_0 w_i^{\text{EB}}$. Notice that,

$$\begin{aligned} \sum_{T_i=0} w^{\text{EB}'} \Phi_j(X_i)/N_0 &\to \int w_i^{\text{EB}'} \Phi_j(x)p_1(x)dx, \\ \sum_{T_i=1} \Phi_j(X_i)/N_1 &\to \int \Phi_j(x)p_1(x)dx, \end{aligned}$$

By the constraints of (8.4.2), we have:

$$\sum_{T_i=0} w^{'\text{EB}}\Phi_j(X_i)/N_0 = \sum_{T_i=0} w^{\text{EB}}\Phi_j(X_i) = \sum_{T_i=1}\Phi_j(X_i)/N_1.$$

Therefore, we have

$$\int \Phi_j(x)p_1(x)dx = \int w_i^{\text{EB}'}\Phi_j(x)p_0(x)dx,$$

which implies

$$\sum_{T_i=0} w_i^{\text{EB}} Y_i \to E(Y_i(0)|T_i = 1).$$

With $\sum_{T_i=1} Y_i/N_1 \to E(Y_i(1)|T_i = 1)$, we establish the consistency if outcome model is correctly specified.

Based on (a) and (b), we show $\hat{\tau}^{\text{EB}}_{\text{ATT}}$ is doubly robust. The proof is largely follows from Zhao and Percival (2017).

8.4.3 Experiments details

Hyperparameter selection

We random sample one combination from all possible choice hyperparameters and train the model on the experimental dataset each time. We perform the hyperparameters selection regime described in section 6 and report only the best one within all possible choices in the random sampling. Table 8.8 lists all possible choice for the parameter. For IHDP data and high-dimensional data, we evaluate $\varepsilon_{\text{PEHE}}$ on the validation dataset. For the Jobs experiments, we evaluate the policy risk R_{POL}.

Table 8.8: Hyperparameter choices

Hyperparameters	Value grid
Imbalance importance κ	$\{10^{k/2}\}_{k=-10}^{6}$
Number of representations layers	$\{1, 2, 3, 4, 5\}$
Dimensions of representations layers	$\{20, 50, 100, 200\}$
Batch size	$\{100, 200, 500\}$

Datasets details

The IHDP and Jobs datasets are public available already. For anonymmous purpose, we will provide the link to download those datasets upon being accepted. We also include the dataset in *npz* files in the supplementary material. For the high-dimensional dataset, we provide a guidance of data generating process in the main text.

Computing infrastructure

We run the code with environment **Tensorflow 1.4.1** and **Numpy 1.16.5** in **Python 2.7**.

8.5 Appendix for Chapter 6

8.5.1 Details on experiments

Details on synthetic auction

We enumerate the steps for generating the synthetic auction data.

- Step 1: We utilize the **scikit-learn.make_classification** function to generate synthetic relevance data (x, y). Each data point corresponds to one ad to be shown.
- Step 2: We fit a random forest model to the data to calculate a relevance score/probability of being click p for each ad.
- Step 3: We run a simulated auction based on the relevance score with some additional noise p'. Each auction determines the ad's layout on one page. In each auction, 20 ads are being considered to compete for the position in the layout with at most 5 slots. Notice that the relevance reserve serves as a filter to determine whether the ad can join the auction.
- Step 4: we assign position based on the p' in the auction with high relevance assigned to the top position.
- Step 5: We generate click based on true relevance score p with Bernoulli trials and randomly pick up one ad to click if the user would click multiple ads on the same page.

For randomized data, we skip the auction stage and simply randomly pick some ads to show on the page. We run 10000 auctions for the randomized data and 25000 auctions on the log data. The final sample size ratio between randomized and log data is approximately 1:5.

Details on end-to-end optimization task

We also provide a detailed description on how we calculate the degree of feature shifts in real-world task and how we pick up the optimization tasks.

In order to compute distribution shift between two different environments, we use discrete bins to represent each feature as a multinomial distribution similar to approach described in Bayir et al. (2019). After that, we applied Jensen-Shannon (JS) divergence metric to compute the similarity of two multinomial distribution for the same feature in counterfactual vs factual environment. We select the typical cases with lower similarity to demonstrate the use of the the proposed method. The JS Divergence of two probability distribution P and Q are given below:

$$JS(P||Q) = \frac{1}{2}D_{KL}(P||M) + \frac{1}{2}D_{KL}(Q||M), M = \frac{1}{2}(P+Q)$$

JS Divergence is the symmetric version of Kullback–Leibler divergence which can be computed as below for a given multinomial distribution with k different bins.

$$D_{KL}(P||Q) = \sum_{i}^{k}(P(i)\ ln(\frac{P(i)}{Q(i)}))$$

Once the JS divergence of each feature is computed based on counterfactual (P) vs factual (P^*) feature distributions, the final distribution shift score (DS) over N features is computed as root mean square of all JS divergence values across all features as follows:

$$DS = \sqrt{\frac{1}{N}\sum_{i}^{N}[JS(P_i||P_i^*)]^2}$$

The distribution shift (DS) scores for selected real use cases are given below in Table 8.9. We calculate the feature shifts of 10 candidate task in total and compare the two tasks in the paper with other eight tasks. Based on the JS-divergence metrics,

the two tasks we demonstrate in the paper serve as good examples for covariates shifts and drastic change in the mechanism.

Table 8.9: Comparison for distribution shifts

DS (Text Ads Case)	10^{-2}
DS (Shopping Ads Case)	$5x10^{-3}$
Average DS (Others)	$45x10^{-5}$
STD of DS (Others)	$35x10^{-5}$

8.5.2 Proof for theorems

First, we give explicit description for the theorems in Section 6.3.3 which are from previous literature. The first theorem in Rojas-Carulla et al. (2018) establishes the relationship between conditional invariant property and robust prediction

Theorem 9 (Adversarial robustness)**.** *Suppose we have training data from various sources.* $\{(x_i^k, z_i^k, y_i^k)\} \sim \mathcal{P}^k, k = 1, 2, \cdots, K$ *and wish to make prediction on targeting* $\{(x_i^{K+1}, z_i^{K+1}, y_i^{K+1})\} \sim \mathcal{P}^{K+1}$*. Assume there exists a unique subset of features* S^* *such that:* $y_i^k | S_i^{*k} \stackrel{d}{=} y_i^{k'} | S_i^{*k'}, k \neq k' \in \{1, 2, \cdots K+1\}$ *(conditional invariant property). Then:*

$$E_{\mathcal{P}^{1,\cdots,K}}(y_i|S_i^*) = \text{argmin}_f \text{sup}_{(x_i,z_i,y_i)\sim\mathcal{P}} E||f(x_i, z_i), y_i||^2,$$

where $\mathcal{P}$ *is the family of distributions of* (x_i, z_i, y_i) *satisfying the invariant property.* $\mathcal{P}^{1,\cdots,K}$ *is the distribution pooling* $\mathcal{P}^1, \mathcal{P}^2 \cdots, \mathcal{P}^k$ *together.*

The second theorem from Peters et al. (2016); Rojas-Carulla et al. (2018) states relationship between conditional invariant property and causality.

Theorem 10 (Relationship to causality)**.** *If we further assume* (x_i, z_i, y_i) *can be expressed with a direct acyclic graph (DAG) or structural equation model (SEM).*

Namely, let $c_i = (x_i, z_i)$, $c_i^j = h_j(c_i^{\boldsymbol{PA}_j}, e_i^j)$, $y_i = h_y(c_i^{\boldsymbol{PA}_Y}, e_i)$. *Then we have* $S_i^* = c_i^{\boldsymbol{PA}_Y}$, *where* $c^{\boldsymbol{PA}_j}$ *denotes the parents for* c_j, $c^{\boldsymbol{PA}_Y}$ *denotes the parents for* y, e_i^j, e_i *are the noises,* $h_j(\cdot,\cdot)$ *and* $h_y(\cdot,\cdot)$ *are deterministic functions.*

Now we prove the Theorem 7 to validate the use of **R-data**, *Proof:* Assuming certain regularity conditions, such as the integrals are well-defined, suppose the model trained can converge to the conditional mean,

$$E(y_i|x_i, z_i) \quad \rightarrow_p \quad \int_{\mathcal{Y}} yp(y|x,z)dy = \int_{\mathcal{Y}} y\frac{p(y,x,z)}{p(x,z)}dy$$

Furthermore, under randomization conditions, we have,

$$\begin{aligned}
\int_{\mathcal{Y}} y\frac{p(y,x,z)}{p(x,z)}dy &= \int_{\mathcal{Y}} y\frac{p(y,x,z)}{p(x_i^1)p(x_i^2\cdots p(x_i^p)p(z_i^1)\cdots p(z_i^{p'}))}dy \\
&= \int_{\mathcal{Y}} y\frac{p(y|c_i^{PA_Y})p(x_i^1)p(x_i^2)\cdots p(x_i^p)p(z_i^1)\cdots p(z_i^{p'})}{p(x_i^1)p(x_i^2)\cdots p(x_i^p)p(z_i^1)\cdots p(z_i^{p'})}dy \\
&= \int_{\mathcal{Y}} y\frac{p(y(\mathrm{do}(c_i^{PA^Y}))p(x_i^1)p(x_i^2)\cdots p(x_i^p)p(z_i^1)\cdots p(z_i^{p'})}{p(x_i^1)p(x_i^2)\cdots p(x_i^p)p(z_i^1)\cdots p(z_i^{p'})}dy \\
&= E(y_i|c_i^{PA_Y}) = E(y_i|S_i^*)
\end{aligned}$$

Bibliography

Alberto Abadie and Guido W Imbens. Large sample properties of matching estimators for average treatment effects. *Econometrica*, 74(1):235–267, 2006.

Alberto Abadie, Alexis Diamond, and Jens Hainmueller. Synthetic control methods for comparative case studies: Estimating the effect of california's tobacco control program. *Journal of the American Statistical Association*, 105:493–505, 2010.

Ahmed M Alaa and Mihaela van der Schaar. Bayesian inference of individualized treatment effects using multi-task gaussian processes. In *Advances in Neural Information Processing Systems*, pages 3424–3432, 2017.

Ahmed M Alaa and Mihaela van der Schaar. Bayesian nonparametric causal inference: Information rates and learning algorithms. *IEEE Journal of Selected Topics in Signal Processing*, 12(5):1031–1046, 2018.

Susan C Alberts and Jeanne Altmann. The amboseli baboon research project: 40 years of continuity and change. In *Long-term Field Studies of Primates*, pages 261–287. Springer, 2012.

Per K Andersen, Elisavet Syriopoulou, and Erik T Parner. Causal inference in survival analysis using pseudo-observations. *Statistics in Medicine*, 36(17):2669–2681, 2017.

Per Kragh Andersen and Maja Pohar Perme. Pseudo-observations in survival analysis. *Statistical Methods in Medical Research*, 19(1):71–99, 2010.

Per Kragh Andersen, John P Klein, and Susanne Rosthøj. Generalised linear models for correlated pseudo-observations, with applications to multi-state models. *Biometrika*, 90(1):15–27, 2003.

Per Kragh Andersen, Mette Gerster Hansen, and John P Klein. Regression analysis of restricted mean survival time based on pseudo-observations. *Lifetime Data Analysis*, 10(4):335–350, 2004.

Michael Anderson and Michael Marmot. The effects of promotions on heart disease: Evidence from whitehall. *The Economic Journal*, 122(561):555–589, 2011.

Michael Anderson and Michael Marmot. The effects of promotions on heart disease: Evidence from whitehall. *The Economic Journal*, 122(561):555–589, 2012.

Adin-Cristian Andrei and Susan Murray. Regression models for the mean of the quality-of-life-adjusted restricted survival time using pseudo-observations. *Biometrics*, 63(2):398–404, 2007.

Joseph Antonelli, Matthew Cefalu, Nathan Palmer, and Denis Agniel. Doubly robust matching estimators for high dimensional confounding adjustment. *Biometrics*, 74 (4):1171–1179, 2018.

Martin Arjovsky, Léon Bottou, Ishaan Gulrajani, and David Lopez-Paz. Invariant risk minimization. *arXiv preprint arXiv:1907.02893*, 2019.

Serge Assaad, Shuxi Zeng, Chenyang Tao, Shounak Datta, Nikhil Mehta, Ricardo Henao, Fan Li, and Lawrence Carin. Counterfactual representation learning with balancing weights. *arXiv preprint arXiv:2010.12618*, 2020.

Onur Atan, James Jordon, and Mihaela van der Schaar. Deep-treat: Learning optimal personalized treatments from observational data using neural networks. In *Thirty-Second AAAI Conference on Artificial Intelligence*, 2018.

Susan Athey and Guido Imbens. Recursive partitioning for heterogeneous causal effects. *Proceedings of the National Academy of Sciences*, 113(27):7353–7360, 2016.

Susan Athey, Guido Imbens, Thai Pham, and Stefan Wager. Estimating average treatment effects: Supplementary analyses and remaining challenges. *American Economic Review*, 107(5):278–81, 2017.

Peter C Austin. Absolute risk reductions and numbers needed to treat can be obtained from adjusted survival models for time-to-event outcomes. *Journal of Clinical Epidemiology*, 63(1):46–55, 2010a.

Peter C Austin. The performance of different propensity-score methods for estimating differences in proportions (risk differences or absolute risk reductions) in observational studies. *Statistics in Medicine*, 29(20):2137–2148, 2010b.

Peter C Austin. Generating survival times to simulate cox proportional hazards models with time-varying covariates. *Statistics in Medicine*, 31(29):3946–3958, 2012.

Peter C Austin. The performance of different propensity score methods for estimating marginal hazard ratios. *Statistics in Medicine*, 32(16):2837–2849, 2013.

Peter C Austin. The use of propensity score methods with survival or time-to-event outcomes: reporting measures of effect similar to those used in randomized experiments. *Statistics in Medicine*, 33(7):1242–1258, 2014.

Peter C Austin and Tibor Schuster. The performance of different propensity score methods for estimating absolute effects of treatments on survival outcomes: a simulation study. *Statistical Methods in Medical Research*, 25(5):2214–2237, 2016.

Peter C. Austin and Elizabeth A. Stuart. Moving towards best practice when using inverse probability of treatment weighting (IPTW) using the propensity score to estimate causal treatment effects in observational studies. *Statistics in Medicine*, 34(28):3661–3679, 2015.

Peter C Austin and Elizabeth A Stuart. The performance of inverse probability of treatment weighting and full matching on the propensity score in the presence of model misspecification when estimating the effect of treatment on survival outcomes. *Statistical Methods in Medical Research*, 26(4):1654–1670, 2017.

Peter C. Austin, Andrea Manca, Merrick Zwarenstein, David N. Juurlink, and Matthew B. Stanbrook. A substantial and confusing variation exists in handling of baseline covariates in randomized controlled trials: a review of trials published in leading medical journals. *Journal of Clinical Epidemiology*, 63(2):142–153, 2010.

Xiaofei Bai, Anastasios A Tsiatis, and Sean M O'Brien. Doubly-robust estimators

of treatment-specific survival distributions in observational studies with stratified sampling. *Biometrics*, 69(4):830–839, 2013.

Jessie P. Bakker, Rui Wang, Jia Weng, Mark S. Aloia, Claudia Toth, Michael G. Morrical, Kevin J. Gleason, Michael Rueschman, Cynthia Dorsey, Sanjay R. Patel, James H. Ware, Murray A. Mittleman, and Susan Redline. Motivational enhancement for increasing adherence to CPAP: a randomized controlled trial. *Chest*, 150 (2):337–345, 2016.

Heejung Bang and James M Robins. Doubly robust estimation in missing data and causal inference models. *Biometrics*, 61(4):962–973, 2005.

Reuben M Baron and David A Kenny. The moderator–mediator variable distinction in social psychological research: Conceptual, strategic, and statistical considerations. *Journal of Personality and Social Psychology*, 51(6):1173, 1986.

Patrick Bateson and Peter Gluckman. Plasticity and robustness in development and evolution. *International Journal of Epidemiology*, 41(1):219–223, 2012.

Patrick Bateson, David Barker, Timothy Clutton-Brock, Debal Deb, Bruno D'udine, Robert A Foley, Peter Gluckman, Keith Godfrey, Tom Kirkwood, Marta Mirazón Lahr, et al. Developmental plasticity and human health. *Nature*, 430(6998):419, 2004.

Murat Ali Bayir, Mingsen Xu, Yaojia Zhu, and Yifan Shi. Genie: An open box counterfactual policy estimator for optimizing sponsored search marketplace. In *Proceedings of the Twelfth ACM International Conference on Web Search and Data Mining*, pages 465–473. ACM, 2019.

Andrea Bellavia and Linda Valeri. Decomposition of the total effect in the presence of multiple mediators and interactions. *American Journal of Epidemiology*, 187(6): 1311–1318, 2018.

Alexandre Belloni, Victor Chernozhukov, and Christian Hansen. Inference on treatment effects after selection among high-dimensional controls. *The Review of Economic Studies*, 81(2):608–650, 2014.

Alexandre Belloni, Victor Chernozhukov, Ivan Fernández-Val, and Christian Hansen. Program evaluation and causal inference with high-dimensional data. *Econometrica*, 85(1):233–298, 2017.

Shai Ben-David, John Blitzer, Koby Crammer, and Fernando Pereira. Analysis of representations for domain adaptation. In *Advances in Neural Information Processing Systems*, pages 137–144, 2007.

Yoshua Bengio, Tristan Deleu, Nasim Rahaman, Rosemary Ke, Sébastien Lachapelle, Olexa Bilaniuk, Anirudh Goyal, and Christopher Pal. A meta-transfer objective for learning to disentangle causal mechanisms. *arXiv preprint arXiv:1901.10912*, 2019.

Andrew Bennett, Nathan Kallus, and Tobias Schnabel. Deep generalized method of moments for instrumental variable analysis. In *Advances in Neural Information Processing Systems*, pages 3559–3569, 2019.

Anirban Bhattacharya and David B Dunson. Sparse bayesian infinite factor models.

Biometrika, pages 291–306, 2011.

Ioana Bica, Ahmed M Alaa, and Mihaela van der Schaar. Time series deconfounder: Estimating treatment effects over time in the presence of hidden confounders. *arXiv preprint arXiv:1902.00450*, 2019.

Steffen Bickel, Michael Brückner, and Tobias Scheffer. Discriminative learning under covariate shift. *Journal of Machine Learning Research*, 10(Sep):2137–2155, 2009.

M-AC Bind, TJ Vanderweele, BA Coull, and JD Schwartz. Causal mediation analysis for longitudinal data with exogenous exposure. *Biostatistics*, 17(1):122–134, 2015.

M-AC Bind, TJ Vanderweele, BA Coull, and JD Schwartz. Causal mediation analysis for longitudinal data with exogenous exposure. *Biostatistics*, 17(1):122–134, 2016.

Nadine Binder, Thomas A Gerds, and Per Kragh Andersen. Pseudo-observations for competing risks with covariate dependent censoring. *Lifetime Data Analysis*, 20 (2):303–315, 2014.

Adam Bloniarz, Hanzhong Liu, Cun-Hui Zhang, Jasjeet S Sekhon, and Bin Yu. Lasso adjustments of treatment effect estimates in randomized experiments. *Proceedings of the National Academy of Sciences*, 113(27):7383–7390, 2016.

Christopher M. Booth. Evaluating patient-centered outcomes in the randomized controlled trial and beyond: Informing the future with lessons from the past. *Clinical Cancer Research*, 16(24):5963–5971, 2010.

Léon Bottou, Jonas Peters, Joaquin Quiñonero-Candela, Denis X Charles, D Max Chickering, Elon Portugaly, Dipankar Ray, Patrice Simard, and Ed Snelson. Counterfactual reasoning and learning systems: The example of computational advertising. *The Journal of Machine Learning Research*, 14(1):3207–3260, 2013.

Leo Breiman. Random forests. *Machine learning*, 45(1):5–32, 2001.

Fernando A Campos, Francisco Villavicencio, Elizabeth A Archie, Fernando Colchero, and Susan C Alberts. Social bonds, social status and survival in wild baboons: a tale of two sexes. *Philosophical Transactions of the Royal Society B*, 375(1811): 20190621, 2020.

Michael Carter. *Foundations of mathematical economics*. MIT Press, 2001.

Anne Case and Christina Paxson. The long reach of childhood health and circumstance: evidence from the whitehall ii study. *The Economic Journal*, 121(554): F183–F204, 2011.

Tarani Chandola, Mel Bartley, Amanda Sacker, Crispin Jenkinson, and Michael Marmot. Health selection in the whitehall ii study, uk. *Social science & medicine*, 56 (10):2059–2072, 2003.

Olivier Chapelle and Lihong Li. An empirical evaluation of thompson sampling. In *Advances in Neural Information Processing Systems*, pages 2249–2257, 2011.

Paidamoyo Chapfuwa, Serge Assaad, Shuxi Zeng, Michael Pencina, Lawrence Carin, and Ricardo Henao. Survival analysis meets counterfactual inference. *arXiv preprint arXiv:2006.07756*, 2020.

Mariette J Chartier, John R Walker, and Barbara Naimark. Separate and cumulative effects of adverse childhood experiences in predicting adult health and health care utilization. *Child abuse & neglect*, 34(6):454–464, 2010.

Zhengping Che, Sanjay Purushotham, Kyunghyun Cho, David Sontag, and Yan Liu. Recurrent neural networks for multivariate time series with missing values. *Scientific reports*, 8(1):6085, 2018.

Guanhua Chen, Donglin Zeng, and Michael R Kosorok. Personalized dose finding using outcome weighted learning. *Journal of the American Statistical Association*, 111(516):1509–1521, 2016.

Pei-Yun Chen and Anastasios A Tsiatis. Causal inference on the difference of the restricted mean lifetime between two groups. *Biometrics*, 57(4):1030–1038, 2001.

Patricia W Cheng and Hongjing Lu. Causal invariance as an essential constraint for creating a causal representation of the world: Generalizing. *The Oxford Handbook of Causal Reasoning*, page 65, 2017.

Victor Chernozhukov, Christian Hansen, and Martin Spindler. Post-selection and post-regularization inference in linear models with many controls and instruments. *American Economic Review*, 105(5):486–90, 2015.

Victor Chernozhukov, Denis Chetverikov, Mert Demirer, Esther Duflo, Christian Hansen, Whitney Newey, and James Robins. Double/debiased machine learning for treatment and structural parameters. *The Econometrics Journal*, 21(1):C1–C68, 2018.

Jody D. Ciolino, Reneé H. Martin, Wenle Zhao, Michael D. Hill, Edward C. Jauch, and Yuko Y. Palesch. Measuring continuous baseline covariate imbalances in clinical trial data. *Statistical Methods in Medical Research*, 24(2):255–272, 2015.

Jody D. Ciolino, Hannah L. Palac, Amy Yang, Mireya Vaca, and Hayley M. Belli. Ideal vs. real: A systematic review on handling covariates in randomized controlled trials. *BMC Medical Research Methodology*, 19(1):1–11, 2019.

Sheldon Cohen and Thomas A Wills. Stress, social support, and the buffering hypothesis. *Psychological Bulletin*, 98(2):310, 1985.

Elizabeth Colantuoni and Michael Rosenblum. Leveraging prognostic baseline variables to gain precision in randomized trials. *Statistics in Medicine*, 34(18):2602–2617, 2015.

Stephen R Cole and Miguel A Hernán. Adjusted survival curves with inverse probability weights. *Computer Methods and Programs in Biomedicine*, 75(1):45–49, 2004.

Thomas D Cook, Donald Thomas Campbell, and William Shadish. *Experimental and quasi-experimental designs for generalized causal inference*. Houghton Mifflin Boston, MA, 2002.

David Roxbee Cox. *Analysis of survival data*. Chapman and Hall/CRC, 2018.

R K Crump, V J Hotz, G W Imbens, and O A Mitnik. Moving the goalposts: Ad-

dressing limited overlap in the estimation of average treatment effects by changing the estimand. Technical Report 330, National Bureau of Economic Research, Cambridge, MA, September 2006. URL `http://www.nber.org/papers/T0330`.

Marco Cuturi and Arnaud Doucet. Fast computation of wasserstein barycenters. In *International conference on machine learning*, pages 685–693. PMLR, 2014.

Rhian M Daniel, SN Cousens, BL De Stavola, Michael G Kenward, and JAC Sterne. Methods for dealing with time-dependent confounding. *Statistics in Medicine*, 32 (9):1584–1618, 2013.

Michael J Daniels, Jason A Roy, Chanmin Kim, Joseph W Hogan, and Michael G Perri. Bayesian inference for the causal effect of mediation. *Biometrics*, 68(4): 1028–1036, 2012.

Hal Daumé III. Frustratingly easy domain adaptation. In *Proceedings of the 45th Annual Meeting of the Association of Computational Linguistics*, pages 256–263, 2007.

Hal Daume III and Daniel Marcu. Domain adaptation for statistical classifiers. *Journal of Artificial Intelligence Research*, 26:101–126, 2006.

Marie Davidian, Anastasios A Tsiatis, and Selene Leon. Semiparametric estimation of treatment effect in a pretest–posttest study with missing data. *Statistical Science*, 20(3):261, 2005.

David L. DeMets and Robert M. Califf. Lessons learned from recent cardiovascular clinical trials: Part I. *Circulation*, 106(6):746–751, 2002.

Jean-Claude Deville and Carl-Erik Särndal. Calibration estimators in survey sampling. *Journal of the American Statistical Association*, 87(418):376–382, 1992.

Vanessa Didelez. Defining causal mediation with a longitudinal mediator and a survival outcome. *Lifetime Data Analysis*, 25(4):593–610, 2019.

Vanessa Didelez, A Philip Dawid, and Sara Geneletti. Direct and indirect effects of sequential treatments. In *Proceedings of the Twenty-Second Conference on Uncertainty in Artificial Intelligence*, pages 138–146, 2006.

Peng Ding and Fan Li. Causal inference: A missing data perspective. *Statistical Science*, 33(2):214–237, 2018.

Peng Ding and Tyler J Vanderweele. Sharp sensitivity bounds for mediation under unmeasured mediator-outcome confounding. *Biometrika*, 103(2):483–490, 2016.

Jing Dong, Junni L. Zhang, Shuxi Zeng, and Fan Li. Subgroup balancing propensity score. *Statistical Methods in Medical Research*, 29(3):659–676, 2020.

Miroslav Dudík, John Langford, and Lihong Li. Doubly robust policy evaluation and learning. *arXiv preprint arXiv:1103.4601*, 2011.

Miroslav Dudík, Dumitru Erhan, John Langford, and Lihong Li. Sample-efficient nonstationary policy evaluation for contextual bandits. *arXiv preprint arXiv:1210.4862*, 2012.

Miroslav Dudík, Dumitru Erhan, John Langford, Lihong Li, et al. Doubly robust policy evaluation and optimization. *Statistical Science*, 29(4):485–511, 2014.

Richard M Dudley and Rimas Norvaiša. *Differentiability of six operators on nonsmooth functions and p-variation, Lecture Notes in Math.* 1703. Springer, Berlin, 1999.

Daniele Durante. A note on the multiplicative gamma process. *Statistics & Probability Letters*, 122:198–204, 2017.

Marko Elovainio, Jane E Ferrie, Archana Singh-Manoux, Martin Shipley, G David Batty, Jenny Head, Mark Hamer, Markus Jokela, Marianna Virtanen, Eric Brunner, et al. Socioeconomic differences in cardiometabolic factors: social causation or health-related selection? evidence from the whitehall ii cohort study, 1991–2004. *American Journal of Epidemiology*, 174(7):779–789, 2011.

Ronald D Ennis, Liangyuan Hu, Shannon N Ryemon, Joyce Lin, and Madhu Mazumdar. Brachytherapy-based radiotherapy and radical prostatectomy are associated with similar survival in high-risk localized prostate cancer. *Journal of Clinical Oncology*, 36(12):1192–1198, 2018.

Gary W Evans, Dongping Li, and Sara Sepanski Whipple. Cumulative risk and child development. *Psychological bulletin*, 139(6):1342, 2013.

Max H Farrell. Robust inference on average treatment effects with possibly more covariates than observations. *Journal of Econometrics*, 189(1):1–23, 2015.

Vincent J Felitti, Robert F Anda, Dale Nordenberg, David F Williamson, Alison M Spitz, Valerie Edwards, and James S Marks. Relationship of childhood abuse and household dysfunction to many of the leading causes of death in adults: The adverse childhood experiences (ace) study. *American Journal of Preventive Medicine*, 14 (4):245–258, 1998.

Jeremy Ferwerda. Electoral consequences of declining participation: A natural experiment in austria. *Electoral Studies*, 35:242–252, 2014.

Laura Forastiere, Alessandra Mattei, and Peng Ding. Principal ignorability in mediation analysis: through and beyond sequential ignorability. *Biometrika*, 105(4): 979–986, 2018.

David A. Freedman. On regression adjustments in experiments with several treatments. *The Annals of Applied Statistics*, 2(1):176–196, 2008.

Yaroslav Ganin, Evgeniya Ustinova, Hana Ajakan, Pascal Germain, Hugo Larochelle, François Laviolette, Mario Marchand, and Victor Lempitsky. Domain-adversarial training of neural networks. *The Journal of Machine Learning Research*, 17(1): 2096–2030, 2016.

Etienne Gayat, Matthieu Resche-Rigon, Jean-Yves Mary, and Raphaël Porcher. Propensity score applied to survival data analysis through proportional hazards models: a monte carlo study. *Pharmaceutical Statistics*, 11(3):222–229, 2012.

Robin Genuer, Jean-Michel Poggi, and Christine Tuleau-Malot. Variable selection using random forests. *Pattern Recognition Letters*, 31(14):2225–2236, 2010.

Peter D Gluckman, Mark A Hanson, Cyrus Cooper, and Kent L Thornburg. Effect of in utero and early-life conditions on adult health and disease. *New England Journal of Medicine*, 359(1):61–73, 2008.

Jeff Goldsmith, Sonja Greven, and CIPRIAN Crainiceanu. Corrected confidence bands for functional data using principal components. *Biometrics*, 69(1):41–51, 2013.

Thore Graepel, Joaquin Quinonero Candela, Thomas Borchert, and Ralf Herbrich. Web-scale bayesian click-through rate prediction for sponsored search advertising in microsoft's bing search engine. In *ICML*, 2010.

Frederik Graw, Thomas A Gerds, and Martin Schumacher. On pseudo-values for regression analysis in competing risks models. *Lifetime Data Analysis*, 15(2):241–255, 2009.

Kerry M Green and Elizabeth A Stuart. Examining moderation analyses in propensity score methods: application to depression and substance use. *Journal of Consulting and Clinical Psychology*, 82(5):773, 2014.

Arthur Gretton, Alex Smola, Jiayuan Huang, Marcel Schmittfull, Karsten Borgwardt, and Bernhard Schölkopf. Covariate shift by kernel mean matching. *Dataset shift in machine learning*, 3(4):5, 2009a.

Arthur Gretton, Alex Smola, Jiayuan Huang, Marcel Schmittfull, Karsten Borgwardt, and Bernhard Schölkopf. Covariate shift by kernel mean matching. *Dataset shift in machine learning*, 3(4):5, 2009b.

J Hahn. On the role of the propensity score in efficient semiparametric estimation of average treatment effects. *Econometrica*, 66(2):315–331, 1998.

Jens Hainmueller. Entropy balancing for causal effects: A multivariate reweighting method to produce balanced samples in observational studies. *Political Analysis*, 20(1):25–46, 2012.

J. Hájek. Comment on "an essay on the logical foundations of survey sampling by d. basu". In V. P. Godambe and D. A. Sprott, editors, *Foundations of Statistical Inference*. Holt, Rinehart and Winson, Toronto, 1971.

Kyunghee Han, Pantelis Z Hadjipantelis, Jane-Ling Wang, Michael S Kramer, Seungmi Yang, Richard M Martin, and Hans-Georg Müller. Functional principal component analysis for identifying multivariate patterns and archetypes of growth, and their association with long-term cognitive development. *PloS one*, 13(11):e0207073, 2018.

Sebastian Haneuse and Andrea Rotnitzky. Estimation of the effect of interventions that modify the received treatment. *Statistics in Medicine*, 32(30):5260–5277, 2013.

Sam Harper and Erin C Strumpf. Commentary: Social epidemiologyquestionable answers and answerable questions. *Epidemiology*, 23(6):795–798, 2012.

Negar Hassanpour and Russell Greiner. Counterfactual regression with importance sampling weights. In *Proceedings of the Twenty-Eighth International Joint Conference on Artificial Intelligence, IJCAI-19*, pages 5880–5887, 2019.

Trevor Hastie, Robert Tibshirani, Jerome Friedman, and James Franklin. The elements of statistical learning: data mining, inference and prediction. *The Mathematical Intelligencer*, 27(2):83–85, 2005.

Walter W. Hauck, Sharon Anderson, and Sue M. Marcus. Should we adjust for covariates in nonlinear regression analyses of randomized trials? *Controlled Clinical Trials*, 19(3):249–256, 1998. ISSN 01972456. doi: 10.1016/S0197-2456(97)00147-5.

Miguel A Hernán. The hazards of hazard ratios. *Epidemiology (Cambridge, Mass.)*, 21(1):13, 2010.

Miguel A Hernan and James M Robins. *Causal Inference*. CRC Boca Raton, FL, 2010.

Miguel A Hernán, Babette Brumback, and James M Robins. Marginal structural models to estimate the joint causal effect of nonrandomized treatments. *Journal of the American Statistical Association*, 96(454):440–448, 2001.

Miguel Ángel Hernán, Babette Brumback, and James M Robins. Marginal structural models to estimate the causal effect of zidovudine on the survival of hiv-positive men. *Epidemiology*, pages 561–570, 2000.

Adrián V. Hernández, Ewout W. Steyerberg, and J. Dik F. Habbema. Covariate adjustment in randomized controlled trials with dichotomous outcomes increases statistical power and reduces sample size requirements. *Journal of Clinical Epidemiology*, 57(5):454–460, 2004.

Jennifer L Hill. Bayesian nonparametric modeling for causal inference. *Journal of Computational and Graphical Statistics*, 20(1):217–240, 2011.

K Hirano and G W Imbens. Estimation of causal effects using propensity score weighting: An application to data on right heart catheterization. *Health Services and Outcomes Research Methodology*, 2:259–278, 2001.

K Hirano, G W Imbens, and G Ridder. Efficient estimation of average treatment effects using the estimated propensity score. *Econometrica*, 71(4):1161–1189, 2003.

Jean-Baptiste Hiriart-Urruty and Claude Lemaréchal. *Fundamentals of convex analysis*. Springer Science & Business Media, 2012.

Paul W Holland. Statistics and causal inference. *Journal of the American Statistical Association*, 81(396):945–960, 1986.

Julianne Holt-Lunstad, Timothy B Smith, and J Bradley Layton. Social relationships and mortality risk: a meta-analytic review. *PLoS Medicine*, 7(7):e1000316, 2010.

Julianne Holt-Lunstad, Timothy B Smith, Mark Baker, Tyler Harris, and David Stephenson. Loneliness and social isolation as risk factors for mortality: a meta-analytic review. *Perspectives on psychological science*, 10(2):227–237, 2015.

Biwei Huang, Kun Zhang, Jiji Zhang, Joseph Ramsey, Ruben Sanchez-Romero, Clark Glymour, and Bernhard Schölkopf. Causal discovery from heterogeneous/nonstationary data. *Journal of Machine Learning Research*, 21(89):1–53, 2020.

Jiayuan Huang, Arthur Gretton, Karsten Borgwardt, Bernhard Schölkopf, and Alex J Smola. Correcting sample selection bias by unlabeled data. In *Advances in Neural Information Processing Systems*, pages 601–608, 2007.

Alan E Hubbard, Mark J Van Der Laan, and James M Robins. Nonparametric locally efficient estimation of the treatment specific survival distribution with right censored data and covariates in observational studies. In *Statistical Models in Epidemiology, the Environment, and Clinical Trials*, pages 135–177. Springer, 2000.

K Imai and M Ratkovic. Covariate balancing propensity score. *Journal of the Royal Statistical Society: Series B*, 76(1):243–263, 2014.

Kosuke Imai, Luke Keele, and Dustin Tingley. A general approach to causal mediation analysis. *Psychological Methods*, 15(4):309, 2010a.

Kosuke Imai, Luke Keele, and Teppei Yamamoto. Identification, inference and sensitivity analysis for causal mediation effects. *Statistical Science*, pages 51–71, 2010b.

Kosuke Imai, Marc Ratkovic, et al. Estimating treatment effect heterogeneity in randomized program evaluation. *The Annals of Applied Statistics*, 7(1):443–470, 2013.

G W Imbens. Nonparametric estimation of average treatment effects under exogeneity: A review. *The Review of Economics and Statistics*, 86(1):4–29, 2004.

Guido W Imbens. The role of the propensity score in estimating dose-response functions. *Biometrika*, 87(3):706–710, 2000.

Guido W Imbens, Whitney K Newey, and Geert Ridder. Mean-square-error calculations for average treatment effects. *IEPR Working Paper No.05.34*, 2005.

GW Imbens and DB Rubin. *Causal Inference for Statistics, Social, and Biomedical Sciences: An Introduction*. Cambridge University Press, New York, 2015.

Martin Jacobsen and Torben Martinussen. A note on the large sample properties of estimators based on generalized linear models for correlated pseudo-observations. *Scandinavian Journal of Statistics*, 43(3):845–862, 2016.

Lancelot F James et al. A study of a class of weighted bootstraps for censored data. *Annals of Statistics*, 25(4):1595–1621, 1997.

Edwin T Jaynes. Information theory and statistical mechanics. *Physical Review*, 106 (4):620, 1957a.

Edwin T Jaynes. Information theory and statistical mechanics. ii. *Physical Review*, 108(2):171, 1957b.

Haomiao Jia and Erica I Lubetkin. Impact of adverse childhood experiences on quality-adjusted life expectancy in the us population. *Child Abuse & Neglect*, 102: 104418, 2020.

Ci-Ren Jiang and Jane-Ling Wang. Covariate adjusted functional principal components analysis for longitudinal data. *The Annals of Statistics*, 38(2):1194–1226, 2010.

Ci-Ren Jiang and Jane-Ling Wang. Functional single index models for longitudinal data. *The Annals of Statistics*, 39(1):362–388, 2011.

Nan Jiang and Lihong Li. Doubly robust off-policy value evaluation for reinforcement learning. In *International Conference on Machine Learning*, pages 652–661, 2016.

Marshall M Joffe, Thomas R Ten Have, Harold I Feldman, and Stephen E Kimmel. Model selection, confounder control, and marginal structural models: review and new applications. *The American Statistician*, 58(4):272–279, 2004.

Fredrik Johansson, Uri Shalit, and David Sontag. Learning representations for counterfactual inference. In *International Conference on Machine Learning*, pages 3020–3029, 2016.

Fredrik D Johansson, Nathan Kallus, Uri Shalit, and David Sontag. Learning weighted representations for generalization across designs. *arXiv preprint arXiv:1802.08598*, 2018.

Edmund Juszczak, Douglas G. Altman, Sally Hopewell, and Kenneth Schulz. Reporting of Multi-Arm Parallel-Group Randomized Trials: Extension of the CONSORT 2010 Statement. *Journal of the American Medical Association*, 321(16):1610–1620, 2019.

Brennan C. Kahan, Vipul Jairath, Caroline J. Doré, and Tim P. Morris. The risks and rewards of covariate adjustment in randomized trials: An assessment of 12 outcomes from 8 studies. *Trials*, 15(1):1–7, 2014.

Brennan C. Kahan, Helen Rushton, Tim P. Morris, and Rhian M. Daniel. A comparison of methods to adjust for continuous covariates in the analysis of randomised trials. *BMC Medical Research Methodology*, 16(1):1–10, 2016.

Nathan Kallus. Balanced policy evaluation and learning. In *Advances in Neural Information Processing Systems*, pages 8895–8906, 2018a.

Nathan Kallus. Deepmatch: Balancing deep covariate representations for causal inference using adversarial training. *arXiv preprint arXiv:1802.05664*, 2018b.

Nathan Kallus. Generalized optimal matching methods for causal inference. *Journal of Machine Learning Research*, 2019.

Nathan Kallus and Masatoshi Uehara. Double reinforcement learning for efficient off-policy evaluation in markov decision processes. *arXiv preprint arXiv:1908.08526*, 2019.

Nathan Kallus, Aahlad Manas Puli, and Uri Shalit. Removing hidden confounding by experimental grounding. In *Advances in Neural Information Processing Systems*, pages 10888–10897, 2018.

Joseph DY Kang, Joseph L Schafer, et al. Demystifying double robustness: A comparison of alternative strategies for estimating a population mean from incomplete data. *Statistical Science*, 22(4):523–539, 2007.

Guolin Ke, Qi Meng, Thomas Finley, Taifeng Wang, Wei Chen, Weidong Ma, Qiwei Ye, and Tie-Yan Liu. Lightgbm: A highly efficient gradient boosting decision tree. In *Advances in Neural Information Processing Systems*, pages 3146–3154, 2017.

Alexander P Keil, Jessie K Edwards, David R Richardson, Ashley I Naimi, and Stephen R Cole. The parametric g-formula for time-to-event data: towards intuition with a worked example. *Epidemiology (Cambridge, Mass.)*, 25(6):889, 2014.

Edward H Kennedy. Semiparametric theory and empirical processes in causal inference. In *Statistical causal inferences and their applications in public health research*, pages 141–167. Springer, 2016.

Chanmin Kim, Michael J Daniels, Bess H Marcus, and Jason A Roy. A framework for bayesian nonparametric inference for causal effects of mediation. *Biometrics*, 73(2):401–409, 2017.

Chanmin Kim, Michael Daniels, Yisheng Li, Kathrin Milbury, and Lorenzo Cohen. A bayesian semiparametric latent variable approach to causal mediation. *Statistics in Medicine*, 37(7):1149–1161, 2018.

Chanmin Kim, Michael J Daniels, Joseph W Hogan, Christine Choirat, and Corwin M Zigler. Bayesian methods for multiple mediators: Relating principal stratification and causal mediation in the analysis of power plant emission controls. *The Annals of Applied Statistics*, 13(3):1927, 2019.

Maiken IS Kjaersgaard and Erik T Parner. Instrumental variable method for time-to-event data using a pseudo-observation approach. *Biometrics*, 72(2):463–472, 2016.

John P Klein and Per Kragh Andersen. Regression modeling of competing risks data based on pseudovalues of the cumulative incidence function. *Biometrics*, 61(1): 223–229, 2005.

John P Klein, Brent Logan, Mette Harhoff, and Per Kragh Andersen. Analyzing survival curves at a fixed point in time. *Statistics in Medicine*, 26(24):4505–4519, 2007.

John P Klein, Mette Gerster, Per Kragh Andersen, Sergey Tarima, and Maja Pohar Perme. Sas and r functions to compute pseudo-values for censored data regression. *Computer Methods and Programs in Biomedicine*, 89(3):289–300, 2008.

Ron Kohavi and Roger Longbotham. Online controlled experiments and a/b testing. *Encyclopedia of machine learning and data mining*, pages 922–929, 2017.

Ron Kohavi, Alex Deng, Brian Frasca, Toby Walker, Ya Xu, and Nils Pohlmann. Online controlled experiments at large scale. In *Proceedings of the 19th ACM SIGKDD international conference on Knowledge discovery and data mining*, pages 1168–1176. ACM, 2013.

Daniel R Kowal. Dynamic function-on-scalars regression. *arXiv preprint arXiv:1806.01460*, 2018.

Daniel R Kowal and Daniel C Bourgeois. Bayesian function-on-scalars regression for high-dimensional data. *Journal of Computational and Graphical Statistics*, 29(3): 629–638, 2020.

Hannes Kröger, Eduwin Pakpahan, and Rasmus Hoffmann. What causes health inequality? a systematic review on the relative importance of social causation and health selection. *The European Journal of Public Health*, 25(6):951–960, 2015.

Kun Kuang, Peng Cui, Susan Athey, Ruoxuan Xiong, and Bo Li. Stable prediction across unknown environments. In *Proceedings of the 24th ACM SIGKDD International Conference on Knowledge Discovery & Data Mining*, pages 1617–1626, 2018.

Sören R Künzel, Jasjeet S Sekhon, Peter J Bickel, and Bin Yu. Metalearners for estimating heterogeneous treatment effects using machine learning. *Proceedings of the National Academy of Sciences*, 116(10):4156–4165, 2019.

Nan M Laird and James H Ware. Random-effects models for longitudinal data. *Biometrics*, pages 963–974, 1982.

Robert J LaLonde. Evaluating the econometric evaluations of training programs with experimental data. *The American Economic Review*, pages 604–620, 1986.

Richard Landerman, Linda K George, Richard T Campbell, and Dan G Blazer. Alternative models of the stress buffering hypothesis. *American Journal of Community Psychology*, 17(5):625–642, 1989.

Theis Lange, Stijn Vansteelandt, and Maarten Bekaert. A simple unified approach for estimating natural direct and indirect effects. *American Journal of Epidemiology*, 176(3):190–195, 2012.

Finnian Lattimore, Tor Lattimore, and Mark D Reid. Causal bandits: Learning good interventions via causal inference. In *Advances in Neural Information Processing Systems*, pages 1181–1189, 2016.

David Lazer, Ryan Kennedy, Gary King, and Alessandro Vespignani. The parable of google flu: traps in big data analysis. *Science*, 343(6176):1203–1205, 2014.

Elisa T Lee and John Wang. *Statistical methods for survival data analysis*, volume 476. John Wiley & Sons, 2003.

Erich L Lehmann and George Casella. *Theory of point estimation*. Springer Science & Business Media, 2006.

Selene Leon, Anastasios A Tsiatis, and Marie Davidian. Semiparametric estimation of treatment effect in a pretest-posttest study. *Biometrics*, 59(4):1046–1055, 2003.

C. Leyrat, A. Caille, A. Donner, and B. Giraudeau. Propensity scores used for analysis of cluster randomized trials with selection bias: A simulation study. *Statistics in Medicine*, 32(19):3357–3372, 2013.

Clémence Leyrat, Agnès Caille, Allan Donner, and Bruno Giraudeau. Propensity score methods for estimating relative risks in cluster randomized trials with low-incidence binary outcomes and selection bias. *Statistics in Medicine*, 33(20):3556–3575, 2014.

Fan Li. Comment: Stabilizing the doubly-robust estimators of the average treatment effect under positivity violations. *Statistical Science*, 0(0):1–10, 2020.

Fan Li and Fan Li. Double-robust estimation in difference-in-differences with an application to traffic safety evaluation. *Observational Studies*, 5:1–20, 2019a.

Fan Li and Fan Li. Propensity score weighting for causal inference with multiple

treatments. *The Annals of Applied Statistics*, 13(4):2389–2415, 2019b.

Fan Li, Alan M Zaslavsky, and Mary Beth Landrum. Propensity score weighting with multilevel data. *Statistics in Medicine*, 32(19):3373–3387, 2013.

Fan Li, Yuliya Lokhnygina, David M. Murray, Patrick J. Heagerty, and Elizabeth R. Delong. An evaluation of constrained randomization for the design and analysis of group-randomized trials. *Statistics in Medicine*, 35(10):1565–1579, 2016. ISSN 10970258.

Fan Li, Elizabeth L. Turner, Patrick J. Heagerty, David M. Murray, William M. Vollmer, and Elizabeth R. Delong. An evaluation of constrained randomization for the design and analysis of group-randomized trials with binary outcomes. *Statistics in Medicine*, 36:3791–3806, 2017. ISSN 10970258.

Fan Li, Kari Lock Morgan, and Alan M Zaslavsky. Balancing covariates via propensity score weighting. *Journal of the American Statistical Association*, 113(521): 390–400, 2018a.

Fan Li, Laine E Thomas, and Fan Li. Addressing extreme propensity scores via the overlap weights. *American Journal of Epidemiology*, 188(1):250–257, 2019.

L Li and T Greene. A weighting analogue to pair matching in propensity score analysis. *International Journal of Biostatistics*, 9(2):1–20, 2013.

Lihong Li, Wei Chu, John Langford, Taesup Moon, and Xuanhui Wang. An unbiased offline evaluation of contextual bandit algorithms with generalized linear models. In *Proceedings of the Workshop on On-line Trading of Exploration and Exploitation 2*, pages 19–36, 2012.

Lihong Li, Shunbao Chen, Jim Kleban, and Ankur Gupta. Counterfactual estimation and optimization of click metrics in search engines: A case study. In *Proceedings of the 24th International Conference on World Wide Web*, pages 929–934. ACM, 2015.

Ya Li, Xinmei Tian, Mingming Gong, Yajing Liu, Tongliang Liu, Kun Zhang, and Dacheng Tao. Deep domain generalization via conditional invariant adversarial networks. In *Proceedings of the European Conference on Computer Vision (ECCV)*, pages 624–639, 2018b.

Kung-Yee Liang and Scott L Zeger. Longitudinal data analysis using generalized linear models. *Biometrika*, 73(1):13–22, 1986.

Bryan Lim. Forecasting treatment responses over time using recurrent marginal structural networks. In *Advances in Neural Information Processing Systems*, pages 7483–7493, 2018.

Sheng-Hsuan Lin, Jessica Young, Roger Logan, Eric J Tchetgen Tchetgen, and Tyler J VanderWeele. Parametric mediational g-formula approach to mediation analysis with time-varying exposures, mediators, and confounders. *Epidemiology (Cambridge, Mass.)*, 28(2):266, 2017a.

Sheng-Hsuan Lin, Jessica G Young, Roger Logan, and Tyler J VanderWeele. Mediation analysis for a survival outcome with time-varying exposures, mediators, and confounders. *Statistics in Medicine*, 36(26):4153–4166, 2017b.

Winston Lin. Agnostic notes on regression adjustments to experimental data: Reexamining freedman's critique. *The Annals of Applied Statistics*, 7(1):295–318, 2013.

Martin A Lindquist. Functional causal mediation analysis with an application to brain connectivity. *Journal of the American Statistical Association*, 107(500):1297–1309, 2012.

Martin A Lindquist and Michael E Sobel. Graphical models, potential outcomes and causal inference: Comment on ramsey, spirtes and glymour. *NeuroImage*, 57(2): 334–336, 2011.

Jan Lindström. Early development and fitness in birds and mammals. *Trends in Ecology & Evolution*, 14(9):343–348, 1999.

Anqi Liu and Brian Ziebart. Robust classification under sample selection bias. In *Advances in Neural Information Processing Systems*, pages 37–45, 2014.

Christos Louizos, Uri Shalit, Joris M Mooij, David Sontag, Richard Zemel, and Max Welling. Causal effect inference with deep latent-variable models. In *Advances in Neural Information Processing Systems*, pages 6446–6456, 2017.

Jared K Lunceford and Marie Davidian. Stratification and weighting via the propensity score in estimation of causal treatment effects: a comparative study. *Statistics in Medicine*, 23(19):2937–2960, 2004a.

JK Lunceford and M Davidian. Stratification and weighting via the propensity score in estimation of causal treatment effects: A comparative study. *Statistics in Medicine*, 23:2937–2960, 2004b.

Laurens van der Maaten and Geoffrey Hinton. Visualizing data using t-sne. *Journal of Machine Learning Research*, 9(Nov):2579–2605, 2008.

David MacKinnon. *Introduction to statistical mediation analysis*. Routledge, 2012.

Sara Magliacane, Thijs van Ommen, Tom Claassen, Stephan Bongers, Philip Versteeg, and Joris M Mooij. Domain adaptation by using causal inference to predict invariant conditional distributions. In *Advances in Neural Information Processing Systems*, pages 10846–10856, 2018.

Huzhang Mao, Liang Li, Wei Yang, and Yu Shen. On the propensity score weighting analysis with survival outcome: Estimands, estimation, and inference. *Statistics in Medicine*, 37(26):3745–3763, 2018.

Huzhang Mao, Liang Li, and Tom Greene. Propensity score weighting analysis and treatment effect discovery. *Statistical Methods in Medical Research*, 28(8):2439–2454, 2019.

Jan Marcus. The effect of unemployment on the mental health of spouses–evidence from plant closures in germany. *Journal of Health Economics*, 32(3):546–558, 2013.

Michael Marmot, Carol D Ryff, Larry L Bumpass, Martin Shipley, and Nadine F Marks. Social inequalities in health: next questions and converging evidence. *Social Science & Medicine*, 44(6):901–910, 1997.

Michael G Marmot, Stephen Stansfeld, Chandra Patel, Fiona North, Jenny Head, Ian White, Eric Brunner, Amanda Feeney, and G Davey Smith. Health inequalities among british civil servants: the whitehall ii study. *The Lancet*, 337(8754):1387–1393, 1991.

Bruce S McEwen. Stress, adaptation, and disease: Allostasis and allostatic load. *Annals of the New York Academy of Sciences*, 840(1):33–44, 1998.

Bruce S McEwen. Central effects of stress hormones in health and disease: Understanding the protective and damaging effects of stress and stress mediators. *European Journal of Pharmacology*, 583(2-3):174–185, 2008.

Nicolai Meinshausen. Causality from a distributional robustness point of view. In *2018 IEEE Data Science Workshop (DSW)*, pages 6–10. IEEE, 2018.

Scott Menard. *Applied logistic regression analysis*, volume 106. Sage, 2002.

Andrea Mercatanti and Fan Li. Do debit cards increase household spending? evidence from a semiparametric causal analysis of a survey. *The Annals of Applied Statistics*, 8(4):2485–2508, 2014.

Gregory E Miller, Sheldon Cohen, and A Kim Ritchey. Chronic psychological stress and the regulation of pro-inflammatory cytokines: a glucocorticoid-resistance model. *Health Psychology*, 21(6):531, 2002.

Gregory E Miller, Edith Chen, and Karen J Parker. Psychological stress in childhood and susceptibility to the chronic diseases of aging: moving toward a model of behavioral and biological mechanisms. *Psychological Bulletin*, 137(6):959, 2011.

Silvia Montagna, Surya T Tokdar, Brian Neelon, and David B Dunson. Bayesian latent factor regression for functional and longitudinal data. *Biometrics*, 68(4): 1064–1073, 2012.

K. L. Moore and Mark J. van der Laan. Covariate adjustment in randomized trials with binary outcomes: Targeted maximum likelihood estimation. *Statistics in Medicine*, 28(1):39–64, 2009.

Kelly L. Moore, Romain Neugebauer, Thamban Valappil, and Mark J. van der Laan. Robust extraction of covariate information to improve estimation efficiency in randomized trials. *Statistics in Medicine*, 30(19):2389–2408, 2011.

Øyvind Næss, Bjøgulf Claussen, and George Davey Smith. Relative impact of childhood and adulthood socioeconomic conditions on cause specific mortality in men. *Journal of Epidemiology & Community Health*, 58(7):597–598, 2004.

Radford M Neal. Annealed importance sampling. *Statistics and Computing*, 11(2): 125–139, 2001.

Daniel Nettle. What the future held: Childhood psychosocial adversity is associated with health deterioration through adulthood in a cohort of british women. *Evolution and Human Behavior*, 35(6):519–525, 2014.

J Neyman. On the application of probability theory to agricultural experiments: Essay on principles, section 9. *Statistical Science*, 5(4):465–480, 1990.

Trang Quynh Nguyen, Ian Schmid, and Elizabeth A Stuart. Clarifying causal mediation analysis for the applied researcher: Defining effects based on what we want to learn. *Psychological Methods*, page in press, 2020.

Martin Nygård Johansen, Søren Lundbye-Christensen, and Erik Thorlund Parner. Regression models using parametric pseudo-observations. *Statistics in Medicine*, 2020.

Morten Overgaard, Erik Thorlund Parner, Jan Pedersen, et al. Asymptotic theory of generalized estimating equations based on jack-knife pseudo-observations. *The Annals of Statistics*, 45(5):1988–2015, 2017.

Morten Overgaard, Erik Thorlund Parner, and Jan Pedersen. Pseudo-observations under covariate-dependent censoring. *Journal of Statistical Planning and Inference*, 202:112–122, 2019.

Vishal M Patel, Raghuraman Gopalan, Ruonan Li, and Rama Chellappa. Visual domain adaptation: A survey of recent advances. *IEEE Signal Processing Magazine*, 32(3):53–69, 2015.

Judea Pearl. Direct and indirect effects. In *Proceedings of the Seventeenth Conference on Uncertainty in Artificial Intelligence*, pages 411–420. Morgan Kaufmann Publishers Inc., 2001.

Judea Pearl. *Causality*. Cambridge university press, 2009.

Judea Pearl et al. Causal inference in statistics: An overview. *Statistics Surveys*, 3: 96–146, 2009.

F. Pedregosa, G. Varoquaux, A. Gramfort, V. Michel, B. Thirion, O. Grisel, M. Blondel, P. Prettenhofer, R. Weiss, V. Dubourg, J. Vanderplas, A. Passos, D. Cournapeau, M. Brucher, M. Perrot, and E. Duchesnay. Scikit-learn: Machine learning in Python. *Journal of Machine Learning Research*, 12:2825–2830, 2011.

Maja Pohar Perme and Per Kragh Andersen. Checking hazard regression models using pseudo-observations. *Statistics in Medicine*, 27(25):5309–5328, 2008.

Jonas Peters, Peter Bühlmann, and Nicolai Meinshausen. Causal inference by using invariant prediction: identification and confidence intervals. *Journal of the Royal Statistical Society: Series B (Statistical Methodology)*, 78(5):947–1012, 2016.

Kaitlyn Petruccelli, Joshua Davis, and Tara Berman. Adverse childhood experiences and associated health outcomes: A systematic review and meta-analysis. *Child abuse & neglect*, 97:104127, 2019.

Stuart J. Pocock, Susan E. Assmann, Laura E. Enos, and Linda E. Kasten. Subgroup analysis, covariate adjustment and baseline comparisons in clinical trial reporting: Current practice and problems. *Statistics in Medicine*, 21(19):2917–2930, 2002.

Jason Poulos and Shuxi Zeng. Rnn-based counterfactual prediction, with an application to homestead policy and public schooling. *arXiv preprint arXiv:1712.03553*, 2017.

Scott Powers, Junyang Qian, Kenneth Jung, Alejandro Schuler, Nigam H Shah, Trevor Hastie, and Robert Tibshirani. Some methods for heterogeneous treatment effect estimation in high dimensions. *Statistics in Medicine*, 37(11):1767–1787,

2018.

Joaquin Quionero-Candela, Masashi Sugiyama, Anton Schwaighofer, and Neil D Lawrence. *Dataset shift in machine learning*. The MIT Press, 2009.

Gillian M. Raab, Simon Day, and Jill Sales. How to select covariates to include in the analysis of a clinical trial. *Controlled Clinical Trials*, 21(4):330–342, 2000.

Hanaya Raad, Victoria Cornelius, Susan Chan, Elizabeth Williamson, and Suzie Cro. An evaluation of inverse probability weighting using the propensity score for baseline covariate adjustment in smaller population randomised controlled trials. *BMC Medical Research Methodology*, 70(20):000, 2020.

James Ramsay and Bernard Silverman. *Functional Data Analysis*. Springer, 2005.

Michelle L Reid, Kevin J Gleason, Jessie P Bakker, Rui Wang, Murray A Mittleman, and Susan Redline. The role of sham continuous positive airway pressure as a placebo in controlled trials: Best apnea interventions for research trial. *Sleep*, 42 (8):zsz099, 2019.

James Robins. A new approach to causal inference in mortality studies with a sustained exposure period—application to control of the healthy worker survivor effect. *Mathematical modelling*, 7(9-12):1393–1512, 1986.

James M Robins. Marginal structural models versus structural nested models as tools for causal inference. In *Statistical models in epidemiology, the environment, and clinical trials*, pages 95–133. Springer, 2000.

James M Robins. Semantics of causal dag models and the identification of direct and indirect effects, 2003.

James M Robins and Dianne M Finkelstein. Correcting for noncompliance and dependent censoring in an aids clinical trial with inverse probability of censoring weighted (ipcw) log-rank tests. *Biometrics*, 56(3):779–788, 2000.

James M Robins and Sander Greenland. Identifiability and exchangeability for direct and indirect effects. *Epidemiology*, pages 143–155, 1992.

James M Robins, Andrea Rotnitzky, and Lue Ping Zhao. Estimation of regression coefficients when some regressors are not always observed. *Journal of the American Statistical Association*, 89(427):846–866, 1994.

James M Robins, Andrea Rotnitzky, and Lue Ping Zhao. Analysis of semiparametric regression models for repeated outcomes in the presence of missing data. *Journal of the American Statistical Association*, 90(429):106–121, 1995.

James M Robins, Sander Greenland, and Fu-Chang Hu. Estimation of the causal effect of a time-varying exposure on the marginal mean of a repeated binary outcome. *Journal of the American Statistical Association*, 94(447):687–700, 1999.

James M Robins, Miguel Angel Hernan, and Babette Brumback. Marginal structural models and causal inference in epidemiology. *Epidemiology*, 11(5), 2000a.

J.M. Robins and A G Rotnitzky. Comment on the bickel and kwon article, 'inference for semiparametric models: Some questions and an answer'. *Statistica Sinica*, 11:

920–936, 01 2001.

JM Robins, MA Hernán, and B Brumback. Marginal structural models and causal inference. *Epidemiology*, 11:550–560, 2000b.

Laurence D. Robinson and Nicholas P. Jewell. Some Surprising Results about Covariate Adjustment in Logistic Regression Models. *International Statistical Review*, 59 (2):227, 1991.

Mateo Rojas-Carulla, Bernhard Schölkopf, Richard Turner, and Jonas Peters. Invariant models for causal transfer learning. *The Journal of Machine Learning Research*, 19(1):1309–1342, 2018.

Tessa Roseboom, Susanne de Rooij, and Rebecca Painter. The dutch famine and its long-term consequences for adult health. *Early human development*, 82(8):485–491, 2006.

Tessa J Roseboom, Jan HP van der Meulen, Clive Osmond, David JP Barker, Anita CJ Ravelli, Jutta M Schroeder-Tanka, Gert A van Montfrans, Robert PJ Michels, and Otto P Bleker. Coronary heart disease after prenatal exposure to the dutch famine, 1944–45. *Heart*, 84(6):595–598, 2000.

P R Rosenbaum and D B Rubin. The central role of the propensity score in observational studies for causal effects. *Biometrika*, 70(1):41–55, 1983.

Paul Rosenbaum. *Observational Studies*. Springer, New York, 2002.

S Rosenbaum, S Zeng, F Campos, L Gesquiere, J Altmann, S Alberts, F Li, and E Archie. Social bonds do not mediate the relationship between early adversity and adult glucocorticoids in wild baboons. *Proceedings of the National Academy of Sciences*, page in press, 2020.

W.F. Rosenberger and J.M. Lachin. *Randomization in clinical trials: theory and practice.* Wiley Interscience, New York, NY, 2002.

David L Roth and David P MacKinnon. Mediation analysis with longitudinal data. *Longitudinal data analysis: A practical guide for researchers in aging, health, and social sciences*, pages 181–216, 2012.

D B Rubin. Estimating causal effects of treatments in randomized and nonrandomized studies. *Journal of Educational Psychology*, 66(1):688–701, 1974.

D. B. Rubin. Bayesian inference for causal effects: The role of randomization. *The Annals of Statistics*, 6:34–58, 1978.

D B Rubin. Using multivariate matched sampling and regression adjustment to control bias in observational studies. *Journal of the American Statistical Association*, 74(366):318–324, 1979.

Donald B Rubin. Randomization analysis of experimental data: The fisher randomization test comment. *Journal of the American Statistical Association*, 75(371): 591–593, 1980.

Donald B Rubin. *Matched sampling for causal effects*. Cambridge University Press, 2006.

Donald B Rubin. For objective causal inference, design trumps analysis. *The Annals of Applied Statistics*, 2(3):808–840, 2008.

DO Scharfstein, A Rotnitzky, and JM Robins. Adjusting for nonignorable drop-out using semiparametric nonresponse models (with discussion). *Journal of the American Statistical Association*, 94:1096–1146, 1999.

E C Schneider, P D Cleary, A M Zaslavsky, and A M Epstein. Racial disparity in influenza vaccination: Does managed care narrow the gap between African Americans and whites? *Journal of the American Medical Association*, 286(12):1455–1460, 2001.

Shaun R Seaman and Stijn Vansteelandt. Introduction to double robust methods for incomplete data. *Statistical Science*, 33(2):184, 2018.

S. J. Senn. Covariate imbalance and random allocation in clinical trials. *Statistics in Medicine*, 8(4):467–475, 1989.

Uri Shalit, Fredrik D Johansson, and David Sontag. Estimating individual treatment effect: generalization bounds and algorithms. In *Proceedings of the 34th International Conference on Machine Learning-Volume 70*, pages 3076–3085. JMLR. org, 2017.

Changyu Shen, Xiaochun Li, and Lingling Li. Inverse probability weighting for covariate adjustment in randomized studies. *Statistics in Medicine*, 33(4):555–568, 2014.

Susan M Shortreed and Ashkan Ertefaie. Outcome-adaptive lasso: Variable selection for causal inference. *Biometrics*, 73(4):1111–1122, 2017.

Ilya Shpitser and Tyler J VanderWeele. A complete graphical criterion for the adjustment formula in mediation analysis. *The International Journal of Biostatistics*, 7(1), 2011.

Joan B Silk. The adaptive value of sociality in mammalian groups. *Philosophical Transactions of the Royal Society B: Biological Sciences*, 362(1480):539–559, 2007.

Joan B Silk, Jeanne Altmann, and Susan C Alberts. Social relationships among adult female baboons (papio cynocephalus) i. variation in the strength of social bonds. *Behavioral Ecology and Sociobiology*, 61(2):183–195, 2006.

Gabrielle Simoneau, Erica EM Moodie, Jagtar S Nijjar, Robert W Platt, and Scottish Early Rheumatoid Arthritis Inception Cohort Investigators. Estimating optimal dynamic treatment regimes with survival outcomes. *Journal of the American Statistical Association*, pages 1–9, 2019.

Noah Snyder-Mackler, Joseph Robert Burger, Lauren Gaydosh, Daniel W Belsky, Grace A Noppert, Fernando A Campos, Alessandro Bartolomucci, Yang Claire Yang, Allison E Aiello, Angela O'Rand, Mullan Harris, C. A. Shively, S. Alberts, and J. Tung. Social determinants of health and survival in humans and other animals. *Science*, 368(6493), 2020.

Michael E Sobel. Identification of causal parameters in randomized studies with mediating variables. *Journal of Educational and Behavioral Statistics*, 33(2):230–

251, 2008.

Leonard A Stefanski and Dennis D Boos. The calculus of m-estimation. *The American Statistician*, 56(1):29–38, 2002.

Alisa J. Stephens, Eric J. Tchetgen Tchetgen, and Victor De Gruttola. Augmented generalized estimating equations for improving efficiency and validity of estimation in cluster randomized trials by leveraging cluster-level and individual-level covariates. *Statistics in Medicine*, 31(10):915–930, 2012.

Alisa J. Stephens, Eric J.Tchetgen Tchetgen, and Victor De Gruttola. Flexible covariate-adjusted exact tests of randomized treatment effects with application to a trial of HIV education. *Annals of Applied Statistics*, 7(4):2106–2137, 2013.

Chien-Lin Su, Robert W Platt, and Jean-François Plante. Causal inference for recurrent event data using pseudo-observations. *Biostatistics*, 2020.

Yi Su, Maria Dimakopoulou, Akshay Krishnamurthy, and Miroslav Dudík. Doubly robust off-policy evaluation with shrinkage. *arXiv preprint arXiv:1907.09623*, 2019.

Masahiro Sugihara. Survival analysis using inverse probability of treatment weighted methods based on the generalized propensity score. *Pharmaceutical Statistics: The Journal of Applied Statistics in the Pharmaceutical Industry*, 9(1):21–34, 2010.

Masashi Sugiyama, Matthias Krauledat, and Klaus-Robert MÃžller. Covariate shift adaptation by importance weighted cross validation. *Journal of Machine Learning Research*, 8(May):985–1005, 2007.

Masashi Sugiyama, Shinichi Nakajima, Hisashi Kashima, Paul V Buenau, and Motoaki Kawanabe. Direct importance estimation with model selection and its application to covariate shift adaptation. In *Advances in Neural Information Processing Systems*, pages 1433–1440, 2008.

Adith Swaminathan and Thorsten Joachims. Batch learning from logged bandit feedback through counterfactual risk minimization. *Journal of Machine Learning Research*, 16(1):1731–1755, 2015a.

Adith Swaminathan and Thorsten Joachims. Counterfactual risk minimization: Learning from logged bandit feedback. In *International Conference on Machine Learning*, pages 814–823, 2015b.

Shiro Tanaka, M Alan Brookhart, and Jason P Fine. G-estimation of structural nested mean models for competing risks data using pseudo-observations. *Biostatistics*, 21 (4):860–875, 2020.

Shuhan Tang, Shu Yang, Tongrong Wang, Zhanglin Cui, Li Li, and Douglas E Faries. Causal inference of hazard ratio based on propensity score matching. *arXiv preprint arXiv:1911.12430*, 2019.

Chenyang Tao, Liqun Chen, Shuyang Dai, Junya Chen, Ke Bai, Dong Wang, Jianfeng Feng, Wenlian Lu, Georgiy Bobashev, and Lawrence Carin. On fenchel mini-max learning. In *Advances in Neural Information Processing Systems*, pages 3559–3569, 2019.

Eric J Tchetgen Tchetgen and Ilya Shpitser. Semiparametric theory for causal me-

diation analysis: efficiency bounds, multiple robustness, and sensitivity analysis. *Annals of Statistics*, 40(3):1816, 2012.

Thomas R Ten Have and Marshall M Joffe. A review of causal estimation of effects in mediation analyses. *Statistical Methods in Medical Research*, 21(1):77–107, 2012.

Laine E Thomas, Fan Li, and Michael J Pencina. Overlap weighting: A propensity score method that mimics attributes of a randomized clinical trial. *Journal of the American Medical Association*, 323(23):2417–2418, 2020a.

Laine E Thomas, Fan Li, and Michael J Pencina. Using propensity score methods to create target populations in observational clinical research. *Journal of the American Medical Association*, 323(5):466–467, 2020b.

Douglas D. Thompson, Hester F. Lingsma, William N. Whiteley, Gordon D. Murray, and Ewout W. Steyerberg. Covariate adjustment had similar benefits in small and large randomized controlled trials. *Journal of Clinical Epidemiology*, 68(9): 1068–1075, 2015.

Einar B Thorsteinsson and Jack E James. A meta-analysis of the effects of experimental manipulations of social support during laboratory stress. *Psychology and Health*, 14(5):869–886, 1999.

Anastasios Tsiatis. *Semiparametric theory and missing data*. Springer Science & Business Media, 2007.

Anastasios A Tsiatis, Marie Davidian, Min Zhang, and Xiaomin Lu. Covariate adjustment for two-sample treatment comparisons in randomized clinical trials: a principled yet flexible approach. *Statistics in Medicine*, 27(23):4658–4677, 2008.

Jenny Tung, Elizabeth A Archie, Jeanne Altmann, and Susan C Alberts. Cumulative early life adversity predicts longevity in wild baboons. *Nature Communications*, 7 (1):1–7, 2016.

Elizabeth L. Turner, Fan Li, John A. Gallis, Melanie Prague, and David M. Murray. Review of recent methodological developments in group-randomized trials: part 1–design. *American Journal of Public Health*, 107(6):907–915, 2017.

Eric Tzeng, Judy Hoffman, Kate Saenko, and Trevor Darrell. Adversarial discriminative domain adaptation. In *Proceedings of the IEEE Conference on Computer Vision and Pattern Recognition*, pages 7167–7176, 2017.

Mark J van der Laan and Maya L Petersen. Direct effect models. *The International Journal of Biostatistics*, 4(1), 2008.

Mark J van der Laan and James M Robins. *Unified methods for censored longitudinal data and causality*. Springer Science & Business Media, 2003.

Mark J Van der Laan and Sherri Rose. *Targeted learning: causal inference for observational and experimental data*. Springer Science & Business Media, 2011.

Mark J Van Der Laan and Daniel Rubin. Targeted maximum likelihood learning. *The International Journal of Biostatistics*, 2(1), 2006.

Mark J Van der Laan, Eric C Polley, and Alan E Hubbard. Super learner. *Statistical*

Applications in Genetics and Molecular Biology, 6(1), 2007.

Aad W Van der Vaart. *Asymptotic statistics. Cambridge Series in Statistical and Probablistic Mathematics*, volume 3. Cambridge university press, 1998.

Tyler VanderWeele. *Explanation in causal inference: methods for mediation and interaction*. Oxford University Press, 2015.

Tyler J VanderWeele. Causal mediation analysis with survival data. *Epidemiology (Cambridge, Mass.)*, 22(4):582, 2011.

Tyler J VanderWeele. A unification of mediation and interaction: a four-way decomposition. *Epidemiology (Cambridge, Mass.)*, 25(5):749, 2014.

Tyler J VanderWeele. Mediation analysis: a practitioner's guide. *Annual Review of Public Health*, 37:17–32, 2016.

Tyler J VanderWeele and Ilya Shpitser. On the definition of a confounder. *Annals of Statistics*, 41(1):196, 2013.

Tyler J VanderWeele and Eric J Tchetgen Tchetgen. Mediation analysis with time varying exposures and mediators. *Journal of the Royal Statistical Society: Series B (Statistical Methodology)*, 79(3):917–938, 2017.

Tyler J VanderWeele, Stijn Vansteelandt, and James M Robins. Effect decomposition in the presence of an exposure-induced mediator-outcome confounder. *Epidemiology (Cambridge, Mass.)*, 25(2):300, 2014.

Stijn Vansteelandt, Martin Linder, Sjouke Vandenberghe, Johan Steen, and Jesper Madsen. Mediation analysis of time-to-event endpoints accounting for repeatedly measured mediators subject to time-varying confounding. *Statistics in Medicine*, 38(24):4828–4840, 2019.

Hal R Varian. Position auctions. *International Journal of Industrial Organization*, 25(6):1163–1178, 2007.

Cédric Villani. *Optimal transport: old and new*, volume 338. Springer Science & Business Media, 2008.

Stefan Wager and Susan Athey. Estimation and inference of heterogeneous treatment effects using random forests. *Journal of the American Statistical Association*, 113 (523):1228–1242, 2018a.

Stefan Wager and Susan Athey. Estimation and inference of heterogeneous treatment effects using random forests. *Journal of the American Statistical Association*, 113 (523):1228–1242, 2018b.

Michael P Wallace and Erica EM Moodie. Doubly-robust dynamic treatment regimen estimation via weighted least squares. *Biometrics*, 71(3):636–644, 2015.

Bingkai Wang, Elizabeth L Ogburn, and Michael Rosenblum. Analysis of covariance in randomized trials: More precision and valid confidence intervals, without model assumptions. *Biometrics*, 75(4):1391–1400, 2019.

Jixian Wang. A simple, doubly robust, efficient estimator for survival functions using pseudo observations. *Pharmaceutical Statistics*, 17(1):38–48, 2018.

Mei Wang and Weihong Deng. Deep visual domain adaptation: A survey. *Neurocomputing*, 312:135–153, 2018.

Rui Wang, Stephen W. Lagakos, James H. Ware, David J. Hunter, and Jeffrey M. Drazen. Statistics in medicine - Reporting of subgroup analyses in clinical trials. *New England Journal of Medicine*, 357(21):2189, 2007.

Shirley V Wang, Yinzhu Jin, Bruce Fireman, Susan Gruber, Mengdong He, Richard Wyss, HoJin Shin, Yong Ma, Stephine Keeton, Sara Karami, et al. Relative performance of propensity score matching strategies for subgroup analyses. *American Journal of Epidemiology*, 187(8):1799–1807, 2018a.

Xuanhui Wang, Nadav Golbandi, Michael Bendersky, Donald Metzler, and Marc Najork. Position bias estimation for unbiased learning to rank in personal search. In *Proceedings of the Eleventh ACM International Conference on Web Search and Data Mining*, pages 610–618. ACM, 2018b.

Yixin Wang and David M Blei. The blessings of multiple causes. *arXiv preprint arXiv:1805.06826*, 2018.

Yu-Xiang Wang, Alekh Agarwal, and Miroslav Dudik. Optimal and adaptive off-policy evaluation in contextual bandits. In *Proceedings of the 34th International Conference on Machine Learning-Volume 70*, pages 3589–3597. JMLR. org, 2017.

John Robert Warren. Socioeconomic status and health across the life course: a test of the social causation and health selection hypotheses. *Social forces*, 87(4): 2125–2153, 2009.

Junfeng Wen, Chun-Nam Yu, and Russell Greiner. Robust learning under uncertain test distributions: Relating covariate shift to model misspecification. In *ICML*, pages 631–639, 2014.

Elizabeth J Williamson, Andrew Forbes, and Ian R White. Variance reduction in randomised trials by inverse probability weighting using the propensity score. *Statistics in Medicine*, 33(5):721–737, 2014.

Jun Xie and Chaofeng Liu. Adjusted kaplan–meier estimator and log-rank test with inverse probability of treatment weighting for survival data. *Statistics in Medicine*, 24(20):3089–3110, 2005.

Ya Xu, Nanyu Chen, Addrian Fernandez, Omar Sinno, and Anmol Bhasin. From infrastructure to culture: A/b testing challenges in large scale social networks. In *Proceedings of the 21th ACM SIGKDD International Conference on Knowledge Discovery and Data Mining*, pages 2227–2236, 2015.

Li Yang and Anastasios A Tsiatis. Efficiency study of estimators for a treatment effect in a pretest–posttest trial. *The American Statistician*, 55(4):314–321, 2001.

Shu Yang. Propensity score weighting for causal inference with clustered data. *Journal of Causal Inference*, 6(2), 2018.

Shu Yang, Guido W Imbens, Zhanglin Cui, Douglas E Faries, and Zbigniew Kadziola.

Propensity score matching and subclassification in observational studies with multi-level treatments. *Biometrics*, 72(4):1055–1065, 2016.

Siyun Yang, Elizabeth Lorenzi, Georgia Papadogeorgou, Daniel M Wojdyla, Fan Li, and Laine E Thomas. Propensity score weighting for causal subgroup analysis. *arXiv preprint arXiv:2010.02121*, 2020.

Fang Yao, Hans-Georg Müller, and Jane-Ling Wang. Functional data analysis for sparse longitudinal data. *Journal of the American Statistical Association*, 100 (470):577–590, 2005.

Jinsung Yoon, James Jordon, and Mihaela Van Der Schaar. Gain: Missing data imputation using generative adversarial nets. *arXiv preprint arXiv:1806.02920*, 2018a.

Jinsung Yoon, James Jordon, and Mihaela van der Schaar. Ganite: Estimation of individualized treatment effects using generative adversarial nets. *International Conference on Learning Representations*, 2018b.

Salim Yusuf. Randomised controlled trials in cardiovascular medicine: Past achievements, future challenges. *British Medical Journal*, 319(7209):564–568, 1999.

Shuxi Zeng, Serge Assaad, Chenyang Tao, Shounak Datta, Lawrence Carin, and Fan Li. Double robust representation learning for counterfactual prediction. *arXiv preprint arXiv:2010.07866*, 2020a.

Shuxi Zeng, Murat Ali Bayir, Joel Pfeiffer, Denis Charles, and Emre Kiciman. Causal transfer random forest: Combining logged data and randomized experiments for robust prediction. *arXiv preprint arXiv:2010.08710*, 2020b.

Shuxi Zeng, Fan Li, and Peng Ding. Is being an only child harmful to psychological health?: evidence from an instrumental variable analysis of china's one-child policy. *Journal of the Royal Statistical Society: Series A (Statistics in Society)*, 183(4): 1615–1635, 2020c.

Shuxi Zeng, Fan Li, Rui Wang, and Fan Li. Propensity score weighting for covariate adjustment in randomized clinical trials. *Statistics in Medicine*, 40(4):842–858, 2020d.

Shuxi Zeng, Stacy Rosenbaum, Elizabeth Archie, Susan Alberts, and Fan Li. Causal mediation analysis for sparse and irregular longitudinal data. *arXiv preprint arXiv:2007.01796*, 2020e.

Kun Zhang, Bernhard Schölkopf, Krikamol Muandet, and Zhikun Wang. Domain adaptation under target and conditional shift. In *International Conference on Machine Learning*, pages 819–827, 2013.

Min Zhang and Douglas E Schaubel. Double-robust semiparametric estimator for differences in restricted mean lifetimes in observational studies. *Biometrics*, 68(4): 999–1009, 2012.

Min Zhang, Anastasios A. Tsiatis, and Marie Davidian. Improving efficiency of inferences in randomized clinical trials using auxiliary covariates. *Biometrics*, 64 (3):707–715, 2008.

Yao Zhang, Alexis Bellot, and Mihaela van der Schaar. Learning overlapping rep-

resentations for the estimation of individualized treatment effects. *arXiv preprint arXiv:2001.04754*, 2020.

Qingyuan Zhao and Daniel Percival. Entropy balancing is doubly robust. *Journal of Causal Inference*, 5(1), 2017.

Yi Zhao, Xi Luo, Martin Lindquist, and Brian Caffo. Functional mediation analysis with an application to functional magnetic resonance imaging data. *arXiv preprint arXiv:1805.06923*, 2018.

Ying Y Zhao, Rui Wang, Kevin J Gleason, Eldrin F Lewis, Stuart F Quan, Claudia M Toth, Michael Morrical, Michael Rueschman, Jia Weng, James H Ware, et al. Effect of continuous positive airway pressure treatment on health-related quality of life and sleepiness in high cardiovascular risk individuals with sleep apnea: Best apnea interventions for research (bestair) trial. *Sleep*, 40(4):zsx040, 2017.

Yingqi Zhao, Donglin Zeng, A John Rush, and Michael R Kosorok. Estimating individualized treatment rules using outcome weighted learning. *Journal of the American Statistical Association*, 107(499):1106–1118, 2012.

Wenjing Zheng and Mark van der Laan. Longitudinal mediation analysis with time-varying mediators and exposures, with application to survival outcomes. *Journal of Causal Inference*, 5(2), 2017.

Wenjing Zheng and Mark J van der Laan. Asymptotic theory for cross-validated targeted maximum likelihood estimation. *U.C. Berkeley Division of Biostatistics Working Paper Series*, 2010.

Wenjing Zheng and Mark J van der Laan. Mediation analysis with time-varying mediators and exposures. In *Targeted Learning in Data Science*, pages 277–299. Springer, 2018.

Tianhui Zhou, Guangyu Tong, Fan Li, and Laine E Thomas. Psweight: An r package for propensity score weighting analysis. *arXiv preprint arXiv:2010.08893*, 2020.

Corwin M Zigler, Francesca Dominici, and Yun Wang. Estimating causal effects of air quality regulations using principal stratification for spatially correlated multivariate intermediate outcomes. *Biostatistics*, 13(2):289–302, 2012.

Matthew N Zipple, Elizabeth A Archie, Jenny Tung, Jeanne Altmann, and Susan C Alberts. Intergenerational effects of early adversity on survival in wild baboons. *Elife*, 8:e47433, 2019.

Guangyong Zou. A Modified Poisson Regression Approach to Prospective Studies with Binary Data. *American Journal of Epidemiology*, 159(7):702–706, 2004. ISSN 00029262. doi: 10.1093/aje/kwh090.

José R Zubizarreta. Stable weights that balance covariates for estimation with incomplete outcome data. *Journal of the American Statistical Association*, 110(511): 910–922, 2015.

Biography

Shuxi Zeng received a B.A. in Economics and B.S. in Mathematics from Tsinghua University in 2017 and a Ph.D. in Statistics from Duke University in 2021.